Czech Technical University in Prague
Faculty of Electrical Engineering
Department of Physics

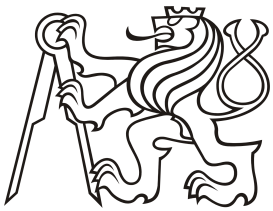

Generation of Fusion Neutrons in *Z*–Pinches

Ing. Daniel Klír, Ph.D.

A habilitation thesis submitted for the degree of 'Docent' (Associate Professor)
in Applied Physics

March 2013

ABSTRACT

A Z-pinch may be defined as a cylindrically symmetric plasma column in which the plasma carrying an axial current is confined, owing to the Lorentz force, by its own magnetic field. Deuterium Z-pinches have produced a large number of fast neutrons from the very beginning of fusion research. Even though the thermonuclear origin of neutrons was not confirmed in the first compressional Z-pinch experiments, a high efficiency of neutron production led to the study of Z-pinches as neutron sources. Z-pinches as pulsed neutron sources can be useful tools in radiation material science, radiobiology, nuclear medicine, cargo inspection, improvised-explosive-device detection and controlled thermonuclear fusion research. In order to produce a significant number of fusion reactions, various Z-pinch configurations have been tested.

The author of this habilitation thesis has been interested in the acceleration of deuterons and production of neutrons in Z-pinches. The thesis presents obtained results in the form of several research articles which were published in peer-reviewed journals. The presented articles are linked together by an additional text between each section. In order to explain the basic idea which lies behind these papers, the purpose of Z-pinch experiments and working methods are also delineated. The results are summarized with respect to neutron production mechanisms and scaling laws. The comparison with other high temperature plasmas is also provided. Finally, the contribution of the Z-pinch group from the Czech Technical University to plasma physics research is presented.

CONTENTS

LIST OF FIGURES

ACKNOWLEDGEMENTS

First and foremost, I would like to make grateful acknowledgement to all members of our research group, particularly to Prof. RNDr. Pavel Kubeš, CSc., Doc. Jozef Kravárik, CSc. , Ing. Karel Řezáč, Ph.D. and Ing. Jakub Cikhardt from the Faculty of Electrical Engineering, Czech Technical University in Prague. Their extensive assistance took many forms but was never lacking.

I also wish to express my gratitude to the research teams at the S-300 *Z*-pinch facility (Kurchatov Institute of Atomic Energy in Moscow), at the PF-1000 plasma focus (Institute of Plasma Physics and Laser Microfusion in Warsaw), at the GIT-12 generator (Institute of High Current Electronics in Tomsk), at the Prague Asterix Laser System (Institute of Plasma Physics in Prague), at the SPEED-2 plasma focus (Comisión Chilena de Energía Nuclear in Santiago de Chile), and at the Phelix laser and Unilac accelarator (GSI Helmholtzzentrum fur Schwerionenforschung GmbH in Darmstadt) for their kind help during our experiments.

I am also grateful to all who provided me with invaluable advice, inspiration, and encouragement.

I thank to the Ministry of Education of the Czech Republic (research programs LC528, LG 13029, LH 13283, and the ECOP project CZ.1.07/2.3.00/20.0279), the Grant Agency of the Czech Republic (grants 202/08/P084, P205/12/0454), the Czech Technical University in Prague (grant SGS-OHK3-053-13), and the International Atomic Energy Agency (grants RC14817 and 17088) for their financial support.

Finally, my sincere thanks go to my wife Michaela for her support.

INTRODUCTION

The research of high-current discharges at the Department of Physics of the Faculty of Electrical Engineering (Czech Technical University in Prague) has a long tradition. The beginnings are connected with the then Heads of the Department, namely with Prof. Ing. Jiří Kracík, DrSc. and Doc. Ing. Jaromír Tobiáš, CSc. They initiated the construction of a plasma gun (Marshall, 1958) which was afterwards studied theoretically and experimentally at the Department in Poděbrady already in the early 1960s. Since that time, several kilojoule apparatus with 100 kA currents and microsecond rise times have been built. The interest was gradually moving from plasma guns and plasma foci in the 1970s and 1980s towards gas embedded Z-pinches and fibre Z-pinches in vacuum in the 1990s. Recently, we have come back to the initial configuration and a plasma focus is being researched again. The main idea behind this research has been to employ attractive properties of Z-pinches and plasma foci, particularly their simplicity of design and very high conversion efficiency of stored electrical energy into X-ray radiation and fast particles.

During the past 50 years, several dozens of scientists, engineers, and students participated in the research. From the 1960s until today, the experiments have been carried out by Jozef Kravárik and Pavel Kubeš. Together they led the experimental group which started its broad international collaboration in the 1990s. During the last 15 years of this collaboration, it was possible to perform measurements at the University of Ferrara, at the Ruhr University in Bochum, at the Imperial College in London, at the Institute of Plasma Physics (IPPLM) in Warsaw, at the Kurchatov Institute of Atomic Energy (KIAE) in Moscow, at the Institute of High Current Electronics (IHCE) in Tomsk, at the Comisión Chilena de Energía Nuclear in Santiago de Chile, and at the GSI Helmholtzzentrum für Schwerionenforschung in Darmstadt. The international collaboration was supported by a significant financial support of the Ministry of Education, Youth and Sports, namely by the INGO project 'Research in the Frame of International Center of Dense and Magnetized Plasma' and by the Czech-Russian bilateral project 'Study of fast Z-pinches'.

The author of this habilitation thesis joined the group in 1998. He has regularly participated in experiments since 2000. His interests then included high temperature plasma diagnostics, Z-pinch energetics, Z-pinch physics, and data analysis. The nanosecond extreme-ultraviolet diagnostics and analysis of fibre Z-pinch experiments at the Department of Physics were the basis for writing his Master and Doctoral thesis in 2002 and 2005, respectively. Later, he was focused on diagnostics of fusion neutrons, high energy density physics and controlled thermonuclear research. Most of the neutron measurements took place at large megajoule devices, namely on the S-300 Z-pinch at KIAE in Moscow, on the GIT-12 Z-pinch in IHCE in Tomsk, and on the PF-1000 plasma focus at the IPPLM in Warsaw. The author's range of activities comprised calibration and testing of detectors, preparation of experiments, participation in measurements, data reduction as well as the interpretation of results together with their presentation at international conferences. The obtained results were published in several research articles of peer-reviewed journals. The summary of the most important articles, the main contributor of which was the author of this thesis, forms Chapter 3. In order to explain the basic idea which lies behind these papers, the purpose of Z-pinch experiments and our working methods are delineated in Chapters 1 and 2, respectively.

Outline

The thesis is divided into 4 chapters as follows:
Chapter 1 contains the explanation of the basic principle of Z-pinches, brief survey of Z-pinch research and state of the art applications. Chapter 2 focuses on purposes and methods used in our fusion experiments. Chapter 3 presents the summary of several research articles which were published in peer-reviewed journals and which are attached to the end of this thesis. The presented articles are linked together by an additional text between each section. This additional text also emphasizes the most important results. Chapter 4 summarizes our results with respect to neutron production mechanisms and scaling laws. The comparison with other high temperature plasmas is also provided. Finally, the contribution of our activity to plasma physics research is presented.

Author's share in presented research articles

The results described in this habilitation thesis have been obtained on the basis of broad collaborations of several international research groups. Nevertheless, the research articles

which are presented within this thesis were written mainly by their first author, i.e. by the author of this habilitation thesis. The participation of the first author in the contents of presented papers can be evaluated as about 90%.

Chapter 1

BASIC PRINCIPLE, HISTORICAL OVERVIEW AND APPLICATIONS OF *Z*-PINCHES

1.1 Principle

The *Z*-pinch may be defined as a cylindrically symmetric plasma column in which the plasma carrying an axial current is confined, owing to the Lorentz force, by its own magnetic field. The term 'pinch' originated in the 20th century, when also the first systematic research of *Z*-pinches began. The prefix '*Z*' was added in the 1950s to denote the confinement driven by the axial (z) current.

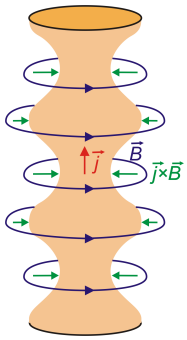

Fig. 1.1: *Z*-pinch being susceptible to $m = 0$ instabilities.

The fluid dynamics of *Z*-pinches can be described by the Euler equation of motion as

$$\rho\left(\frac{\partial \mathbf{v}}{\partial t} + (\mathbf{v}\cdot\nabla)\mathbf{v}\right) = -\nabla p + \mathbf{j}\times\mathbf{B} \tag{1.1}$$

where the pressure gradient $-\nabla p$ and the magnetic force density $\mathbf{j}\times\mathbf{B}$ are included, whereas the viscous force $\eta\Delta\mathbf{v}$ and other terms are neglected.

Z-pinches belong to the most fascinating objects in plasma physics because of their simple principle, natural occurrence including lightings and current channels in galactic scales as well as variety of applications.

1.2 Historical overview

It was the simple principle and geometry in particular why magnetic pinches enjoyed great attention in the early 1950s in conjunction with controlled thermonuclear fusion research (Post, 1956). The idea behind this research was to heat a fusion mixture by Joule heating and by adiabatic or shock compression, and then to confine the plasma by the pinch effect until a sufficient amount of fusion energy was released. One of the first experiments was performed with compressional *Z*-pinches. In this configuration, the electric current started at an insulating wall and when the magnetic pressure exceeded the gas pressure, a current carrying plasma shell together with the preceding shock wave radially collapsed (see Fig. 1.2). Characteristic parameters of compressional *Z*-pinches were 50 cm long and 5 cm diameter vessels, 0.1 Torr initial pressures of a D_2 gas, 20 kV charging voltages, μF capacitor banks and μs implosion times (Andrianov et al., 1958; Anderson et al., 1958; Mather and Williams, 1958).

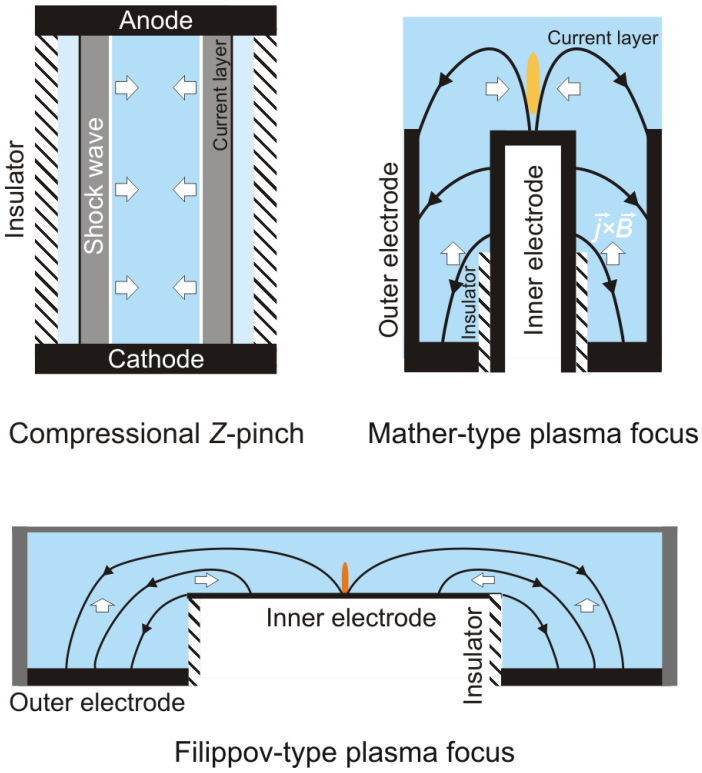

Fig. 1.2: Compressional *Z*-pinch and plasma focus configuration.

The compressional *Z*-pinches produced a high number of neutrons, above 10^8 per one pulse on a 100 kA current level. However, S. Colgate with his colleagues showed that the neutrons were not produced by a Maxwellian plasma. They proposed that deuterons were

accelerated by axial electric fields created by the growth of $m = 0$ instabilities (Anderson et al., 1958). This was consistent with Kurchatov's explanation (Kurchatov, 1957), Kruskal's and Schwarzschild's theoretical work (Kruskal and Schwarzchild, 1954), and earlier experiments carried by Carruthers and Davenport (1957). All these facts together, particularly the conclusion that neutrons were not of thermal origin, led to the abandonment of a straight Z-pinch as a fusion power source. As a result, more complex schemes of magnetically confined plasma devices, such as tokamaks and stellarators that are also free from electrode phenomena and end-losses, were suggested and researched in an attempt to reduce MHD instabilities.

During the research of one of more stable schemes, namely the Scylla-θ pinch[1] at Los Alamos, a plasma gun was used to inject a plasma into the device. When the plasma gun was studied, it was found that a large number of neutrons were generated from this plasma gun itself. This was the main reason why a so-called Mather-type plasma focus[2] was researched from that time on (Mather, 1965). The plasma focus is a device also based on the pinch effect. The dense plasma focus is filled with a gas of ≈Torr pressures (several hundreds of Pa), and consists of a two coaxial electrodes which are insulated from each other by an insulator sleeve. After a breakdown, the current sheath is accelerated along the coaxial electrodes as shown in Fig. 1.2. At the end of this axial phase, when the current rises to its peak, a radial collapse occurs in the way similar to Z-pinches[3]. The maximum yield on sub-MJ devices approached the value of 10^{12} DD neutrons per pulse (cf. Bernard et al., 1977b; Brzosko et al., 1987).

The interest in Z-pinches was renewed in the 1970s when high voltage, >100 kV pulsed power technology was developed and used to drive a Z-pinch load. Using the pulsed power technology, it has become possible to deliver an electrical power of ≈50 TW and an energy of ≈10 MJ to a load. The compression of an electrical energy in time and space is enabled by a Marx generator, (water) pulse forming line and magnetically insulated (vacuum) transmission line[4]. When the pinch effect is used as a final stage of these

[1] The names Scylla and Charybda indicated the difficulty with achievement of controlled nuclear fusion. On the Scylla theta pinch, the first thermonuclear fusion is said to be proved.

[2] In the former Soviet Union, a plasma focus was constructed independently from a compressional Z-pinch with a conducting wall (cf. Andrianov et al., 1958; Filippov et al., 1962). In a so-called Fillipov type plasma focus, the ratio between an anode diameter and a length is higher than in the Mather type.

[3] The main advantages of a plasma focus are as follows: Firstly, the radial compression occurs at a peak current without the necessity of a high voltage pulsed power generator. Secondly, an insulator is protected against direct irradiation by stagnating plasmas. Finally, in comparison with compressional Z-pinches, plasma foci are usually smaller and the final increase of a plasma column inductance is lower.

[4] More recently, lower voltage linear transformer drivers have been developed to deliver a current into

devices, the energy stored in capacitors can be deposited into a small volume of $\approx$cm^3 within several nanoseconds with a high efficiency of about 30%. Due to a low impedance of these current generators, the implosion of a low inductance cylindrical plasma onto its axis is a more effective way to generate radiation than resistive heating of an exploding wire with an initial low diameter (Linhart, 1961). For this reason, cylindrical arrays of wires, thin cylindrical foils, annular gas puffs, etc. have been used. With these loads, the stored electrical energy is converted into a kinetic energy of magnetically confined, imploding plasmas. At stagnation, the kinetic energy is thermalized. In the case of high atomic number material, the significant part of the energy is radiated in sub-keV and keV radiation. Since observed radiation yields were sometimes higher than the kinetic energy input (Riordan et al., 1981), other mechanisms also contribute to the total X-ray output.

More recently, by using nested arrays of $\approx\mu$m diameter wires, *Z*-pinches have become the world's most powerful (350 TW power, 2.8 MJ radiated energy) and most efficient (15%) laboratory X-ray sources (Sanford et al., 1996; Deeney et al., 1997; Spielman et al., 1998). In addition to that, the measured Doppler-width of iron spectral lines indicated that the ion temperature in wire-arrays on the *Z*-machine exceeded 200 keV (Haines et al., 2006). This was believed to be the record temperature for a magnetically confined plasma[5]. From other significant parameters of the most powerful *Z*-machine in Sandia, we can mention magnetic and kinetic pressures of the order of 10 Mbar, electron temperatures of about 1 keV, radiated powers of 100 TW, magnetic fields of 1000 T, and the energy density of about 10 MJ/cm^3. Matter with these parameters fulfills the conditions required for high energy density physics.

1.3 State of the art

At present, *Z*-pinches are being intensively researched as the most powerful and efficient laboratory sources of soft X-rays. The refurbished *Z* machine in the Sandia National Laboratories is now capable of producing 5 ns X-ray pulses with 350 TW peak powers and 2.8 MJ radiated energies.

The primary interest of the research is to use *Z*-pinch sources as drivers for the controlled thermonuclear fusion. However, there are more reasons for studying *Z*-pinches

a load with a short rise-time (Kim et al., 2009; Mazarakis et al., 2009).

[5] Since the broadening of the spectral lines was influenced by residual fluid motion, the real ion temperature was lower.

since they can be used in other high-energy-density physics experiments, such as for example:

- Laboratory measurements of material and radiation properties under extreme conditions, i.e. at densities, temperatures and pressures that could be otherwise reached only in underground nuclear explosions or at the National Ignition Facility (shock physics, measurement of the equation of state under multi-mega-bar pressures, the study of radiation hydrodynamics, radiation transport, opacity measurements, Matzen et al. 2005).
- Stockpile stewardship programme (survivability of weapons systems, etc.).
- Development of X-ray lasers (Rocca et al., 1994) and X-ray sources for EUV lithography and X-ray microscopy (Bailey et al., 1982; McGeoch, 1998).
- Laboratory astrophysics (the generation of highly supersonic plasma jets, etc. Remington et al., 2006).
- Controlled generation of high magnetic fields of the order of 1000 T by magnetic flux compression in an imploding cylindrical shell (Felber et al., 1985; Slutz et al., 2010).
- Optical guidance of terawatt laser pulses in a capillary discharge (Hosokai et al., 2000).
- Spectroscopy of highly charged ions (cf. Pereira and Davis, 1988 and references herein).
- Generation of charged and neutral particles for industrial, scientific and medical applications (Bogolubov et al., 2009; Roshan et al., 2010; Gribkov et al., 2010; Rawat, 2012).

1.4 Production of neutrons

Besides the successful achievements mentioned above, Z-pinches have also been used as efficient sources of fusion neutrons from the very beginning of the controlled thermonuclear fusion research. A large number of produced neutrons in Z-pinches led to the study

of acceleration of deuterons to fusion energies. In order to cope with this reality satisfactorily and to achieve even higher neutron yields, various configurations based on the *Z*-pinch effect have been suggested and tested from that time on (see the survey in the introductory part of Klir et al., 2008, article No. 2 of this habilitation thesis). The most promising configurations seem to be deuterium gas puff *Z*-pinches (Batyunin et al., 1990) and a plasma focus with a deuterium gas filling (Mather, 1965). An illustrative result is 4×10^{13} neutrons produced with a double-shell D_2 gas puff on the 17 MA *Z*-machine in 2005. In addition to that, MHD and particle-in-cell simulations showed that there is a hope of a large thermonuclear component (Velikovich et al., 2007; Welch et al., 2009). In the case of the 29 *ZR* machine, up to 6×10^{16} DT neutrons are expected which was a lower estimate for ICF (Inertial Confinement Fusion) capsules on the National Ignition Facility.

Z-pinches as pulsed neutron sources are useful tools particularly in two areas. The first area involves important broad-band applications of *Z*-pinches in radiation material science (Bogolubov et al., 2009), radiobiology, nuclear medicine (brachytherapy, PET radionuclide production, Roshan et al., 2010), cargo inspection (Bures et al., 2010), improvised-explosive-device detection (Gribkov et al., 2010), etc. The various use of *Z*-pinches is one of the main reasons why they are researched in many countries all over the world, particularly in Chile, China, India, Poland, Russia, Singapore, and USA.

The second area is closely related to the controlled thermonuclear fusion research. Firstly, *Z*-pinches might support the main streams of nuclear fusion programme. For instance, *Z*-pinches could be used to solve fusion engineering problems (e.g. neutron tests of materials of the first wall, blankets). Furthermore, since *Z*-pinches provide plasma densities and time-scales which can be relatively easily diagnosed, it is possible to study plasma phenomena which are of a great interest for inertial confinement fusion (self-generated magnetic fields, Rayleigh-Taylor instability, isoentropic compression, equation of state, etc.) as well as for magnetic confinement fusion (anomalous resistance, plasma turbulences, current disruption, heating by deuteron beams). Secondly, it is also possible to research *Z*-pinches as fusion devices. The application of a *Z*-pinch as an indirect X-ray driver for ICF capsules is well known (Ruiz et al., 2004). However, there is also a possibility of novel fusion approaches based on the *Z*-pinch effect.

There are two principal reasons for novel fusion approaches. The first one is the idea to employ the effect of inertial as well as magnetic confinement in a large space of plasma

densities between 10^{20} and 10^{29} m^{-3} (so-called Magneto-Inertial Fusion or Magnetized-Target Fusion). This density region has not been investigated in such details as ICF and MCF (Magnetic Confinement Fusion) concepts but it seems worthwhile to do so. The second reason follows from basic principles of particle diffusion which show that alternative approaches based on the Z-pinch effect could provide much smaller fusion reactors than tokamaks and ICF drivers (Siemon et al., 1999). This is an important fact because it means cheaper way of fusion research which has not been finished yet. In this respect we can mention the MagLIF concept (Magnetized Liner Inertial Fusion, Slutz et al., 2010; Slutz and Vesey, 2012) which is a very promising even though there are many technological challenges that need to be overcome.

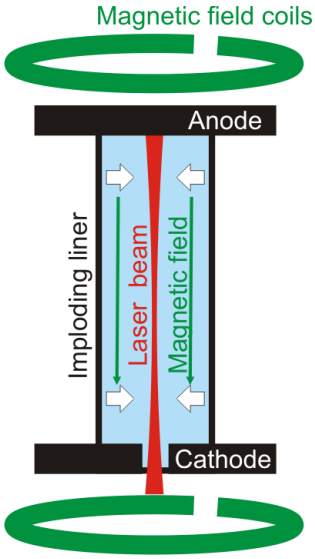

Fig. 1.3: Imploding liner heated by laser in the MagLIF concept.

The basic idea of the MagLIF project is based on magnetically driven compression of a solid liner that contains a fuel preheated by a powerful laser and magnetized by an embedded axial magnetic field, as shown in Fig. 1.3. In comparison with gas puffs, solid metal liners provide higher initial conductivity and they enable us to use a DT mixture with much higher initial pressure of about 100 Mbar. Due to the preheating by a laser to ≈500 eV temperatures, a relatively low implosion velocity of the order of 10^5 m/s is required to obtain the ignition temperature. The axial magnetic field of ≈10 T is expected to stabilize the implosion, to suppress thermal conduction losses, and to enhance the energy deposition by alpha particles. When a 100 ns current generator is used, a modest laser energy is required and a purely axial magnetic field is sufficient to confine α particles

within a 2 cm long cylindrical column. According to numerical predictions, conditions sufficient for breakeven might be reached even with the Z-machine and Z-beamlet at the Sandia National Laboratories. But even if the issue of controlled fusion is not solved in the near future, Z-pinches might be applied as efficient neutron sources in fusion-fission reactors (Leonard, 1973; Gerstner, 2009).

Chapter 2

AIMS, METHODS AND TECHNIQUES

2.1 Purpose of our research

At the end of the previous chapter, we pointed out the importance of applications of *Z*-pinches as neutron sources. Before *Z*-pinches are used in these applications, however, it is necessary to address all issues which are specific for the implosion of deuterium plasma. In this respect, more experimental data are needed to benchmark numerical codes.

The last but not least reason for being interested in experiments with deuterium is related to plasma diagnostics. As far as the fusion of two deuterons is concerned, there are four products of two main branches of the DD reaction, one of them is a neutron. Because neutrons are influenced neither by magnetic nor by electric fields[1], neutron detection is a favourable diagnostic tool of fast deuterons in plasma. While a large number of scientific papers in the last years were devoted to studies of X-ray radiation, the information about fast ions was rather rare. Therefore fusion neutron measurements could provide invaluable data about fast ions for plasma physics and for a large variety of modern applications.

2.2 Methods used in our research

A significant part of our diagnostic instruments and methods was prepared and tested on a small plasma focus PFZ-200 at the Faculty of Electrical Engineering, Czech Technical University in Prague (Kubes et al., 2009). This device with DD neutron yields of 10^7-10^8/shot could be easily modified with respect to applied diagnostic techniques and methods. When diagnostic instruments had been successfully tested, it was possible to use them abroad at larger facilities.

[1] Finite electric dipole and magnetic moments of neutrons are not taken into account.

Z-pinch discharges showed specific experimental results in each shot and shot-to-shot variations were large. Therefore it was important to use simultaneously comprehensive set of diagnostic tools with temporal, spatial, and spectral resolution. In our fusion experiments, the emphasis was put on finding information about (i) neutron yields, (ii) energy distributions of fusion neutrons, (iii) anisotropy of neutron emission, (iv) a spatial region of neutron generation, and (v) a time and duration of neutron production with respect to general plasma dynamics. In what follows, we will restrict ourselves to the description of the measurement of time resolved neutron energy distribution function and neutron flux. The description of these quantities is important for a better insight into our work.

2.2.1 Neutron flux

The neutron flux carries important information about velocities of colliding deuterons. Figure 2.1 shows the dependence of the fusion cross-section on a deuteron energy E_d and on the angle θ between a fast deuteron and an outgoing neutron. It can be seen in graph 2.1 that the fewest neutrons are emitted perpendicularly to the direction of fast deuteron motion. It means that the ratio is the highest between the end-on and side-on yield.

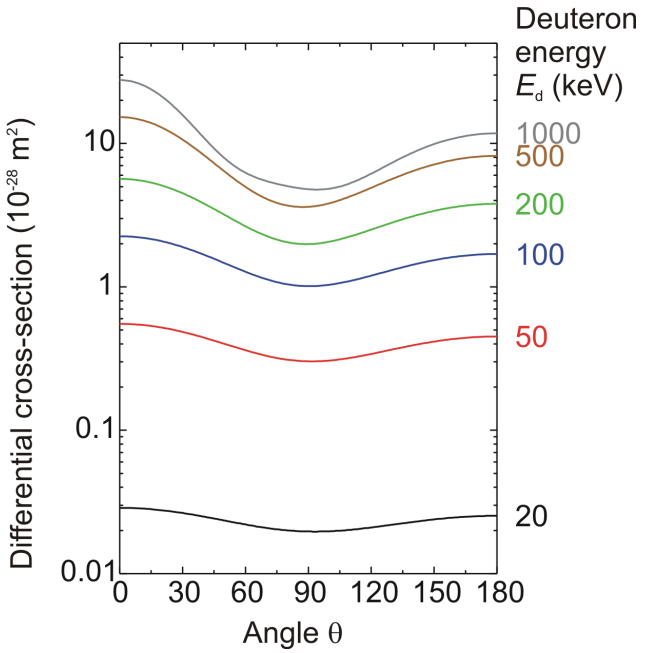

Fig. 2.1: Energy–angle dependence of the differential cross-section of the D(d,n)^{3}He fusion reaction in the laboratory frame of reference using data from Drosg (1987).

In our experiments, the neutron flux/fluence was measured by several techniques, e.g. by indium and silver activation counters (Bienkowska et al., 2006), by thermoluminiscence dosimeters placed in Bonner spheres (Velyhan et al., 2006; Krasa et al., 2008; Kralik et al., 2010), by superheated fluid detectors (Ing et al., 1997), and by time-of-flight detectors calibrated to a single neutron sensitivity (Klir et al., 2011).

2.2.2 Neutron energy distribution function

Another piece of information about colliding deuterons is carried by a neutron energy spectrum. If we assume the binary reaction of a fast deuteron with a stationary target deuteron[2], the neutron energy E_n depends on the deuteron energy E_d and on the laboratory angle θ between the colliding fast deuteron and the outgoing neutron as

$$\begin{aligned} E_\mathrm{n}(E_\mathrm{d},\theta) &= E_\mathrm{d}\frac{m_\mathrm{n}m_\mathrm{d}}{(m_\mathrm{n}+m_\mathrm{He})^2}\cdot \\ &\cdot \left(\cos\theta + \sqrt{\frac{m_\mathrm{He}(m_\mathrm{n}+m_\mathrm{He}-m_\mathrm{d})E_\mathrm{d}+m_\mathrm{He}(m_\mathrm{He}+m_\mathrm{n})Q}{m_\mathrm{n}m_\mathrm{d}E_\mathrm{d}}-\sin^2\theta}\right)^2 \end{aligned} \tag{2.1}$$

where $Q \doteq 3.27$ MeV represents the energy released from the D(d,n)^{3}He fusion reaction, m_n is the neutron mass, and m_He is the mass of helium $^3_2$He. It can be seen in Fig. 2.2, that 200 keV deuterons, for instance, could produce 3 MeV neutrons forwards, 2.5 MeV neutrons side-on and 2 MeV neutrons backwards.

One of the most accurate methods of measuring energy spectra of fast neutrons which are produced by the D(d,n)^{3}He fusion reactions is time-of-flight (ToF) diagnostics. This is why the ToF analysis was applied to diagnose fusion processes in our experiments.

In the time-of-fligh method, the time-resolved neutron energy distribution function $f(E_\mathrm{n},\theta,\phi,t)$ is being reconstructed from time-resolved neutron signals $S(x,T)$ which are recorded by several detectors in one direction at different distances x. The relation between the time-of-flight signals $S(x,T)$ and the energy distribution function $f(E_\mathrm{n},\theta,\phi,t)$ is given by

[2] If the velocity of target deuterons cannot be neglected, e.g. in themonuclear plasmas, a different approach has to be applied. For instance, the approach presented by Appelbe and Chittenden (2011) might be helpful.

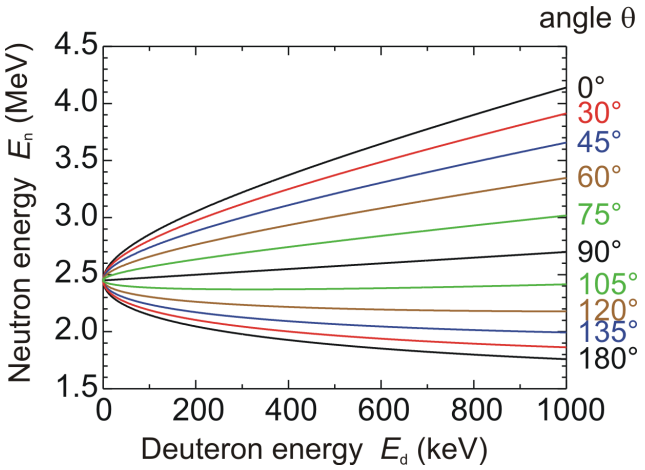

Fig. 2.2: Energy–angle dependence of neutron energies for the D(d,n)^{3}He fusion reaction in the laboratory frame of reference.

$$S(x,T) = \int_{\phi} d\phi \int_{\theta} d\theta \int_{-\infty}^{+\infty} dE_{\mathrm{n}} \int_{-\infty}^{+\infty} d\tau \int_{-\infty}^{+\infty} dt f(E_{\mathrm{n}},\theta,\phi,t) \cdot \\ \cdot \; \delta\left(t-\tau+\frac{x}{\sqrt{2E_{\mathrm{n}}/m_{\mathrm{n}}}}\right) h(E_{\mathrm{n}},T-\tau) \tag{2.2}$$

where T is the neutron detection time, t is the emission time and $h(E_{\mathrm{n}},\tau)$ is the pulse response of the ToF detector. The lower and upper limits of the integration $\int_{\phi}\int_{\theta} d\phi d\theta$ depend on the detector surface and on its distance from a source.

There are several numerical algorithms how to obtain the $f(E_{\mathrm{n}},\theta,\phi,t)$ function. We chose the Monte Carlo method (Tiseanu et al., 1996). The author with his Ph.D. student Karel Řezáč improved this method by using ToF detectors in mutually opposite directions (Rezac et al., 2012). Another Ph.D. student, Ondřej Šíla, calculates the influence of neutron scattering on ToF signals by the Monte Carlo N-Particle code (Briesmeister, J. F., 2000). In the near future, it will be possible to obtain corrected time-of-flight signals $S(x,T)$ by deconvolution of measured signals with a simulated response including scattering at the whole experimental arrangement.

2.3 Article No. 1: Fusion neutron detector for time-of-flight measurements in Z-pinch and plasma focus experiments

For our Z-pinch and plasma focus experiments, we constructed a set of neutron time-of-flight detectors which operate in current mode. These detectors consist of a fast plastic scintillator, a photomultiplier and shielding. The reconstruction of neutron energy spectrum from Eq. 2.2 requires the knowledge of the detector pulse response $h(E_n, \tau)$ on a single neutron. Therefore we carefully calibrated each detector. The results were published in *Review of Scientific Instruments* (Klir et al., 2011). During the calibration procedure, the author developed a novel method of the acquisition of a pulse height distribution. In this method, the PF-1000 plasma focus was used as a pulsed neutron source. When the detector was placed at a sufficient distance from the source, it was possible to record individual neutrons and also to calculate the neutron energy by its time-of-flight. It enabled us to calibrate *in-situ* the neutron detector for absolute neutron yields at about 2.45 MeV and to determine the single neutron sensitivity in the energy range between 1.8 and 3.0 MeV. Despite the fact that the dependence of the light output on a neutron energy is not taken into account in many experiments, it could strongly influence results in the case of a broad neutron spectrum. Therefore our calibration and testing are useful for other plasma physics groups, namely at the Nanyang Technological University in Singapoure and at the Comisión Chilena de Energía Nuclear in Santiago de Chile where very similar detectors are used.

Chapter 3

RESULTS GAINED ON S-300, PF-1000 AND GIT-12 GENERATORS

One of the main aim of our research is to discuss various mechanisms of deuteron acceleration and fusion neutron production, and to specify suitable usage of Z-pinch neutron sources in various applications and fusion research. In the previous chapter we showed that neutron flux and neutron energies carry important information about colliding deuterons. Therefore, if the space and time resolved information together with the anisotropy of neutron production are known, it is possible to study the generation of fast deuterons.

In our case, neutron measurements were performed on the large Z-pinches S-300 in Moscow and GIT-12 in Tomsk, and on the PF-1000 plasma focus in Warsaw. The obtained results are presented in this chapter which combines the research articles published by the author of this thesis during the past 5 years.

Article No. 2 contains the experimental results from the S-300. It also demonstrates the method of neutron time-of-flight analysis. Articles No. 3, 4 and 9 show that the deuterium gas puff is one of the most efficient Z-pinch configurations with respect to neutron emission. In the case of the S-300 Z-pinch, a total energy of deuterons accelerated to fusion energies was higher than 15% of the energy input into a plasma. As a result, the abundace of fusion neutrons was produced. On the GIT-12 generator, the number of neutrons from the D(d,n)^{3}He reaction exceeded 3×10^{11} per one shot. In articles No. $5-7$, the authors provide an unambiguous experimental evidence of thermonuclear neutrons in a plasma focus, after 50 years of the research. Finally, purely theoretical article No. 8 is devoted to a so-called drive parameter. This parameter is often used for the design of a neutron optimized plasma focus and it has become a debated issue during the last decade. In our paper, the history of this parameter is traced and the real meaning of the drive parameter is derived and explained.

3.1 Article No. 2: Neutron emission generated during wire-array Z-pinch implosion onto deuterated fiber

The experiments described in Klir et al. (2008) were carried out on the S-300 generator. This low, 0.15 Ω, impedance generator with a 3.5 MA peak current and a 100 ns rise-time (Chernenko et al., 1996) was built at the Kurchatov Institute of Atomic Energy under the supervision of L.I. Rudakov. The collaboration between the *Z*-pinch group of prof. Kubeš from the Czech Technical University and Dr. Rudakov from the Kurchatov Institute of Atomic Energy began in 1996. At the beginning, the possibility of population inversion in single wire explosions was studied (Kubes et al., 2002, 2003). Later, the focus of the research was shifted towards neutron production.

As far as the article with the title 'Neutron emission generated during wire-array *Z*-pinch implosion onto deuterated fiber' is concerned, there were several ideas behind this paper published in *Physics of Plasmas*. Firstly, cylindrical arrays of wires are suitable loads for low impedance current generators such as the S-300. Secondly, wire-arrays provide not only high efficiency of energy conversion to X-rays but they could also deliver a significant part of the current onto the axis with a very fast rise time. There was a presumption that the fast current rise-time could suppress the development of magnetohydrodynamic instabilities and the early expansion of an on-axis deuterated fiber. Then the significant number of thermonuclear neutrons was expected (Lorenz et al., 1998, 1999). Finally, the reason of using a deuterated fiber in the experiment was related to the diagnostics of the most energetic processes in wire-array *Z*-pinches, namely the acceleration of ions to >100 keV energies.

We intended to build on our long-term experience with neutron producing plasma foci and to draw on it in *Z*-pinch research. For instance, we used and improved the Monte Carlo method for neutron energy spectrum reconstruction (Rezac et al., 2006, 2012). The author with his Ph.D. student developed the method of obtaining distribution functions of the kinetic energy component of fusing deuterons. This way, the information about the energy of deuterons was obtained. In the experiment described in Klir et al. (2010), the total number of fast deuterons reached 10^{15} and the average kinetic energy of "reacting" deuterons was about 150 keV. As far as the neutron production mechanism is concerned, the key results were the anisotropy of neutron emission and broad neutron energy spectra. These results indicated that neutrons were not of thermonuclear origin. We used such

an orientation of the conical wire array that we were able to exclude the possibility of a moving thermonuclear boiler[1]. Instead of the thermonuclear mechanism, a beam of fast deuterons was accelerated towards the cathode and then it was colliding with 'cold' target deuterons. Broad neutron energy spectra in the radial direction implied also a high radial component of deuteron velocities. Therefore trajectories of deuterons seemed to be strongly influenced by magnetic fields and the linear motion did not occur. As regards the time of neutron emission, it correlated with soft and hard X-rays. We found the strong correlation also between neutron signals and voltage waveforms. On the basis of neutron measurements, we concluded that the acceleration of fast deuterons is not a secondary process but it reflects the global dynamics of Z-pinch plasmas. For this reason it is useful to add deuterium as a 'tracer' in Z-pinch loads more often.

[1] A moving thermonuclear boiler is a thermonuclear source which is moving in the laboratory frame of the reference.

3.2 Article No. 3: Neutron energy distribution function reconstructed from time-of-flight signals in deuterium gas-puff Z-pinch

On the S-300 generator, various Z-pinch loads containing deuterium were explored, e.g. a deuterated polyethylene fibre (Klir et al., 2006), cylindrical and conical wire arrays imploding onto a deuterated fibre (Klir et al., 2008), deuterated cylindrical foams (Bakshaev et al., 2006) or X-pinch from deuterated fibres (Anan'ev et al., 2010). As shown in Fig. 3.1, the most efficient configuration with respect to the neutron yield was a deuterium gas puff (see Fig. 3.2).

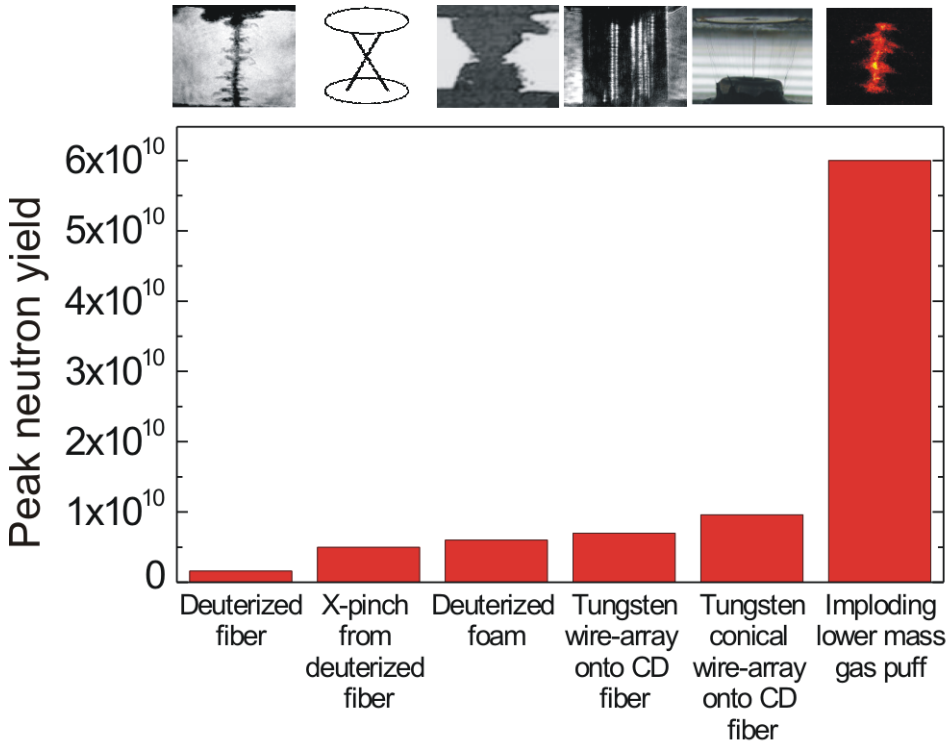

Fig. 3.1: Peak neutron yields obtained with various Z-pinch configurations on the S-300 generator.

We were encouraged to try deuterium gas puffs by the Z-pinch research group from the Sandia National Laboratories. The motivation was to support gas puff experiments on the Z-machine. At the most powerful Z-pinch in Sandia, only a few shots per one year are devoted to fusion research. For instance, the last deuterium gas puff experiment consisting of 2 shots was carried out in 2005 and new experiments are scheduled on 2013. Therefore, in order to acquire more details on neutron production, experiments on a MA current level with advanced neutron diagnostics were required.

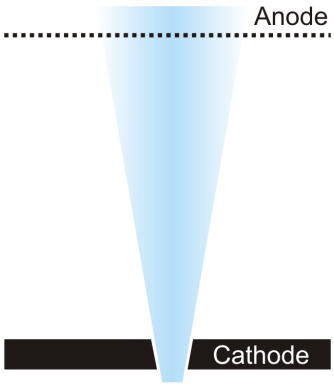

Fig. 3.2: Solid fill deuterium gas puff Z-pinch.

For our first experiments, we constructed a solid fill deuterium gas puff driven by burning gun powder similarly as on the Angara at Troitsk (Batyunin et al., 1990). With such a gas puff, the peak neutron yield of 10^{10} was achieved on the current level of 2 MA. The main contribution of this experiment was the result from neutron TOF diagnostics. It was for the first time in Z-pinch research when 12 nTOF detectors were used and the radial isotropy of neutron emission was studied by TOF signals. The most important data were published in *IEEE Transactions on Plasma Science* and Welch et al. (2010) used these experimental results to verify PIC simulations of Sandia's Z-machine.

3.3 Article No. 4: Efficient production of 100 keV deuterons in deuterium gas puff Z-pinches at 2 MA current

In our first gas puff experiment, the result of which were described in Article No. 3, the injection of gas into vacuum was not reproducible. In addition to that, the deuterium gas was likely interfused with the burning gun powder and thus a linear mass density was higher than expected (above 200 μg/cm). It resulted in a low implosion velocity and lower neutron yields. Therefore we prepared a new electromagnetic valve to drive a gas puff in the following experiments. We asked the group from the Faculty of Mechanical Engineering to help us with the numerical simulation of a gas flow by the ANSYS FLUENT flow modeling software (Stodůlka, 2010). The gas flow simulation confirmed our expectation that the maximum achievable linear mass density was about 20 μg/cm. Such a low mass proved to be suitable for a higher neutron yield. For 20 μg/cm, we increased the neutron yield up to 6×10^{10} neutrons in one shot.

Another important conclusion was related to the efficiency of ion acceleration. The estimation of the total energy of deuterons accelerated to fusion energies was enabled by the simultaneous measurement of the energy input into a plasma, the plasma diameter, the neutron yield and neutron TOF signals in the radial and axial direction. The total energy of fast deuterons was 1.5 kJ. This represented more than 15% of the energy input into a plasma. Therefore gas puff Z-pinches seem to be not only powerful sources of X-ray radiation but also efficient sources of 100 keV deuterons. These results were published in Article No. 4 that was awarded as one of the most frequently downloaded articles in *Plasma Physics and Controlled Fusion* in 2010.

3.4 Article No. 5: Experimental evidence of thermonuclear neutrons in a modified plasma focus

The principal neutron emission and the beam-target mechanism of MA devices were observed after stagnation, more precisely after disruptive development of instabilities. However, the characteristic feature of our deuterium gas puff experiments was the observation of multiple neutron pulses. As a result, neutron production seems to be a multiphase process in which more than one mechanism occurs during the implosion, stagnation, expansion and disruption of the plasma column. The first neutron pulse usually occurs during stagnation. It is therefore natural to ask whether a fraction of neutrons in the first pulse may be explained by thermonuclear mechanism, i.e. whether deuterons are accelerated to fusion energies by multiple elastic collisions in a high-temperature plasma. To prove the thermonuclear mechanism experimentally has been the challenging issue for fifty years of the Z-pinch research. For example, at the end of the well diagnosed experiment at Limeil, Dr. Bernard wrote that he had never seen any piece of evidence indicating that neutrons have thermonuclear origin (Bernard, 1978). On other devices, researchers arrived at similar conclusions. Despite these results, it is important to search for thermonuclear neutrons from two main reasons. The first being the uniqueness of the thermonuclear mechanism which offers the possibility of energy gain. The second reason is promising scaling of a fusion yield with a current $Y_{\mathrm{n}} \propto I^4$.

From these reasons, we wanted to continue with D_2 gas puff experiments on the S-300. However, the S-300 generator at the Kurchatov Institute of Atomic Energy had to be closed due to fire safety regulations in 2010 and our research had to be transferred to the the Institute of Plasma Physics and Laser Microfusion in Warsaw where the PF-1000 plasma focus was built (2.0 MA peak current, 24 kV charging voltage, 400 kJ stored energy, Scholz et al., 2001). The PF-1000 plasma focus demonstrated similar behaviour as the MA deuterium gas puff Z-pinch, particularly the first neutron pulse was observed during the quiet phase. The PF-1000 facility was equipped with Mather-type coaxial electrodes of a 480 mm length and a 230 mm anode diameter. The cathode composed of twelve 80 mm diameter stainless-steel rods distributed around a cylinder of 400 mm diameter. There was one significant advantage of PF-1000 after all, and that was the interferometry diagnostics which enables to provide 16 interferograms from each shot (Zielinska et al., 2011).

In order to search for thermonuclear neutrons, we modified the plasma focus discharge. Firstly, we used a relatively low deuterium pressure between 160 and 240 Pa, i.e. lower than is usual because we wanted to increase the implosion velocity and the ion temperature. Secondly, we placed the cathode disk 3 cm in front of the anode to localize the region where deuterons are accelerated. There were two great advantages of such a modification, namely (i) a higher current during the stagnation and (ii) more straightforward interpretation of plasma dynamics. Despite these changes, however, the evaluation of the neutron energy spectrum of the first, small pulse was still rather complicated. Nevertheless, there was one more advantage of the PF-1000 – its horizontal position of a discharge axis. The horizontal orientation of the PF-1000 enabled us to place neutron TOF detectors on the axis in an upstream direction[2]. In the upstream direction, 2.45 MeV neutrons were one of the fastest and they could be distinguished from scattered and beam-target neutrons which were emitted after the first compression.

After the preparation of neutron and interferometric diagnostics mentioned above, we proved that (i) the time, (ii) the energy spectrum, (iii) the emission isotropy and (iv) the neutron yield of 10^9 during the first neutron pulse corresponded to theoretical predictions for thermonuclear neutrons. The author believes that we provided the first unambiguous experimental evidence of thermonuclear neutrons in Z-pinches after 60 years of the research. In addition to that, an ion temperature of 1.2 keV was calculated from the width of the neutron energy spectrum. These achievements were published in *Applied Physics Letters* in 2011.

[2] Most of the ions are accelerated by the beam-target direction in the downstream direction. The term "downstream" means the direction of current sheath propagation.

3.5 Article No. 6: Response to "Comment on 'Experimental evidence of thermonuclear neutrons in a modified plasma focus'"

The thermonuclear mechanism has been a source of controversy since the beginning of *Z*-pinch research. Some researchers suppose that almost all neutrons are of thermonuclear origin whereas others do not believe in the thermonuclear mechanism even during stagnation. Our letter in *Applied Physics Letters* initiated the discussion on this subject again. The comment in the *APL* can serve as an example. In our response, we tried to clarify our contribution to the confirmation of the thermonuclear mechanism in plasma foci. We showed that it was actually for the first time in the plasma focus research when the ion temperature of a thermonuclear plasma was calculated from neutron energy spectra.

3.6 Article No. 7: Search for thermonuclear neutrons in a mega-ampere plasma focus

Since all articles in *Applied Physics Letters* are limited to 3−4 pages, we decided, in order to explain our findings in more detail, to publish another full-length article in *Plasma Physics and Controlled Fusion*. There, the way how to recognize the thermonuclear mechanism from the beam target one was presented. The thermonuclear neutrons were researched not only during the first neutron pulse but also in the post-stagnation phase. At the end of the article, we made some conclusions on the thermonuclear mechanism in Z-pinches and on the prospects of various Z-pinch configurations for the fusion research. It was shown that the MagLIF concept (Slutz et al., 2010; Slutz and Vesey, 2012) is the most promising Z-pinch project with respect to the controlled thermonuclear fusion research. By writing this, however, we would not wish to forget that dense plasma foci remain very simple devices that do not require pulsed power high voltage technology and, at the same time, they are extremely efficient.

3.7 Article No. 8: Drive parameter of neutron optimized plasma foci

The efficiency of neutron production can be expressed as a number of DD fusion neutrons per joule of energy stored in capacitor banks. In plasma foci, the efficiency up to 3×10^6 DD neutrons/joule was reported (Bernard et al., 1977b). Such a high efficiency was achieved during optimization procedure. It was found that neutron optimized plasma foci with 50 J – 1 MJ stored energy work at an almost constant drive parameter $I_0/(a\sqrt{p_0})$, where I_0, a and p_0 represent the peak discharge current, the inner electrode radius, and the initial filling pressure, respectively (Lee and Serban, 1996). Several papers on the drive parameter have been published. On the one hand, it has been pointed out that the constant value of the drive parameter means almost the same values of axial and radial velocities, an ion temperature, an Alfvén velocity, and magnetic energy per unit mass. But on the other hand, the explanation why the drive parameter has almost the same value of 77 kA/cm/$\sqrt{\text{mbar}}$ has not been provided. It was the reason why the author of this thesis decided to research this phenomenon[3]. In the article published in *IEEE Transactions on Plasma Science*, the authors show that the drive parameter is closely related to the geometry of electrodes and to the properties of a current generator, namely to the rise rate of a current. Then the constancy of the drive parameter can be explained by similar current rise-rates of low voltage generators. In order to confirm our conclusion, the examples of optimized plasma foci with different drive parameters were presented.

The only presumption of our derivation was the coincidence of a current peak and the end of an axial phase. This is necessary but not sufficient condition for efficient neutron production. It is generally accepted that there are more preconditions for optimized neutron emission and that dense plasma foci operate at a certain range of the drive parameter. To find this range is the subject of future research. In standard plasma foci, all phases are interconnected and it is not easy to change independently conditions suitable for the breakdown, for the rundown, and for the pinch phase. In this respect, gas puff Z-pinches might be very useful since they possess the advantage of causing no difficulties with an insulator, namely, with its conditioning and re-strikes during the pinch phase.

[3] The interest in this subject was initiated during the discussions with Dr. Leopoldo Soto at Comisión Chilena de Energía Nuclear in Santiago de Chile.

3.8 Article No. 9: Deuterium gas puff Z-pinch at currents of 2 to 3 mega-ampere

Plasma foci demonstrated very efficient neutron production and $Y_n \propto I^4$ scaling law up to MA currents. They were able to produce 10^{11} DD neutrons in one shot at a stored energy of 100 kJ. Unfortunately, the favorable scaling law was not prolonged above 1 MA on megajoule devices at Associazione Euratom in Frascati and at the Institute of Plasma Physics and Laser Microfusion in Warsaw. The saturation of a neutron yield at the value of 10^{12} was observed and this was one of the most important arguments for shutting down the largest plasma focus facilities in the 1980s.

One possible explanation of this saturation effect is a low impedance of MJ generators (Lee and Saw, 2008). During the axial and radial phase, the impedance/inductance of a plasma focus is significantly higher than the impedance of a generator. As a result, the current at the pinch phase is reduced and plasma focus experiments cannot be carried out so easily at currents above 2 MA. In this respect, multi-megaampere *Z*-pinch experiments with deuterium gas puffs in vacuum could provide valuable information about neutron production mechanisms and scaling laws above 2 MA. In addition to that, deuterium gas puff *Z*-pinches possess higher variability than plasma foci. For instance, deuterium gas puffs enable us to study the influence of shorter current rise times, various implosion velocities, various gas density profiles, and different gases and admixtures inside inner and/or outer shells.

Therefore we decided to carry out experiments with deuterium gas puffs on the GIT-12 in Tomsk. The GIT-12 is the current generator with an intermediate inductive storage of an energy and a microsecond plasma opening switch. At a 50 kV charging voltage, the generator stored an energy of 2.6 MJ. When the plasma-opening-switch (POS) is applied, a current reaches a peak of about 2.7 MA with a 200 ns risetime (10%-90%) and a rate of up to 20 kA/ns. The generator can be used also without the POS. Then the GIT-12 allows us to study the influence of different current rise-times on neutron emission and neutron energy spectra. The great advantage of the experiment on the GIT-12 was that we could use electromagnetic valve, nozzles, preionization and also the experience which was gained during previous experiments with argon and neon gas puffs (Shishlov et al., 2002; Labetsky et al., 2008).

In 2011, we used double shell gas puffs with the outer shell diameter of 8 cm. As far as neutron TOF diagnostics is concerned, it was implemented in the radial direction. Even though there were strong gamma rays and harsh electromagnetic noise from the current generator, we succeeded in using one nTOF detector at 140 cm, i.e. very close to the source. It enabled us a very precise measurement of neutron emission time. This way, we observed the first neutron pulse during the stagnation. However, similarly to dense plasma foci, the principal neutron peak occurred 35 ns later, at the beginning of the expansion. The main neutron emission in the post-stagnation phase strongly depended on the quality of implosion. We showed that the issue of considerable importance to deuterium gas puffs, the one with serious implications, is the spread of the gas at a large diameter inside the energy concentrator. The significant spread of hydrogen is likely caused by a lower mass of hydrogen molecules and their higher thermal velocity. The spread could influence the breakdown process, the implosion velocity, the plasma diameter at the stagnation, the peak load voltage, and consequently the energy input into a plasma. We would like to focus on this phenomenon in our future experiments which will be devoted to the optimization of a deuterium gas puff at 3 MA currents. We believe that the yield could exceed 10^{12} DD neutrons/shot.

Chapter 4

DISCUSSION AND PROSPECTS

The following pages first discuss the results presented in our research articles. After that, prospects of the future Z-pinch research are proposed.

4.1 Neutron production mechanisms

The first aim of our research has been related to neutron production mechanisms. We intended to recognize processes which lead to the acceleration of deuterons. Then we tried to study the properties and efficiency of these mechanisms and the ways how to influence them.

4.1.1 Beam-target mechanism during the principal emission

Even though the neutron production in Z-pinches has been studied since the 1950s, the mechanism of deuteron acceleration has remained unresolved. On the one hand, it has been clear from the very beginning of Z-pinch fusion research that the nonlinear evolution of instabilities, the sausage instability in particular, plays an important role in the production of fast particles. But on the other hand, a large number of mutually contradictory mechanisms were suggested to explain how particles are accelerated within instabilities. Recent reviews on the generation of fast particles was given by Ryutov et al. (2000), Haines (2001, 2011) and Vikhrev and Korolev (2007). According to Haines's model, the disruptive development of necks causes a significant decrease of linear density of plasmas. A low linear density then leads to the occurrence of microturbulences (Bernard et al., 1975), high resistivity (Bernard, 1978; Decker et al., 1983), rapid dissipation of magnetic fields, and high Alfvén and ion-acoustic velocities. Consequently, a fast redistribution of current and magnetic fields together with a rapid plasma expansion result in the acceleration of ions to high velocities towards the cathode near the axis and to lower

velocities towards the anode at larger radii. This model qualitatively explains our neutron energy spectra, neutron emission anisotropy, peak neutron production after the disruption, the correlation of neutron emission with hard X-rays above 1 MeV and the conservation of total axial momentum. In contrast, the Fermi acceleration mechanism (Deutsch and Kies, 1988) and the adiabatic heating of necks (Vikhrev, 1986) produce the peak neutron emission exactly at the maximum compression of the neck and they cannot account for the occurrence of 1 MeV photons. As for the formation of a high-energy ion tail due to the onset of ion-acoustic turbulences (Ryutov et al., 2000), it cannot easily explain the observed end-on neutron emission anisotropy[1]. On the basis of our experimental data, we may conclude that the mechanism proposed by prof. Haines (2001, 2011) explains best the principal neutron emission on the MA current level.

The mechanism mentioned above is quite efficient since we found that about 15% of the plasma energy is converted into fast deuterons. Such an efficiency is comparable with light ion beam accelerators. The main difference is that deuterons in megaampere Z-pinches are magnetized and their trajectories are not linear. It enables to increase the path length of deuterons in hot plasmas and then the efficiency of fusion neutron production.

At present, our scientific group researches the way of optimizing fusion neutron yields. For this purpose, several Z-pinch configurations have been tried so far. In the most efficient configurations, that is in a deuterium gas puff and a plasma focus, we look for convenient parameters. For instance, during our recent experiment on the GIT-12 (Klir et al., 2013), we have found out that the proper mass is more important for higher neutron yields than the coincidence of the stagnation with a peak current.

4.1.2 Thermonuclear mechanism during the stagnation

The thermonuclear mechanism was discussed in articles No. 5 – 7 of this habilitation thesis. In these research articles, we presented the method of how to recognize thermonuclear neutrons. The way of increasing the thermonuclear neutron yield was also demonstrated. In this respect, the MagLIF project seems to be very promising and highly reasonable fusion concept (Slutz et al., 2010; Slutz and Vesey, 2012). In contrast, parameters of deuterium gas puff Z-pinches and dense plasma foci are still far from those required for fusion energy gain. However, in terms of the total number of neutrons, deu-

[1] It should be mentioned that the neutron emission could be strongly influenced not only by the anisotropic energy distribution function of fast deuterons but also by an inhomogeneous density of target deuterons.

terium gas puffs are efficient neutron sources. There is an open question of the neutron production mechanism and scaling laws at high currents. The neutron yield scaling with a current is presented in the next subsection.

4.2 Scaling law

4.2.1 Neutron yield scaling of the thermonuclear mechanism

The thermonuclear neutron yield is given by the equation

$$Y_{\mathrm{th}} = \frac{1}{4} n_{\mathrm{d}}^2 \langle \sigma v \rangle_T \pi R^2 l \tau \tag{4.1}$$

where n_{d} is the ion density, $\langle \sigma v \rangle$ stands for the DD fusion reaction rate, R is the plasma radius, l is the plasma length, and τ means the confinement time. Assuming a constant ion temperature, confinement time and dimensions, the fusion yield scales as

$$Y_{\mathrm{th}} \propto n_{\mathrm{d}}^2. \tag{4.2}$$

If the stagnation of dynamic Z-pinches is matched to the peak current, the density is given by (see Ryutov et al., 2000)

$$n_{\mathrm{d}} \propto \frac{I^2 t_0^2}{R_0} \tag{4.3}$$

where R_0 is the initial radius and t_0 is the rise-time of the current to its peak.

Combining two previous equations together, we obtain the neutron yield being proportional to the current to the fourth power for the same initial diameter and the same current rise time

$$Y_{\mathrm{th}} \propto n_{\mathrm{d}}^2 \propto I^4. \tag{4.4}$$

Such promising scaling is expected for >10 MA Z-pinches where the thermonuclear mechanism can be dominant[2] (Velikovich et al., 2007; Welch et al., 2010).

4.2.2 Neutron yield scaling of the beam-target mechanism

At lower currents, e.g. at 100 kA, the neutron yield is determined mainly by the beam-target mechanism and the scaling could differ from the one described above. In the beam-

[2] The main issue of high thermonuclear yields is ion collisionality of Z-pinch plasmas during nanosecond stagnation. At >5 keV temperatures and 10^{21} cm^{-3} densities, the collisionality of ions is too low.

target mechanism, the neutron yield Y_n is given by the number of accelerated deuterons N_d, their energy E_d, the target particle density n_d, and the path length l as

$$Y_n = \sigma_{fusion}(E_d) N_d n_d l. \tag{4.5}$$

It is reasonable to suppose that the deuteron energy E_d increases with the current I. Since the fusion cross-section σ_{fusion} strongly depends on the deuteron energy E_d, e.g. $\sigma_{fusion} \propto E_d^5$ at about 10 keV, the neutron yield could scale with the current to the power higher than 4. This was confirmed experimentally by McCall (1989); Serban and Lee (1998); Pouzo and Milanese (2003); Sadowski and Scholz (2012). In contrast, at even higher currents and higher deuteron energies, the increase of the fusion cross-section with deuteron energy is slower, e.g. $\sigma_{fusion} \propto E_d^{1.5}$ at about 100 keV. As a result, the scaling might not be so favourable. Assuming the 'worst' case where the number of fast deuterons N_d and their energies E_d remain constant, the neutron yield depends on the product of the target density and the path length $n_d l$. Keeping dimensions of deuterium gas puffs constant, as is the usual case, the final ion density scales with the current as $n_d \propto I^2$ and the pessimistic scaling is $Y_n \propto n_d \propto I^2$. In contrast, plasma foci of all energies have almost the same ion densities. Higher currents therefore require larger dimensions $l \propto I$ (Lee and Serban, 1996) and the yield should scale approximately as $Y_n \propto n_d l \propto l \propto I$. This dependence could be also one of the reasons why there was the saturation of DD neutron yields at $10^{11} - 10^{12}$ in megajoule plasma foci. At present, it is important to find out at which currents this saturation will be overcome by a more efficient mechanism, namely by the thermonuclear mechanism. We would like to study this region in our future experiments on the GIT-12 at the IHCE in Tomsk.

4.3 Future experiments

There are three main purposes of our future experiment. The first purpose of our experiment on the GIT-12 is to obtain knowledge about the neutron production mechanisms at about 3 MA. Next, we would like to increase the neutron yield up to 10^{12}. At these yields, it should be possible to measure secondary DT neutrons. The Y_{DT}/Y_{DD} ratio provides valuable information about parameters of fusion plasmas.

In order to reach 10^{12} neutrons, a deuterium gas puff has to be optimized. On the GIT-12, we have unique possibilities now. It is possible to try various gases, gas admixtures,

pressures, nozzles, delays, etc. Since a deuterium gas is less compressible than higher-Z elements, one of very attractive configurations is a neon–on–deuterium gas puff. According to calculations made at the Naval Research Laboratory for the Z-machine (Chong et al., 2011), the thermonuclear neutron yield with higher-Z pusher could be even higher than for pure deuterium.

Finally, the third reason we have for carrying out further research is to perform experiments which will be related more closely to magnetic flux compression and the MagLIF project.

4.4 Comparison with other high temperature plasmas

At this point, it seems useful to compare the neutron production efficiency of the most powerful Z-pinch with high energy lasers and tokamaks. The JT-60U tokamak with the total energy input of about 4 GJ and 8×10^{16} DD neutrons provides the efficiency 2×10^7 neutrons/joule (Fujita et al., 2003). Direct drive capsules at the Omega[3] laser produced much lower DD neutron yields of about 4×10^{11} at a 40 MJ stored energy and at an efficiency of 10^4 neutrons/J (Laboratory for Laser Energetics, 2011). In our experiments, the peak neutron efficiency was 6×10^5 DD neutrons per one joule of stored energy with a gas puff Z-pinch on the S-300. The neutron yield of 4×10^{13} neutrons on the 10 MJ Z-machine implies almost 4×10^6 neutrons/J. Such a value is comparable with the JT-60U and JET tokamaks (cf. Fig. 4.1). In addition to that, even higher neutron yields are expected on future higher current generators and for the MagLIF project on the refurbished Z. Of course, a lot of technological and material issues have to be solved in order to use Z-pinches in the controlled thermonuclear fusion research. Nevertheless, it is evident that Z-pinches are efficient sources of fusion neutrons that might be useful for hybrid fusion-fission concepts or for other applications.

As for other applications, smaller repetitive devices are usually more suitable. In this respect, a small dense plasma focus in the range of 100 – 1000 J reaches the efficiency of about 10^5 neutrons/J (Verma et al., 2013). It seems to be lower than 10^6 neutrons/J which is the typical value of femtosecond laser systems (Disdier et al., 1999; Lee et al., 2009). However, here 1 J represents the energy of a laser beam whereas the stored electrical

[3] The lowest estimate of the NIF is about 6×10^{16} DT neutrons. Therefore the expected DD yield of about 10^{15} at a 400 MJ stored energy gives 2.5×10^6 neutrons/J, however, the ignition has not been achieved so far.

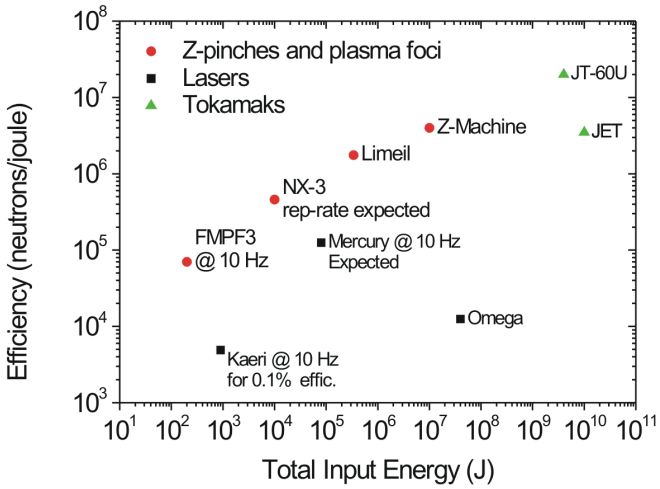

Fig. 4.1: Wall-plug efficiency of DD neutron production in various plasma-based sources: JET (Jarvis and Conroy, 2002) and JT-60U (Fujita et al., 2003) tokamaks; FMPF-3 (Verma et al., 2013), NX-3 (Verma et al., 2012) and Limeil (Bernard et al., 1977a) plasma foci; Omega (Laboratory for Laser Energetics, 2011), Kaeri (Lee et al., 2009), and Mercury (Bayramian et al., 2009) lasers; gas puff Z-pinch on *Z* (Coverdale et al., 2007).

energy is higher. As a result, on the one hand, the efficiency of a small DPF is higher than the efficiency of ultra-short laser systems. On the other hand, laser-based neutron source is more localized and the properties of neutron emission can be modified by parameters of laser beams and targets more easily.

4.5 Prospects

It has been mentioned several times in this thesis that *Z*-pinches and plasma foci are now being researched as efficient sources of X-rays and neutrons. Nevertheless, as it has been also pointed out, several technological issues need to be solved before they are put into practice more extensively. For instance, the usefulness of small plasma foci as neutron sources depends on the development of a higher repetition device with a long lifetime ($>10^7$ shots). As far as *Z*-pinches are concerned, we suppose that their future will be strongly influenced either by the success or failure of the MagLIF project. Next, we believe that the further progress of *Z*-pinches is dependent on the construction of petawatt class generators. Always, when a new machine with a higher current is constructed, the significant progress and breakthroughs might be expected. Now, the most powerful current generator provides the >50 TW peak power and the current of 25 MA. To con-

centrate a twofold current into a small volume is not as simple as to reach a twofold laser energy by increasing the number of beams. Since it is difficult to concentrate the charge into a small volume, the construction of 50 MA devices requires a new technology. Such a challenging project has been solved by Stygar et al. (2007). The construction of 50 MA device is now in the preparatory phase at TRINITY in Troitsk as well as at the Sandia National Laboratories in Albuquerque, New Mexico.

CONLUSIONS

The research of high-current discharges at the Faculty of Electrical Engineering has made a significant progress during the last 15 years. This was accompanied with the international experimental campaigns on the megajoule plasma focus and Z-pinch devices and with the significant financial support of our research by the Ministry of Education of the Czech Republic. The progress has been documented in a number of articles published in peer-reviewed journals by members of our Z-pinch group, namely by prof. RNDr. Pavel Kubeš, CSc. and Daniel Klír, Ph.D. A significant part of Daniel Klír's results forms Chapter 3 of this habilitation thesis.

Contribution of our research group

The contribution of our group to international Z-pinch and plasma focus research lies in fusion related experiments. Our group participated in almost all neutron measurements in Z-pinches during the last 5 years. Our further progress will be strongly affected by the usage of Z-pinches in fusion research, particularly by the success or failure of the MagLIF project. The contribution of our experiments can also be seen in the development of a comprehensive set of X-ray and neutron diagnostics and methods for data analysis. Since the Z-pinch community is rather small, it is important to keep in touch with main streams in plasma physics. In our case, this is enabled by means of plasma diagnostics which could be used not only in Z-pinches but also in other types of high-energy density physics experiments. For instance, our experimental group has used nanosecond XUV diagnostics in experiments with laser-produced jets at the Prague Asterix Laser System since 2007 (Nicolai et al., 2008; Tikhonchuk et al., 2008; Kasperczuk et al., 2009; Nicolai et al., 2010; Kasperczuk et al., 2011, 2012). We also performed neutron measurements on the Prague Asterix Laser System during the interaction of the laser beam with solid deuterated targets. Recently, we have been asked to help with the extreme-UV diagnostics of homogeneous plasma created for the measurement of the heavy ion stopping power at the GSI Helmholtzzentrum für Schwerionenforschung in Darmstadt. On the ba-

sis of these interdisciplinary collaborations, the author of this habilitation thesis became a member of Laser Plasma Center and Extreme Light Infrastructure (ELI).

Contribution of the author

The contemporary scientific effort is hardly conceivable without teamwork in domestic and foreign research groups. Therefore it is somewhat difficult to identify the contribution of individual researchers. However, in the following paragraph, the author tries to reflect briefly on this issue and to give account of his part in the effort.

In the last 5 years, the field of activity has been divided as follows:

Prof. RNDr. Pavel Kubeš, CSc. has continued with the organization of the research at the PF-1000 plasma focus whereas the experiments on Z-pinches have been led and experimental data have been analyzed mainly by Daniel Klír. The author of this thesis also established new contacts with the Sandia National Laboratories[4], with the Imperial College in London and with Comisión Chilena de Energía Nuclear in Santiago de Chile. The author used his contacts to negotiate the possibility of new experiments on the GIT-12 generator at IHCE in Tomsk after the S-300 had been shut down because of fire safety. Most of the financial support of our research has been arranged by prof. Pavel Kubeš. Daniel Klír has been the principal investigator of the post-doc and standard GACR projects No. 202/08/P084 and No. P205/12/0454, respectively.

Training of students

Last but not least, it should be mentioned what the prospects of Z-pinch research in the Czech Republic are. In this respect we really appreciate one particular advantage of Z-pinches which is their simple construction and low cost. This is important not only for the testing of new diagnostic methods and calibration of scientific instruments, but also for the training of students in experimental plasma physics and controlled thermonuclear fusion. In our laboratory at the Department of Physics, students have the opportunity to diagnose fusion plasmas, to detect fusion neutrons every working day. They can take the advantage of a smallscale experiment which could be easily modified and, in some cases, better diagnosed, while it remains interesting from the physical point of view. Furthermore, at megajoule devices, they obtain experience with harsch electromagnetic environment, with strong hard X-rays and gammas as well as with the teamwork and

[4] The agreement with the Czech Technical University has not been signed from nuclear security reasons.

multi-national partnership. Young scientists with such experience may usefully participate in the ELI beamlines project which is expected to be accomplished at the end of 2015.

The author of this thesis supervised/supervises 4 students, namely Karel Řezáč (Ph.D. degree), Ondřej Šíla (Ph.D., M.Sc., B.Sc. degree), Jakub Cikhardt (Ph.D. degree) and Vojtěch Munzar (B.Sc. degree). These students are expected to influence strongly the future of Z-pinch research in the Czech Republic.

Some portion of knowledge and experience from the scientific research could obviously be transferred to teaching. The author gives several lectures within the undergraduate courses at the Faculty of Nuclear Sciences and Engineering, namely Data analysis and signal processing (12ZSD), Plasma diagnostics (02DPLA), Pinches (02PINC), and Selected topics in inertial confinement fusion (02PICF). At the Faculty of Electrical Engineering, he teaches seminars and supervises laboratory exercises in basic courses of physics.

BIBLIOGRAPHY

Anan'ev, S. S., Bakshaev, Y. L., Blinov, P. I., Bryzgunov, V. A., Vikhrev, V. V., Dan'ko, S. A., Zelenin, A. A., Kazakov, E. D., Kalinin, Y. G., Kingsep, A. S., Korolev, V. D., Smirnova, E. A., Ustroev, G. I., Chernenko, A. S., and Shchagin, V. A. (2010). X-Pinch-Based Neutron Source. *Plasma Physics Reports*, 36(7):601–608.

Anderson, O., Baker, W., Stirling, A., Ise, J., and Pyle, R. (1958). Neutron production in linear deuterium pinches. *Physical Review*, 110(6):1375–1383.

Andrianov, A., Bazilevskaia, O., Braginskii, S., Brezhnev, B., Khvaschevski, S., Khrabrov, V., Kovalski, N., Filippov, N., Filippova, T., Palchikov, V., Podgorny, I., Prokhorov, Y., and Sulkovskaya, M. (1958). High-current pulse discharges. In J. H. M. t., editor, *Proc. 2nd United Nations International Conference on Peaceful Uses of Atomic Energy, Vol. 31*, pages 348–364, Geneva, Switzerland. United Nations.

Appelbe, B. and Chittenden, J. (2011). The production spectrum in fusion plasmas. *Plasma Physics and Controlled Fusion*, 53(4):045002.

Bailey, J., Ettinger, Y., Fisher, A., and Feder, R. (1982). Evaluation of the gas puff *Z*–pinch as an X–ray lithography and microscopy source. *Applied Physics Letters*, 40:33–35.

Bakshaev, Y. L., Blinov, P. I., Vikhrev, V. V., Dan'ko, S. A., Korolev, V. D., Meshcherov, B. R., Nedoseev, S. L., Smirnova, E. A., Ustroev, G. I., Chernenko, A. S., and Shashkov, A. Y. (2006). Measurements of neutron emission from a Z-pinch constriction. *Plasma Physics Reports*, 32(7):531–538.

Batyunin, A., Bulatov, A., and Vikharev, V. (1990). *Soviet Journal of Plasma Physics*, 16:597.

Bayramian, A. J., Armstrong, J. P., Beer, G., Campbell, R., Cross, R., Erlandson, A., Freitas, B., Menapace, J., Molander, W., Perkins, L. J., Schaffers, K., Siders, C., Sutton,

S., Tassano, J., Telford, S., Ebbers, C. A., Caird, J., and Barty, C. P. J. (2009). High Average Power Petawatt Laser Pumped by the Mercury Laser for Fusion Materias Engineering. *Fusion Science And Technology*, 56(1):295–300.

Bernard, A. (1978). Recent developements in plasma focus research. *Atomkernenergie*, 32(1):73–75.

Bernard, A., Cloth, P., Conrads, H., Coudeville, A., Gourlan, G., Jolas, A., Maisonnier, C., and Rager, J. (1977a). Dense-Plasma Focus - High-Intensity Neutron Source. *Nuclear Instruments & Methods*, 145(1):191–218.

Bernard, A., Coudeville, A., Garconnet, J., and A. Jolas, J. de Mascureau, C. N. (1977b). Structure of current sheath and fast-particle beams in the focus experiment. In *Plasma Physics and Controlled Nuclear Fusion Research 1976 (IAEA-CN-35), 6th IAEA Conference on Plasma Physics and Controlled Nuclear Fusion Vol. III*, pages 471–482, Vienna, Austria. IAEA.

Bernard, A., Coudeville, A., Jolas, A., Launspach, J., and Mascureau, J. (1975). Experimental studies of plasma focus and evidence for nonthermal processes. *Physics of Fluids*, 18(2):180–194.

Bienkowska, B., Karpinski, L., Paduch, M., Scholz, M., Pytel, K., Prokopowicz, R., and Szydlowski, A. (2006). Measurements of neutron yield from PF-1000 device by activation method. *Czechoslovak Journal of Physics*, 56(Part 2):B377–B382.

Bogolubov, Y. P., Koltunov, M. V., Lemeshko, B. D., Mikerov, V. I., Samosyuk, V. N., Sidorov, P. P., and Yurkov, D. I. (2009). Application of a plasma focus-based source for fast neutron and X-ray radiography. *Nuclear Instruments & Methods in Physics Research Section A-Accelerators Sprectrometers Detectors and Associated Equipment*, 605(1-2):62–64.

Briesmeister, J. F. (2000). MCNP - A General Monte Carlo N-Particle Transport Code - Version 4C. Los Alamos National Laboratory report LA-13709-M.

Brzosko, J., Robouch, B., and Klobukowska, J. (1987). A macroscopic study of neutron, gamma and X-ray emissivity in the Frascati plasma focus. *Fusion Technology*, 12(1):71–91.

Bures, B. L., Krishnan, M., Madden, R. E., and Blobner, F. (2010). Enhancing Neutron Emission From a 500-J Plasma Focus by Altering the Anode Geometry and Gas Composition. *IEEE Transactions on Plasma Science*, 38(4):667–671.

Carruthers, R. and Davenport, P. (1957). Observation of the instability of constricted gaseous discharge. *Proc. Phys. Soc. B*, 70:49–50.

Chernenko, A., Kalinin, Y., and Kingsep, A. (1996). S-300, New pulsed power installation in Kurchatov Institute, Investigation of stable liner implosion. In Jungwirth, K. and Ullschmied, J., editors, *BEAMS 1996*, pages 154–157, Prague, Czech Republic.

Chong, Y., Velikovich, A., Thornhill, J., Giuliani, J., Coverdale, C., Flicker, D., and Clark, R. (2011). Multidimensional radiation MHD modeling of argon on deuterium gas puff z-pinch loads as a neutron source. In *IEEE International Conference on Plasma Science - ICOPS*, page DOI: 10.1109/PLASMA.2011.5993198, Chicago, IL. IEEE.

Coverdale, C. A., Deeney, C., Velikovich, A. L., Clark, R. W., Chong, Y. K., Davis, J., Chittenden, J., Ruiz, C. L., Cooper, G. W., Nelson, A. J., Franklin, J., LePell, P. D., Apruzese, J. P., Levine, J., Banister, J., and Qi, N. (2007). Neutron production and implosion characteristics of a deuterium gas-puff Z pinch. *Physics of Plasmas*, 14(2):022706.

Decker, G., Kies, W., and Pross, G. (1983). The 1st and the final 50 nanoseconds of a fast focus discharge. *Physics of Fluids*, 26(2):571–578.

Deeney, C., Nash, T., Spielman, R., Seaman, J., Chandler, G., Struve, K., Porter, J., Stygar, W., McGurn, J., Jobe, D., Gilliland, T., Torres, J., Vargas, M., Ruggles, L., Breeze, S., Mock, R., Douglas, M., Fehl, D., McDaniel, D., Matzen, M., Peterson, D., Matuska, W., Roderick, N., and MacFarlane, J. (1997). Power enhancement by increasing the initial array radius and wire number of tungsten Z pinches. *Physical Review E*, 56(5):5945–5958.

Deutsch, R. and Kies, W. (1988). Manifestation of an ion acceleration mechanism in computer simulations and plasma focus experiments. *Plasma Physics and Controlled Fusion*, 30:921.

Disdier, L., Garconnet, J., Malka, G., and Miquel, J. (1999). Fast neutron emission from a high-energy ion beam produced by a high-intensity subpicosecond laser pulse. *Physical Review Letters*, 82(7):1454–1457.

Drosg, M. (1987). Handbook on Nuclear Activation Data. Technical reports series no. 273, International Atomic Energy Agency, Vienna.

Felber, F., Liberman, M., and Velikovich, A. (1985). Methods for producing ultrahigh magnetic fields. *Applied Physics Letters*, 46:1042–1044.

Filippov, N., Filippova, T., and Vinogradov, V. (1962). Dense, high-temperature plasma in a noncylindrical *Z*-pinch compression. *Nuclear Fusion*, (2):577–587.

Fujita, T., Akasaka, H., Akino, N., Anno, K., Arai, M., Arai, T., and JT-60 Team (2003). Overview of JT-60U results leading to high integrated performance in reactor-relevant regimes. *Nuclear Fusion*, 43(12):1527–1539.

Gerstner, E. (2009). The hybrid returns. *Nature*, 460(7251):25–28.

Gribkov, V. A., Latyshev, S. V., Miklaszewski, R. A., Chernyshova, M., Drozdowicz, K., Wiacek, U., Tomaszewski, K., and Lemeshko, B. D. (2010). A dense plasma focus-based neutron source for a single-shot detection of illicit materials and explosives by a nanosecond neutron pulse. *Physica Scripta*, 81(3):035502.

Haines, M. (2001). Kinetic effects in *Z*–pinches. *Laser and Particle Beams*, 19:345–353.

Haines, M., LePell, P., Coverdale, C., Jones, B., Deeney, C., and Apruzese, J. (2006). Ion Viscous Heating in a Magnetohydrodynamically Unstable Z Pinch at Over 2×10^9 Kelvin. *Physical Review Letters*, 96:075003.

Haines, M. G. (2011). A review of the dense Z-pinch. *Plasma Physics and Controlled Fusion*, 53(9):093001.

Hosokai, T., Kando, M., Dewa, H., Kotaki, H., Kondo, S., Hasegawa, N., Nakajima, K., and Horioka, K. (2000). Optical guidance of terrawatt laser pulses by the implosion phase of a fast *Z*–pinch discharge in a gas–filled capillary. *Optics Letters*, 25:10–12.

Ing, H., Noulty, R., and McLean, T. (1997). Bubble detectors - A maturing technology. *Radiation Measurements*, 27(1):1–11.

Jarvis, O. and Conroy, S. (2002). Prediction/modelling of the neutron emission from JET discharges. *Plasma Physics and Controlled Fusion*, 44(8):1651–1687.

Kasperczuk, A., Pisarczyk, T., Badziak, J., Borodziuk, S., Chodukowski, T., Gus'kov, S. Y., Demchenko, N. N., Klir, D., Kravarik, J., Kubes, P., Rezac, K., Ullschmied, J., Krousky, E., Masek, K., Pfeifer, M., Rohlena, K., Skala, J., and Pisarczyk, P. (2011). Interaction of a laser-produced copper plasma jet with ambient plastic plasma. *Plasma Physics and Controlled Fusion*, 53(9):095003.

Kasperczuk, A., Pisarczyk, T., Chodukowski, T., Kalinowska, Z., Gus'kov, S. Y., Demchenko, N. N., Klir, D., Kravarik, J., Kubes, P., Rezac, K., Ullschmied, J., Krousky, E., Pfeifer, M., Rohlena, K., Skala, J., and Pisarczyk, P. (2012). Plastic plasma as a compressor of aluminum plasma at the PALS experiment. *Laser and Particle Beams*, 30(1):1–7.

Kasperczuk, A., Pisarczyk, T., Nicolai, P. H., Stenz, C. H., Tikhonchuk, V., Kalal, M., Ullschmied, J., Krousky, E., Masek, K., Pfeifer, M., Rohlena, K., Skala, J., Klir, D., Kravarik, J., Kubes, P., and Pisarczyk, P. (2009). Investigations of plasma jet interaction with ambient gases by multi-frame interferometric and X-ray pinhole camera systems. *Laser and Particle Beams*, 27(1):115–122.

Kim, A. A., Mazarakis, M. G., Sinebryukhov, V. A., Kovalchuk, B. M., Visir, V. A., Volkov, S. N., Bayol, F., Bastrikov, A. N., Durakov, V. G., Frolov, S. V., Alexeenko, V. M., McDaniel, D. H., Fowler, W. E., LeChien, K., Olson, C., Stygar, W. A., Struve, K. W., Porter, J., and Gilgenbach, R. M. (2009). Development and tests of fast 1-MA linear transformer driver stages. *Physical Review Special Topics-Accelerators and Beams*, 12(5):050402.

Klir, D., Kravarik, J., Kubes, P., Bakshaev, Y. L., Blinov, P. I., Chernenko, A. S., Danko, S. A., Korolev, V. D., Ustroev, G. I., Ivanov, M. I., and Cai, H. (2006). Deuterated fibre Z-pinch on the S-300 generator. *Physica Scripta*, T123:116–119.

Klir, D., Kravarik, J., Kubes, P., Rezac, K., Anan'ev, S. S., Bakshaev, Y. L., Blinov, P. I., Chernenko, A. S., Kazakov, E. D., Korolev, V. D., Meshcherov, B. R., Ustroev, G. I., Juha, L., Krasa, J., and Velyhan, A. (2008). Neutron emission generated during wire array Z-pinch implosion onto deuterated fiber. *Physics of Plasmas*, 15(3):032701.

Klir, D., Kravarik, J., Kubes, P., Rezac, K., Cikhardt, J., Litseva, E., Hyhlik, T., Ananev, S. S., Bakshaev, Y. L., Bryzgunov, V. A., Chernenko, A. S., Kalinin, Y. G., Kazakov, E. D., Korolev, V. D., Ustroev, G. I., Zelenin, A. A., Juha, L., Krasa, J., Velyhan, A., Vysin, L., Sonsky, J., and Volobuev, I. V. (2010). Efficient production of 100 keV deuterons in deuterium gas puff Z-pinches at 2 MA current. *Plasma Physics and Controlled Fusion*, 52(6):065013.

Klir, D., Kravarik, J., Kubes, P., Rezac, K., Litseva, E., Tomaszewski, K., Karpinski, L., Paduch, M., and Scholz, M. (2011). Fusion neutron detector for time-of-flight measurements in z-pinch and plasma focus experiments. *Review of Scientific Instruments*, 82(3):033505.

Klir, D., Shishlov, A. V., Kokshenev, V. A., Kubes, P., Labetsky, A. Y., Rezac, K., Cikhardt, J., Fursov, F. I., Kovalchuk, B. M., Kravarik, J., Kurmaev, N. E., Ratakhin, N. A., Sila, O., and Stodulka, O. (2013). Characterization of neutron emission from megaampere deuterium gas puff *Z*-pinch at microsecond implosion times. *Plasma Physics and Controlled Fusion*, 55:submitted on 27th February 2013.

Kralik, M., Krasa, J., Velyhan, A., Scholz, M., Ivanova-Stanik, I. M., Bienkowska, B., Miklaszewski, R., Schmidt, H., Rezac, K., Klir, D., Kravarik, J., and Kubes, P. (2010). Application of a Bonner sphere spectrometer for determination of the energy spectra of neutrons generated by approximate to 1 MJ plasma focus. *Review of Scientific Instruments*, 81(11):113503.

Krasa, J., Kralik, M., Velyhan, A., Solc, J., Juha, L., Scholz, M., Bienkowska, B., Ivanova-Stanik, I. M., Karpinski, L., Miklaszewski, R., Paduch, M., Schmidt, H., Tomaszewski, K., Klir, D., Kravarik, J., Kubes, P., and Rezac, K. (2008). Anisotropy of the emission of DD-fusion neutrons caused by the plasma-focus vessel. *Plasma Physics and Controlled Fusion*, 50(12):125006.

Kruskal, M. and Schwarzchild, M. (1954). Some instabilities of a completely ionized gas. *Proc. Royal Soc. London A*, 223:348.

Kubes, P., Klir, D., Kravarik, J., and Rezac, K. (2009). Neutron Production at the Small Plasma-Focus Device With Antianode. *IEEE Transactions on Plasma Science*, 37(9):1786–1791.

Kubes, P., Kravarik, J., Bakshaev, Y., Blinov, P., Gordeev, E., Dan'ko, S., Klir, D., Korel'skii, A., Korolev, V., Kravehenko, E., Krasa, J., Krousky, E., Renner, O., Ustroev, G., Chernenko, A., Juha, L., and Shashkov, A. (2003). The dynamics of and radiation from a copper-wire corona in a megaampere Z-pinch. *Plasma Physics Reports*, 29(11):971–977.

Kubes, P., Kravarik, J., Renner, O., Krousky, E., Bakshaev, Y., Blinov, P., Chernenko, A., Gordeev, E., Dan'ko, S., Korolev, V., and Shashkov, A. (2002). Dynamics of an Al wire corona of a megaampere Z-pinch. *Plasma Physics Reports*, 28(4):296–302.

Kurchatov, I. (1957). On the possibility of producing thermonuclear reactions in a gas discharge. *Journal of Nuclear Energy*, 4:193.

Labetsky, A. Y., Kokshenev, V. A., Kurmaev, N. E., Oreshkin, V. A., Rousskikh, A. G., Fedyunin, A. V., Fursov, F. I., Chaikovsky, S. A., Shishlov, A. V., and Zhidkova, N. A. (2008). Study of the current-sheath formation during the implosion of multishell gas puffs. *Plasma Physics Reports*, 34(3):228–238.

Laboratory for Laser Energetics (2000-2011). LLE Review Quarterly Report. Technical report, University of Rochester.

Lee, S., Park, S., Yea, K.-H., Kwon, D.-H., Park, S.-K., Jeong, Y. U., and Cha, H. (2009). Efficient Fast Neutron Generation in a Femtosecond, Deuterated, Polystyrene Plasma. *Journal of the Korean Physical Society*, 55(2):543–548.

Lee, S. and Saw, S. H. (2008). Pinch current limitation effect in plasma focus. *Applied Physics Letters*, 92(2):021503.

Lee, S. and Serban, A. (1996). Dimensions and lifetime of the plasma focus pinch. *IEEE Transactions on Plasma Science*, 24(3):1101–1105.

Leonard, B. (1973). Review of Fusion-Fission (Hybrid) Concepts. *Nuclear Technology*, 20(3):161–178.

Linhart, J. (1961). Dynamic stability of a conducting cylindrical shell in a magnetic field. *Journal of Applied Physics*, 32:500.

Lorenz, A., Beg, F., Ruiz-Camacho, J., Worley, J., and Dangor, A. (1998). Influence of a prepulse current on a fiber *Z*–pinch. *Physical Review Letters*, 81:361–364.

Lorenz, A., Peacock, N., O'Mullane, M., and Neely, D. (1999). Diagnostic characterization of a prepulsed carbon fiber *Z*–pinch using spectral line intensity analyses. *Review of Scientific Instruments*, 70:1425–1429.

Marshall, J. (1958). Acceleration of plasma into vacuum. In J. H. M. t., editor, *Proc. 2nd United Nations International Conference on Peaceful Uses of Atomic Energy, Vol. 31*, page 341, Geneva, Switzerland. United Nations.

Mather, J. (1965). Formation of a high-density deuterium plasma focus. *Physics of Fluids*, 8:366.

Mather, J. and Williams, A. (1958). Neutron production in Columbus II. In J. H. M. t., editor, *Proc. 2nd United Nations International Conference on Peaceful Uses of Atomic Energy, Vol. 32*, page 26, Geneva, Switzerland. United Nations.

Matzen, M., Sweeney, M., Adams, R., Asay, J., Bailey, J., Bennett, G., et al. (2005). Pulsed-power-driven high energy density physics and inertial confinement fusion research. *Physics of Plasmas*, 12(5):055503.

Mazarakis, M. G., Fowler, W. E., Kim, A. A., Sinebryukhov, V. A., Rogowski, S. T., Sharpe, R. A., McDaniel, D. H., Olson, C. L., Porter, J. L., Struve, K. W., Stygar, W. A., and Woodworth, J. R. (2009). High current, 0.5-MA, fast, 100-ns, linear transformer driver experiments. *Physical Review Special Topics-Accelerators and Beams*, 12(5):050401.

McCall, G. (1989). Calculation of neutron yield from a dense *Z*-pinch. *Physical Review Letters*, 62(17):1986–1988.

McGeoch, M. (1998). Radio–frequency preionized xenon *Z*–pinch source for extreme ultraviolet lithography. *Applied Optics*, 37:1651.

Nicolai, P., Stenz, C., Kasperczuk, A., Pisarczyk, T., Klir, D., Juha, L., Krousky, E., Masek, K., Pfeifer, M., Rohlena, K., Skala, J., Tikhonchuk, V., Ribeyre, X., Galera, S., Schurtz, G., Ullschmied, J., Kalal, M., Kravarik, J., Kubes, P., Pisarczyk, P., and Schlegel, T. (2008). Studies of supersonic, radiative plasma jet interaction with gases at the Prague Asterix Laser System facility. *Physics of Plasmas*, 15(8):082701.

Nicolai, P., Stenz, C., Tikhonchuk, V., Kasperczuk, A., Pisarczyk, T., Juha, L., Krousky, E., Masek, K., Pfeifer, M., Rohlena, K., Skala, J., Kmetik, V., Ullschmied, J., Kalal, M., Klir, D., Kravarik, J., Kubes, P., Rezac, K., Pisarczyk, P., and Tabakhoff, E. (2010). Experimental evidence of multimaterial jet formation with lasers. *Physics of Plasmas*, 17(11):112903.

Pereira, N. and Davis, J. (1988). X–rays from *Z*–pinches on relativistic electron–beam generator. *Journal of Applied Physics*, 64:R1–R27.

Post, R. (1956). Controlled fusion research – an application of physics of high temperature plasmas. *Reviews of Modern Physics*, 28(3):338–362.

Pouzo, J. and Milanese, M. (2003). Applications of the dense plasma focus to nuclear fusion and plasma astrophysics. *IEEE Transactions on Plasma Science*, 31(6):1237–1242.

Rawat, R. S. (2012). High Energy Density Pulsed Plasmas in Plasma Focus: Novel Plasma Processing Tool for Nanophase Hard Magnetic Material Synthesis. *Nanoscience and Nanotechnology Letters*, 4(3, SI):251–274.

Remington, B., Drake, R., and Ryutov, D. (2006). Experimental astrophysics with high power lasers and *Z*-pinches. *Reviews of Modern Physics*, 78:755.

Rezac, K., Klir, D., Kubes, P., Kravarik, J., and Stransky, M. (2006). Monte Carlo simulations for reconstruction of neutron time-resolving energy distribution in D-D fusion reactions. *Czechoslovak Journal of Physics*, 56(Part 2):B357–B363.

Rezac, K., Klir, D., P., K., and J., K. (2012). Improvement of Time-of-flight Methods for Reconstruction of Neutron Energy Spectra from D(d,n)3He Fusion Reactions. *Plasma Physics and Controlled Fusion*, 54(9).

Riordan, J., Pearlman, J., Gersten, M., and Rauch, J. (1981). Sub-kilovolt X–ray emission from imploding wire plasmas. In Attwood, D. and Henke, B., editors, *Proceedings of the Topical Conference on Low Energy X–Ray Diagnostics, AIP conference proceedings, vol. 75*, pages 35–43, APS, New York. American Institute of Physics.

Rocca, J., Shlyaptsev, V., Tomasel, F., Cortazar, O., Hartshorn, D., and Chilla, J. (1994). Demonstration of a discharge pumped table–top soft X–ray laser. *Physical Review Letters*, 73:2192–2195.

Roshan, M. V., Springham, S. V., Rawat, R. S., and Lee, P. (2010). Short-Lived PET Radioisotope Production in a Small Plasma Focus Device. *IEEE Transactions on Plasma Science*, 38(12):3393–3397.

Ruiz, C., Cooper, G., Slutz, S., Bailey, J., Chandler, G., Nash, T., Mehlhorn, T., Leeper, R., Fehl, D., Nelson, A., Franklin, J., and Ziegler, L. (2004). Production of thermonuclear neutrons from deuterium-filled capsule implosions driven by Z-pinch dynamic hohlraums. *Physical Review Letters*, 93(1):015001.

Ryutov, D., Derzon, M., and Matzen, M. (2000). The physics of fast Z–pinches. *Reviews of Modern Physics*, 72(1):167–223.

Sadowski, M. J. and Scholz, M. (2012). Important issues in high-current plasma experiments of the Z-pinch type. *Nukleonika*, 57(1):11–24.

Sanford, T., Allshouse, G., Marder, B., Nash, T., Mock, R., Spielman, R., Seamen, J., McGurn, J., Jobe, D., Gilliland, T., Vargas, M., Struve, K., Stygar, W., Douglas, M., Matzen, M., Hammer, J., DeGroot, J., Eddleman, J., Peterson, D., Mosher, D., Whitney, K., Thornhill, J., Pulsifer, P., Apruzese, J., and Maron, Y. (1996). Improved symmetry greatly increases X-ray power from wire-array Z-pinches. *Physical Review Letters*, 77(25):5063–5066.

Scholz, M., Karpinski, L., Paduch, M., Tomaszewski, K., Miklaszewski, R., and Szydlowski, A. (2001). Recent progress in 1 MJ Plasma-Focus research. *Nukleonika*, 46(1):35–39.

Serban, A. and Lee, S. (1998). Experiments on speed-enhanced neutron yield from a small plasma focus. *Journal of Plasma Physics*, 60(Part 1):3–15.

Shishlov, A., Baksht, R., Labetsky, A., Oreshkin, V., Rousskikh, A., Fedunin, A., Chaikovsky, S., Kokshenev, V., Kurmaev, N., and Fursov, F. (2002). Experimental study of an argon-hydrogen Z pinch plasma radiation source. *IEEE Transactions on Plasma Science*, 30(2):498–511.

Siemon, R., Lindemuth, I., and Schoenberg, K. F. (1999). Why magnetized target fusion offers a low-cost development path for fusion energy. *Comments Plasma Physics and Controlled Fusion*, 18:363.

Slutz, S. A., Herrmann, M. C., Vesey, R. A., Sefkow, A. B., Sinars, D. B., Rovang, D. C., Peterson, K. J., and Cuneo, M. E. (2010). Pulsed-power-driven cylindrical liner implosions of laser preheated fuel magnetized with an axial field. *Physics of Plasmas*, 17(5):056303.

Slutz, S. A. and Vesey, R. A. (2012). High-Gain Magnetized Inertial Fusion. *Physical Review Letters*, 108(2):025003.

Spielman, R., Deeney, C., Chandler, G., Douglas, M., Fehl, D., Matzen, M., McDaniel, D., Nash, T., Porter, J., Sanford, T., Seamen, J., Stygar, W., Struve, K., Breeze, S., McGurn, J., Torres, J., Zagar, D., Gilliland, T., Jobe, D., McKenney, J., Mock, R., Vargas, M., Wagoner, T., and Peterson, D. (1998). Tungsten wire-array Z-pinch experiments at 200 TW and 2 MJ. *Physics of Plasmas*, 5(5):2105–2111.

Stodůlka, J. (2010). Numerické rešení proudění deuteria v katodě pulzního generátoru proudu. Bachelor thesis. Czech Technical University, Prague.

Stygar, W. A., Cuneo, M. E., Headley, D. I., Ives, H. C., Leeper, R. J., Mazarakis, M. G., Olson, C. L., Porter, J. L., Wagoner, T. C., and Woodworth, J. R. (2007). Architecture of petawatt-class z-pinch accelerators. *Physical Review Special Topics-Accelerators and Beams*, 10(3):030401.

Tikhonchuk, V. T., Nicolai, P., Ribeyre, X., Stenz, C., Schurtz, G., Kasperczuk, A., Pisarczyk, T., Juha, L., Krousky, E., Masek, K., Pfeifer, M., Rohlena, K., Skala, J., Ullschmied, J., Kalal, M., Klir, D., Kravarik, J., Kubes, P., and Pisarczyk, P. (2008). Laboratory modeling of supersonic radiative jets propagation in plasmas and their scaling to astrophysical conditions. *Plasma Physics and Controlled Fusion*, 50(12):124056.

Tiseanu, I., Decker, G., and Kies, W. (1996). A Monte-Carlo technique for the reconstruction of time dependent spectra of short-pulse neutron sources. *Nuclear Instruments & Methods in Physics Research Section A-Accelerators Sprectrometers Detectors and Associated Equipment*, 373(1):73–80.

Velikovich, A. L., Clark, R. W., Davis, J., Chong, Y. K., Deeney, C., Coverdale, C. A., Ruiz, C. L., Cooper, G. W., Nelson, A. J., Franklin, J., and Rudakov, L. I. (2007). Z-pinch plasma neutron sources. *Physics of Plasmas*, 14(2):022701.

Velyhan, A., Krasa, J., Bienkowska, B., Ivanova-Stanik, I. M., Juha, L., Karpinski, L., Klir, D., Kralik, M., Kravarik, J., Kubes, P., Paduch, M., Scholz, M., and Tomaszewski, K. (2006). Use of thermoluminescent dosimeters for measurement of fast-neutron spatial-distribution at the plasma focus device PF-1000. *Physica Scripta*, T123:112–115.

Verma, R., Rawat, R. S., Lee, P., Springham, S. V., and Tan, T. L. (2013). High Performance High Repetition Rate Miniature Plasma Focus Device: Record Time Averaged Neutron Yield at 200 J with Enhanced Reproducibility. *Journal of Fusion Energy*, 32(1):2–10.

Verma, R., Rawat, R. S., Lee, P., Tan, A. T. L., Shariff, H., Ying, G. J., Springham, S. V., Talebitaher, A., Ilyas, U., and Shyam, A. (2012). Neutron Emission Characteristics of NX-3 Plasma Focus Device: Speed Factor as the Guiding Rule for Yield Optimization. *IEEE Transactions on Plasma Science*, 40(12):3280–3289.

Vikhrev, V. (1986). Mechanism for neutron production in *Z*–pinches. *Soviet Journal of Plasma Physics*, 12:262–270.

Vikhrev, V. V. and Korolev, V. D. (2007). Neutron generation from Z-pinches. *Plasma Physics Reports*, 33(5):356–380.

Welch, D. R., Rose, D. V., Clark, R. E., Mostrom, C. B., Stygar, W. A., and Leeper, R. J. (2009). Fully Kinetic Particle-in-Cell Simulations of a Deuterium Gas Puff Z-Pinch. *Physical Review Letters*, 103(25):255002.

Welch, D. R., Rose, D. V., Thoma, C., Clark, R. E., Mostrom, C. B., Stygar, W. A., and Leeper, R. J. (2010). Kinetic simulation of thermonuclear-neutron production by a 10(7)-A deuterium Z pinch. *Physics of Plasmas*, 17(7):072702.

Zielinska, E., Paduch, M., and Scholz, M. (2011). Sixteen-Frame Interferometer for a Study of a Pinch Dynamics in PF-1000 Device. *Contributions to Plasma Physics*, 51(2-3, SI):279–283.

ARTICLE NO. 1

Fusion neutron detector for time-of-flight measurements in *z*-pinch and plasma focus experiments

D. Klir,[1,a)] J. Kravarik,[1] P. Kubes,[1] K. Rezac,[1] E. Litseva,[1] K. Tomaszewski,[2] L. Karpinski,[3] M. Paduch,[3] and M. Scholz[3]
[1]*Faculty of Electrical Engineering, Czech Technical University in Prague, Technicka 2, 16627 Prague 6, Czech Republic*
[2]*ACS Ltd., Advanced Diagnostics Laboratory, Warsaw, Poland*
[3]*Institute of Plasma Physics and Laser Microfusion, Warsaw, Poland*

(Received 8 October 2010; accepted 2 February 2011; published online 11 March 2011)

We have developed and tested sensitive neutron detectors for neutron time-of-flight measurements in *z*-pinch and plasma focus experiments with neutron emission times in tens of nanoseconds and with neutron yields between 10^6 and 10^{12} per one shot. The neutron detectors are composed of a BC-408 fast plastic scintillator and Hamamatsu H1949-51 photomultiplier tube (PMT). During the calibration procedure, a PMT delay was determined for various operating voltages. The temporal resolution of the neutron detector was measured for the most commonly used PMT voltage of 1.4 kV. At the PF-1000 plasma focus, a novel method of the acquisition of a pulse height distribution has been used. This pulse height analysis enabled to determine the single neutron sensitivity for various neutron energies and to calibrate the neutron detector for absolute neutron yields at about 2.45 MeV. [doi:10.1063/1.3559548]

I. INTRODUCTION

Time-of-flight (ToF) diagnostics is one of the most accurate methods of measuring energy spectra of fast neutrons which are produced by D(d, n)^{3}He fusion reactions. That is why the ToF analysis has been applied to diagnose fusion processes in controlled thermonuclear fusion research.[1–4] This method is also commonly used for diagnostics of *z*-pinches and plasma foci with neutron yields between 10^6 and 10^{13} (see Refs. 5–12). Such neutron yields enable to acquire ToF signals within a single shot. The duration of neutron ToF signals in *z*-pinches is typically tens of nanoseconds; therefore, it is necessary to use neutron detectors with a fast time response. Nanosecond temporal resolutions can be easily achieved with plastic scintillators which are relatively inexpensive and easy to handle. These properties are important when a large number of ToF detectors are used, such as at the PF-1000 facility.[8] In this paper, we describe the design, the calibration, and the initial test of a neutron detector which is composed of the BC-408 fast plastic scintillator and the Hamamatsu H1949-51 PMT assembly. The description of the neutron detector is provided in Sec. II. Section III deals with the issues of temporal resolution and timing of the detector. Section IV presents a novel method of the measurement of single neutron sensitivity in the energy range between 1.8 and 3.0 MeV. Section V brings forward the calibration of the neutron detector for absolute neutron yields at 2.45 MeV. Finally, Sec. VI describes the initial test of the neutron ToF detector during the measurement of a neutron production time.

II. DESCRIPTION OF NEUTRON TIME-OF-FLIGHT DETECTOR

One of the most common ways of detecting fusion neutrons is to produce a recoil proton through elastic scattering in a hydrogen-containing scintillator.[13] Because the free path length of recoil protons is usually negligible in comparison with scintillator dimensions, the recoil proton energy is fully deposited into a scintillator. The fluorescence of excited atoms in a scintillator can be converted into an electrical pulse by a PMT combined with a high-bandwidth transient digitizer. For purposes of ToF analysis with the temporal resolution on the order of several nanoseconds, fast plastic scintillators based on a polyvinyltoluene matrice are used since they can be easily fabricated and handled. In our plasma focus and *z*-pinch experiments,[8,10,12,14] we mostly used Saint Gobain BC-408 plastic scintillators with a 0.9 ns rise time, a 2.5 ns FWHM, a 2.1 ns decay time, and a 425 nm peak emission wavelength.[15] The general characteristics of the BC-408 scintillator are the density of 1.032 g/cc and the atomic ratio between hydrogen and carbon of 1.104. The front surface of our cylindrical scintillator is 45 mm in diameter. The 50 mm thickness of the scintillator is approximately equal to the mean free path of 2.45 MeV neutron in the polyvinyltoluene matrice. The fast plastic scintillator is coupled to the Hamamatsu H1949-51 PMT assembly which is composed of a high voltage divider and the R1828-01 photomultiplier tube.[16] This type of the PMT with a 1.3 ns rise time (at a 2.5 kV voltage), the peak cathode sensitivity at 420 nm and the photocathode of a 46 mm effective diameter is well matched to the parameters of the scintillator. A large dynamic range of the PMT ($>10^6$, see Ref. 17) enables us to use a neutron detector for a broad range of neutron yields. The neutron detector described in this paper was used at small plasma foci with 10^6 neutrons/shot,[10,11] at the mega-ampere PF-1000 plasma focus[8,36] and the S-300

a)Electronic mail: daniel.klir@fel.cvut.cz.

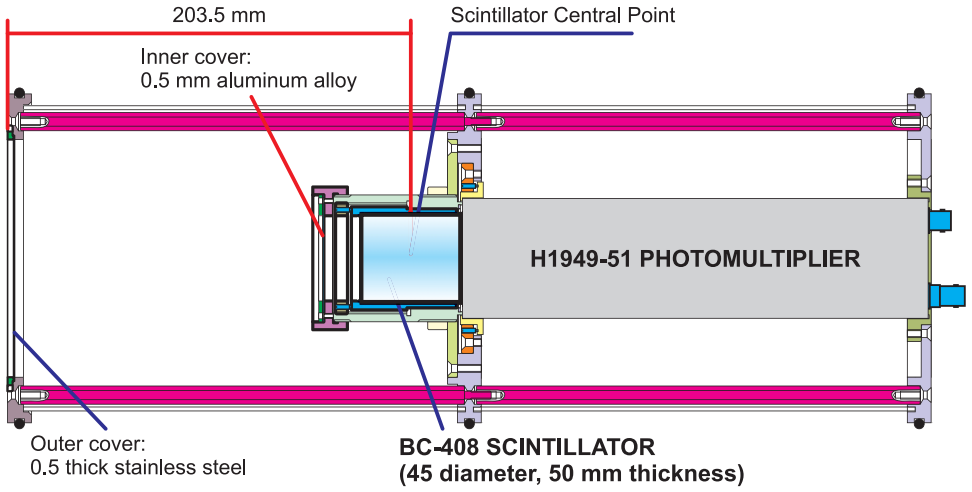

FIG. 1. (color online) Cross section of the neutron time-of-flight detector showing the BC-408 scintillator and the H1949-51 photomultiplier tube inside the stainless-steel housing. The inside cover of the scintillator is from black-anodized aluminum. In order to minimize the interface reflection, a silicone grease was applied between the scintillator and the PMT entrance window.

z-pinch[12] with neutron yields up to 10^{12} as well as at the PALS laser facility.[20]

As far as the electromagnetic shielding is concerned, each scintillator-PMT combination was put inside a heavy duty housing which was manufactured by ACS Ltd.[18] (see Fig. 1). At the PF-1000 facility, the housing with the detector was placed into a AS16U-8 mobile stand at 1.2 m above the floor.[19] In the presence of a harsh x-ray environment, such as at the S-300 z-pinch[12] or the PALS laser system,[20] scintillators were shielded with up to 10 cm of lead. It was also suitable to place the scintillator-PMT combination in such a position to avoid a direct exposure of the photomultiplier tube or to shield the PMT by even larger amount of lead or tungsten. In both cases, it was essential to place shielding close to the neutron detector in order not to influence significantly the time-of-flight of neutrons. Further details on the design of the ToF detector can be found in Ref. 18.

III. TEMPORAL RESOLUTION AND TIMING CALIBRATION

The temporal resolution of the neutron detector is given by the pulse width of the scintillator (2.5 ns FWHM) and by the width of a PMT time response which depends on a photomultiplier voltage (cf. Fig. 2). The response of an acquisition system below 1 ns and a transit time of 2.5 MeV neutrons through 50-mm-thick scintillators (1 ns uncertainty) do not limit the temporal resolution. For the most commonly used PMT voltage of 1.4 kV, the typical time response to a 3 MeV neutron recorded with a 500 MHz oscilloscope is shown in Fig. 3. The observed signal corresponds to the result obtained by the convolution of the PMT time response with the scintillator decay (see a dashed line in Fig. 3). The width (FWHM) of the neutron signal was 5.7 ± 0.6 ns ($\pm 2\sigma$). The rise time and fall time were 2.9 ± 0.2 and 8 ± 1 ns, respectively. As far as the detection of two neutrons is concerned, it was possible to distinguish them when the temporal shift was about 5.5 ns.[18] The temporal resolution could be slightly improved by a higher PMT voltage. At a 1.9 kV voltage, for example, the width of the neutron signal was by 0.4 ns smaller, i.e., 5.3 ns. (At even higher voltages, a single neutron produces >10 mA peaks and, if a large number of neutrons are detected, the PMT may operate in a nonlinear regime, i.e., the anode current is above 250 mA. For that purpose, a neutral density filter may be placed between the scintillator and the PMT. Because it reduces the signal-to-noise ratio, we do not use operating voltages above 2.0 kV.)

The applied voltage determines not only what the temporal resolution shall be but also influences a PMT delay, the information that is necessary to know in order to synchronize all neutron detectors between each other as well as with other diagnostic tools. The dependence of the PMT delay on the applied voltage was measured for each PMT and the result of one of PMTs can be seen in Fig. 4. An uncertainty of the PMT delay was below 1 ns and differences between various PMTs did not exceed 2 ns for >1 kV voltages.

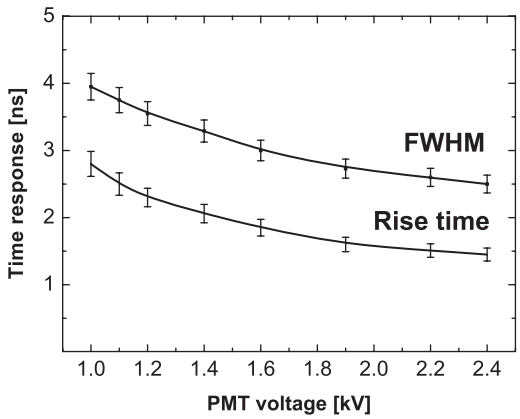

FIG. 2. The dependence of the PMT response (FWHM and rise time) on the operating voltage. The error bars indicate $\pm 2\sigma$ uncertainty.

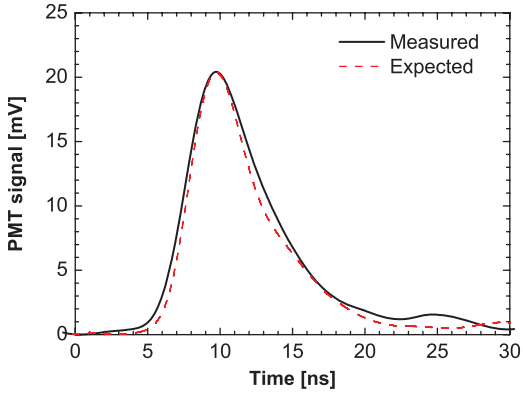

FIG. 3. (color online) The typical time response to a 3 MeV neutron recorded with a 500 MHz oscilloscope (solid line) and the convolution of the PMT time response with the scintillator decay (dashed line). The measurement was based on the technique which is described in Sec. IV. Since only a single neutron was detected, the uncertainty caused by a neutron transit time through 50-mm-thick scintillators is not included in this time response.

IV. LIGHT OUTPUT AND SINGLE NEUTRON SENSITIVITY

The pulse height distribution for a specific scintillator and for various neutron energies can be calculated by the MCNP code[21] postprocessed by the PoliMi package, similarly as it was simulated by Pozzi *et al.*[22,23] Such a numerical simulation is useful for a calibration of detectors operating in the counting mode. In the case of our ToF measurements,[8,12,24] the detectors are operating in the current mode. It means that a large number of neutrons create a ToF signal. Therefore, it is necessary to know what the average light output for neutrons with a given time-of-flight is.

The calculation of the average light output for neutron energies between 1.8 and 3.0 MeV is not as straightforward as it may seem. First, recoil proton energies are distributed uniformly from zero energy to the full kinetic energy of an incident neutron.[13] Second, the response to protons and carbons is nonlinear for energies below 5 MeV.[15,25] Third, neutrons can lose their kinetic energy during the transport from the source to the detector. If a neutron loses its energy near the scintillator (especially at the PMT and lead shielding), the measured time-of-flight corresponds to a higher neutron energy than the energy of a detected neutron. Finally, it is necessary to calculate the coupling efficiency of a scintillator light by the PMT tube, the photocathode quantum efficiency, and the electron gain.

To include all these effects, we developed a novel method of calibrating a neutron detector for different neutron energies between 1.8 and 3.0 MeV. We experimentally estimated *in situ* the response to a single neutron at the PF-1000 plasma focus (2 MA peak current, 5 μs rise time, Ref. 26). It means that the detector described in this paper was developed for the application at this device. When a deuterium gas is used, this facility is capable to produce more than 10^{11} D(d, n)^{3}He neutrons with energies from 1.8 to 3.5 MeV within 100 ns. In the case of such a high neutron yield, it is possible to detect individual neutrons at a distant place from the neutron source and to calculate the energy of a detected neutron by the ToF method. An illustrative ToF signal is displayed in Fig. 5. In comparison with the method described in Refs. 27 and 28, where the neutron detector was calibrated at a 2 m distance, the detector at the PF-1000 was positioned upstream at a distance of 83.7 m from the plasma. Such a great distance enables us to measure the single neutron sensitivity for neutron energies between 1.8 and 3.0 MeV.

The kinetic energy of a neutron, E, could be calculated from the basic time-of-flight method. The energy resolution of the ToF method ΔE is determined mainly by the duration of neutron emission $\Delta\tau$ as

$$\frac{\Delta E}{E} = \frac{2\Delta\tau}{\tau}, \tag{1}$$

where τ is the neutron time-of-flight from a source to a detector. At the PF-1000 plasma focus, the FWHM of neutron emission $\Delta\tau$ is usually below 100 ns. Then, for a 83.7 m distance and for 2.45 MeV neutron with the ToF of 3860 ns, we obtain the uncertainty of a neutron energy ΔE on the order of 0.1 MeV.

If the energy estimated from the time-of-flight is known, it is possible to measure a pulse height response of the detector to neutrons with various neutron energies. During the calibration at the PF-1000 facility, the noise level was 0.2 mV (root mean square). Therefore, the discrimination level was set at 1 mV and only single peaks above this threshold were taken into account. The response to a single neutron was

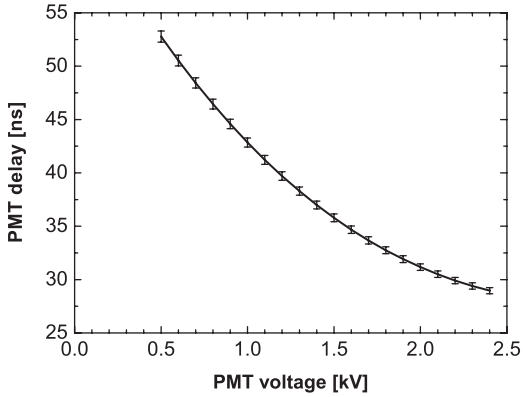

FIG. 4. The dependence of the PMT delay on the PMT voltage. The error bars indicate $\pm 2\sigma$ uncertainty.

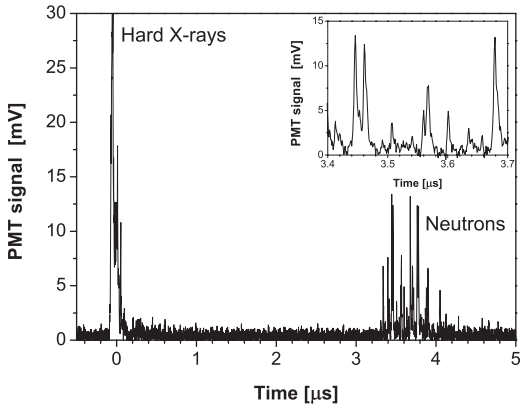

FIG. 5. An example of a ToF signal recorded at 83.7 m.

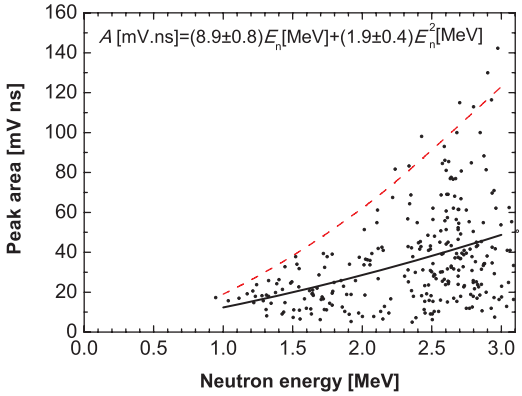

FIG. 6. (color online) The dependence of peak areas on neutron energies calculated from the neutron ToF. A dashed line represents a relative dependence of the light output for recoil protons according to Ref. 15.

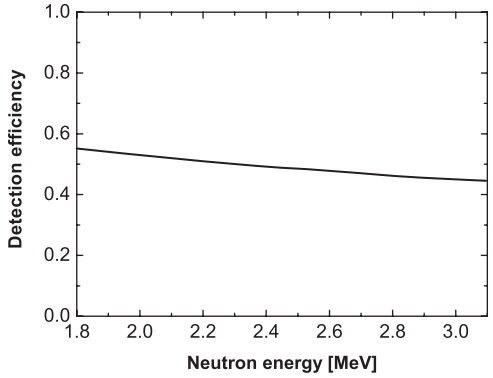

FIG. 7. The dependence of the detection efficiency of the neutron energy for 50 mm thick BC-408 scintillator.

recognized by its FWHM which should be between 5 and 7 ns. In order to avoid pile-up effect, we excluded from the analysis those parts of a ToF signal where the coincidence of two neutrons was expected. During 20 shots (these correspond to 1 day operation of the PF-1000 facility), we accumulated ~5000 peaks and analyzed 300 well separated peaks (see Fig. 6). Even though the operating regime of the PF-1000 facility was not optimized for the pulse height analysis and neutron yields were higher than optimal, 300 well separated pulses ensured sufficient accuracy for our Monte Carlo reconstruction of neutron energy spectra.[12,24,29,30] If a higher accuracy is required, more shots in an optimized regime of the device can be easily achieved.

Figure 6 shows that the maximum light output observed for a given energy of the incident neutron is rising more than linearly. Such a result agrees with the fact that the response to recoil protons with the full neutron energy is nonlinear for energies below 5 MeV.[13,15,25] Since only a portion of the neutron energy is usually transferred to a recoil proton in a single scattering event, there are more events with pulse heights lower than the maximum for the incident neutron energy in Fig. 6. As far as the average values are concerned, the dependence of the light output on the neutron energy was fitted by a polynomial of the second order. The result was influenced by the 1 mV discrimination level because events with 0–5 mV ns peak areas were not included and, thus, the average light output is somewhat overestimated. If we assume that a number of events in the 0–10 mV ns region was the same as in the 10–20 mV ns region, the average neutron light yield should be decreased by about 3 mV ns for all energies and we receive fit parameters which are presented in Fig. 6. Error estimates of fit parameters include the uncertainty of neutron energies and the influence of a discrimination level and Poisson statistics.

On the one hand, Fig. 6 shows that colliding neutrons with higher energies produce higher light outputs. But on the other hand, more energetic neutrons have usually lower probability of a scattering event with protons in a scintillator. In order to include this effect in our measurement with the BC-408 scintillator, we estimate the dependence of the detection efficiency on a neutron energy using the ENDF database.[31] In the first order approximation, we assume a thin target and we calculate the probability of the elastic interaction of an incident neutron with a recoil proton. The result can be seen in Fig. 7. Since the detection efficiency is not so strongly dependent on a neutron energy and since the light output caused by scattering on carbon is very small and can be neglected (cf. Ref. 15), the error of our approximation is expected to be on the order of a few percent. As a result, the detector sensitivity to multiple neutrons with various energies is given by the multiplication of the dependencies presented in Figs. 6 and 7.

Such a calibration of the current mode neutron ToF detector does not occur often in fusion experiments. Usually, the detector response is assumed to be independent on a neutron energy. This assumption is valid only in the case of a narrow neutron energy spectrum. In the case of z-pinch and plasma focus experiments,[5,12,24,32,33] the width of neutron energy spectra could exceed 500 keV and thus the dependence of a detector sensitivity on a neutron energy should be taken into account. For instance, the difference between 2.1 and 2.9 MeV neutrons reaches 35%. Such a value is comparable with the axial neutron emission anisotropy observed in z-pinches.[24]

V. NEUTRON YIELD AND NUMBER OF DETECTED NEUTRONS

The calibration mentioned in Sec. IV was carried out mainly for the purpose of more precise reconstruction of neutron energy spectra.[24,29,30] In addition to that, the known response of the detector to a single neutron can be used for the estimation of the number of detected neutrons by the current mode detector. Figure 8 shows the histogram of a peak area for neutrons with energies between 2.2 and 2.7 MeV. The average peak area A was about (37 ± 5) mV ns, i.e., 0.75 pC, for the 1.4 kV operating voltage (as regards the calibration at various voltages, it was possible to use the measured dependence of the radiant sensitivity of the PMT tube on a voltage published in Ref. 18). Then, if we determine the charge produced by the current mode detector, Q, the number of detected neutrons can be estimated as $N_{\text{detected}} = Q/A$.

If the number of detected neutrons is known, a neutron ToF detector can be calibrated for absolute neutron yields.

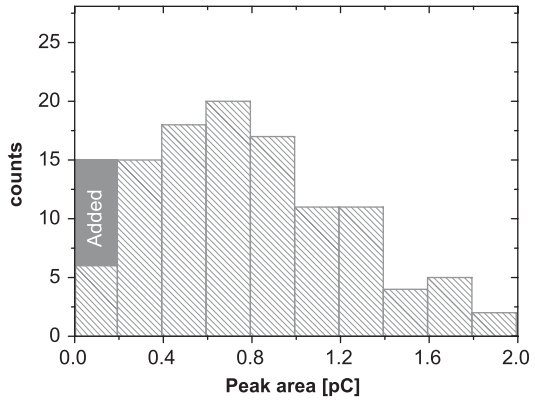

FIG. 8. The histogram of peak areas for 2.2–2.7 MeV neutrons. In order to include the effect of the discrimination limit, several counts were added into a 0–0.2 pC region.

Assuming the isotropic emission, the neutron yield is given by

$$Y = \frac{4\pi}{\Omega}\frac{N_{\text{detected}}}{\eta}, \tag{2}$$

where Ω and η stand for the solid angle and the efficiency of neutron detection, respectively. The solid angle Ω covered by a detector can be simply inferred from the experimental arrangement. As for the detection efficiency, η, i.e., the ratio between detected and impinging neutrons, it is ~50% in the case of 2.45 MeV neutrons (cf. Fig. 7). At the PF-1000, we were able to compare the neutron yield measured by this technique with the one determined by four silver activation detectors.[34] When we considered the influence of neutrons scattered at the experimental chamber (see Ref. 35 and 37), the neutron yields measured by scintillators were by about 30% lower. The observed difference could be ascribed to a neutron flux anisotropy and to the accuracy of neutron yield measurements by these methods.

On the contrary, if the neutron yield Y is known, we can calculate the expected number of detected neutrons N_{detected}. At the PF-1000 facility, for instance, neutron yields are on the order of 10^{11} per one shot. At the distance of 30 m, the 4.5 cm diameter of the cylindrical detector corresponds to the solid angle Ω of 2×10^{-7} srad. Calculating with the 50% detection efficiency, we obtain more than 7000 detected neutrons. As far as the number of detected neutrons is concerned, a neutron detector operating in the current mode requires a sufficiently high number of scattering events in order to reduce the quantum noise. The quantum noise is given not only by the stochastic nature of neutron detection but also by the stochastic transfer of a neutron energy to recoil protons and, therefore, by the stochastic distribution of pulse heights for a given neutron energy. Therefore, it is necessary for ToF measurements to detect at least several tens of neutrons within the temporal resolution of the detector. At the PF-1000 facility, the typical duration of ToF signals at 30 m is about 300 ns.[8] In the case of 7000 detected neutrons, we obtain about 115 neutrons within the 5 ns temporal resolution. Such a value seems to be high enough to reduce the quantum noise. In the case of the 85 m distance, the quantum noise is much more significant since the number of detected neutrons is lower and also the width of a ToF signal is broader. For this reason, it seems better to use cylindrical scintillators with a larger diameter.[18] Another possibility is to use a longer cylindrical scintillator positioned perpendicularly to the source–detector axis.

VI. TIME OF NEUTRON PRODUCTION, TEMPORAL ACCURACY, AND TEMPORAL RESOLUTION

An illustrative test of the fast neutron detector is the measurement of neutron production time at a small plasma focus PFZ at the Czech Technical University in Prague. The time of neutron production is usually estimated from the nearest neutron ToF signals, therefore, it is convenient to place the neutron detector as close to the source as possible. The shortest possible distance is given by an experimental arrangement and by the fact that a neutron signal has to be temporally separated from hard x-ray emission or harsh electromagnetic noise. At the PFZ device, the time of neutron production is estimated from the nearest side-on ToF detector at about 150 cm from the plasma. The advantage of side-on detectors is usually less amount of hardware in the direction of diagnostic ports which implies a smaller influence of scattered neutrons.[14] Another advantage of side-on detectors is that neutron energy spectra are centered at about 2.45 MeV. Therefore, in order to obtain the temporal evolution of neutron emission, it is possible to shift the observed neutron signals by the time-of-flight of 2.45 MeV neutrons (69.4 ns in the case of 150 cm distance, 64.4 ns delay after hard x-rays). For example, Fig. 9 shows a radial neutron signal shifted by the ToF together with waveforms of soft and hard x-ray radiations and current derivative $\mathrm{d}I/\mathrm{d}t$.

In Fig. 9, we can see the temporal correlation of the $\mathrm{d}I/\mathrm{d}t$ dip (maximum compression) and soft and hard x-ray signals. All these waveforms were recorded by the same oscilloscope and were adjusted to account for different transit times from each detector. A 2 ns temporal uncertainty between these waveforms is given by the uncertainty of a detector distance, length of cables, a PMT delay, and a 500 MHz bandwidth of the oscilloscope. As regards the shift between hard x-rays and neutron signals, they are taken from the same waveform. Therefore, the temporal uncertainty is determined only by the accuracy of the distance from the source to the detector. In

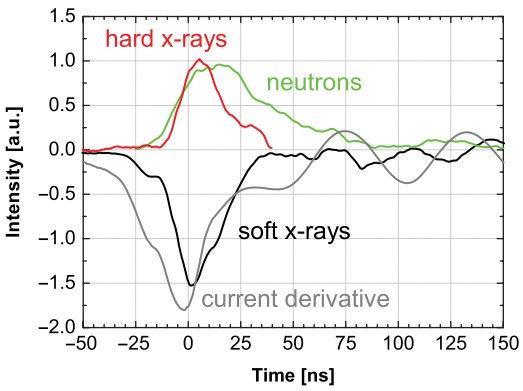

FIG. 9. (Color online) The waveforms of current derivative, soft x-rays, hard x-rays, and neutron emission recorded in discharge No. 090429-23 with a neutron yield of about 10^7.

the case of 2.45 MeV neutrons, the distance of about 2 cm corresponds to a 1 ns temporal uncertainty.

Much more important than the 2 ns temporal uncertainty (temporal accuracy) is the temporal resolution of neutron detection. Since the neutron emission is detected at a certain, nonzero, distance from the neutron source, the temporal resolution is given not only by the 5.7 ns pulse response of the neutron detector (see Sec. II), but also by the width of a neutron energy spectrum. The difference between neutron kinetic energies implies the broadening of ToF signals. In the case of a 500 keV width of side-on energy spectra which was observed in most of plasma focus and z-pinch experiments,[5,12,24,32] the instant neutron emission is broadened to a 6.5 ns FWHM at 1.5 m distance. Calculating with the 5.7 ns pulse response to a single neutron, we obtain the overall temporal resolution of about 8.5 ns.

The overall temporal resolution of 8.5 ns seems to be sufficient for most neutron measurements in gas puff z-pinches and plasma foci. In these devices, temporal changes of neutron emission are not so fast since it takes some time to produce fusion neutrons from accelerated deuterons. For instance, the free path length of 100 keV deuterons in z-pinch plasmas is typically several centimeters long. Each 3 cm then represents the time period of about 10 ns. This time delay can partly explain differences between the hard x-ray and neutron signal in Fig. 9. The application of a faster neutron detector is, therefore, valuable especially in the case of a shorter neutron emission, a narrow energy spectrum, and a small distance of the neutron detector.

VII. CONCLUSION

We have developed and tested sensitive neutron detectors which are designed for neutron ToF measurements in z-pinch and plasma focus experiments. The pulse response of the neutron detector is ~5 ns. During the calibration procedure at the PF-1000 facility, we demonstrated the applicability of a novel method of the acquisition of the pulse height distribution. With the ToF detector at the distance of 85 m, it was possible to measure the single neutron sensitivity for neutron energies between 1.8 and 3.0 MeV. The detector described in this paper has been successfully used in z-pinch and plasma focus experiments with neutron yields from 10^6 to 10^{12} neutrons/shot.

ACKNOWLEDGMENTS

This research has been supported by Grant Nos. 202-08-P084, 202-08-H057 of the Grant Agency of the Czech Republic, by research program Nos. LA08024, ME09087, LC528 of the Ministry of Education, by IAEA Grant No. RC14817 and CTU Grant No. SGS10/266/OHK3/3T/13.

[1] O. N. Jarvis, Plasma Phys. Controlled Fusion **36**, 209 (2010).
[2] T. Elevant, P. van Belle, O. N. Jarvis, and G. Sadler, Nucl. Instrum. Methods Phys. Res. A **364**, 333 (1995).
[3] R. A. Lerche, V. Yu. Glebov, M. J. Moran, J. M. McNaney, J. D. Kilkenny, M. J. Eckart, R. A. Zacharias, J. J. Haslam, T. J. Clancy, M. F. Yeoman, D. P. Warwas, T. C. Sangster, C. Stoeckl, J. P. Knauer, and C. J. Horsfield, Rev. Sci. Instrum. **81**, 10D319 (2010).
[4] V. Y. Glebov, T. C. Sangster, C. Stoeckl, J. P. Knauer, W. Theobald, K. L. Marshall, M. J. Shoup, T. Buczek, M. Cruz, T. Duffy, M. Romanofsky, M. Fox, A. Pruyne, M. J. Moran, R. A. Lerche, J. McNaney, J. D. Kilkenny, M. J. Eckart, D. Schneider, D. Munro, W. Stoeffl, R. Zacharias, J. J. Haslam, T. Clancy, M. Yeoman, D. Warwas, C. J. Horsfield, J. L. Bourgade, O. Landoas, L. Disdier, G. A. Chandler, and R. J. Leeper, Rev. Sci. Instrum. **81**, 10D325 (2010).
[5] A. Bernard, A. Coudeville, A. Jolas, J. Lauspach, and J. de Mascreau, Phys. Fluids **18**, 180 (1975).
[6] I. Tiseanu, G. Decker, and W. Kies, Nucl. Instrum. Methods Phys. Res. A **373**, 73 (1996).
[7] R. Aliaga-Rossel and P. Choi, IEEE Trans. Plasma Sci. **26**, 1138 (1998).
[8] P. Kubes, J. Kravarik, D. Klir, K. Rezac, M. Scholz, M. Paduch, K. Tomaszewski, I. Ivanova-Stanik, B. Bienkowska, L. Karpinski, M. Jan Sadowski, and H. Schmidt, IEEE Trans. Plasma Sci. **34**, 2349 (2006).
[9] C. A. Coverdale, C. Deeney, A. L. Velikovich, J. Davis, R. W. Clark, Y. K. Chong, J. Chittenden, S. Chantrenne, C. L. Ruiz, G. W. Cooper, A. J. Nelson, J. Franklin, P. D. LePell, J. P. Apruzese, J. Levine, and J. Banister, Phys. Plasmas **14**, 056309 (2007).
[10] P. Kubes, D. Klir, J. Kravarik, K. Rezac, IEEE Trans. Plasma Sci. **37**, 1786 (2009).
[11] R. Verma, R. S. Rawat, P. Lee, M. Krishnan, S. V. Springham, and T. L. Tan, Plasma Phys. Controlled Fusion **51**, 075008 (2009).
[12] D. Klir, J. Kravarik, P. Kubes, K. Rezac, J. Cikhardt, E. Litseva, T. Hyhlik, S. S. Ananev, Yu. L. Bakshaev, V. A. Bryzgunov, A. S. Chernenko, Yu. G. Kalinin, E. D. Kazakov, V. D. Korolev, G. I. Ustroev, A. A. Zelenin, L. Juha, J. Krasa, A. Velyhan, L. Vysin, J. Sonsky, and I. V. Volobuev, Plasma Phys. Controlled Fusion **52**, 065013 (2010).
[13] G. F. Knoll, *Radiation Detection and Measurement*, 3rd ed. (Wiley, New York, 1999).
[14] D. Klir, J. Kravarik, P. Kubes, K. Rezac, S. S. Ananev, Yu. L. Bakshaev, P. I. Blinov, A. S. Chernenko, E. D. Kazakov, V. D. Korolev, G. I. Ustroev, L. Juha, J. Krasa, A. Velyhan, IEEE Trans. Plasma Sci. **37**, 425 (2009).
[15] Saint-Gobain Crystals, Scintillation Products, Organic Scintillator. Available: http://www.detectors.saint-gobain.com/uploadedFiles/SGdetectors/Documents/Brochures/Organics-Brochure.pdf.
[16] Hamamatsu, Photomultiplier Tubes. Available: http://sales.hamamatsu.com/assets/pdf/catsandguides/PMT_TPMO0009E01.pdf.
[17] Hamamatsu, Photomultiplier Tube R1828-01. Available: http://sales.hamamatsu.com/assets/pdf/parts_R/R1828-01.pdf.
[18] K. Tomaszewski, in *AIP Conference Proceedings*, *17th IAEA Technical Meeting on Research Using Small Fusion Devices*, Lisbon, 2007 (American Institute of Physics, New York, 2008), Vol. 996, p. 89.
[19] K. Tomaszewski, in *AIP Conference Proceedings*, *16th IAEA Technical Meeting on Research Using Small Fusion Devices*, Mexico, 2005 (American Institute of Physics, New York, 2006), Vol. 875, p. 41.
[20] K. Jungwirth, A. Cejnarova, L. Juha, B. Kralikova, J. Krasa, E. Krousky, P. Krupickova, L. Laska, K. Masek, T. Mocek, M. Pfeifer, A. Präg, O. Renner, K. Rohlena, B. Rus, J. Skala, P. Straka, and J. Ullschmied, Phys. Plasmas **8**, 2495 (2001).
[21] See National Technical Information Service Document No. DE87000708 (J. F. Briesmeister, MCNP: A general Monte Carlo code for neutron and photon transport, LANL Report No. DE87000708, 1986). Copies may be ordered from National Technical Information Service, Springfield, VA.
[22] S. A. Pozzi, J. A. Mullens, J. T. Mihalczo, Nucl. Instrum. Methods Phys. Res. A **524**, 92 (2004).
[23] S. A. Pozzi, M. Flaska, A. Enqvist, and I. Pazsit, Nucl. Instrum. Methods Phys. Res. A **582**, 629 (2007).
[24] D. Klir, J. Kravarik, P. Kubes, K. Rezac, S. S. Ananev, Yu. L. Bakshaev, P. I. Blinov, A. S. Chernenko, E. D. Kazakov, V. D. Korolev, B. R. Meshcherov, G. I. Ustroev, L. Juha, J. Krasa, and A. Velyhan, Phys. Plasmas **15**, 032701 (2008).
[25] A. A Naqvi, A. Aksoy, F. Z. Khiari, A. Coban, M. M. Nagadi, M. A. Al-Ohali, and M. A. Al-Jalal, Nucl. Instrum. Methods Phys. Res. A **345**, 514 (1994).
[26] M. Scholz, L. Karpinski, M. Paduch, K. Tomaszewski, R. Miklaszewski, and A. Szydlowski, Nukleonika **46**, 35 (2001).
[27] L. E. Ruggles, J. L. Porter, W. W. Simpson, M. F. Vargas, D. M. Zagar, R. Hartke, F. Buersgens, D. R. Symes, and T. Ditmire, Rev. Sci. Instrum. **75**, 3595 (2004).
[28] R. Hartke, D. R. Symes, F. Buersgens, L. E. Ruggles, J. L. Porterb, and T. Ditmire, Nucl. Instrum. Methods Phys. Res. A **540**, 464 (2005).
[29] K. Rezac, D. Klir, P. Kubes, J. Kravarik, and M. Stransky, Czech J. Phys. **56**, B357 (2006).

[30]K. Rezac, D. Klir, P. Kubes, J. Kravarik, in *AIP Conference Proceedings, 7th International Conference on Dense Z-Pinches*, Alexandria, VA, 2008 (American Institute of Physics, New York, 2009), Vol. 1088, p. 211.
[31]M. B. Chadwick, P. Obložinský, M. Herman, N. M. Greene, R. D. McKnight, D. L. Smith, P. G. Young, R. E. Macfarlane, G. M. Hale, S. C. Frankle, A. C. Kahler, T. Kawano, R. C. Little, D. G. Madland, P. Moller, R. D. Mosteller, P. R. Page, P. Talou, H. Trellue, M. C. White, W. B. Wilson, R. Arcilla, C. L. Dunford, S. F. Mughabghab, B. Pritychenko, D. Rochman, A. A. Sonzogni, C. R. Lubitz, T. H. Trumbull, J. P. Weinman, D. A. Brown, D. E. Cullen, D. P. Heinrichs, D. P. McNabb, H. Derrien, M. E. Dunn, N. M. Larson, L. C. Leal, A. D. Carlson, R. C. Block, J. B. Briggs, E. T. Cheng, H. C. Huria, M. L. Zerkle, K. S. Kozier, A. Courcelle, V. Pronyaev, and S. C. van der Marck, Nucl. Data Sheets **107**, 2931 (2006).
[32]M. J. Bernstein and G. G. Comisar, Phys. Fluids **15**, 700 (1972).
[33]D. R. Welch, D. V. Rose, C. Thoma, R. E. Clark, C. B. Mostrom, W. A. Stygar, and R. J. Leeper, Phys. Plasmas **17**, 072702 (2010).
[34]M. Scholz, B. Bienkowska, I. M. Ivanova-Stanik, L. Karpinski, M. Paduch, E. Zieliñska, J. Kravarik, P. Kubes, M. J. Sadowski, and A. Szydlowski, H. Schmidt, Czech. J. Phys. Suppl. B **56**, 243 (2006).
[35]J. Krasa, M. Kralik, A. Velyhan, J. Solc, L. Juha, M. Scholz, B. Bienkowska, I. M. Ivanova-Stanik, L. Karpinski, R. Miklaszewski, M. Paduch, H. Schmidt, K. Tomaszewski, D. Klir, J. Kravarik, P. Kubes, and K. Rezac, Plasma Phys. Controlled Fusion **50**, 125006 (2008).
[36]D. Klir, P. Kubes, M. Paduch, T. Pisarczyk, T. Chodukowski, M. Scholz, Z. Kalinowska, E. Zielinska, B. Bienkowska, J. Hitschfel, S. Jednorog, L. Karpinski, J. Kortanek, J. Kravarik, K. Rezac, I. Ivanova-Stanik, and K. Tomaszewski, Appl. Phys. Lett. **98**, 071501 (2011).
[37]M. Králík, J. Krása, A. Velyhan, M. Scholz, I. M. Ivanova-Stanik, B. Bienkowska, R. Miklaszewski, H. Schmidt, K. Řezáč, D. Klír, J. Kravárik, and P. Kubeš, Rev. Sci. Instrum. **81**, 113503 (2010).

ARTICLE NO. 2

Neutron emission generated during wire array Z-pinch implosion onto deuterated fiber

D. Klir,[1] J. Kravarik,[1] P. Kubes,[1] K. Rezac,[1] S. S. Anan'ev,[2] Yu. L. Bakshaev,[2] P. I. Blinov,[2] A. S. Chernenko,[2] E. D. Kazakov,[2] V. D. Korolev,[2] B. R. Meshcherov,[2] G. I. Ustroev,[2] L. Juha,[3] J. Krasa,[3] and A. Velyhan[3]
[1]*Czech Technical University, Faculty of Electrical Engineering, Department of Physics, Technicka 2, 166 27 Prague 6, Czech Republic*
[2]*Russian Research Center, Kurchatov Institute, 1 Kurchatov Sq., 123182 Moscow, Russia*
[3]*Institute of Physics, Na Slovance 2, 182 21 Prague 8, Czech Republic*

(Received 20 November 2007; accepted 10 January 2008; published online 12 March 2008)

The implosion of both cylindrical and conical wire arrays onto a deuterated polyethylene fiber was studied on the S-300 pulsed power generator [A. S. Chernenko *et al.*, *Proceedings of the 11th International Conference on High Power Particle Beams* (Academy of Science of Czech Republic, Prague, 1996), p. 154]. Neutron measurements were used to obtain information about acceleration of fast deuterons. An average neutron yield approached 10^9 on the current level of 2 MA. In the case of conical wire arrays, side-on neutron energy spectra peaked at 2.48 ± 0.05 MeV with 450 ± 100 keV full width at half-maximum. In the downstream direction, the peak neutron energy and the width of a neutron spectrum were 2.65 ± 0.10 MeV and 350 ± 100 keV, respectively. The total number of fast deuterons was 10^{15} and their average kinetic energy was about 150 keV. Most of the deuterons were directed toward the cathode. The broad width of neutron spectra in the side-on direction implied a high radial component of deuteron velocity. With regard to the emission time, neutron pulses temporally correlated with hard x rays and also with measured voltage. The neutron emission lasted on average 30 ± 5 ns and it was observed during the stagnation and at the beginning of the expansion of a plasma column. At this moment, the plasma impedance reached 0.2–0.4 Ω. In the post-stagnation phase, this value was formed significantly by enhanced plasma resistance. Similar experimental results were observed also with cylindrical wire arrays imploding onto a deuterated fiber. © *2008 American Institute of Physics*. [DOI: 10.1063/1.2839352]

I. INTRODUCTION

At present, Z pinches belong to the most intensive laboratory sources of soft x rays,[1] and that is also the main reason why they are studied. The application of Z pinches as neutron sources has been somewhat problematic from the beginning of Z-pinch research primarily because of serious doubts in issues of crucial importance. More specifically, two fundamental questions have been studied: (i) the origin of neutrons and (ii) the scaling of a neutron yield with a current. In order to solve these questions and to achieve a higher neutron yield, various types of Z-pinch configurations have been tested from that time on.

In the 1950s, the controlled thermonuclear research was conducted with toroidal and straight compressional Z pinches mainly in the United Kingdom,[2] the United States,[3,4] the former Soviet Union,[5] but also in Canada, Germany, Japan, and Sweden.[6] During that time, teams of researchers were concerned with the idea of heating and confining a fusion mixture within a small diameter by a pinch effect. In compressional Z pinches, an electric current started at an insulating wall, and when a magnetic pressure exceeded a gas pressure, a current-carrying plasma shell together with a preceding shock wave radially collapsed. In the late 1950s, the researchers arrived at the conclusion that neutrons in Z pinches were not produced by thermal collisions of deuterons. This conclusion led to the abandonment of the straight Z pinch as a fusion power source. As a result, more complex schemes of magnetically confined plasma devices (such as θ pinches, stellarators, and tokamaks) were suggested and researched.

During the research of one of more stable schemes, namely Scylla θ pinch at Los Alamos, a plasma gun was used to inject a plasma into the device.[7] In this configuration, the plasma was accelerated between two coaxial electrodes. During the investigation of how the plasma gun worked, it was found that a large number of neutrons (up to 2×10^{10}) was generated from this plasma gun itself. This was the main reason why the so-called Mather-type plasma focus was researched from that time on. The maximum yield exceeded the value of 10^{12} neutrons per pulse.[8] In the former Soviet Union, the Filippov-type plasma focus was constructed independently from a gas embedded Z pinch with a conducting wall.[5,9]

The progress in nanosecond pulsed-power technology in the 1970s led to new attempts to use Z pinches in fusion research. A new effort was made at Los Alamos during high density Z-pinch experiments. It was known that a 100 μm current channel had to be created in order to reach fusion conditions (10^{26} m^{-3} density, 1 μs confinement time, 10 keV temperature) with the Pease–Braginski current of 1.4 MA.[10] It thus seemed reasonable enough to start with a small initial diameter of a plasma column. The idea was to initiate the

pinch by a focused laser or electron beam that would ionize a channel on the axis of a gas filled vessel. This is how a gas-embedded pinch is formed. Gas-embedded experiments demonstrated the possibility of producing stable Z pinches. However, the pinched plasma could not reach a high enough temperature because it rapidly accreted particles from the surrounding gas.

One suggestion on how to overcome the accretion and how to confine a high-density and high-temperature plasma column within a small diameter was to initiate Z pinches from fibers of cryogenic solid deuterium in vacuum.[11] Z-pinch plasmas in the first fiber experiments seemed to be stable for many radial Alfven transit times, whereas the neutron yield approached 10^{10} (Ref. 12). However, the enhanced stability was not confirmed in further and better diagnosed experiments on new generators at NRL[13] and Los Alamos[14] as well as on KALIF at Kernforschungszentrum Karlsruhe[15] or on MAGPIE at Imperial College in London.[16] Particularly, the early development of plasma instabilities and the rapid expansion decreased a plasma density substantially and thus eliminated the possibility of using a fiber Z pinch as a fusion reactor.

During fiber Z-pinch experiments, fibers from deuterated polyethylene were also employed because they were easily available in comparison with frozen deuterium fibers and at the same time neutron yields were almost identical.[17] In the case of fiber pinches, neutrons originated from several points distributed over the entire length of a fiber. For some applications it seemed better to have more localized neutron emission. For that purpose, an X pinch (that is, two crossed fibers) was tried.[18] Another possibility of energy concentration into one localized region was to employ a vacuum spark[19] or to preform an $m=0$ instability in a Z-pinch load.[20,21]

In the 1990s, most Z-pinch experiments were carried out with imploding wire arrays or gas-puffs. So far, the highest neutron yields in Z pinches have been reached with gas-puffs. One of the first deuterium gas-puff experiments was carried on the Angara 5-1 device at Troitsk.[22] The characteristic feature of this experiment was the relatively small mass of a liner and the axial gradient of a linear density. This way, a very high neutron yield above 10^{12} neutrons per shot was reached at the current of "only" 2–3 MA. The strong anisotropy of neutron fluxes and neutron energy spectra gave evidence of deuterons accelerated to 200–500 keV energies. Even more DD fusion neutrons were generated on the Z machine with a double-shell deuterium gas-puff on the current level of 17 MA.[23] With regard to the overall neutron yield in this experiment, there is a hope of a large thermonuclear component because it is difficult to explain the yield of about 6×10^{13} neutrons by the beam-target mechanism.

On the basis of experimental results of several research groups (see Refs. 24 and 25), solid fibers appear less suitable than deuterium gas-puffs when a high neutron yield is required. Nevertheless, it seemed interesting to see what would happen if a deuterated fiber were put in the center of a wire array or a hollow gas-puff. Two shots (Nos. 293 and 294) with 240 aluminum wires imploding onto a $(CD_2)_n$ fiber were carried out on Sandia's Z machine in 1998 but the obtained results have not been published. On the Saturn generator, $(2.8\pm0.2)\times10^{12}$ neutrons were generated during the implosion of a hollow deuterium gas-puff onto a 250 μm deuterated polyethylene fiber located on the pinch axis.[24] In addition to such a high neutron yield, the neutron emission was almost isotropic.

This short overview brings us to the purpose of this paper, which is concerned with Z-pinch experiments in which a wire array imploded onto a deuterated fiber. Since results with aluminum wire arrays have already been published,[26] we focus in particular on experiments with conical tungsten wire arrays here. The purpose of our experiment is described in Sec. II. Section III provides the description of a current generator and diagnostics used in our experiment. Section IV brings forward the most important results we have obtained. Section V contains the overall discussion within the framework of other experiments.

II. PURPOSE OF OUR EXPERIMENT AND METHOD USED

The primary objective of our experiments at the S-300 generator is to get deeper insight into the process of generating fast electrons, ions, and hard x rays in Z-pinch plasmas. Whereas a large number of papers are devoted to studies of EUV, soft-, and hard-x-ray radiation, and in some cases electrons, information about fast ions is rather rare. At this point we can mention the recent measurement of an ion temperature in wire arrays. The Doppler width of iron spectral lines indicated that the ion temperature exceeded 200 keV.[27] Such a result suggests that also a fusion neutron measurement could provide invaluable data for Z-pinch physics since it helps us to understand the issue of the acceleration of fast ions. And that is precisely why we are interested in the research of fusion reactions in Z pinches.

At the S-300 generator, the easiest way to produce fusion neutrons seemed to be putting a deuterated fiber in the center of a wire array. As regards the fusion of two deuterons, there are two branches of the reaction. They both occur with nearly equal probability.

$$\mathrm{D}+\mathrm{D}\rightarrow \mathrm{T}\ (1.01\ \mathrm{MeV})+\mathrm{p}\ (3.02\ \mathrm{MeV}),$$

$$\mathrm{D}+\mathrm{D}\rightarrow {}^{3}_{2}\mathrm{He}(0.82\ \mathrm{MeV})+\mathrm{n}(2.45\ \mathrm{MeV}).$$

Since neutrons are influenced neither by magnetic nor by electric fields, the detection of neutrons is a favorable diagnostic tool for fast deuterons in a plasma. This very fact is also taken into account when studying plasmas not only in Z pinches but also in tokamaks,[28] nanosecond, and femtosecond lasers.[29] A great advantage of neutron diagnostics is weak absorption and scattering of neutrons in the air, which enables us to use the extended time-of-flight (TOF) analysis for the determination of neutron energy spectra.

The time-resolved neutron energy distribution function $f(E_n,t)$ can be reconstructed from time-resolved neutron signals $S(x,T)$, which are recorded by several detectors in one direction at different distances x. The relation between the neutron flux $S(x,T)$ and the energy distribution function $f(E_n,t)$ is given by

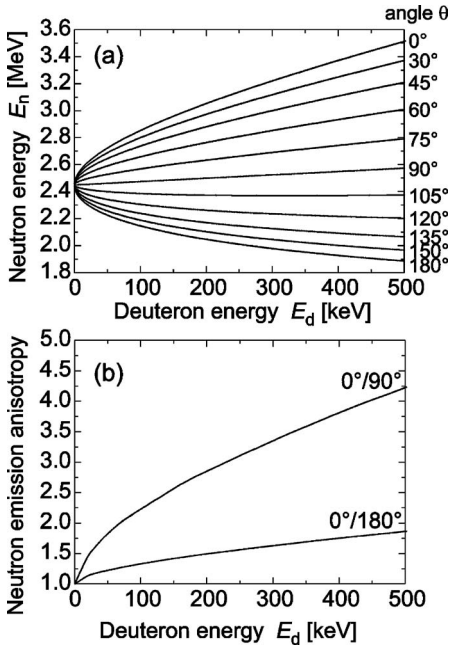

FIG. 1. (a) The energy-angle dependence of neutron energies for the $D(d,n)^3He$ fusion reaction. (b) The ratio between differential cross sections for θ=0°, 90°, and 180° as a function of a deuteron energy for the $D(d,n)^3He$ reaction. The angle θ is the laboratory angle between the incoming fast deuteron and the outgoing neutron.

$$S(x,T) = \int dt \int dE_n f(E_n,t)\,\delta\left(t - T + \frac{x}{\sqrt{2E_n/m_n}}\right), \qquad (1)$$

where E_n is the neutron energy, m_n is the neutron mass, T is the neutron detection time, and t is the emission time. It follows from this equation that the time of neutron production is estimated mainly from the nearest neutron signal and the energy of neutrons is determined mainly from the most distant neutron detector. There are several developed algorithms for the deconvolution of the $f(E_n,t)$ function. In our case, a Monte Carlo method[30] was used and subsequently improved. Our improvement is based on the fact that it is possible to use neutron detectors in mutually opposite directions. In other words, neutron spectra could be evaluated from the chain of neutron detectors on both sides of the neutron source. On the one hand, such a procedure significantly improved results of neutron spectra reconstruction[31] and limited the influence of scattered neutrons (see the Appendix). But on the other hand, neutron emission anisotropy had to be included into the Monte Carlo reconstruction. We included the anisotropy of neutron energies [see Fig. 1(a)] and differential cross sections [see Fig. 1(b)] into our reconstruction.[32] Recently, we have taken into account the fact that deuteron velocities could have an arbitrary direction with respect to the chain of neutron detectors (i.e., with respect to the line of sight). Our calculation of the anisotropy was based on the scattering theory. The nuclear data of the D–D fusion reaction were taken from Refs. 28, 33, and 34.

III. APPARATUS AND DIAGNOSTICS

A. Current generator and Z-pinch load

The implosion of a conical tungsten wire array Z pinch onto a deuterated fiber was studied on the S-300 device (4 MA peak current, 700 kV voltage, 100 ns rise time, 0.15 Ω impedance) at the Kurchatov Institute in Moscow.[35] In this paper, we present results from the experimental series of 15 shots at the current level of 2 MA. The diameter of a conical wire array was 10 and 7 mm at the anode and at the cathode, respectively. The wires were inclined at an angle of 13° to the array axis. The conical wire arrays consisted of 30 tungsten wires 7 μm in diameter. The deuterated polyethylene $(CD_2)_n$ fibers with diameters between 80 and 120 μm were placed on the axis of the array. The enrichment of deuterium in the polyethylene was higher than 98%. The mass percentage of tungsten, carbon, and deuterium ions in Z-pinch load was about 73%, 20%, and 7%, respectively.

B. Diagnostics

In order to study dynamics of Z-pinch plasmas, we applied optical, x-ray, and neutron diagnostics, part of which was described in Refs. 36 and 37. Each shot was observed with the following set of diagnostic tools (cf. Fig. 2):

(i) An optical streak camera was performed in the radial mode, i.e., with a slit perpendicular to the Z-pinch

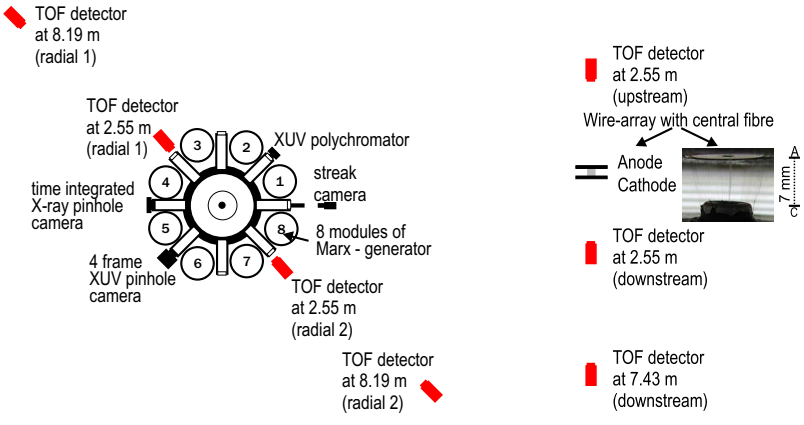

FIG. 2. (Color online) A schematic diagram of our diagnostic setup with seven time-of-flight neutron detectors.

axis. The plasma 3 mm away from the cathode was imaged on the slit of the streak camera.

(ii) A time-integrated pinhole camera was differentially filtered (without a filter, and with 5 and 24 μm Mylar).

(iii) A gated pinhole camera recorded four frames with 2 ns exposure and 5 or 10 ns interframe separation.

(iv) A time-resolved soft-x-ray polychromator was used for the estimation of radiated energy and also for the measurement of spectral power density in various spectral channels.

(v) Seven scintillators and photomultiplier tubes enabled the TOF analysis of fusion neutrons. Three axial (end-on) neutron detectors were located at distances of −2.55 m (the minus sign means upstream, i.e., behind the anode), 2.55 m, and 7.43 m (downstream, behind the cathode). Four radial (side-on) detectors were positioned in a row at distances of −8.19, −2.55, 2.55, and 8.19 m from the Z-pinch plasma. To prevent hard x rays from saturating photomultipliers, detectors were shielded by 5–10 centimeters of lead. The detector time resolution of about 4 and 7 ns was given mainly by the decay time of scintillators, by the rise-time of the photomultiplier tube, and by a neutron transit time through 5 and 10 cm thick scintillators, respectively. The time resolution of neutron detection was further strongly influenced by the detector distance from the neutron source. For example, at the distance of 2.55 m, the instant neutron emission was broadened to 7 ns in the case of the neutron energy spectrum with 2.45 MeV peak and 300 keV full width at half-maximum (FWHM). Because it was possible to distinguish two neutron peaks 11 ns apart from each other, the experimentally estimated temporal resolution of neutron detection was about 10 ns.

(vi) The neutron yield was measured with the use of an indium activation counter and thermoluminescent dosimeters.

(vii) High-voltage and dI/dt probes provided information about electrical characteristics and the power input into the discharge.

This set of diagnostic tools enabled us to observe results that are presented in the following section. All times described in this paper refer to the start of a current when $t=0$. All signals were adjusted to account for different transit times from each detector to oscilloscopes. The temporal uncertainty between waveforms of soft x rays, hard x rays, neutrons, and electrical characteristics was below 5 ns.

IV. EXPERIMENTAL RESULTS

In order to describe Z-pinch discharges that show specific experimental results in each shot, it is important to use simultaneously comprehensive diagnostics with temporal, spatial, and spectral resolution. For this reason, we illustrate the most important results on carefully chosen individual shots that most evidently describe general characteristics of the experiment.

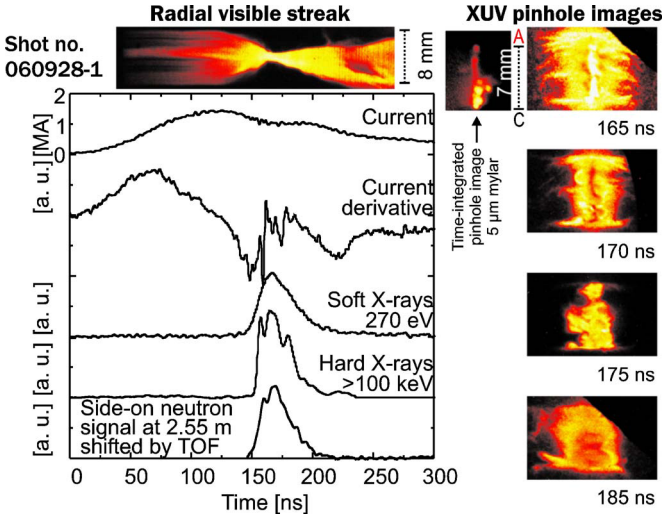

FIG. 3. (Color online) A visible streak image, XUV pinhole images and waveforms of current, current derivative, soft x rays, hard x rays, and neutron emission recorded in Discharge No. 060928-1, with a neutron yield of about 9×10^8. Note: The detection efficiency varied between frames of the XUV pinhole camera.

Figure 3 presents typical results of the implosion of the conical tungsten wire array onto the deuterated polyethylene fiber. Evidently, the streak image shows the radiation from the fiber and/or precursor plasma already at 50 ns. At about 130 ns, the tungsten wire array started to implode with the velocity approaching the value of 2×10^5 m/s. The most intense soft x rays were emitted near the cathode at about 160 ns during the stagnation of imploded tungsten wires onto the $(CD_2)_n$ fiber. The power of soft x rays (above 100 eV) reached 100 GW. The total emitted energy was about 5 kJ. The maximum spectral power density of about 0.5 GW/eV was measured at a photon energy of 120 eV. The radiation was close to the radiation of a black body with a temperature of 40 eV.

Hard-x-ray emission started at the final stage of the wire array implosion. The rise time of a hard-x-ray signal was very short and usually did not exceed 3 ns. In all shots, the onset of x-ray emission corresponded to a dip in the dI/dt signal. After that, the hard-x-ray emission lasted for about 30 ns, i.e., during the stagnation and expansion phase.

As far as neutron emission is concerned, it temporally correlated with hard x rays within 5 ns accuracy. The neutron pulse lasted on average 30 ± 5 ns (FWHM). In Fig. 4, we can see the neutron spectrum obtained perpendicularly to the Z-pinch axis. In this particular shot, the peak neutron energy detected in the side-on direction was slightly shifted from 2.45 MeV. On average, the peak neutron energy was 2.48 ± 0.05 MeV and the FWHM of neutron energy spectra was 450 ± 100 keV. As regards the axial direction [see Fig. 4(c)], the energy of neutrons detected downstream was always above 2.45 MeV. When we calculated the average downstream neutron energy spectrum from 15 shots, it peaked at 2.65 ± 0.10 MeV with 350 ± 100 keV FWHM.

The knowledge of neutron spectra at different directions relative to the Z-pinch axis carries important information about the energy of deuterons that produce fusion reactions.

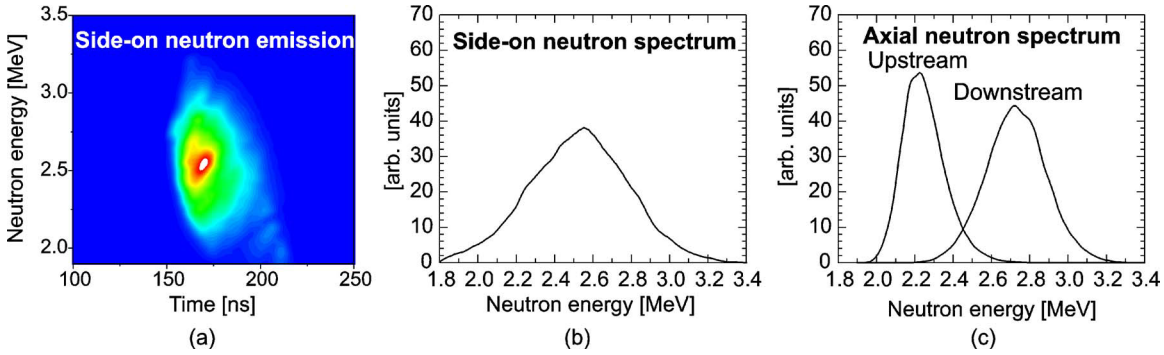

FIG. 4. (Color online) (a) and (b) Side-on neutron emission time and neutron energy spectrum. (c) Axial neutron energy spectrum, Shot No. 060928-1.

Assuming a binary reaction of a fast deuteron with a stationary one, the neutron energy E_n depends on the deuteron energy E_d and on the laboratory angle between the colliding fast deuteron and the outgoing neutron θ as

$$E_n(E_d,\theta) = E_d \frac{m_n}{2(m_n+m_{He})} \cdot \left(\cos\theta + \sqrt{\frac{m_{He}}{m_n}\left(1+\frac{2Q}{E_d}\right)-\sin^2\theta}\right)^2, \quad (2)$$

where $Q \doteq 3.27$ MeV is the energy released from D–D fusion reactions, m_n is the neutron mass, and m_{He} is the mass of helium. It follows from this equation that it is necessary to know the angle θ in order to estimate the deuteron energy from the neutron energy. Fortunately, if the deuteron energy E_d is much smaller than the fusion energy Q, we obtain

$$E_n(E_d,\theta) \approx E_d \frac{m_n}{2(m_n+m_{He})} \cdot \left(\cos\theta + \sqrt{\frac{m_{He}}{m_n}\cdot\frac{2Q}{E_d}}\right)^2, \quad (3)$$

$$E_n(E_d,\theta) \approx g(E_d\cos^2\theta) + \frac{m_{He}}{m_n+m_{He}}\cdot Q \doteq g(E_d\cos^2\theta) + 2.45\ \text{MeV}. \quad (4)$$

Then the neutron energy E_n is only a function of the component of the deuteron kinetic energy in the direction of neutron detection $g(E_d\cos^2\theta)$.

On the basis of Eq. (4), it was possible to transform neutron energy spectra into distribution functions of side-on and end-on energy components of deuterons (see Fig. 5). The divergence around small deuteron energies in Fig. 5 is given by a large dE_n/dE_d near 2.45 MeV neutron energy (cf. Fig. 1).

In Fig. 5, we can see that neutrons were produced mainly by deuterons with a kinetic energy component below 100 keV. The mean axial component of the deuteron kinetic energy $\langle|E_\parallel|\rangle$ was 60 keV while the mean side-on component $\langle|E_\perp|\rangle$ was 40 keV. Therefore, the average kinetic energy of reacting deuterons was $\langle E_d\rangle = \langle E_\parallel\rangle + 2\langle|E_\perp|\rangle \doteq 150$ keV. Our Monte Carlo reconstruction also estimated the downstream/upstream anisotropy of neutron flux as 1.2.

In Shot No. 060928-1, there were only a few downstream neutrons below 2.45 MeV and thus most of the deuterons were directed toward the cathode. In some other shots, a different case occurred. Figure 6 shows results from Shot No. 060922-2, in which the same number of neutrons as in Shot No. 060928-1 was detected. In this particular shot it is also evident that neutrons were emitted together with hard and soft x rays. In addition to that, the neutron emission temporally correlated with the voltage rise up to 400 kV. As regards distribution functions of neutron and deuteron energy, they are displayed in Fig. 7. In comparison with Shot No. 060928-1, neutron and deuteron energy distribution functions were more isotropic. The mean neutron energy observed downstream was about 2.55 MeV. According to our calculation, the side-on and end-on neutron spectra imply the neutron flux anisotropy below 1.2.

A. Correlation of neutron emission with hard x rays and electrical characteristics

Figures 3 and 6 show how neutron emission temporally correlated with hard x rays. Because the Monte Carlo reconstruction could blur a real neutron signal, we displayed the waveform of the nearest side-on neutron detector to obtain more accurate values of the shift between hard-x-ray and neutron emission. In Fig. 8(a), we can see how neutron emission correlated with hard x rays with a small delay, which

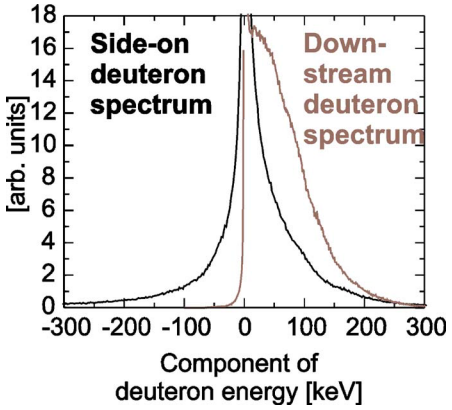

FIG. 5. (Color online) Distribution functions of the kinetic energy component of deuterons that produced fusion neutrons, Shot No. 060928-1. (The energy distribution function of all deuterons was not obtained because the assumption of a thin target is not valid and therefore it is not sufficient to include the fusion cross section and the stopping power into the calculation. One has to include also the slowing-down of fast deuterons.)

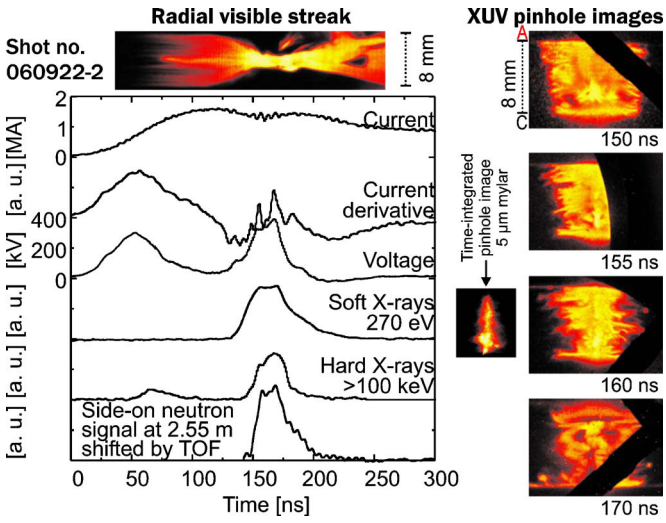

FIG. 6. (Color online) A visible streak image, XUV pinhole images and waveforms of current, current derivative, voltage, soft x rays, hard x rays, and neutron emission recorded in Discharge No. 060922-2, with a neutron yield of about 9×10^8.

was about 4 ns. A part of this delay could be attributed to the transit time of neutrons through the TOF detector and to the uncertainty of neutron energy estimation.

As regards measured voltage, there was also a strong correlation with side-on and end-on neutron emission. An exemplary result can be seen in Fig. 8(b).

Another common feature of our experiment was the rapid rise of hard-x-ray and neutron emission after the dip in the dI/dt signal. After this dip, the current derivative oscillated for about 50 ns and during this period neutrons and hard x rays were detected. It was clear that neutron emission correlated with dI/dt peaks rather than with minima [see Fig. 8(c)] and that the induced voltage $L\mathrm{d}I/\mathrm{d}t$ contributed to voltage peaks [see Fig. 8(d)].

On the basis of voltage V, current I, and dI/dt measurements, it was possible to calculate the plasma resistance R_P and time-varying inductance $\dot{L}_P$ from the equation

$$R_P+\dot{L}_P=\frac{V-L\dot{I}}{I}, \tag{5}$$

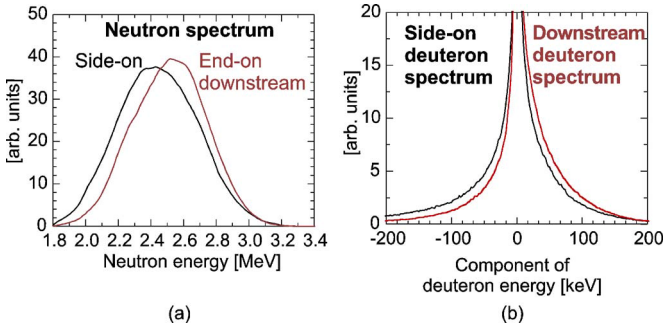

FIG. 7. (Color online) (a) Side-on and end-on energy spectra of neutrons. (b) Distribution functions of the kinetic energy component of reacting deuterons, Shot No. 060922-2.

where $L(t)=L_P(t)+L_0$ is the inductance including the external inductance of transmission line L_0. We assumed that the inductance $L(t)$ of about 9 nH was approximately constant during the implosion. But results would not change qualitatively even if we calculated with the increased inductance of about 14 nH. The results of the $R_P+\dot{L}_P$ term from shots No. 060922-2 and No. 060921-1 are displayed together with neutron emission and a streak image in Fig. 9. In each shot, the neutron emission started at the end of the wire array implosion and lasted for about 40 ns up to the expansion phase. During this period, the energy input $\int(R_P+\dot{L}_P)I^2\mathrm{d}t$ approached 20 kJ.

B. Neutron yield

The study of neutron generation in our experiments at the S-300 generator was focused mainly on the estimation of emission time and neutron energies. The neutron yield was estimated from one indium activation detector assuming the 4π isotropy. Values of neutron yields are therefore important mainly for a relative comparison of individual shots. In this respect, we wanted to know whether the neutron yield was dependent on any parameter of the Z-pinch discharge. The only parameter that we recognized that played some role was the peak of an electric current. Figure 10 shows the scaling of the neutron yield with the magnitude of an electric current. The average neutron yield from 15 shots was 6×10^8 while the peak neutron yield reached the value of 10^9 for 1.65 MA current.

In order to improve neutron yield measurements, we tried to use thermoluminescent dosimeters (TLDs), which were placed inside a 10–in.-thick Bonner sphere, 1 m from the neutron source (cf. Ref. 38). As regards the experiments described in this paper, neutron signals from TLDs were overlaid by a strong hard-x-ray background. In preliminary deuterium gas-puff experiments in which hard x rays were less intensive in comparison with neutron emission, results from TLDs were used for cross-calibration of our indium activation detector *in situ*. According to this cross-calibration, there was an indication that our indium activation detector underestimated neutron yields. We are going to pay more attention to the absolute measurement of neutron yields in future experimental campaigns.

C. Comparison with cylindrical wire array imploding onto deuterated fiber

In this subsection, we present results from the implosion of standard cylindrical tungsten wire arrays onto a fiber as we believe it is valuable to compare the experiment with conical wire arrays with other configurations with similar initial parameters. In the following subsection, we also show results from shots when only a fiber without any imploding wire array was used.

The experimental series with standard tungsten wire-arrays consisted of 17 shots whereas the series with conical wire arrays consisted of 15 shots. We present more detailed results from conical wire array experiments in this paper

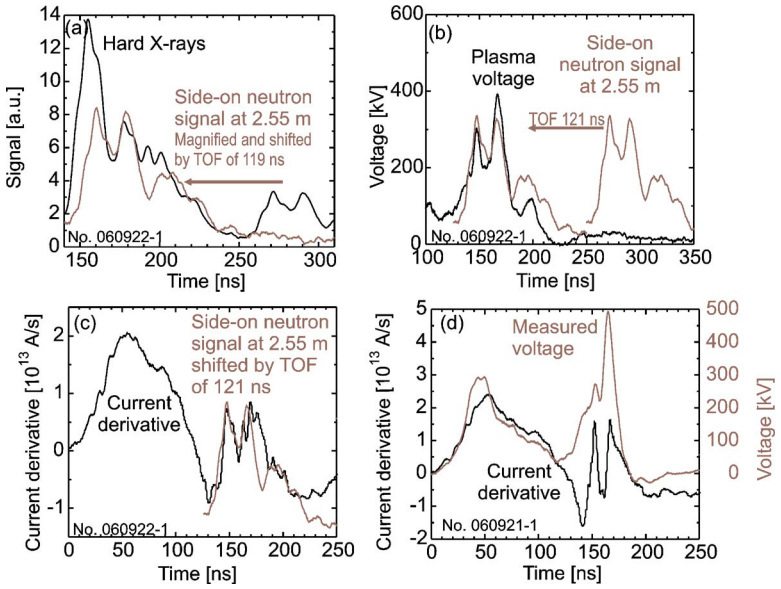

FIG. 8. (Color online) (a)–(c) Examples of the correlation of hard x rays, plasma voltage, and dI/dt signal with neutron emission at the side-on detector in Shot No. 060922-1. 120 ns represents the time-of-flight of 2.4 MeV neutrons to the detector located at 2.55 m. (d) An example of plasma voltage and current dI/dt measured in Shot No. 060921-1.

because diagnostics of cylindrical wire arrays consisted of a lower number of neutron detectors. In the case of the standard wire array, 40 tungsten wires of 5 μm diameter and 10 mm length were used. As far as the conical wire array is concerned, it consisted of 30 tungsten wires of 7 μm diameter and 7 mm length. Both experiments were carried out on the same current generator with similar deuterated fibers and similar currents of about 2 MA.

Also experimental results demonstrated a lot of similarities. The average neutron yield from a standard wire array was about 9×10^8. Thus the neutron yield per length was similar to the one presented above for conical wire arrays. Statistical data from cylindrical and conical wire arrays showed that differences in neutron emission time and neutron spectra were smaller than the shot to shot variation. As an example, we chose the shot displayed in Fig. 11. We would like to present this shot in order to demonstrate that neutrons were emitted after 180 ns, i.e., during the plasma expansion. These features were not so obvious in all shots, but late or delayed neutron emission was observed in the case of conical wire arrays as well.

D. Comparison with fiber Z pinch

During the experimental series with standard tungsten wire arrays, we also tried to initiate the Z pinch from one deuterated fiber only, i.e., without any wire array. Such an experiment seemed to be interesting for comparing our results with those obtained in the 1970s and 1980s.[12,15–17] The average neutron yield of about 1×10^8 was several times lower than in our experiments with the implosion of a wire array onto a fiber. The typical results that we obtained are displayed in Fig. 12. From these images, it can be clearly seen how $m=0$ unstable plasma was expanding from the very beginning of the current. The neutron emission was triggered at about 70 ns and lasted for a relatively long time of more than 60 ns. At this point, it should be said that hard-x-ray and neutron signals in Fig. 12 were taken from the same waveform recorded by the TOF detector at 2.55 m. The temporal uncertainty given by the spread of neutron energies was below 5 ns. This means that there was a real delay between the neutron production and the hard-x-ray emission. Figure 12 shows that the peak neutron energy in the axial (down-

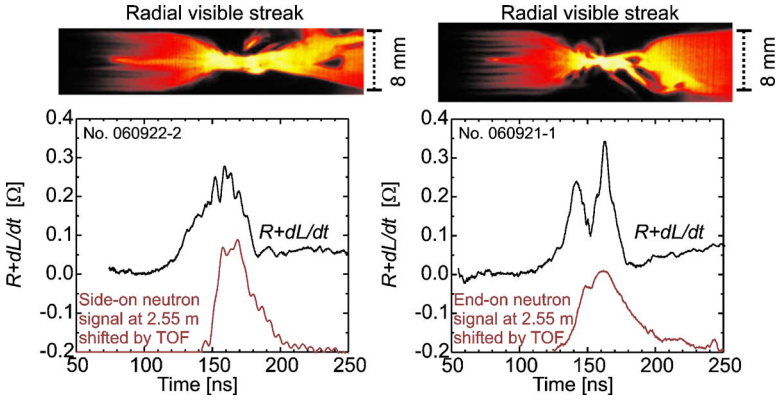

FIG. 9. (Color online) The plasma impedance $R_P+\dot{L}_P$, neutron emission, and streak images in shots No. 060922-2 and No. 060921-1.

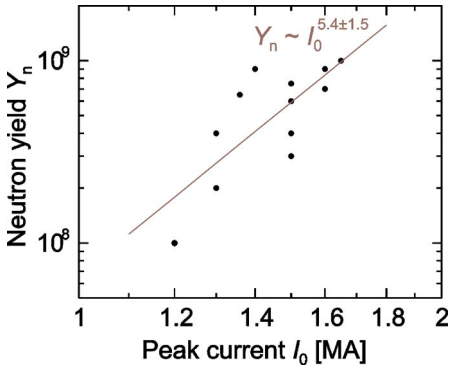

FIG. 10. (Color online) Neutron yield scaling with the current. The conical tungsten wire array imploding onto a deuterated polyethylene fiber.

stream) direction was about 2.65 MeV. Whereas the plasma dynamics and the neutron emission time completely differed from the ones obtained with an imploding wire array, the neutron spectra were very similar (cf. Fig. 12 with Fig. 7). In addition to that, similar spectra were acquired also in our preliminary experiments with a deuterium gas-puff.

V. DISCUSSION OF NEUTRON PRODUCTION MECHANISM

During the past 60 years, plasma theory and modeling were improved to such a degree that it was possible to explain gross dynamics of the discharge as well as a lot of "fine" phenomena of Z pinches. However, several crucial issues such as the mechanism of neutron production have remained unresolved. A recent review on the generation of fast particles was given by Ryutov *et al.*,[39] Haines,[40] and Vikhrev and Korolev.[21] In plasma foci, a lot of experimental results have been obtained and also the neutron production mechanism has been studied up to the present time (see Ref. 41 and references therein). In this respect, experimental data from Z pinches are more rare.

A. Neutron emission anisotropy and beam-target model

Measurements of neutron energies and neutron emission time play an important role in the discussion of the neutron production mechanism. As regards experiments on the S-300 generator, the peak neutron energy detected downstream was shifted from 2.45 MeV toward higher energies in all shots. One could therefore think that a deuteron beam was accelerated toward the anode. However, a small shift above 2.45 MeV could also be a result of significant kinetic energies of fast deuterons (e.g., in a very high-temperature plasma). To exclude this, it was favorable to use neutron detectors also in the upstream axial direction. In our case, upstream neutron energies were smaller than downstream ones. That is why most fusion reactions were realized in the center-of-mass frame, which was moving with respect to the laboratory frame of reference.

Of course, there is still a possibility of a thermonuclear source moving toward the cathode, a so-called moving thermonuclear boiler. But the observed shift to 2.7 MeV [cf. Fig. 4(c)] requires the unreasonable high velocity of about 2×10^8 cm/s toward the cathode. In addition to that, we used such an orientation of the conical wire array that the zippering occurred in the opposite direction, i.e., toward the anode (see Fig. 3). This result indicated that the neutron emission anisotropy was caused by a beam of fast deuterons that were directed toward the cathode and which were colliding with "cold" target deuterons. At this point, we should mention that the neutron emission could be strongly influenced not only by the anisotropic energy distribution function of fast deuterons but also by an inhomogeneous density of target deuterons.

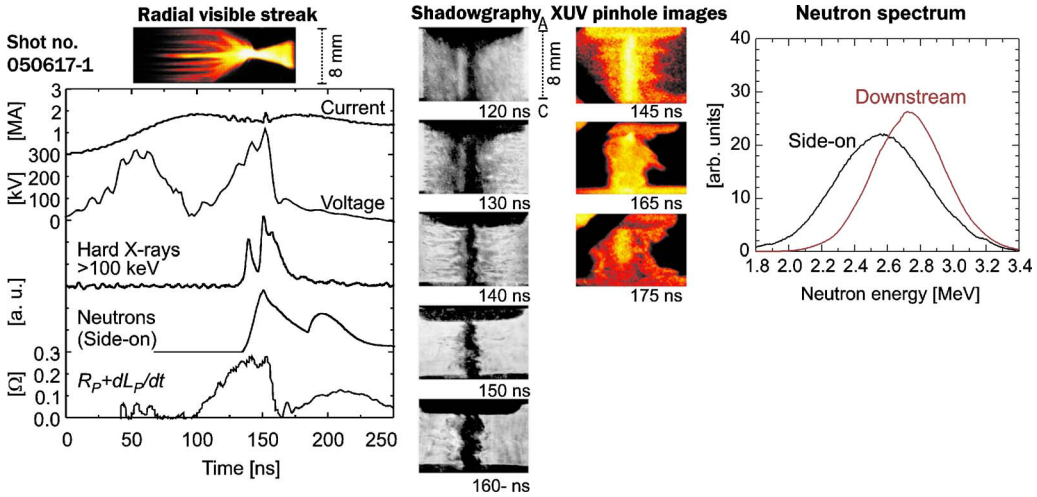

FIG. 11. (Color online) A visible streak image, an XUV pinhole image, shadow images, neutron energy spectra and waveforms of current, voltage, hard x rays, and neutron emission time recorded with the standard tungsten wire array imploding onto a deuterated fiber. Shot No. 050617-1, a neutron yield of about 2.5×10^9.

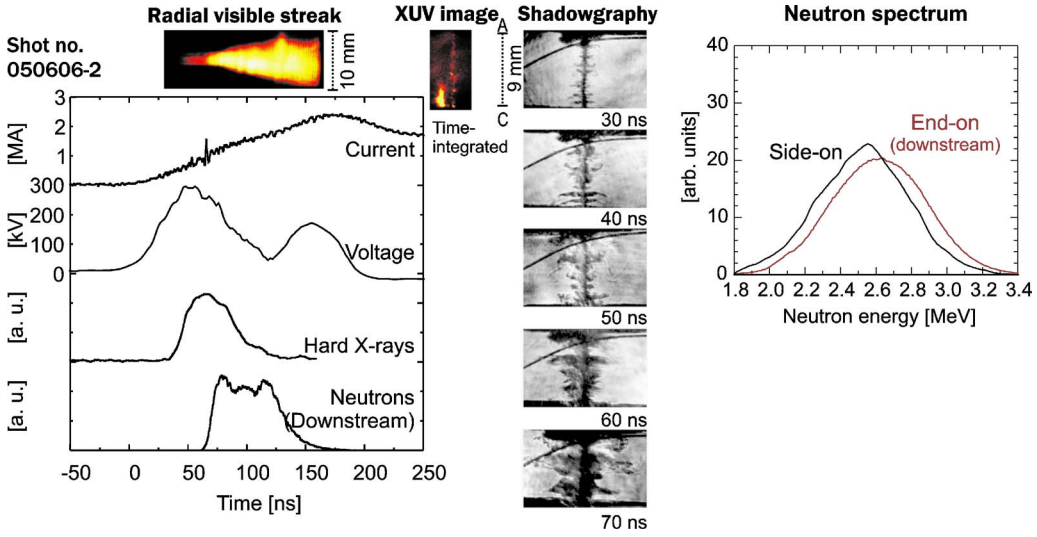

FIG. 12. (Color online) A visible streak image, an XUV pinhole image, shadow images, neutron energy spectra and waveforms of current, voltage, hard x rays, and neutron emission time recorded without an imploding wire array, i.e., only with the deuterated fiber of 100 μm diameter. Shot No. 050606-2, a neutron yield of about 4×10^8.

B. Radial energy component of deuterons and the generalized beam-target model

So far we have discussed results from axial neutron detectors. As regards the side-on direction, an important result is the 450 keV FWHM of neutron energy spectra. Almost the same value was observed in our experiments with a standard wire array (see Fig. 11) or with a fiber (see Fig. 12) as well as in other Z-pinch configurations (gas-embedded Z pinch,[3–5] gas-puff Z pinch,[22] and plasma focus[42,43]). Such a broad width of neutron spectra implies high radial velocity of deuterons. Figures 5 and 7 show that the side-on component of deuteron kinetic energy is comparable with the axial one. It might be a result of magnetic and/or electric fields in Z pinches.

As regards the influence of electric fields, a large component of velocity in all directions could be achieved for instance in a turbulent plasma. If this is not the case, trajectories of deuterons accelerated axially could be curved by magnetic fields. The influence of magnetic field can be evaluated by the ratio between the Larmor r_{Larmor} and pinch radius R. For a deuteron with the kinetic energy E_{d}, the mass m_{d}, the charge e in the magnetic field B produced by the cylindrical current I, the ratio r_{Larmor}/R is given by

$$\frac{r_{\mathrm{Larmor}}}{R}=\frac{m_{\mathrm{d}}\sqrt{2E_{\mathrm{d}}/m_{\mathrm{d}}}}{eBR}=\frac{2\pi\sqrt{2E_{\mathrm{d}}m_{\mathrm{d}}}}{e\mu_0 I}\approx\frac{\sqrt{E_{\mathrm{d}}[\mathrm{MeV}]}}{I[\mathrm{MA}]}. \quad (6)$$

For the deuteron energy $E_{\mathrm{d}}=150$ keV and the current $I=1.5$ MA, we obtain the ratio $r_{\mathrm{Larmor}}/R\approx0.25$, which means that fast deuterons could be confined by the magnetic field within the pinch diameter. In such a case, the classical linear beam target model does not occur. Instead of the rectilinear motion, trajectories of fast deuterons could be rather complex. If we simplify trajectories, deuterons can move similarly as described earlier by Bernstein and Comisar.[42] Such curved trajectories of deuterons could explain not only the observed neutron spectra but also the neutron flux anisotropy. It is known that the neutron emission probability is highly anisotropic at high deuteron energies [cf. Fig. 1(b)]. In the case of the classical rectilinear beam target model, the neutron flux ratio $Y_{\theta_1}/Y_{\theta_2}$ for $\theta_1=0°$ and $\theta_2=90°$ is 2.5 for 150 keV deuterons. If we take into account curved trajectories, however, the flux anisotropy can be substantially decreased. This is probably the reason why the neutron flux anisotropy in most Z-pinch[17,23,24,44] and plasma focus[42,45] experiments was below 1.7.

C. Stopping power and number of accelerated deuterons

Another parameter that determines trajectories of deuterons is the stopping power of fast deuterons. According to Ref. 46, the Coulomb energy loss of fast deuterons E_{d} in a plasma target of the length x could be expressed as

$$\frac{dE_{\mathrm{d}}}{dx}=\frac{n_{\mathrm{bound}}}{n_{\mathrm{bound}}+n_{\mathrm{free}}}\left(\frac{dE_{\mathrm{d}}}{dx}\right)_{\mathrm{cold}}+\frac{n_{\mathrm{free}}}{n_{\mathrm{bound}}+n_{\mathrm{free}}}\left(\frac{dE_{\mathrm{d}}}{dx}\right)_{\mathrm{free}}+\left(\frac{dE_{\mathrm{d}}}{dx}\right)_{\mathrm{ions}}, \quad (7)$$

where n_{bound} and n_{free} represent the density of bound and free electrons, respectively. If we assume homogeneously mixed ions in a stagnated Z pinch and the ratio $n_{\mathrm{bound}}/(n_{\mathrm{bound}}+n_{\mathrm{free}})$ above 1/2, fast deuterons are decelerated mainly by electrons bounded in tungsten ions. This means that

$$\frac{dE_{\mathrm{d}}}{dx}\approx\frac{n_{\mathrm{bound}}}{n_{\mathrm{bound}}+n_{\mathrm{free}}}\left(\frac{dE_{\mathrm{d}}}{dx}\right)_{\mathrm{cold}}\geq\frac{1}{2}\left(\frac{dE_{\mathrm{d}}}{dx}\right)_{\mathrm{cold}}. \quad (8)$$

In the case of 30 tungsten wires of 7 μm diameter and the plasma diameter of about 2 mm, the density of tungsten ions is estimated as 2×10^{19} cm^{-3}. For a 150 keV deuteron, the stopping power $\frac{1}{2}(dE_{\mathrm{d}}/dx)_{\mathrm{cold}}$ calculated with SRIM tables[47] is $\approx$50 keV/mm and the deuteron is decelerated on the length l_{free} of the order of 3 mm.

The number of accelerated deuterons N_d depends on the neutron yield N_n, the D–D fusion cross section $\sigma_{fusion}(E_d)$, the deuteron density n_d, and the length l_{free} as

$$N_d = \frac{N_n}{\sigma_{fusion}(E_d) n_d l_{free}}. \quad (9)$$

For the neutron yield $N_n = 10^9$, the fusion cross section $\sigma_{fusion}(150\ \text{keV}) = 2.8 \times 10^{-30}\ \text{m}^{-2}$ (see Ref. 34), the deuteron density $n_d \approx 10^{20}\ \text{cm}^{-3}$, and the length $l_{free} = 3 \times 10^{-3}$ m, we obtain the number of accelerated deuterons $N_d \approx 10^{15}$.

D. Acceleration mechanisms

When we talk about the neutron production mechanism here, we mean the way deuterons are accelerated. We showed in previous paragraphs that the generalized beam-target model played an important role in our wire array and also fiber Z-pinch experiments. However, it is still not clear how the beam of fast deuterons was created. To discuss this issue, we must look at waveforms of plasma voltage, current, and current derivative.

1. Acceleration by induced electric fields

An obvious result of our experiment was the correlation of 400–500 kV voltage peaks with neutron emission (see Fig. 8). Therefore, it seems reasonable to explain the deuteron acceleration to 150 keV energies by diode action. Also one of the first explanations in the 1950s suggested that charged particles in Z pinches were accelerated by the diode action in a large induced voltage. The observed induced voltage was ascribed to a large increase of the inductance $\dot{L}_P > 0$, which resulted from the growth of instabilities[4] or from the collapsing of the main plasma column.[48] The question we should ask here is what electric field $\vec{E}$ occurs in the plasma? Even though the voltage peak across the plasma is measured, it is not clear that a high electric field is also seen by deuterons. In the presence of time-varying magnetic fields, it cannot be assumed that the measured voltage is given only by the integration of the axial electric field E_z along the length of a plasma column. Besides that, as has already been pointed out,[49] the electric field seen by ions in an imploding plasma is $\vec{E} + \vec{v} \times \vec{B} = 0$.

The drawback of the acceleration model described above is its limitation on the imploding plasma. As regards our results, we observed similar phenomena as other researchers in many Z-pinch and plasma focus experiments (see, for instance, Refs. 5, 44, and 50–53): neutrons were generated mainly after the plasma implosion during the stagnation and during the global plasma expansion when the dI/dt signal was rising. That is, for example, why Trubnikov[54] and Uhm[55] extended the acceleration mechanism based on induced fields also for the plasma expansion. Trubnikov considered a rapid transfer of a current to a peripheral plasma. A high transient electric field then accelerates deuterons that are not coiled by the magnetic field. Because it is necessary to explain high radial velocities of deuterons, axially accelerated deuterons have to be bent by magnetic fields before they produce fusion neutrons. Another issue that should be discussed here is the negative value of induced voltage $\dot{L}_P I$ during the expansion.

2. Role of microturbulence and enhanced resistance

A more realistic approach was considered by the authors in Refs. 40, 42, 44, 51, and 56. Even though there are differences in argumentation, all these authors emphasized the role of microturbulence and anomalous resistance during the plasma stagnation and expansion. The role of microturbulence lies in the fact that it can cause rapid magnetic field diffusion and fast current redistribution. Then, a large $\partial \vec{B}/\partial t$ could accelerate ions in one direction near the axis and in the opposite direction in the peripheral plasma. Besides, microturbulence could not only generate induced electric fields but also form a high-energy tail of the ion distribution function.[39,57] From an experimental point of view, the onset of microinstabilities just before neutron emission was clearly shown by Bernard *et al.* with laser scattering in a plasma focus discharge.[43] The measured plasma resistance during the plasma stagnation exceeded the Spitzer value and reached 0.2–0.4 Ω for a broad energy range of plasma focus machines.[56,57]

As regards our experiment, we measured the $(R_P + \dot{L}_P)$ term (see Fig. 9). On the one hand, the measured value of about 0.2–0.4 Ω during the implosion could be ascribed to a time-varying inductance. Then the energy would be naturally coupled from the generator through the $\dot{L}_P$ term. But on the other hand, it is impossible to explain a 40 ns duration of 0.2 Ω by a constantly increasing plasma inductance only. If the plasma resistance is neglected, there is no evidence of the plasma expansion and the total increase of inductance $\Delta L_P = \int \dot{L}_P dt$ is about 10 nH. Such an inductance increase of the 7 mm long plasma column requires the collapse to a 10 μm diameter. A more likely explanation of the inductance rise is the increase of the effective plasma length. This might be a result of complex helical structures that develop usually after the stagnation.[58] However, the main argument against neglecting plasma resistance is that the magnetic energy $\frac{1}{2}\Delta L_P I^2 \doteq 10$ kJ could be hardly stored at the time when the plasma column expanded to a few millimeter diameter and when a significant fraction of the energy had already emitted from the plasma. This led us to a conclusion that the influence of resistive heating during the stagnation was growing. For the Spitzer resistance and for experimentally estimated values during the stagnation (plasma radius $R = 1$ mm, length $l = 5 \times 10^{-3}$ m, electron temperature $kT_e = 50$ eV, effective charge $\bar{z} = 10$, and Coulomb logarithm $\ln \Lambda \doteq 10$), we get

$$R_P \doteq \frac{10^{-4} \bar{z} \ln \Lambda}{kT_e^{3/2}} \cdot \frac{l}{\pi R^2} \doteq 0.05\ \Omega.$$

Since the result comes out less than 0.2 Ω, the classical Spitzer resistivity is also insufficient to explain the measured value of the plasma impedance.

Here, the research of neutron emission is related to the energy conservation, which has recently become a debated issue in wire-array Z pinches (see, e.g., Refs. 27, 58, and 59).

Already 25 years ago, however, Riordan *et al.* pointed out that the observed radiation yield was significantly higher than the kinetic energy input.[60] From that time on, several models have been suggested to explain the observed discrepancy. In this respect, the enhanced resistance was considered as an explanation, for instance, by Whitney with his colleagues in Saturn experiments.[61] On the MAGPIE generator, Chittenden explained the enhancement of ohmic heating by the onset of $m=1$ instabilities after the secondary implosion of trailing mass.[62]

3. Thermonuclear neutrons

Our experiments demonstrated the strong correlation between neutron emission and measured plasma voltage. The question that still remains is whether the acceleration mechanism is connected with a high voltage induced across a plasma column (see Sec. V D 1), or with ion acceleration in microturbulence (see Sec. V D 2), or with the power input into a plasma. The process mentioned last is closely related to the thermonuclear origin of neutrons and it was explored mainly by Vikhrev in Refs. 21, 63, and 64. The adiabatic heating in necks of $m=0$ instabilities was considered also by Young *et al.* in experiments with deuterated polyethylene fibers of >50 μm diameter.[17] Riley and colleagues pointed out that it is impossible to interpret neutron measurements in fiber Z pinches if the ion temperature equals the electron temperature. Instead of it, they explained observed neutron yields by the direct heating of ions within turbulence arising from instability growth.[65] Recently, the ion temperature higher than the temperature of electrons was assumed by Velikhovich *et al.* in the calculation of thermonuclear yields in a deuterium gas-puff.[23]

From the experimental point of view, thermonuclear D–D fusion reactions in the center-of-mass frame of reference are characterized by isotropic neutron emission and by a mean neutron energy of about 2.45 MeV. It is evident from Figs. 4(b) and 4(c) that most of the neutrons in our experiments came from the beam-target interaction. However, it is still possible that the beam originated from a Maxwellian plasma or from another isotropic ion energy distribution. For example, the beam of fast deuterons could be accelerated within a high-temperature plasma and afterwards it escaped and penetrated through a low-temperature plasma where fusion neutrons were produced. Consequently, the observed neutron emission anisotropy could be a result of strong magnetic and electric fields[21,64] as well as a result of anisotropy of target deuterons. In all cases, however, a broad neutron energy spectrum requires a relatively high temperature. According to the equation $\Delta E_{\mathrm{d}}(\mathrm{keV})=82.5\sqrt{kT_{\mathrm{i}}[\mathrm{keV}]}$ (e.g., Ref. 28), the width of a neutron spectrum $\Delta E_{\mathrm{d}}=500$ keV corresponds to the equivalent ion temperature $kT_i \approx 30$ keV. Such a high temperature could be achieved locally in a small volume, otherwise the neutron yield would be much higher. In our experiment, for instance, if we assume that the neutron yield of 10^9 was thermonuclear and originated from the bulk of plasma, we obtain plasma temperatures of about 2 and 100 keV width of a neutron spectrum.

But even though we admitted that a fraction of fast deuterons was accelerated by elastic collisions in a high-temperature locality, it could not be referred to as thermonuclear fusion and also it would not be useful for energy production. If deuterons escape a high-temperature region, they are slowed down by cold deuterons usually without undergoing fusion reactions. The fusion energy released is always smaller than the energy expended on the acceleration of fast deuterons. The only way how to achieve the energy gain is to transfer the lost energy of fast deuterons to the acceleration of other deuterons in the same plasma, i.e., to achieve the energy feedback. For that purpose, it is necessary to keep fast deuterons in a high-temperature region or to use fast deuterons for heating of a surrounding plasma to a fusion temperature. As regards Z pinches, a magnetic field seems to have the crucial importance in prevention of fast deuterons from escaping a plasma.

At this point, we would like to go back to the discussion of the model of deuteron acceleration. The problem of the acceleration mechanism is that it should clarify not only the observed peak value of plasma voltage but also a comparatively long duration of neutron emission. On the one hand, there does not seem to be a problem to ascribe 400 kV voltage peaks to a large rise of the inductance dL_P/dt, the current rise dI/dt, and the resistance R_P. But on the other hand, it is necessary to elucidate up to 40 ns long neutron emission at the post-stagnation phase. We believe that the acceleration mechanism in a turbulent plasma perhaps fits best to a prolonged neutron emission and to broad side-on neutron spectra. The onset of microturbulence then could induce high plasma voltage as well as form a high-energy tail in deuteron velocity distribution. Nevertheless, the origin of microturbulence and a more detailed description of the acceleration mechanism are beyond our possibilities of experimental data interpretation. However unclear this issue may be, it holds that the research of the neutron origin is connected with the study of plasma voltage and with the power input into a plasma. It follows that the acceleration is connected with the global plasma dynamics and that the deuteron acceleration is not a "secondary" process in plasma.

VI. CONCLUSION

The implosion of a conical wire array Z pinch onto a deuterated polyethylene fiber was studied on the S-300 pulsed power generator at the Kurchatov Institute. The study of neutron emission in these experiments was focused mainly on the estimation of neutron energies and neutron emission time. The neutron measurement was used to obtain significant data about acceleration of fast ions in Z-pinch plasmas.

First, as regards neutron energies in the side-on direction, the neutron energy spectrum peaked at 2.48 ± 0.05 MeV with 450 ± 100 keV FWHM. In the downstream direction, the peak neutron energy and the width of a neutron spectrum were 2.65 ± 0.10 MeV and 350 ± 100 keV, respectively. The knowledge of neutron spectra at different directions relative to the Z-pinch axis provided information about the energy of deuterons that produced fusion reactions.

The average kinetic energy of reacting deuterons was about 150 keV. Most of the deuterons were directed toward the cathode. The broad width of neutron spectra implied a high radial velocity of deuterons. Therefore, trajectories of deuterons producing fusion reactions seemed to be strongly influenced by magnetic and/or turbulent electric fields. This observation was made also in experiments with an imploding standard wire array as well as in fiber Z pinch.

Moving to the second subject of our interest, i.e., neutron emission time, the neutron pulse temporally correlated with hard x rays and also with measured voltage. The neutron emission lasted on average 30 ± 5 ns (FWHM) and was observed at the end of implosion and during the expansion of a plasma column. At this moment, the $R_P + \dot{L}_P$ term reached $0.2-0.4\ \Omega$. During the implosion, this value could be ascribed to a time-varying inductance $\dot{L}_P$ whereas in the post-stagnation phase the plasma impedance was probably dominated by enhanced resistance, R_P. For that reason, the neutron emission is supposed to be a multiphase process and we believe that the prolonged neutron emission is connected with the enhanced resistance. We would like to prove this in future experiments.

Recently, we have prepared a deuterium gas-puff in order to interpret experimental results and to compare them with those obtained in other Z-pinch devices. Should we conclude with what we expect from this modification, we do hope that the interpretation of Z-pinch experiments with pure deuterium will be more straightforward in comparison with a heterogeneous mixture of tungsten, carbon, and deuterium ions.

ACKNOWLEDGMENTS

We wish to thank Professor A. S. Kingsep (RRC Kurchatov Institute, Moscow) for his valuable comments and Dr. G. N. Timoshenko (Laboratory of Radiation Biology of JINR, Dubna) for his kind help with Bonner spheres.

This research has been supported by Research Program Nos. LA08024, 1P05ME761, and LC528 of the Ministry of Education and by Grant No. 202-08-P084 of the Grant Agency of the Czech Republic.

APPENDIX: SCATTERED NEUTRONS

The advantage of time-of-flight (TOF) detectors located in mutually opposite directions concerns neutron scattering. A large number of scattered neutrons forms the tail of TOF signals. It causes the shift of measured neutron energies to lower values. So far, the Monte Carlo ray-tracing of neutrons[66] between the neutron source and TOF detectors has been performed only for a small part of the diagnostic arrangement. Therefore, we tested the influence of scattered neutrons on our reconstruction by the use of artificial energy distribution function $f_0(E_n,t)$ which was modified by scattered neutrons (the average energy decrease of about 0.1 MeV). According to this modified distribution function $f_M(E_n,t)$, test neutron signals $S(x,T)$ were generated at the TOF detectors. On the basis of these TOF signals, we wanted to reconstruct the original distribution function $f_0(E,t)$ by our Monte Carlo simulation. In the case of TOF detectors on both sides of the neutron source, it was not possible to simulate a large number of low-energy neutrons in one direction from the neutron source because it required a large number of high-energy neutrons in the opposite direction. As a result, we found out that our Monte Carlo reconstruction suppressed the influence of scattered neutrons and that the test energy spectrum was reconstructed correctly. Including the temporal resolution of TOF detectors, the systematic error of neutron energy reconstruction in our experiment was estimated below 0.1 and 0.05 MeV for the end-on and side-on direction, respectively. With regard to the time of neutron emission, it was a little delayed in comparison with the original test distribution function. Therefore, it seemed more accurate to calculate the emission time from the nearest TOF detector. Of course, due to a small number of TOF detectors, it was not possible to determine unambiguously the shape of the neutron energy spectrum. Yet from the chain of four TOF detectors, two basic moments of the energy distribution function (i.e., the mean energy and the width of spectrum) could be estimated.

[1] T. Sandford, G. Allshouse, B. Marder *et al.*, Phys. Rev. Lett. **77**, 5063 (1996). R. Spielman, C. Deeney, G. Chandler *et al.*, Phys. Plasmas **5**, 2105 (1998).
[2] M. G. Haines, Plasma Phys. Controlled Fusion **38**, 643 (1996); S. W. Cousins and A. A. Ware, Proc. Phys. Soc. London, Sect. B **64**, 159 (1951); P. Thonemann, Nature **181**, 217 (1958).
[3] J. W. Mather and A. H. Williams, in *Proceedings of the 2nd United Nations International Conference on Peaceful Uses of Atomic Energy, Geneva, 1958*, edited by J. H. Martens *et al.* (United Nations, Geneva, Switzerland, 1958), Vol. 32, p. 26; J. L. Tuck, *ibid.*, Vol. 32, p. 3; R. F. Post, Rev. Mod. Phys. **28**, 338 (1956).
[4] O. A. Anderson, W. R. Baker, S. A. Colgate, J. Ise, and R. V. Pyle, Phys. Rev. **110**, 1375 (1958).
[5] A. M. Andrianov, O. A. Bazilevskaia, S. I. Braginski *et al.*, in *Proceedings of the 2nd United Nations International Conference on Peaceful Uses of Atomic Energy, Geneva, 1958*, edited by J. H. Martens *et al.* (United Nations, Geneva, Switzerland, 1958), Vol. 31, p. 348; L. A. Artsimovich, *ibid.*, p. 6; I. V. Kurchatov, At. Energy **1**, 359 (1956).
[6] E. von Funfer, H. Herold, G. Lehner, H. Tuczek, and C. Andelfinger, Z. Naturforsch. A **13A**, 524 (1958); K. Nishiguchi, H. Maruo, Y. Arata, and M. Okada, J. At. Energy Soc. Jpn. **1**, 115 (1959); S. Berglund, R. Nilsson, P. Ohlin, K. Siegbahn, T. Sundstrom, and S. Svennerstedt, Nucl. Instrum. **1**, 233 (1957).
[7] See National Technical Information Service Document No. LA3253 (Review of Controlled Thermonuclear Research at Los Alamos 1965, LANL Rep. LA-3253-MS, 1965). Copies may be ordered from National Technical Information Service, Springfield, VA 22161.
[8] A. Bernard, J. P. Garconnet, A. Jolas, J. P. Le Breton, and J. de Mascureau, in *Plasma Physics and Controlled Fusion Research (IAEA-CN-37), 7th IAEA Conference on Plasma Physics and Controlled Nuclear Fusion, Innsbruck, 1978* (IAEA, Vienna, 1979), Vol. 2, p. 159.
[9] N. V. Filippov, T. I. Filippova, and V. P. Vinogradov, Nucl. Fusion **2**, 577 (1962).
[10] J. E. Hammel, D. W. Scudder, and J. S. Shlachter, Nucl. Instrum. Methods Phys. Res. **207**, 161 (1983).
[11] D. W. Scudder, Bull. Am. Phys. Soc. **30**, 1408 (1985); N. R. Pereira, N. Rostoker, J. Riordan, and M. Gersten, in *Proceedings of the 1st International Conference on Dense Z-Pinches for Fusion, Alexandria, VA, 1984*, edited by J. D. Sethian and K. A. Gerber (Naval Research Laboratory, Washington, DC, 1984), p. 71; J. E. Hammel, D. W. Scudder, and J. S. Schlachter, *ibid.*, p. 13.
[12] J. D. Sethian, A. E. Robson, K. A. Gerber, and A. W. DeSilva, Phys. Rev. Lett. **59**, 892 (1987).
[13] J. Sethian, A. Robson, K. Gerber, and A. DeSilva, *Proceedings of the*

Workshop on Physics of Alternative Magnetic Confinement Schemes, Varenna, 1990, edited by S. Ortolani and E. Sindoni (Editrice Compositori, Bologna, Italy, 1991), p. 511.
[14]D. W. Scudder, *Proceedings on the Workshop on Physics of Alternative Magnetic Confinement Schemes, Varenna, 1990*, edited by S. Ortolani and E. Sindoni (Editrice Compositori, Bologna, Italy, 1991), p. 519.
[15]W. Kies, G. Decker, M. Malzig *et al.*, J. Appl. Phys. **70**, 7261 (1991).
[16]S. V. Lebedev, R. Aliaga-Rossel, J. P. Chittenden, I. H. Mitchell, A. E. Dangor, M. G. Haines, and J. F. Worley, Phys. Plasmas **5**, 3366 (1998).
[17]S. Stephanakis, L. Levine, D. Mosher, I. Vitkovitsky, and F. Young, Phys. Rev. Lett. **29**, 568 (1972); F. Young, S. Stephanakis and D. Mosher, J. Appl. Phys. **48**, 3642 (1977).
[18]K. C. Mittal, K. A. Gerber, and J. D. Sethian, J. Appl. Phys. **70**, 6712 (1991).
[19]S. Lee and H. Conrads, Phys. Lett. **57A**, 233 (1976).
[20]Yu. L. Bakshaev, P. I. Blinov, V. V. Vikhrev *et al.*, Plasma Phys. Rep. **32**, 531 (2006).
[21]V. V. Vikhrev and V. D. Korolev, Plasma Phys. Rep. **33**, 356 (2007).
[22]A. Batyunin, Sov. J. Plasma Phys. **16**, 597 (1990).
[23]A. L. Velikovich, R. W. Clark, J. Davis *et al.*, Phys. Plasmas **14**, 022701 (2007); C. A. Coverdale, C. Deeney, A. L. Velikovich *et al.*, *ibid.* **14**, 022706 (2007); **14**, 056309 (2007).
[24]See National Technical Information Service Document No. DE98007273 (R. B. Spielman *et al.*, D–D fusion experiments using fast Z pinches, Sandia National Laboratories, Rep. SAND98-0705, 1998). Copies may be ordered from National Technical Information Service, Springfield, VA 22161.
[25]I. Mitchell, J. Gomez, S. Lebedev, S. Bland, J. Chittenden, D. Ampleford, S. Bott, and G. Hall, Bull. Am. Phys. Soc. **49**, 334 (2004).
[26]D. Klir, P. Kubes, J. Kravarik *et al.*, Plasma Devices Oper. **13**, 39 (2005).
[27]M. G. Haines, P. D. LePell, C. A. Coverdale, B. Jones, C. Deeney, and J. P. Apruzese, Phys. Rev. Lett. **96**, 075003 (2006).
[28]B. Wolle, Phys. Rep. **312**, 1 (1999).
[29]C. K. Li, F. H. Seguin, D. G. Hicks *et al.*, Phys. Plasmas **8**, 4902 (2001); G. Pretzler, A. Saemann, A. Pukhov *et al.*, Phys. Rev. E **58**, 1165 (1998); T. Ditmire, J. Zweiback, V. P. Yanovky, T. E. Cowan, G. Hays, and K. B. Wharton, Nature **398**, 489 (1999); V. P. Krainov and M. B. Smirnov, Phys. Rep. **370**, 237 (2002).
[30]I. Tiseanu, G. Decker, and W. Kies, Nucl. Instrum. Methods Phys. Res. A **373**, 73 (1996); I. Tiseanu and I. Craciunescu, Nucl. Sci. Eng. **47**, 384 (1996).
[31]K. Rezac, D. Klir, P. Kubes, J. Kravarik, and M. Stransky, Czech. J. Phys. **56**, B357 (2006).
[32]K. Rezac, D. Klir, J. Kravarik *et al.*, *Conference Proceedings of Contributed Papers, 34th EPS Conference on Plasma Physics, Warsaw, 2007*, edited by P. Gasior and J. Wolowski (European Physical Society, Petit Lancy, 2007), Vol. 31F, p. P-1.016.
[33]M. Drosg and O. Schwerer, in *Production of Monoenergetic Neutrons Between 0.01 and 23 MeV*, Handbook of Nuclear Activation Data (IAEA, Vienna, 1987), p. 111.
[34]M. B. Chadwick, P. Oblozinsky, M. Herman *et al.*, Nucl. Data Sheets **107**, 2931 (2006).
[35]A. S. Chernenko, Yu. M. Gorbulin, Yu. G. Kalinin *et al.*, in *Proceedings of the 11th International Conference on High Power Particle Beams, Prague, 1996*, edited by J. Ullschmied (Academy of Science of Czech Republic, Prague, 1996), Vol. 1, p. 154; Yu. L. Bakshaev, A. S. Chernenko, V. D. Korolev *et al.*, *ibid.*, Vol. 2, p. 962.
[36]Yu. L. Bakshaev, P. I. Blinov, A. S. Chernenko *et al.*, Rev. Sci. Instrum. **72**, 1210 (2001).
[37]D. Klir, P. Kubes, and J. Kravarik, IEEE Trans. Plasma Sci. **34**, 2303 (2006).
[38]A. Velyhan, J. Krasa, B. Bienkowska *et al.* Phys. Scr., T **123**, 112 (2006).
[39]D. D. Ryutov, M. S. Derzon, and M. K. Matzen, Rev. Mod. Phys. **72**, 167 (2000).
[40]M. G. Haines, Laser Part. Beams **19**, 345 (2001).
[41]L. Soto, Plasma Phys. Controlled Fusion **47**, A361 (2005); Y. Mizuguchi, J. I. Sakai, H. R. Yousefi, T. Haruki, and K. Masugata, Phys. Plasmas **14**, 032704 (2007); V. A. Gribkov, A. Banaszak, B. Bienkowska *et al.*, J. Phys. D **40**, 3592 (2007).
[42]M. J. Bernstein and G. G. Comisar, Phys. Fluids **15**, 700 (1972).
[43]A. Bernard, A. Coudeville, A. Jolas, J. Lauspach, and J. de Mascreau, Phys. Fluids **18**, 180 (1975).
[44]I. H. Mitchell, R. Aliaqa-Rossel, J. P. Chittenden, A. Robledo, H. Schmidt, and M. G. Haines, IEEE Trans. Plasma Sci. **26**, 1267 (1998).
[45]H. Schmidt, P. Kubes, M. Sadowski, and M. Scholz, IEEE Trans. Plasma Sci. **34**, 2363 (2006).
[46]G. Belyaev, M. Basko, A. Cherkasov *et al.*, Phys. Rev. E **53**, 2701 (1996).
[47]J. F. Ziegler, Nucl. Instrum. Methods Phys. Res. B **219-220**, 1027 (2004).
[48]H. A. Bodin, R. A. Fitch, and N. J. Peacock, J. Nucl. Energy, Part C **1**, 206 (1960).
[49]M. G. Haines, Nucl. Instrum. Methods Phys. Res. **207**, 179 (1983); G. McCall, Phys. Rev. Lett. **62**, 1986 (1989).
[50]M. J. Bernstein, Phys. Rev. Lett. **24**, 724 (1970); M. J. Bernstein and F. Hai, *ibid.* **25**, 641 (1970).
[51]T. Yamamoto, K. Shimoda, K. Kobayashi, and K. Hirano, Jpn. J. Appl. Phys., Part 1 **23**, 242 (1984).
[52]W. Kies, G. Decker, U. Berntien, Yu. V. Sidelnikov, D. A. Gluskov, K. N. Koshelev, D. M. Simanovskii, and S. V. Bobashev, Plasma Sources Sci. Technol. **9**, 279 (2000).
[53]P. Kubes, J. Kravarik, D. Klir *et al.*, IEEE Trans. Plasma Sci. **34**, 2349 (2006).
[54]B. A. Trubnikov, Sov. J. Plasma Phys. **12**, 271 (1986).
[55]H. S. Uhm and T. N. Lee, Phys. Rev. A **40**, 3915 (1989).
[56]G. Decker, W. Kies, and G. Pross, Phys. Fluids **26**, 571 (1983).
[57]A. Bernard, Atomkernenergie **32**, 73 (1978).
[58]R. B. Spielman, J. S. DeGroot, T. J. Nash, J. McGurn, L. Ruggles, M. Vargas, and K. G. Estabrook, AIP Conf. Proc. **299**, 404 (1994).
[59]L. I. Rudakov, A. L. Velikhovich, J. Davis, J. W. Thornhill, J. L. Giuliani, and C. Deeney, Phys. Rev. Lett. **84**, 3326 (2000).
[60]J. Riordan, J. Pearlman, M. Gersten, and J. Rauch, AIP Conf. Proc. **75**, 35 (1981).
[61]K. G. Whitney, J. W. Thornhill, J. P. Apruzese, J. Davis, C. Deeney, and C. A. Coverdale, Phys. Plasmas **11**, 3700 (2004).
[62]J. P. Chittenden, S. V. Lebedev, C. A. Jennings, S. N. Bland, and A. Ciardi, Plasma Phys. Controlled Fusion **46**, B457 (2004).
[63]V. V. Vikhrev, Sov. J. Plasma Phys. **12**, 262 (1986).
[64]V. V. Vikhrev, Sov. J. Plasma Phys. **15**, 339 (1989).
[65]R. Riley, D. Scudder, J. Shlachter, and R. Lovberg, Phys. Plasmas **3**, 1314 (1996).
[66]See National Technical Information Service Document No. DE87000708 (J. F. Briesmeister, MCNP: A general Monte Carlo code for neutron and photon transport, LANL Report, 1986). Copies may be ordered from National Technical Information Service, Springfield, VA 22161.

ARTICLE NO. 3

Neutron Energy Distribution Function Reconstructed From Time-of-Flight Signals in Deuterium Gas-Puff Z-Pinch

Daniel Klir, Jozef Kravarik, Pavel Kubes, *Member, IEEE*, Karel Rezac, Sergey S. Ananev, Yuriy L. Bakshaev, Peter I. Blinov, Andrey S. Chernenko, Evgeny D. Kazakov, Valery D. Korolev, Gennadiy I. Ustroev, Libor Juha, Josef Krasa, and Andriy Velyhan

***Abstract*—The implosion of a solid deuterium gas-puff Z-pinch was studied on the S-300 pulsed power generator [A. S. Chernenko, *et al.*, Proceedings of 11th Int. Conf. on High Power Particle Beams, 154 (1996)]. The peak neutron yield above 10^{10} was achieved on the current level of 2 MA. The fusion neutrons were generated at about 150 ns after the current onset, i.e., during the stagnation and at the beginning of the expansion of a plasma column. The neutron emission lasted on average 25 ns. The neutron energy distribution function was reconstructed from 12 neutron time-of-flight signals by the Monte Carlo simulation. The side-on neutron energy spectra peaked at 2.42 $\pm$ 0.04 MeV with about 450-keV FWHM. In the downstream direction (i.e., the direction of the current flow from the anode toward the cathode), the peak neutron energy and the width of a neutron spectrum were 2.6 $\pm$ 0.1 MeV and 400 keV, respectively. The average kinetic energy of fast deuterons, which produced fusion neutrons, was about 100 keV. The generalized beam-target model probably fits best to the obtained experimental data.**

***Index Terms*—Deuterium, fusion reaction, gas puff, Monte Carlo reconstruction, neutron energy spectra, neutrons, Z-pinch.**

I. Introduction

AT PRESENT, Z-pinches are intensively researched as powerful and efficient laboratory sources of soft X-rays [1], [2]. Whereas a large number of papers is devoted to studies of EUV and soft X-ray radiation, experimental data about fast ions are rather rare. One of those very few examples is the recent measurement of an ion temperature in wire-arrays at the Z-machine [3]. The Doppler-width of iron spectral lines indicated that the ion temperature exceeded 200 keV. In this respect, also fusion neutron measurements could provide invaluable data for Z-pinch physics since they give insight into the acceleration of fast ions. Recently, the highest neutron yield from the $\mathrm{D}(d,\mathrm{n})^3\mathrm{He}$ fusion reaction of 6×10^{13} has been achieved with a double-shell deuterium gas puff on the 17 MA current level [4], [5]. With regard to the overall neutron yield in this experiment, there is a hope for a large thermonuclear component; however, an unambiguous evidence has not been yet provided.

The results previously mentioned indicate that there is a need of more experimental data about fast ions. For that purpose, we measured the production of fusion neutrons on the S-300 generator at the Kurchatov Institute in Moscow. We carried out Z-pinch experiments with: 1) deuterated fibers; 2) various types of wire arrays imploding onto a deuterated fiber; and 3) deuterium gas puffs as Z-pinch loads. Because results from fiber and wire-array Z-pinches have been already published in [6], in this paper, we particularly focus on experiments with deuterium gas puffs. The structure of this paper is the following: The experimental arrangement and diagnostics used in our experiment are described in Section II (the emphasis was put mainly on the comprehensive neutron time-of-flight (TOF) diagnostics). Section III provides the most important experimental results which are then discussed in Section IV. Finally, results are summarized in Section V.

II. Experimental Arrangement and Diagnostics

A. Experimental Setup

The implosion of a solid deuterium gas-puff Z-pinch was studied on the S-300 pulsed power generator (4-MA peak current, 700-kV voltage, 100-ns rise time, 0.15-Ω impedance) at the Kurchatov Institute in Moscow [7], [8]. This paper presents results from the experimental series of ten shots at the current level of 2 MA.

The gas-puff hardware was designed according to the gas valve used on the Angara-5 device [9]. A photograph of the gas-puff anode and cathode can be seen in Fig. 1. The separation between the cathode and the anode was 10 mm. The

Manuscript received July 25, 2008; revised October 3, 2008. First published February 10, 2009; current version published March 11, 2009. This work was supported in part by the Grant Agency of the Czech Republic under Grant 202-08-P084, by the Ministry of Education under Research Programs LA08024, ME09087, and LC528, and by the IAEA under Grant RC14817.

D. Klir, J. Kravarik, P. Kubes, and K. Rezac are with Czech Technical University in Prague, 166 27 Prague, Czech Republic (e-mail: klird1@fel.cvut.cz; kravarik@fel.cvut.cz; kubes@fel.cvut.cz; rezack@fel.cvut.cz).

S. S. Ananev, Y. L. Bakshaev, P. I. Blinov, A. S. Chernenko, E. D. Kazakov, V. D. Korolev, and G. I. Ustroev are with the Russian Research Center "Kurchatov Institute," 123182 Moscow, Russia (e-mail: seregin2000@mail.ru; bak@dap.kiae.ru; blinov@dap.kiae.ru; chernenko@dap.kiae.ru; evgenische@gmail.com; korolev@dap.kiae.ru; gustroev@dap.kiae.ru).

L. Juha and J. Krasa are with the Institute of Physics, Academy of Sciences of the Czech Republic, 182 21 Prague, Czech Republic (e-mail: juha@fzu.cz; krasa@fzu.cz).

A. Velyhan is with the Institute of Physics, Academy of Sciences of the Czech Republic, 182 21 Prague, Czech Republic (e-mail: velyhan@fzu.cz).

Color versions of one or more of the figures in this paper are available online at http://ieeexplore.ieee.org.

Digital Object Identifier 10.1109/TPS.2008.2010860

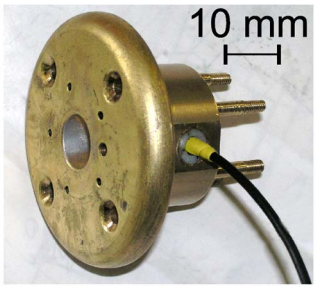

(a)

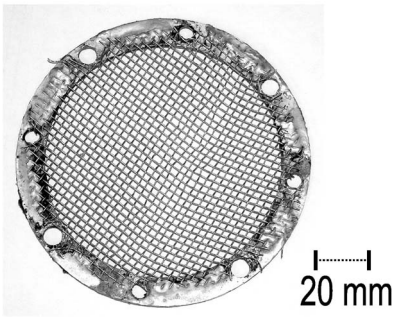

(b)

Fig. 1. Deuterium gas-puff hardware. (a) Cathode, gas-puff nozzle. (b) Anode, stainless steel mesh.

anode was formed by a stainless steel mesh. The gas puff was triggered by an electrical spark which ignited gunpowder. A Teflon piston driven by the burning gunpowder then compressed the deuterium gas in a closed volume below the nozzle. The deuterium gas entered the nozzle when the gas pressure broke through a 0.2-mm-thick stainless steel foil. The delay between the detection of the deuterium gas in the nozzle and the current generator start-up was set up between 10 and 40 μs. The outer diameter of the conical solid deuterium gas puff was 10 mm and about 15 mm at the cathode and at the anode, respectively. At the time of the current onset, we expected the line deuterium gas density of $5 \div 50$ μg/cm. The gas density profile has not been characterized so far since our primary intention was to implement and to test extended TOF method for the determination of neutron energy spectra [10], [11]. We would like to apply a high number of neutron TOF detectors in order to study the anisotropy of neutron energy distribution function in Z-pinch plasmas, and we used the deuterium gas puff as a suitable source of neutrons.

B. Diagnostics

In order to observe Z-pinch discharges that show specific experimental results in each shot, it is important to use simultaneously comprehensive diagnostics with temporal, spatial, and spectral resolution. The diagnostic setup, part of which was described in [12], is shown in Fig. 2.

First, in order to provide time and space resolved information about visible emission, a radial optical streak camera was used. The plasma 5 mm away from the cathode was imaged on the streak camera slit. Furthermore, an optical frame camera provided three 2-D images with 3-ns exposure and 20-ns interframe separation.

Second, X-ray radiation was detected with a pinhole camera and a semiconductor diode. The X-ray pinhole camera, time integrated and differentially filtered (with 2-μm Al, 10-μm Al, and 15-μm Cu filters), was used to observe the plasma in various spectral ranges with a spatial resolution of 100 μm. Time-resolved information about X-rays from 1 to 40 keV was obtained with the semiconductor diode SPPD11-4 [13].

Third, high-voltage and dI/dt probes provided information about electrical characteristics and the power input into a discharge. The load current was measured by current loops which were placed 6 cm from the Z-pinch axis.

Finally, neutron yields were measured with an indium activation counter and with thermoluminescent dosimeters which were placed inside 10-in-thick Bonner sphere, 1 m from the neutron source (cf., [14]). As far as the reconstruction of neutron energy spectra is concerned, it is the main subject of this paper, and therefore, neutron TOF analysis is presented separately in the following paragraphs.

C. Neutron TOF Diagnostics

Twelve fast plastic scintillators and photomultiplier tubes enabled the TOF analysis of fusion neutrons. All detectors were shielded by $1 \div 10$ cm of lead. The energy dependent sensitivity of neutron TOF detectors was calculated by the Monte Carlo N-Particle code [15]. The detector time resolution of about 4.5 and 5.0 ns was given mainly by the decay time of scintillators, by the electron transit time spread within the photomultiplier tube and by a neutron transit time through 5- and 10-cm-thick scintillators, respectively. Four axial (end-on) neutron detectors were located at distances of -5.07, -2.55 (the minus sign means upstream, i.e., at the top of the S-300 device, behind the anode), 2.55, and 7.43 m (downstream, i.e., at the bottom of the S-300 device, behind the cathode). We should make a note here that the term "downstream" does not mean the direction of current sheet acceleration as in plasma foci but the direction of current flow (from the anode toward the cathode). With regard to eight radial (side-on) detectors, they were positioned in two mutually perpendicular rows at distances of -8.31, -2.55, 2.55, and 8.31 m from the Z-pinch plasma (see Fig. 2). The choice of distances, where neutron TOF detectors were placed, fulfilled the following criteria.

First, it is necessary to place several neutron detectors as close to the neutron source as possible because the time of neutron production is estimated mainly from the nearest neutron signals. In our case, the time of neutron production was estimated from the nearest side-on TOF detectors at 2.55 m from the Z-pinch plasmas. The advantage of side-on detectors was smaller influence of scattered neutrons because side-on diagnostic ports of 10-cm diameter and 1.5-m length were surrounded by water (cf., scattered neutrons on the side-on and downstream detectors in Fig. 3). Another advantage of side-on detectors was the fact that neutron energy spectra were usually centered at about 2.45 MeV. Therefore, in order to obtain the temporal evolution of neutron emission, it was possible to shift the observed neutron signals at 2.55 m by the TOF of 2.45-MeV neutrons (which was about 118 ns, the temporal uncertainty was 2 ns). The temporal resolution (FWHM of pulse response) of

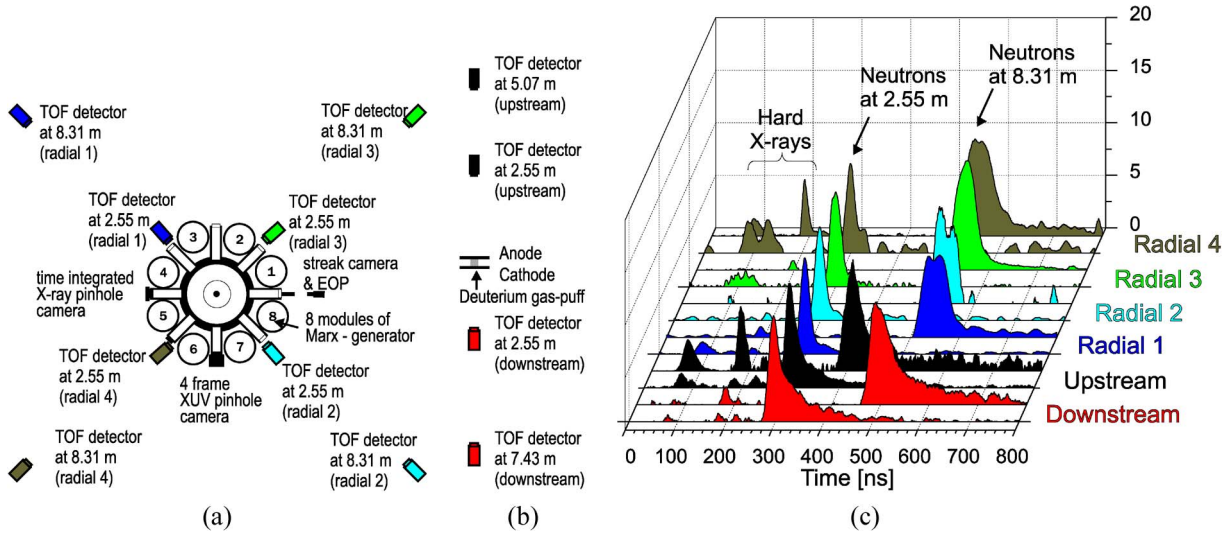

Fig. 2. Schematic diagram of our diagnostic setup with 12 TOF neutron detectors. (a) End-on view. (b) Side-on view. (c) Examples of neutron TOF signals in shot No. 070614-1, the neutron yield of about 2×10^9.

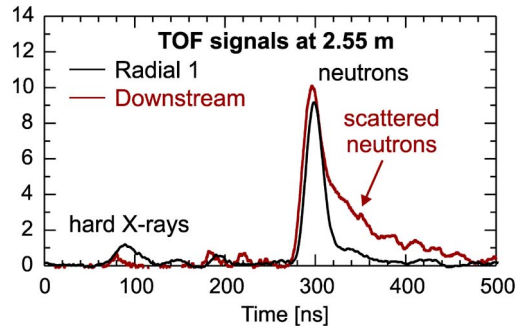

Fig. 3. TOF signals on the side-on (radial 1) and downstream detectors at 2.55 m, shot No. 070614-1, the neutron yield of about 2×10^9. Hard X-rays at about 100 ns were produced by current leakages before the gas-puff implosion.

neutron detection at 2.55 m was given mainly by the width of a neutron energy spectrum and was experimentally estimated below 10 ns.

Second, since energies of neutrons are determined mainly from the most distant detectors, several neutron TOF detectors were placed far from the experimental chamber. The neutron energy distribution function $f(E_{\rm n}, t)$ was reconstructed from time-resolved neutron signals $S(x, T)$ by the Monte Carlo method [6], [10], [16]. Including the temporal resolution of TOF detectors and neutron scattering, the systematic error of mean neutron energy estimated in our experiment was below 0.1 and 0.05 MeV for the end-on and side-on direction, respectively. As far as the error in the estimation of the width of neutron energy spectra is concerned, it was well below 100 keV (cf., downstream spectrum in Fig. 7). Of course, due to a low number of TOF detectors in a row, it was not possible to determine unambiguously the shape of neutron energy spectrum, nevertheless, the mean energy and the width of spectrum could be estimated.

Third, it is convenient to place detectors in various directions at the same distance. It enables instantaneous and unambiguous measurement of the neutron emission anisotropy (together with the anisotropy of the experimental arrangement) by simple comparison of TOF signals without any specific data processing such as the Monte Carlo simulation. The same distance is also useful for cross-calibration of detectors.

Fourth, neutron detectors can be used in mutually opposite directions (i.e., neutron spectra are evaluated from the chain of neutron detectors on the both sides of the neutron source). Such a procedure significantly improved results of neutron spectra reconstruction and limited the influence of scattered neutrons [6]. Besides that, it was possible to quantitatively estimate the role of scattered neutrons: The sum of the mean neutron energy in one direction and in the opposite direction should be about $2.45 + 2.45$ MeV $= 4.9$ MeV. If the sum is higher then 4.9 MeV, it can be caused by significant kinetic energies of fast deuterons. However, if the sum is lower, it is caused by lowering of neutron energies because of scattering.

The aforementioned set of diagnostic tools enabled us to observe results which are presented in the following section.

III. Experimental Results

A. Plasma Dynamics

We carried out a series of ten shots with a deuterium gas puff. The typical waveforms and images obtained are shown in Fig. 4. The times described in this paper refer to the start of a current when $t = 0$. All signals were adjusted to account for different transit times from each detector to oscilloscopes. The temporal uncertainty between waveforms of X-rays, neutrons, and electrical characteristics was below 5 ns.

The visible image in Fig. 4 recorded the conical shape of a deuterium gas puff. The conical implosion resulted also in the formation of a jet which was observed in the time-integrated X-ray pinhole image (see Fig. 5). The streak camera in Fig. 4 clearly showed the implosion of a deuterium gas puff. The implosion started at about 60 ns, and the velocity reached the modest value of 6×10^4 m/s. At about 150 ns, during the stagnation of deuterium plasmas on the axis, the voltage signal, hard X-ray emission, and neutron production peaked. The plasma

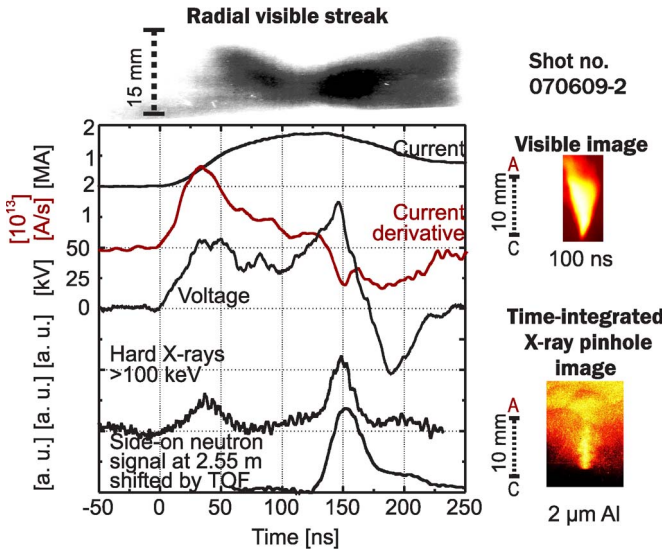

Fig. 4. Visible streak image, visible image, X-ray pinhole image and waveforms of current, current derivative, voltage, hard X-rays, and neutron emission recorded in discharge No. 070609-2, the neutron yield of about 4×10^9.

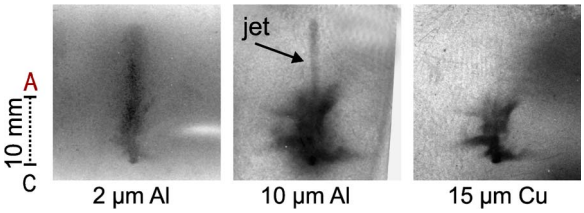

Fig. 5. Collimated jet above the anode in time integrated X-ray pinhole images in discharge No. 070614-1, the neutron yield of about 2×10^9.

impedance during the implosion and stagnation $R_{\mathrm{P}} + \dot{L}_{\mathrm{P}} = (V - L_{\mathrm{P}}\dot{I})/I$ exceeded 0.04 Ω (in the shot with the highest neutron yield, the plasma impedance was about 0.15 Ω). A relatively low implosion velocity together with a small plasma impedance and inductance indicate that a significant part of the electric current was flowing near the return current post, i.e., near the radius of 5 cm. It is likely that this fact was caused by a large spread of the deuterium gas in the central anode–cathode region.

B. Time of Hard X-Ray and Neutron Production

X-ray emission started at the stagnation of a deuterium gas puff on the axis. In all shots, the peak of X-ray emission corresponded to a voltage spike and to a dip in a dI/dt signal. The hard X-ray emission lasted during the stagnation and expansion phase. As far as neutron peaks are concerned, they temporally correlated with hard X-ray peaks within 5-ns accuracy. The neutron pulse lasted on average 25 ± 10 ns (FWHM). The error of 10 ns represents the shot-to-shot variation and the variation between four nearest radial detectors.

C. Neutron Energy Distribution Function

Neutron energy spectra were reconstructed from TOF signals by the Monte Carlo simulation which was described in [6] and [16]. A typical example of neutron TOF signals detected with

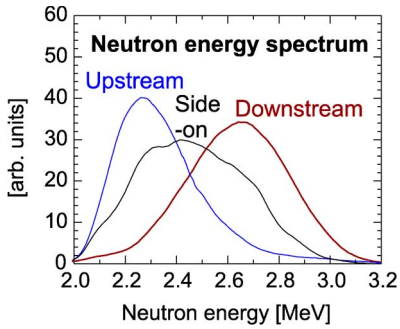

Fig. 6. End-on and side-on (radial 3) energy spectra of neutrons, shot No. 070614-1, the neutron yield of about 2×10^9.

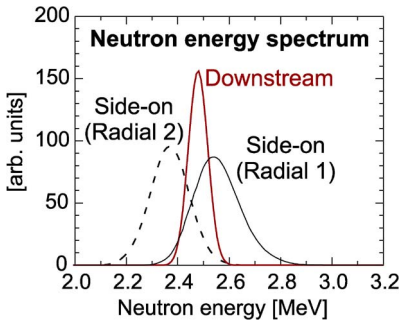

Fig. 7. End-on and side-on (radial 1 and 2) energy spectra of neutrons, shot No. 070605-1, the neutron yield of about 9×10^8.

12 detectors is shown in Fig. 2(c). In Fig. 6, we can see end-on and side-on neutron spectra obtained from these 12 waveforms. Each of the three spectra in Fig. 6 was reconstructed from 4 TOF detectors in a row.

On average, the side-on neutron energy peaked at 2.42 ± 0.04 MeV, and the FWHM of neutron energy spectra was 450 keV. In the downstream direction, the peak neutron energy and the width of a neutron spectrum were 2.60 ± 0.10 and 400 keV, respectively. In the upstream direction, the peak neutron energy was 2.30 ± 0.10 MeV.

As regards side-on neutron TOF signals at 8.31 m in Fig. 2 and the side-on neutron energy spectrum in Fig. 6, they showed a multipeak structure. It follows that time-integrated neutron energy spectra could be formed by a multiphase process. An interesting result was achieved in several other shots. For example, in shot No. 070605-1 (see Fig. 7), we observed a relatively narrow width of an end-on neutron energy spectrum together with an anisotropic emission in the side-on direction (see also radial 1 and radial 2 directions in Fig. 2). At this point, it should be noted that these results are not just artifacts of our Monte Carlo reconstruction. The radial anisotropy was evident even before any data were processed. Fig. 8 shows signals from radial TOF detectors at the same distance of about 8.31 m. Hard X-rays on the radial 1 detector coincided with the radial 2 detector (see Fig. 8). In most cases, also the temporal differences between neutron TOF signals were below the temporal uncertainty of about 3 ns. However, in this particular shot, the temporal difference was 13 ns. It means that most fusion reactions were really realized in the center of mass frame which was moving in the side-on direction (with respect to the laboratory frame of reference).

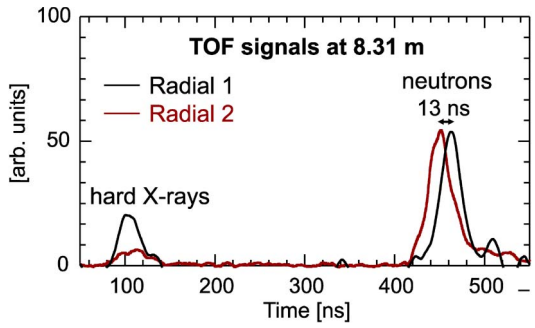

Fig. 8. TOF signals on the side-on detectors (radial 1 and 2) at 8.31 m, shot No. 070605-1, the neutron yield of about 9×10^8. Hard X-rays at about 100 ns were produced by current leakages before the gas-puff implosion.

D. Neutron Yield

We detected neutrons from D-D fusion reactions in eight cases over a series of ten shots. The peak neutron yield was achieved in the case of the highest plasma voltage of about 300 kV, the highest plasma impedance of 0.15 Ω, and the highest implosion velocity. The peak neutron yield exceeded 10^{10} on the current level of 2 MA.

On the one hand, such a number of neutrons was a common yield in fiber Z-pinch experiments [17]–[20]. The neutron yield of 10^{10} on 2-MA current level is also consistent with I^4 scaling and neutron yields obtained on the Saturn generator (2×10^{12} at 7.5 MA current [21]) and on the Z machine (3×10^{13} at 15 MA current [5]). However, on the other hand, neutron yields up to 10^{12} were achieved with a plasma focus [22] and with a gas-puff Z-pinch on the ANGARA-5-1 [9] on the current level of 2–3 MA. Therefore, it is possible that there are two different neutron production mechanisms, and we would like to focus on this issue during our future gas-puff experiments on the S-300 generator.

It would be interesting to know if we succeed in increasing the neutron yield with the gas-puff optimization on the S-300 generator. In our preliminary gas-puff experiments, we suppose that a significant current did not flow through the central part of a gas puff because of the large spread of a deuterium gas. In these cases, the plasma compression and subsequently the neutron yield were reduced. Even though the deuterium gas puff was not optimized for the highest neutron yield, these experiments confirmed our assumption that neutron yields with deuterium gas puffs are higher than with other Z-pinch configurations presented in [6] (on average, 5×10^8 for a deuterated fiber Z-pinch and 10^9 for a wire-array Z-pinch with an on-axis deuterated fiber).

IV. Discussion

A. Distribution Function of Deuteron Kinetic Energy Components

The knowledge of neutron spectra at different directions relative to the Z-pinch axis gives us important information about the energy of deuterons which produce fusion reactions. If energies of reacting deuterons are much smaller than the energy released from the $\mathrm{D}(d,\mathrm{n})^3\mathrm{He}$ fusion reaction (i.e., much lower than 3.3 MeV), the neutron energy is given mainly by the component of deuteron kinetic energy in the direction of neutron detection, and it is possible to transform neutron energy spectra into distribution functions of side-on and end-on energy components of deuterons (cf., [6]). Results obtained in shots previously mentioned are shown in Fig. 9.

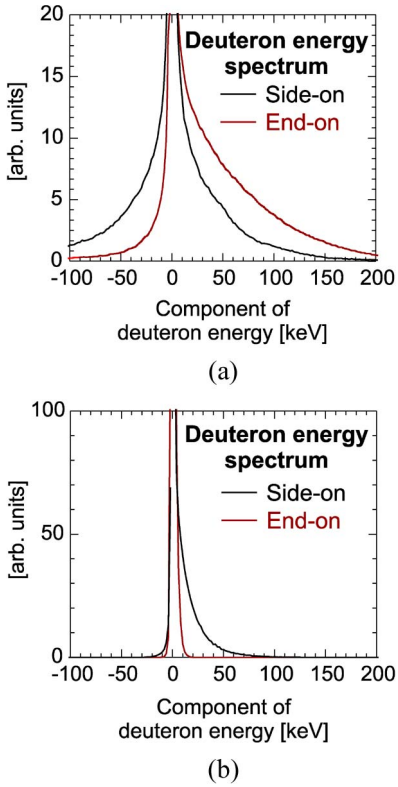

Fig. 9. Distribution functions of kinetic energy components of reacting deuterons. The plus and minus signs of kinetic energy component reflect the direction of deuteron velocity. (a) Shot no. 070614-1. (b) Shot no. 070605-1.

In Fig. 9(a), we can see that fusion neutrons were produced mainly by deuterons with a kinetic energy component below 100 keV. The mean axial component of the deuteron kinetic energy $\langle |E_\parallel| \rangle$ was 50 keV while the mean side-on component $\langle |E_\perp| \rangle$ was 35 keV. The average kinetic energy of reacting deuterons was $\langle E_\mathrm{d} \rangle = \langle E_x + E_y + E_z \rangle = 2\langle |E_\perp| \rangle + \langle |E_\parallel| \rangle \doteq 120$ keV. Our Monte Carlo reconstruction also estimated the downstream/upstream anisotropy of neutron flux as 1.1.

B. Generalized Beam-Target Model

If we are to discuss the neutron production mechanism in our gas-puff experiments, we should perhaps start with the discussion of an important result that was observed: the anisotropy of neutron energy spectra. The neutron emission anisotropy was most likely caused by a beam of fast deuterons which were accelerated in certain directions and thereafter collided with "cold" target deuterons. Usually, most of the fast deuterons were directed toward the cathode. We used such an orientation of the conical gas puff that a hydrodynamic flow occurred toward the anode, i.e., in the opposite direction than the one in which deuterons were directed. That is why it seems reasonable to explain the deuteron acceleration to 100 keV energies by the

diode action. However, in some shots, the anisotropy was also apparent in the side-on direction. This very fact leads us to a supposition that the deuteron acceleration and fusion neutron production is a rather complicated multiphase process which could result in broad widths of neutron energy spectra on the order of 400 keV. Such a broad width of neutron energy spectra then caused a relatively small anisotropy of neutron flux. Similar neutron energy spectra were obtained in our previous wire-array Z-pinch experiments on the S-300 generator (cf., [6]) as well as in plasma focus discharges [23], [24].

With regard to plasma focus discharges, a high radial component of deuteron velocities was explained by: 1) the Fermi acceleration mechanism and/or 2) the generalized beam-target model. In the Fermi acceleration mechanism, deuterons acquire the energy from the radially imploding current sheet [25] whereas in the generalized beam-target model (gyrating particle model), axially accelerated deuterons are bent by magnetic fields before they produce fusion neutrons [23], [26], [27].

With regard to our experiments, we can draw similar conclusions as in previous experiments on the S-300 generator (cf., [6]). The neutron emission anisotropy and the broad width of neutron spectra are the main arguments against the thermonuclear origin of neutrons. Furthermore, the observed radial neutron spectra could be explained neither by a monoenergetic deuteron beam nor by deuteron beams moving at a single angle to axis. The observed spectra have to be explained by a broad angular dependence and by monotonically decreasing energy dependence of deuteron energy distribution function. These conclusions are far from the simple concept of a linear beam-target model, and this is why Bernstein with his colleagues introduced the term generalized beam-target model [23]. On the basis of our experimental data, we are not able to decide how the beam of fast deuterons was created. Nevertheless, the aforementioned results put unambiguous restrictions on models of deuteron acceleration. For instance, the radial Fermi acceleration mechanism is inconsistent with spectra in Figs. 6 and 9(a) whereas it cannot be completely excluded in the shot with spectra in Figs. 7 and 9(b).

C. Plasma Voltage and Resistance

The discussion part of this paper shall be concluded by a description of the temporal correlation of neutron emission with plasma voltage, the characteristic feature of our experiment, and the issue of plasma resistance. The origin of voltage peaks during the neutron emission is discussed here because it could elucidate the process of accelerating fast deuterons. The positive voltage peaks could be explained by the plasma resistance R_{P}, by the increasing inductance $\dot{L}_{\mathrm{P}} > 0$ or by the increasing current $\dot{I} > 0$. In our experiment with a deuterium gas puff as well as in deuterium gas-puff experiments on the Angara 5-1 device at Troitsk [9], neutrons were emitted at the stagnation and at the beginning of plasma expansion. This means that the measured voltage peaks could be hardly ascribed to an increasing plasma inductance $\dot{L}_{\mathrm{P}}$. Furthermore, it is highly probable that the resistive voltage $R_{\mathrm{P}}I$ significantly contributed to voltage peaks because the induced voltage $L_{\mathrm{P}}\dot{I}$ was negative during the neutron emission.

On the Angara 5-1 generator, the plasma impedance was between 0.1 and 0.3 Ω. Such a value could not be explained by the Spitzer resistivity and the possibility of anomalous resistance was discussed. The characteristic feature of the experiment at Troitsk was the relatively small mass of a liner and the axial gradient of a linear density. Therefore, microturbulences were supposed to occur near the anode where the gas density was low.

The anomalous resistance does not seem to be a unique feature of a few experiments. The enhanced plasma resistance $(0.2 \div 0.4\ \Omega)$ during the neutron emission was measured also for a broad energy range of plasma focus machines [28], [29] and in our previous experiments on the S-300 generator [6]. As far as the gas-puff experiment described in this paper is concerned, the plasma impedance was usually below 0.05 Ω. However, the peak neutron yield was achieved in the case of plasma impedance of 0.15 Ω. Such a value does not indicate only that the resistance could play an important role in our gas-puff experiment but also that the enhanced resistance could be a general phenomenon in Z-pinches at the poststagnation phase.

V. Conclusion

The implosion of a deuterium gas-puff Z-pinch was studied on the S-300 generator. The emphasis was put mainly on the reconstruction of the neutron energy distribution function from 12 neutron TOF signals by the Monte Carlo simulation. The neutron measurements were used to obtain data about acceleration of deuterons in Z-pinch plasmas.

The peak neutron yield above 10^{10} was achieved on the current level of 2 MA. The fusion neutrons were generated at about 150 ns after the current onset and the emission lasted on average 25 ns. The side-on neutron energy spectra peaked at 2.42 ± 0.04 MeV with about 450-keV FWHM. In the downstream direction, the peak neutron energy and the width of a neutron spectrum were 2.6 ± 0.1 MeV and 400 keV, respectively. The average kinetic energy of fast deuterons, which produced fusion neutrons, was about 100 keV. The generalized beam-target model probably fits best to the obtained experimental data.

In future experimental campaigns, we shall pay special attention to the reduction of a deuterium gas spread in the energy concentrator and to the optimization of a deuterium gas puff. We would like to increase the neutron yield and to measure the gas-puff density profile. This, we believe, is necessary for further experimental data processing and for the subsequent discussion of deuteron acceleration mechanisms.

Acknowledgment

The authors would like to thank Prof. A. S. Kingsep for his valuable comments and Dr. G. N. Timoshenko (Laboratory of Radiation Biology of JINR, Dubna) for his kind assistance with Bonner spheres. The authors would also like to thank M. Kralik (Czech Metrology Institute) for his help with the MCNP code.

REFERENCES

[1] T. Sandford, G. Allshouse, B. Marder *et al.* "Improved symmetry greatly increases X-ray power from wire-array Z-pinches," *Phys. Rev. Lett.*, vol. 77, no. 25, pp. 5063–5066, Dec. 1996.

[2] R. Spielman, C. Deeney, G. Chandler *et al.*, "Tungsten wire-array Z-pinch experiments at 200 TW and 2 MJ," *Phys. Plasmas*, vol. 5, no. 5, pp. 2105–2111, May 1998.

[3] M. G. Haines, P. D. LePell, C. A. Coverdale, B. Jones, C. Deeney, and J. P. Apruzese, "Ion viscous heating in a magnetohydrodynamically unstable Z-pinch at over 2×10^9 kelvin," *Phys. Rev. Lett.*, vol. 96, no. 7, p. 075 003, Feb. 2006.

[4] A. L. Velikovich, R. W. Clark, J. Davis *et al.*, "Z-pinch plasma neutron sources." *Phys. Plasmas*, vol. 14, no. 2, pp. 022 701-1–022 701-16, Feb. 2007.

[5] C. A. Coverdale, C. Deeney, A. L. Velikhovich *et al.*, "Neutron production and implosion characteristics of a deuterium gas-puff Z pinch," *Phys. Plasmas*, vol. 14, no. 2, pp. 022 706-1–022 706-7, Feb. 2007.

[6] D. Klir, J. Kravarik, P. Kubes *et al.*, "Neutron emission generated during wire array Z-pinch implosion onto deuterated fiber," *Phys. Plasmas*, vol. 15, no. 3, pp. 032 701.1–032 701.13, Mar. 2008.

[7] A. S. Chernenko, Y. M. Gorbulin, Y. G. Kalinin *et al.*, "S-300, new pulsed power installation in Kurchatov Institute, investigation of stable liner implosion," in *Proc. 11th Int. Conf. High Power Particle Beams*, J. Ullschmied, Ed. Prague, Czech Republic: Acad. Sci. Czech Republic, 1996, vol. 1, p. 154.

[8] Y. L. Bakshaev, A. S. Chernenko, V. D. Korolev *et al.*, "Energy concentration on S-300 pulsed power generator," in *Proc. 11th Int. Conf. High Power Particle Beams*, J. Ullschmied, Ed. Prague, Czech Republic: Acad. Sci. Czech Republic, 1996, vol. 2, p. 962.

[9] A. V. Batyunin, A. N. Bulatov, V. D. Vikharev *et al.*, "Study of an ultrafast Z-pinch on the Angara 5-1 device," *Sov. J. Plasma Phys.*, vol. 16, pp. 597–601, 1990.

[10] I. Tiseanu, G. Decker, and W. Kies, "A Monte-Carlo technique for the reconstruction of time dependent spectra of short-pulse neutron sources," *Nucl. Instrum. Methods Phys. Res. A, Accel. Spectrom. Detect. Assoc. Equip.*, vol. 373, no. 1, pp. 73–80, Feb. 1996.

[11] I. Tiseanu and I. Craciunescu, "Evaluation of reconstruction methods for time-resolved spectroscopy of short-pulsed neutron sources," *Nucl. Sci. Eng.*, vol. 122, no. 3, pp. 384–394, 1996.

[12] Y. L. Bakshaev, P. I. Blinov, A. S. Chernenko *et al.*, "Diagnostic arrangement on S-300 facility," *Rev. Sci. Instrum.*, vol. 72, no. 1, pp. 1210–1213, Jan. 2001.

[13] Y. L. Bakshaev, P. I. Blinov, V. V. Vikhrev *et al.*, "Measurements of neutron emission from a Z-pinch constriction," *Plasma Phys. Rep.*, vol. 32, no. 7, pp. 531–538, Jul. 2006.

[14] A. Velyhan, J. Krasa, B. Bienkowska *et al.*, "Use of thermoluminescent dosimeters for measurement of fast-neutron spatial-distribution at the plasma focus device PF-1000," *Phys. Scr.*, vol. T123, pp. 66–78, Mar. 2006.

[15] J. F. Briesmeister, "MCNP—A general Monte Carlo N-particle transport code," Los Alamos Nat. Lab., Los Alamos, NM, Report No. LA-12625-M, 1993.

[16] K. Rezac, D. Klir, P. Kubes, J. Kravarik, and M. Stransky, "Monte Carlo simulations for reconstruction of neutron time-resolving energy distribution in D-D fusion reactions," *Czech J. Phys.*, vol. 56, pp. B357–B363, Oct. 2006.

[17] F. Young, S. Stephanakis, and D. Mosher, "Neutron and energetic ion production in exploded polyethylene fibers," *J. Appl. Phys.*, vol. 48, no. 9, pp. 3642–3650, Sep. 1977.

[18] J. D. Sethian, A. E. Robson, K. A. Gerber, and A. W. DeSilva, "Enhanced stability and neutron production in a dense Z-pinch plasma formed from a frozen deuterium fiber," *Phys. Rev. Lett.*, vol. 59, no. 8, pp. 892–899, Aug. 1987.

[19] W. Kies, G. Decker, M. Malzig *et al.*, "Terawatt fiber pinch experiments," *J. Appl. Phys.*, vol. 70, no. 12, pp. 7261–7272, Dec. 1991.

[20] V. V. Vikhrev and V. D. Korolev, "Neutron generation from Z-pinches," *Plasma Phys. Rep.*, vol. 33, no. 5, pp. 356–380, May 2007.

[21] R. Spielman, G. Baldwin, G. Cooper *et al.*, "D-D fusion experiments using fast Z-pinches," Sandia Nat. Lab., Albuquerque, NM, Rep. SAND98-07-05, 1998.

[22] A. Bernard, J. P. Garconnet, A. Jolas, J. P. Le Breton, and J. de Mascureau, "Turbulence caused by the interaction between plasma and electric current in the focus experiment," in *Proc. 7th IAEA Conf. Plasma Phys. Controlled Nucl. Fusion, Innsbruck, 1978—Plasma Physics and Controlled Fusion Research (IAEA-CN-37)*. Vienna, Austria: IAEA, 1979, vol. 2, pp. 159–172.

[23] M. J. Bernstein and G. G. Comisar, "Neutron energy and flux distributions from a crossed-field acceleration model of plasma focus and Z-pinch discharges," *Phys. Fluids*, vol. 15, no. 4, pp. 700–707, Apr. 1972.

[24] A. Bernard, A. Coudeville, A. Jolas, J. Lauspach, and J. de Mascreau, "Experimental studies of the plasma focus and evidence for nonthermal processes," *Phys. Fluids*, vol. 18, no. 2, pp. 180–194, Feb. 1975.

[25] R. Deutsch and W. Kies, "Ion acceleration and runaway in dynamical pinches," *Plasma Phys. Control. Fusion*, vol. 30, no. 3, pp. 263–276, Mar. 1988.

[26] U. Jager and H. Herold, "Fast ion kinetics and fusion reaction-mechanism in the plasma-focus," *Nucl. Fusion*, vol. 27, no. 3, pp. 407–423, 1987.

[27] V. A. Gribkov, A. Banaszak, and B. Bienkowska *et al.*, "Plasma dynamics in the PF-1000 device under full-scale energy storage: II. Fast electron and ion characteristics versus neutron emission parameters and gun optimization perspectives," *J. Phys. D, Appl. Phys.*, vol. 40, no. 12, pp. 3592–3607, Jun. 2007.

[28] G. Decker, W. Kies, and G. Pross, "The first and the final fifty nanoseconds of a fast focus discharge," *Phys. Fluids*, vol. 26, no. 2, pp. 571–578, Feb. 1983.

[29] A. Bernard, "Recent developments in plasma focus research," *Atomkernenergie*, vol. 32, pp. 73–75, 1978.

Daniel Klir was born in Podebrady, Czech Republic, on March 4, 1979. He received the M.Sc. degree in applied physics and the Ph.D. degree in plasma physics from Czech Technical University in Prague (CTU), Prague, Czech Republic, in 2002 and 2005, respectively.

Since 2005, he has been a Research Associate with the Department of Physics, Faculty of Electrical Engineering, CTU. His research interests include Z-pinch physics and plasma diagnostics based on X-ray and neutron detection.

Jozef Kravarik was born in Bosaca, Slovakia, on August 9, 1936. He received the M.Sc. degree in electrical engineering and the Ph.D. degree in plasma physics from Czech Technical University in Prague (CTU), Prague, Czech Republic, in 1960 and 1967, respectively.

Since 1963, he has been with the Faculty of Electrical Engineering, CTU, where he has been an Associate Professor since 1976. His research activities concentrate on the visual, X-ray, laser, and high-energy particle diagnostics of the Z-pinch and plasma focus discharges.

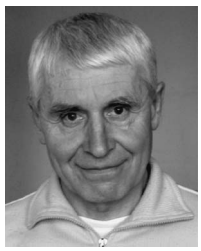

Pavel Kubes (M'07) was born in Prague, Czech Republic, on May 23, 1943. He received the M.Sc. degree from the Charles University, Prague, and the Ph.D. degree in plasma physics from Czech Technical University in Prague (CTU), Prague, in 1965 and 1977, respectively.

Since 1966, he has been with the Department of Physics, Faculty of Electrical Engineering, CTU, where he has been a Professor of applied physics since 1991. His research interests concentrate on the study of X-rays and neutrons in Z-pinch and plasma focus discharges.

Karel Rezac was born in Kladno, Czech Republic, on June 16, 1980. He received the M.Sc. degree in computer science and engineering from Czech Technical University in Prague, Prague, Czech Republic, in 2004, where he is currently working toward the Ph.D. degree in the Faculty of Electrical Engineering.

His research interests include plasma diagnostics and numerical simulations in neutron diagnostics.

Sergey S. Ananev was born in Moscow, Russia, in 1982. He received the M.Sc. degree in physics from Moscow Institute of Natural Sciences and Ecology, Moscow, in 2005.

Since 2002, he has been with the Russian Research Center "Kurchatov Institute," Moscow, working in the field of X-ray and EUV plasma spectroscopy and plasma visualization with the time resolution. His research interests include Z-pinch and plasma diagnostics based on laser probing and electooptical systems.

Yuriy L. Bakshaev was born in Jaransk, Russia, on July 31, 1938. He received the degree in radio physics and electronics from NNGU in Gorki in 1960.

Up to 1969, was with VNIIF in Snezhinsk as the Senior Engineer. Since 1969, he has been with the Russian Research Center "Kurchatov Institute," Moscow, Russia, as a Senior Scientist. His scientific interests include the physics of hot dense Z-pinch plasma and engineering of powerful pulse accelerators.

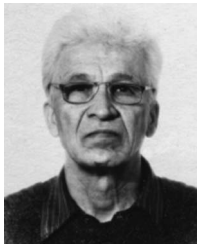

Peter I. Blinov was born in Russia in 1932. He received the M.Sc. degree in technical physics from Leningrad Polytechnic Institute, Saint Petersburg, Russia, in 1955.

Since 1976, he has been with the Russian Research Center "Kurchatov Institute," Moscow. In 1971, he became an Associate Professor with Kharkov University, Kharkov, Russia. His research interests include Z-pinch and plasma diagnostics.

Andrey S. Chernenko was born in Moscow, Russia, in 1951. He received the degree in physics from Moscow Institute of Physics and Technologies, Moscow, in 1974 and the Ph.D. degree from the Kurchatov Institute of Atomic Energy, Moscow, in 1984.

Since 1974, he has been with the Russian Research Center "Kurchatov Institute," Moscow, working in the field of intense electron beams and plasma diagnostics. His research interests include high-power current generators, Z-pinch, and plasma diagnostics.

Evgeny D. Kazakov was born in Moscow, Russia, in 1982. He received the degree in physics from Moscow Engineering Physics Institute (State University), Moscow, in 2005 and the Ph.D. degree from the Alikhanov Institute for Theoretical and Experimental Physics, Moscow, in 2008.

Since 2003, he has been with the Russian Research Center "Kurchatov Institute," Moscow, working in the field of X-ray and EUV plasma spectroscopy and plasma visualization. His research interests include Z-pinch and laser plasma physics and diagnostics.

Valery D. Korolev was born in Moscow, Russia, in 1943. He received the degree in physics from Moscow Engineering Physics Institute (State University), Moscow, in 1967 and the Ph.D. and Doctor of Science degrees from the Russian Research Center "Kurchatov Institute," Moscow, in 1978 and 2004, respectively.

His research interests include physics of relativistic electron beams, Z-pinch physics, and diagnostics of dense plasma.

Gennadiy I. Ustroev was born in Volsk, Russia, in 1941. He received the degree in physics from Moscow Engineering Physics Institute (State University), Moscow, Russia, in 1972.

Since 1970, he has been with the Russian Research Center "Kurchatov Institute," Moscow. His research interests include neutron physics, physics of fission, and structure of nuclei. Recently, his interests have included also Z-pinch physics, and the study of X-rays and neutrons produced by Z-pinches.

Libor Juha was born in Krnov, Czech Republic, on February 28, 1964. He received the M.Sc. and Ph.D. degrees from Czech Technical University in Prague, Prague, Czech Republic, in 1987 and 1995, respectively.

Since 1992, he has been a staff member with the Laser Plasma Department, Institute of Physics, Academy of Sciences of the Czech Republic, Prague. His research interests include interaction of intense XUV/X-ray radiation with matter, radiometry of intense short-wavelength radiation, and laser-plasma chemistry.

Josef Krasa was born in Borotice, Czech Republic, in 1946. He received the M.Sc. degree in experimental physics from the Charles University, Prague, Czech Republic, in 1969 and the Ph.D. degree in plasma physics from the Czechoslovak Academy of Sciences, 1977.

Since 1970, he has been with the Institute of Physics, Academy of Sciences of the Czech Republic, Prague. As a Senior Scientist, he was involved in the diagnostics of ions emitted from laser-produced plasmas, mainly in the analysis of time-of-flight spectra of pulsed ion currents. Moreover, he is interested in the neutron diagnostics with the use of thermoluminescent dosimeters in the PF-1000 Facility, IPPLM, Warsaw.

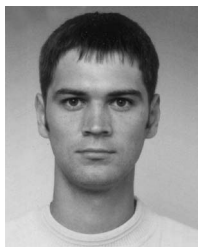

Andriy Velyhan was born in Uzhgorod, Ukraine, in 1976. He received the M.Sc. degree in physics from Uzhgorod State University, Uzhgorod, Ukraine, in 1999 and the Ph.D. degree from the Charles University, Prague, Czech Republic, in 2008. The topic of his doctoral thesis relates to the secondary emission and field emission from micrometer-size cosmic grains.

He is currently with the Institute of Physics, Academy of Sciences of the Czech Republic, Prague, where he is involved in the research of laser-induced highly charged ion beams and detection of neutron radiation by means of thermoluminescent dosimetry.

ARTICLE NO. 4

Plasma Phys. Control. Fusion **52** (2010) 065013 (17pp) doi:10.1088/0741-3335/52/6/065013

Efficient production of 100 keV deuterons in deuterium gas puff Z-pinches at 2 MA current

D Klir[1], J Kravarik[1], P Kubes[1], K Rezac[1], J Cikhardt[1], E Litseva[1], T Hyhlik[2], S S Ananev[3], Yu L Bakshaev[3], V A Bryzgunov[3], A S Chernenko[3], Yu G Kalinin[3], E D Kazakov[3], V D Korolev[3], G I Ustroev[3], A A Zelenin[3], L Juha[4], J Krasa[4], A Velyhan[4], L Vysin[4], J Sonsky[5] and I V Volobuev[6]

[1] Czech Technical University in Prague, Faculty of Electrical Engineering, Department of Physics, Technicka 2, 166 27 Prague 6, Czech Republic
[2] Czech Technical University, Faculty of Mechanical Engineering, Department of Fluid Dynamics and Power Engineering, Technicka 4, 166 27 Prague, Czech Republic
[3] Institute of Nuclear Synthesis, RRC Kurchatov Institute, 1 Kurchatov Sq., 123182 Moscow, Russia
[4] Institute of Physics, Academy of Sciences of the Czech Republic, Na Slovance 2, 182 21 Prague 8, Czech Republic
[5] Institute of Thermomechanics, Academy of Sciences of the Czech Republic, Dolejskova 5, 182 00 Praha 8, Czech Republic
[6] P.N. Lebedev Physical Institute, Russian Academy of Sciences, Leninsky prospect 53, 119991 Moscow, Russia

E-mail: klirdani@fel.cvut.cz

Received 11 March 2010, in final form 28 April 2010
Published 12 May 2010
Online at stacks.iop.org/PPCF/52/065013

Abstract

Deuterium gas puff experiments were carried out on the S-300 Z-pinch at the Kurchatov Institute in Moscow. Gas puffs imploded onto the axis before a current peak at about 100 ns. Fusion neutrons were generated after the gas puff implosion during global expansion of a plasma column. Neutron emission lasted on average 35 $\pm$ 5 ns (full width half maximum, FWHM). In the downstream direction (on the Z-pinch axis behind the cathode), a mean neutron energy was 2.6 $\pm$ 0.1 MeV. Side-on neutron energy spectra peaked at 2.40 $\pm$ 0.05 MeV with about 600 $\pm$ 150 keV FWHM. A broad width of side-on neutron spectra implied a high radial component of deuteron velocities. An average kinetic energy of fast deuterons, which produced fusion neutrons, was 150 keV. A peak neutron yield reached a value of 6×10^{10} on a current level of 1.5 MA. It was by one order higher in comparison with other deuterated loads used on the same current generator. On the basis of experimental observations, we concluded that a total energy of deuterons accelerated to fusion energies was above 1.5 kJ. It is more than 15% of the energy input into a plasma. Therefore gas puff Z-pinches seem to be not only powerful sources of x-ray radiation but also efficient sources of 100 keV deuterons. Such a result is consistent with high

neutron yields observed on the Angara Z-pinch and plasma foci with similar currents.

(Some figures in this article are in colour only in the electronic version)

1. Introduction

The first systematic study of Z-pinches started in the 1950s in connection with controlled thermonuclear fusion research. Straight compressional Z-pinches were found to produce a large number of neutrons which originated from the D(d,n)^{3}He fusion reaction [1–3]. Shortly afterwards, researchers arrived at the conclusion that neutrons were not of thermonuclear origin and that straight Z-pinches were not useful for fusion power production. Nevertheless, a large number of produced neutrons in Z-pinches led to the study of acceleration of deuterons to fusion energies. In order to cope with this reality satisfactorily and to achieve even higher neutron yields, various configurations based on the Z-pinch effect have been suggested and tested from that time on. The most promising configuration seemed to be a plasma focus with a deuterium gas filling (a record yield exceeded 10^{12} neutrons/shot on a megaampere current level [4]). In plasma foci (PF), many experimental results have been obtained and also neutron production mechanisms have been studied up to the present time [5–8]. In this respect, experimental data from Z-pinches are rather rare. One of those few examples is a Z-pinch which is formed from a frozen deuterium fibre or a deuterated plastic fibre. The first fibre Z-pinches in the 1980s seemed to be promising due to enhanced stability of plasma [9]. However, the enhanced stability was not confirmed in further and better diagnosed experiments and, in addition to that, peak neutron yields did not exceed 10^{10} with a megaampere current [10–13]. When a higher neutron yield was required, solid fibres appeared to be less suitable than a deuterium gas.

The first deuterium gas puff experiment was carried out on the Angara 5-1 Z-pinch at Troitsk at the end of the 1980s [14, 15]. Characteristic features of a solid deuterium gas puff were the axial gradient of a linear density $\mathrm{d}N/\mathrm{d}z \approx 10^{18}\,\mathrm{cm}^{-2}$ and a relatively small mass of a deuterium gas near the anode. This way, more than 10^{12} neutrons were emitted within 50 ns at a current of 'only' 2 MA. Neutron energy spectra gave evidence of deuterons accelerated to 200–500 keV energies.

A few years later, a hollow deuterium gas puff Z-pinch was researched on the Saturn generator [16]. Even though the current was higher (about 7–9 MA), a peak neutron yield of about 2×10^{12} was comparable to that achieved on the Angara. We should perhaps comment here on the fact that the saturation of a neutron yield at the value of 10^{12} has been also observed during plasma focus research and this was one of the most important arguments for shutting down the largest plasma focus facilities. In this respect, 4×10^{13} neutrons from a double-shell D_2 gas puff on the 17 MA Z-machine in 2005 seemed to be a crucial finding [17–19]. In addition to that, MHD [19] and particle-in-cell [20] simulations showed that there is a hope of a large thermonuclear component. Higher ratio between thermonuclear and beam–target neutrons could also explain the overcoming of the saturation at 10^{12} neutrons/shot.

Since 2007 we have carried out deuterium gas puff experiments on the S-300 generator at the Kurchatov Institute. The first reason for our experiments is our interest in the study of the neutron production mechanism. The second reason is to learn more about fast deuterons because the information about ions in Z-pinches is rather rare. Since neutrons are influenced neither by magnetic nor by electric fields, the detection of neutrons is a favourable diagnostic

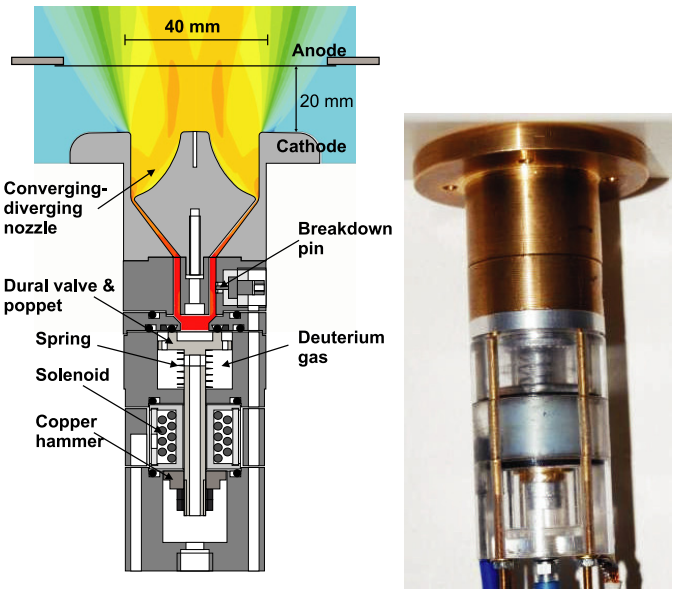

Figure 1. Electromagnetic valve.

Table 1. Parameters of electromagnetic valve.

Inductance of solenoid	$L = 2.5\,\mu$H
Capacitance	$C = 200\,\mu$F
Charging voltage	$V = 1.6$–2.8 kV
Current (at 2.6 kV)	$I_{\max} = 17$ kA
Opening speed of the poppet (at 17 kA)	$v = 3\,\mathrm{m\,s^{-1}}$
Deuterium pressure	$p = 1$–4 bar
Voltage at breakdown pin	$V_{\mathrm{PIN}} = 400$–1000 V
Initiation of the current generator after the breakdown pin pulse	$t = 150$–$1000\,\mu$s

tool for fast deuterons in a plasma. The third reason is to perform deuterium gas puff experiments on a 1–2 MA level, i.e. with a comparable current as in experiments on the Angara and on the largest plasma focus devices PF-1000 [21] and PF-3 [22]. Not only do we intend to repeat successful results achieved on the Angara, but we would also like to provide more experimental data from a deuterium gas puff Z-pinch by means of a comprehensive set of neutron and x-ray diagnostics. Last but not least, our experiments make it possible to enlarge the neutron scaling law for deuterium gas puffs below 2 MA currents.

In our preliminary gas puff experiments at the S-300 [23], the gas puff was driven by burning gun powder similarly as at Troitsk on the Angara. However, in our experiments, the deuterium gas was likely interfused with the burning gun powder and thus a mass density was too high (above $200\,\mu\mathrm{g\,cm^{-1}}$). In this paper, we present results from experiments with the linear mass density of about $20\,\mu\mathrm{g\,cm^{-1}}$ which was achieved with a new electromagnetic valve. The construction of this valve, an experimental arrangement and diagnostics used in our experiment are described in section 2. Section 3 provides the most important experimental results. The discussion of these results is the subject of section 4. Finally, section 5 brings an overall summary.

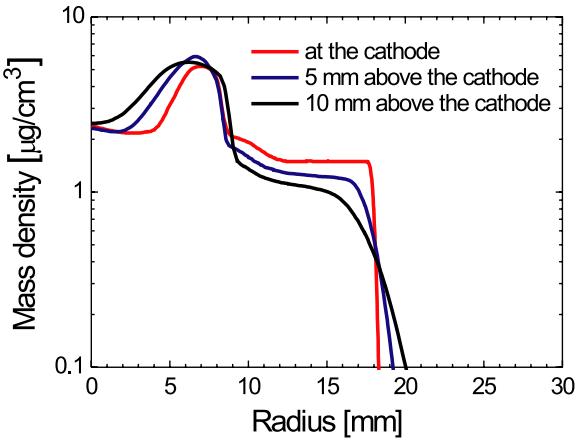

Figure 2. Simulated mass density profiles at various distances above the cathode in the case of a 20 μg cm^{-1} linear mass density.

2. Experimental arrangement and diagnostics

2.1. Experimental setup

The experimental series of 11 shots with a deuterium gas puff was carried out on the S-300 pulsed power generator (4 MA peak current, 700 kV voltage, 100 ns rise time, 0.15 Ω impedance [24, 25]) at the Kurchatov Institute (Moscow) in September 2009. The peak current in these shots varied between 1.4 and 1.7 MA. For the last experimental campaign, we constructed the electromagnetic valve the schematic diagram of which is displayed in figure 1. Parameters of the electromagnetic valve are displayed in table 1. By means of a fast optical framing camera, we measured a modest opening speed of the valve of 3 m s^{-1}.

As regards the design of a supersonic nozzle, we aim at testing various nozzles for both annular and solid gas puffs. We started with a convergent–divergent de Laval nozzle displayed in figure 1. When we calculated the steady state with the ANSYS FLUENT flow modelling software, we received the Mach number of about 6 and the linear density up to 50 μg cm^{-1} at 4 bar plenum pressure. At the initiation of the current generator, the plenum pressure significantly decreased. Therefore we calculated the linear mass density from observed implosion velocities and implosion time. In this paper, we present lower mass shots with the linear density of about 20 μg cm^{-1}. Calculated density profiles at various distances above the cathode can be seen in figure 2. The separation between the cathode and the anode was 11 or 20 mm.

2.2. Diagnostics

In order to study dynamics of the deuterium gas puff Z-pinch, we applied optical, x-ray and neutron diagnostics, part of which has already been described in more detail in [23, 26]. Each shot was observed with the following set of diagnostic tools (see also figure 3):

(i) A high-voltage probe (resistive divider) located at a radial distance of 2 cm [27].
(ii) $\mathrm{d}I/\mathrm{d}t$ probes placed at a 6.8 cm radius. From the differential equation $\dot{L}I = V - L\dot{I}$, we could numerically calculate the inductance $L(t)$ during the implosion when the resistive voltage RI is assumed to be negligible (for more details see [28]). Further, it was possible

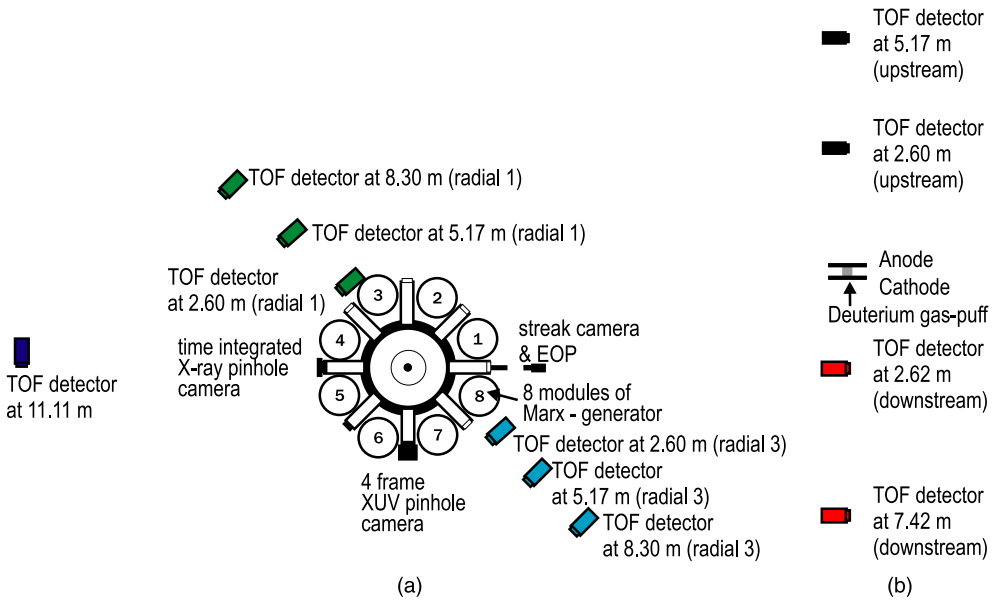

Figure 3. Schematic diagram of diagnostic setup with 11 TOF neutron detectors. (*a*) End-on view, (*b*) side-on view.

to evaluate the $\dot{L}I$ voltage and the active energy input into a plasma during the implosion $W_{\text{input}} = \int_0^{t_{\text{imp}}} VI\mathrm{d}t - \Delta(\frac{1}{2}LI^2) = \frac{1}{2}\int_0^{t_{\text{imp}}} \dot{L}I^2\mathrm{d}t$.

(iii) A radial optical streak camera. The plasma 5 mm above the cathode was imaged on the slit of the streak camera.

(iv) A 6-frame optical camera with 1 ns exposure and 10 ns inter-frame separation.

(v) A 3-fast-frame optical camera with 0.5 ns exposure and 0.9–1.0 ns inter-frame separation.

(vi) A 4-frame XUV pinhole camera with 2 ns exposure and 5 or 10 ns inter-frame separation.

(vii) A time-integrated x-ray pinhole camera (differentially filtered with 10 μm aluminium foil, 5 μm Mylar and 12 μm Mylar).

(viii) Two calibrated AXUV-5 semiconductor diodes with 36 μm and 121 μm Mylar filters.

(ix) Indium and silver activation counters located axially at 1 m above the anode.

(x) Thermoluminescent dosimeters (TLDs) placed inside a 10 inch thick Bonner sphere, 1 m from the neutron source (cf [29]).

(xi) Eleven hard x-ray and neutron time-of-flight (TOF) detectors based on a fast plastic scintillator (BC408 or its equivalent) and photomultiplier tube combination. Four axial (end–on) neutron detectors were located at distances of −5.17 m, −2.6 m (the minus sign stands for upstream, i.e. behind the anode), 2.6 m and 7.42 m (downstream, behind the cathode). Six radial (side-on) detectors were positioned in a row at distances of −8.3 m, −5.17 m, −2.6 m, 2.6 m, 5.17 m, 8.3 m from the Z-pinch plasma. One TOF detector was placed at 11.11 m, i.e. at the most distant place in the experimental hall. For preventing hard x-rays from saturating photomultipliers, detectors were shielded by 1–10 cm of lead. Neutron TOF diagnostics was used to give an insight into the acceleration of fast deuterons. The emphasis was put on finding more about the energy distribution of deuterons which produced fusion neutrons, about anisotropy of neutron emission and about the time and duration of neutron production with respect to general Z-pinch dynamics. A temporal resolution of neutron detectors was about 5 ns. The full width at half maximum

(FWHM) of neutron signals was more than 20 ns; therefore the 5 ns temporal resolution could not seriously affect neutron energy spectra reconstruction by the Monte Carlo simulation [30, 31]. Since hard x-ray and neutron signals were recorded on the same waveform and they were separated only by the TOF, the temporal uncertainty between hard x-rays and neutrons was on the order of the temporal resolution of a neutron detector. More details about our neutron diagnostics and Monte Carlo reconstruction of neutron energy spectra can be found in [23, 26].

This comprehensive set of diagnostic tools enabled us to achieve results that are described in the following section.

3. Experimental results

3.1. Plasma dynamics

During the experimental campaign in 2009, we carried out 11 shots with a linear mass density of 20 μg cm^{-1}. Typical waveforms obtained in shot No 090930-2 with the deuterium gas puff Z-pinch are displayed in figure 4. The time described in this figure refers to the start of a current when $t = 0$.

In the case of 20 μg cm^{-1}, the gas puff imploded onto the axis before the current peak at about 100 ns. An implosion velocity exceeded the value of 3×10^5 m s^{-1}. The implosion recorded by visible and XUV imaging seemed to be with a $<$10 ns zipper and with a diameter during the stagnation of about 2 mm (see also images in figure 5). The peak power of soft ($>$1.5 keV) x-rays was 70 MW with a total emitted energy of 2 J. It was a negligible fraction of the total energy input into a plasma $W_{\text{input}} = \frac{1}{2}\int_0^{t_{\text{imp}}} \dot{L} I^2 \mathrm{d}t$ which approached 9 kJ. Measured load impedances were consistent with the observed implosion velocities. The peak plasma impedance reached 0.30–0.45 Ω before the stagnation.

3.2. Hard x–ray and neutron production

Figure 4(*b*) shows waveforms of hard x-rays and neutrons recorded in the same shot as in figure 4(*a*). All signals were adjusted to account for different transit times from each detector to the oscilloscopes. The time of neutron production was estimated from the nearest side-on TOF detectors at 2.6 m from the Z-pinch plasmas. We shifted the observed neutron signals by 118 ns, i.e. by the TOF of 2.45 MeV neutrons. Therefore the temporal resolution of neutron detection was given by the width of a neutron energy spectrum and was experimentally estimated as 10 ns.

As regards the neutron emission in figure 4(*b*), there was a small neutron pulse which started during the stagnation and correlated with a hard x-ray peak. However, it was usually possible to distinguish two neutron pulses and the main emission (the second neutron pulse) corresponded to a small x-ray and hard x-ray peak. In all shots, the neutron emission started immediately after the maximum of $\dot{L} I$ voltage but it reached the peak 35 ns later. The neutron emission lasted for a quite long period with a 35 ± 5 ns FWHM. At this time, we did not observe any significant voltage peak and also the x-ray emission detected by silicon diodes was quite low. During the neutron emission, visible and XUV imaging recorded only a bright spot at the cathode whereas the streak camera showed the plasma expansion.

The total number of neutrons measured by the indium and silver activation counters in shot No 090930-2 was 2.6×10^{10} and 2.9×10^{10}, respectively. TLDs showed the neutron yield on the order of 10^{10}. The average neutron yield in all 11 shots was 3.5×10^{10} while the peak number of fusion neutrons in one shot approached 6×10^{10} at the maximum current of 1.3 MA. In comparison with previous experiments on the S-300, the yield is by one order

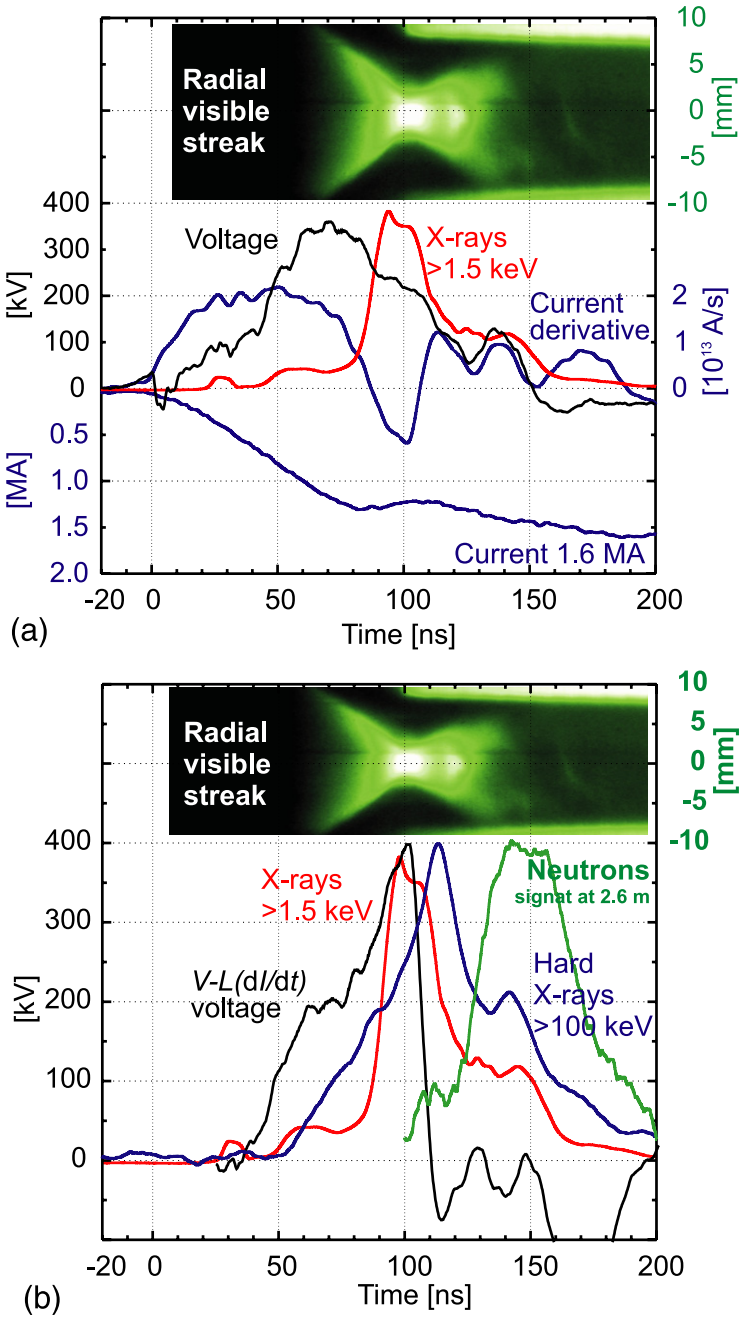

Figure 4. Discharge No 090930-2, the linear mass density of $20\,\mu g\,cm^{-1}$, the neutron yield of 3×10^{10}. (*a*) A visible streak image and waveforms of current, current derivative, voltage and x-rays. (*b*) A visible streak image and waveforms of $\dot{L}I$ voltage, x-ray, hard x-ray and neutron signals.

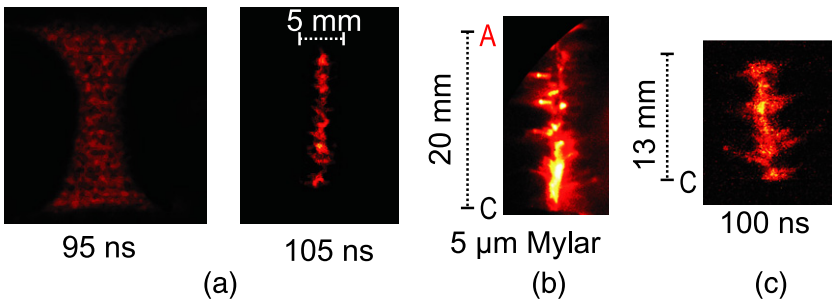

Figure 5. An example of images achieved with the deuterium gas puff. (*a*) Visible frames, shot No 090930-1, neutron yield of 4.5×10^{10}. (*b*) Time-integrated x-ray pinhole image, shot No 090928-1, neutron yield of 2×10^{10}. (*c*) XUV pinhole image, shot No 090930-2, neutron yield of 3×10^{10}.

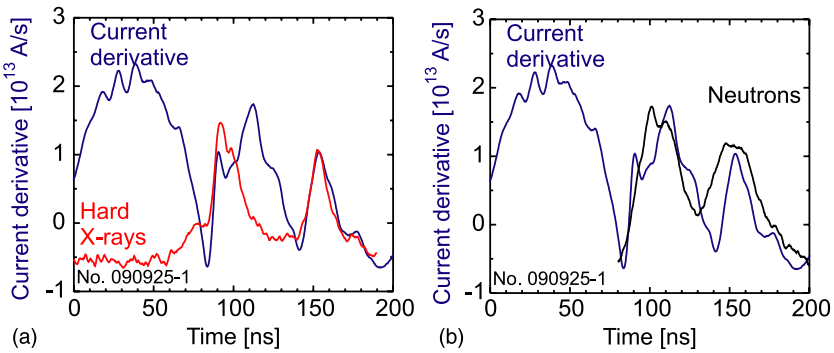

Figure 6. An example of the correlation of the $\mathrm{d}I/\mathrm{d}t$ signal with hard x-ray and neutron emission detected at the side-on detector at 2.6 m. The neutron signal was shifted by the TOF of 2.45 MeV neutrons. Shot No 090925, neutron yield of 3×10^{10}. (*a*) $\mathrm{d}I/\mathrm{d}t$ signal and hard x-rays. (*b*) $\mathrm{d}I/\mathrm{d}t$ signal and neutrons.

higher than the one with deuterated fibres [26, 32], X-pinches, deuterated foams [33, 34] and imploding wire-arrays [26].

3.3. Correlation of neutron and hard x-ray emission with $\mathrm{d}I/\mathrm{d}t$ *signal*

Temporal correlations of neutron and hard x-ray emission with electrical characteristics were investigated because we believe that it could throw more light on the process of accelerating charged particles. A common feature of our experiment was the correlation of hard x-rays with the signal of the $\mathrm{d}I/\mathrm{d}t$ probe. The most exemplary result was observed in the shot with one additional neutron pulse at 150 ns (cf figure 6). In all shots, the rapid increase of hard x-rays started immediately after the dip in the $\mathrm{d}I/\mathrm{d}t$ signal. Further, it was clear that the maxima of hard x-rays corresponded to the $\mathrm{d}I/\mathrm{d}t$ peaks. The current increase caused by these $\mathrm{d}I/\mathrm{d}t$ peaks was 100–200 kA.

Similar correlations were observed also in the case of neutron emission. However, neutrons were usually a little delayed which could be ascribed (i) to the time separation between deuteron acceleration and neutron production, (ii) to the transit time of neutrons through the TOF detector and (iii) to the uncertainty of neutron energy estimation.

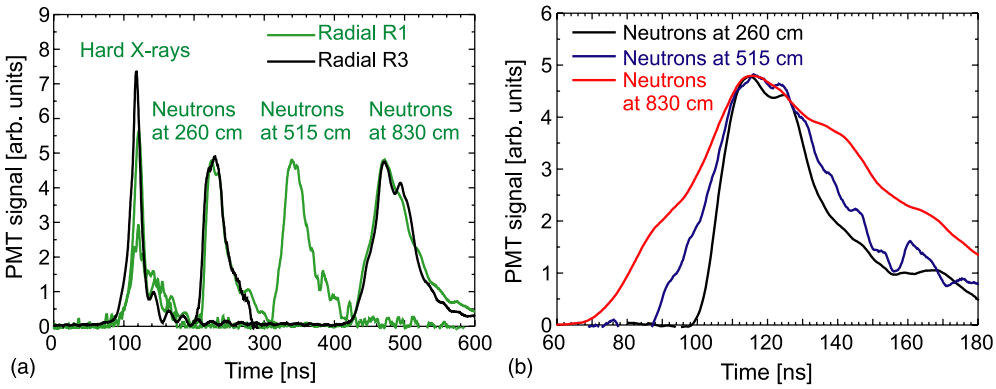

Figure 7. Neutron TOF signals on the side-on detectors in discharge No 090922, the neutron yield of 3×10^{10}. (*a*) Side-on TOF signals shifted by the TOF of x-rays. Neutron TOF detector (R3) at 515 cm was saturated in this particular shot. (*b*) Neutron TOF signals at various radial positions shifted by the TOF of 2.45 MeV neutrons.

3.4. Neutron energy spectra

Eleven fast plastic scintillators and photomultiplier tubes enabled the TOF analysis of fusion neutrons. In figure 7 we can see a typical example of TOF signals measured in the side-on direction. The first peak at 120 ns corresponds to hard x-rays above 200 keV. Other pulses represent neutron signals at various distances. It can be seen how the neutron signal shifts and broadens with increasing distance from the neutron source. It was caused by different velocities of neutrons. Qualitatively, we calculated neutron energy spectra from TOF signals by a Monte Carlo reconstruction [23, 35]. The neutron spectra which we received are displayed in figure 8. In the downstream direction (on the Z-pinch axis behind the cathode), the mean neutron energy was 2.60 ± 0.08 MeV with a 700 ± 200 keV width. Let us remind the reader here that the term 'downstream' means the direction of current flow (from the anode towards the cathode). In the side-on direction, the mean neutron energy was 2.40 ± 0.05 MeV and the width of the neutron spectra was 600 ± 150 keV. As regards neutron spectra from all 11 shots, average values were almost the same as in figure 8.

3.5. Energy distribution function of reacting deuterons

The knowledge of neutron energy spectra at different directions could provide important information about kinetic energies of deuterons which produce fusion neutrons. If we assume a binary reaction of a fast deuteron with a stationary one, the neutron energy E_n depends on the deuteron energy E_d and on the laboratory angle between the colliding fast deuteron and the outgoing neutron θ as

$$E_n(E_d, \theta) = E_d \frac{m_n}{2(m_n + m_{He})} \cdot \left(\cos\theta + \sqrt{\frac{m_{He}}{m_n}\left(1 + \frac{2Q}{E_d}\right) - \sin^2\theta} \right)^2, \quad (1)$$

where $Q \doteq 3.27$ MeV represents the energy released from the D(d,n)^{3}He fusion reaction, m_n is the neutron mass and m_{He} is the mass of helium $^3_2$He. If the deuteron energy (below 300 keV in our experiment) is much smaller than the fusion energy of 3.3 MeV, it is possible to simplify

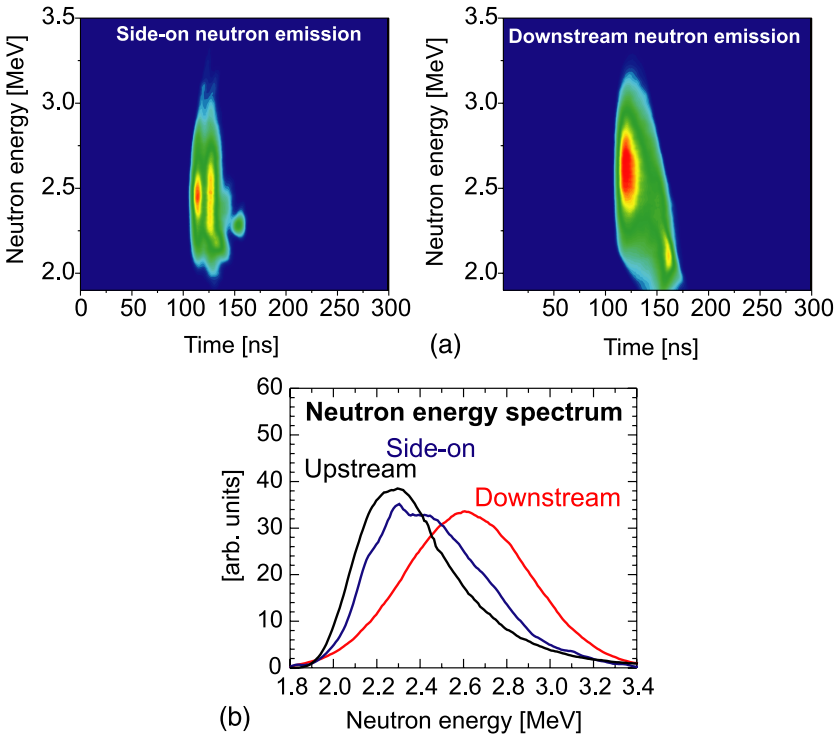

Figure 8. Neutron energy distribution functions in the side-on and end-on direction in shot No 090922, the neutron yield of 3×10^{10}. (*a*) Time-dependent. (*b*) Time-integrated.

the previous equation as

$$E_{\mathrm{n}}(E_{\mathrm{d}}, \theta) \doteq E_{\mathrm{d}} \frac{m_{\mathrm{n}}}{2(m_{\mathrm{n}} + m_{\mathrm{He}})} \cdot \left(\cos\theta + \sqrt{\frac{m_{\mathrm{He}}}{m_{\mathrm{n}}} \frac{2Q}{E_{\mathrm{d}}}} \right)^2 . \tag{2}$$

Then the component of deuteron kinetic energy in the direction of neutron detection can be calculated as

$$E_{\mathrm{d}} \cos^2\theta \doteq \frac{2(m_{\mathrm{n}} + m_{\mathrm{He}})}{m_{\mathrm{n}}} \cdot \left(\sqrt{E_{\mathrm{n}}} - \sqrt{\frac{m_{\mathrm{He}} Q}{m_{\mathrm{n}} + m_{\mathrm{He}}}} \right)^2 . \tag{3}$$

On the basis of the last equation, it was possible to transform the neutron spectra into energy distribution functions of deuterons which produced fusion neutrons. The distribution functions of the end-on and side-on component of kinetic energy obtained in the shot mentioned above can be seen in figure 9.

It can be clearly seen in figure 9 that most of the fusion neutrons were produced by deuterons with the kinetic energy component below 300 keV. It agrees with the fact that we observed the maximum neutron energy of about 3.2 MeV both in the side-on and end-on directions (see figure 8). As regards mean values, the mean axial component of the deuteron kinetic energy $\langle |E_{\parallel}| \rangle$ was 60 keV whereas the mean side-on component $\langle |E_{\perp}| \rangle$ was 40 keV. This means that the average kinetic energy of reacting deuterons was $\langle E_{\mathrm{d}} \rangle = \langle E_x + E_y + E_z \rangle = 2\langle |E_{\perp}| \rangle + \langle |E_{\parallel}| \rangle = 140\,\mathrm{keV} \doteq 150\,\mathrm{keV}$. From the deuteron energy spectra in figure 9, our Monte Carlo reconstruction estimated the downstream/upstream anisotropy of neutron flux as 1.1.

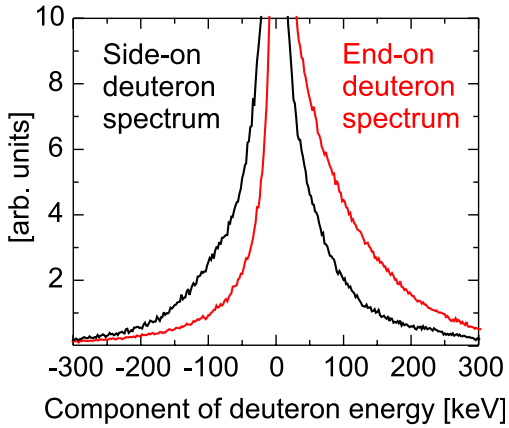

Figure 9. Distribution functions of kinetic energy components of reacting deuterons. The plus and minus signs of kinetic energy component reflect the direction of deuteron velocity. Shot No 090922, the neutron yield of 3×10^{10}.

4. Discussion

4.1. Mechanism of neutron production

On the basis of results presented above, we should be able to discuss neutron production mechanisms now. In this respect, two findings are of great importance. The first one concerns the time of neutron generation whereas the second one relates to neutron energy spectra.

4.1.1. Time of neutron emission. The first fundamental result is the time of neutron emission because most of the neutrons were not produced during the stagnation. Instead of that, they were produced during the global plasma expansion for quite a long period (35 ± 5 ns FWHM) after the soft x-ray peak. At this time, voltage peaks or a significant power input were not observed. However, the impedance was almost 0 despite the fact that the plasma was expanding. This means that the negative value of time-varying inductance $\dot{L}$ (which should be on the order of 0.1 Ω) was likely compensated by the plasma resistance R. The anomalously high resistance was reported on the Angara [14] and in PF [36, 37]. From the experimental point of view, the onset of microinstabilities just before neutron emission was clearly shown by Bernard *et al* with laser scattering in a plasma focus discharge [38]. With respect to PF, it seems worthy of remark that two neutron pulses were observed too. The first pulse was recorded during the so-called quiet phase of the stagnation and the second, i.e. the principal one, after the development of $m = 0$ instabilities [39].

As regards the temporal correlations in our experiment, the neutron and hard x-ray emission corresponded to peaks of the $\mathrm{d}I/\mathrm{d}t$ signal. This could be explained by the fact that charged particles accelerated to high energies carry a significant part of a fast changing electrical current. It follows that the acceleration mechanism is connected with global plasma dynamics and therefore it cannot be regarded as a 'secondary' process in plasma.

4.1.2. Neutron energy spectra. The second important topic in the discussion of neutron production mechanism is the analysis of measured neutron energies. As regards deuterium gas puff experiments on the S-300 generator, the mean neutron energy detected downstream was shifted from 2.45 MeV towards higher energies whereas the upstream neutron energy spectrum

had the maximum at about 2.2 MeV. That is why most fusion reactions were realized in the centre of the mass frame which was moving with respect to the laboratory frame of reference. One could therefore think that a deuteron beam was accelerated towards the cathode. However, a small shift from 2.5 MeV could have been either a result of a thermonuclear source moving towards the cathode or a consequence of an inhomogeneous density of target deuterons. And because the observed neutron emission anisotropy was too small to exclude a significant part of thermonuclear neutrons, the much more important result was the neutron energy spectrum measured in the side-on direction. What were the advantages that this direction brought to us? The first advantage of the side-on direction was a higher number of detectors in a row. The second advantage was a smaller influence of scattered neutrons because side-on diagnostic ports of 10 cm diameter and 1.5 m length were surrounded by water without significant mass distributed along the line of sight. On account of both these advantages side-on neutron energy spectra could be reconstructed more accurately. The important parameter regarding the side-on direction is a width of neutron energy spectra. In our experimental campaign, the broad width of side-on neutron energy spectra implied a high radial velocity of deuterons. If we assume the significant part of thermonuclear neutrons, the width of neutron energy spectrum would be given by $\triangle E_{\mathrm{n}}\,(\mathrm{keV}) = 82.5\sqrt{kT_{\mathrm{i}}[\mathrm{keV}]}$ (e.g. [40]). Therefore the 500 keV FWHM would require an unreasonably high temperature of 40 keV.

All these facts together, i.e. the time of neutron emission and the energy spectra, imply that most of the neutrons were not of thermonuclear origin. This could perhaps lead us to speak about the beam–target model. Nevertheless, the neutron production cannot be explained by a simple concept of the linear beam–target model because of a significant radial component of deuteron velocities. The observed spectra have to be explained by a broad angular dependence of the deuteron energy distribution function. The question of how deuterons are accelerated (e.g. if axially accelerated deuterons are bent by magnetic fields before they produce fusion neutrons or if the acceleration could occur also in the side-on direction) is being investigated and it is the subject of our future experiments.

4.2. Thermonuclear yield

Apparently, the thermonuclear mechanism was not dominant. In order to support such an observation, it is possible to calculate an expected thermonuclear yield from plasma parameters reached in our experiment. The thermonuclear yield is given by the equation

$$Y_{\mathrm{thermonuclear}} = \tfrac{1}{2} n_{\mathrm{i}}^2 \langle \sigma v \rangle_T \pi R^2 l \tau. \tag{4}$$

Plasma parameters are estimated in table 2. The ion temperature $T = 1$ keV was calculated from the energy input W_{input} and the total numbers of deuterons N_{total}.

For the plasma density $n_{\mathrm{i}} = 2 \times 10^{20}\ \mathrm{cm}^{-3}$, the plasma length $l = 2$ cm, the plasma radius $R = 1$ mm and the confinement time $\tau = 5$ ns, one obtains 2×10^8 thermonuclear neutrons. This is on the order of one per cent of the total neutron yield and on the order of the first neutron pulse observed immediately after the stagnation in figure 4(*b*).

4.3. Total energy of deuterons accelerated to fusion energies

The beam–target mechanism was identified in Z-pinches already in the 1950s. It was considered as a very pessimistic result with respect to fusion energy production. However, high neutron yields need to be studied and explained in more detail. This is the reason why it is interesting to calculate the number and energy of fast deuterons similarly to the way it was done for the Z-machine by Velikhovich *et al* in [19].

Table 2. Estimated plasma parameters.

Linear mass density	$m = 20\,\mu\mathrm{g\,cm^{-1}}$
Line density	$N = 6 \times 10^{18}$ deuterons $\mathrm{cm^{-1}}$
Length of plasma column	$l = 2\,\mathrm{cm}$
Total number of deuterons	$N_{\mathrm{total}} = Nl = 6 \times 10^{18} \cdot 2 \doteq 10^{19}$
Plasma radius during stagnation	$R \gtrsim 0.1\,\mathrm{cm}$
Ion density	$n_{\mathrm{i}} = N/\pi R^2 \approx 2 \times 10^{20}\,\mathrm{cm^{-3}}$
Energy input	$W_{\mathrm{input}} = \frac{1}{2}\int_0^{t_{\mathrm{imp}}} \dot{L} I^2 \mathrm{d}t \approx 8\,\mathrm{kJ}$
Temperature	$k(T_{\mathrm{i}} + T_{\mathrm{e}}) = \frac{2}{3} W_{\mathrm{input}}/N_{\mathrm{total}} \doteq 2\,\mathrm{keV}$
Ion temperature for $kT_{\mathrm{i}} = kT_{\mathrm{e}}$	$T = T_{\mathrm{i}} \doteq 1\,\mathrm{keV}$
D(d,n)^{3}He fusion reaction rate [41]	$\langle \sigma v \rangle_{T=1\,\mathrm{keV}} = 0.75 \times 10^{-22}\,\mathrm{cm^3}$
Confinement time	$\tau = 5\,\mathrm{ns}$
Ion–ion collision time	$\tau_{\mathrm{ii}} = 1/\nu_{\mathrm{ii}} = 0.4\,\mathrm{ns} \ll 5\,\mathrm{ns}$

The number of accelerated deuterons N_{d} depends on the neutron yield Y_{n}, the fusion cross-section $\sigma_{\mathrm{fusion}}(E_{\mathrm{d}})$, the deuteron density n_{d} and the path length l as

$$N_{\mathrm{d}} = \frac{Y_{\mathrm{n}}}{\sigma_{\mathrm{fusion}}(E_{\mathrm{d}}) n_{\mathrm{d}} l}. \tag{5}$$

In our experiment we measured the neutron yield $Y_{\mathrm{n}} \doteq 4 \times 10^{10}$ and the average energy of reacting deuterons $\langle E_{\mathrm{d}} \rangle \approx 150\,\mathrm{keV}$. Deuterons with such a kinetic energy have the fusion cross-section $\sigma_{\mathrm{fusion}}(150\,\mathrm{keV}) = 2.8 \times 10^{-30}\,\mathrm{m^{-2}}$ (see [42]).

During the main neutron emission, the plasma was expanded to the radius R greater than 5 mm. Because the line density of deuterons was $N = 6 \times 10^{18}$ deuterons $\mathrm{cm^{-1}}$, the upper value of ion density $n_{\mathrm{d}} = N/\pi R^2$ was $7.5 \times 10^{18}\,\mathrm{cm^{-3}}$. Further, one can estimate the path length of fast deuterons as $l \approx 3\,\mathrm{cm}$. For these values one obtains the number of accelerated deuterons $N_{\mathrm{d}} \approx 6 \times 10^{16}$. It is only a small fraction of the total number of deuterons $N_{\mathrm{total}} \doteq 10^{19}$ but it can be connected with a significant current and energy. The velocity of 150 keV deuterons is $3 \times 10^6\,\mathrm{m\,s^{-1}}$; therefore 6×10^{16} deuterons carry 30 kA current (cf with a 100–200 kA rise of the current during the hard x-ray and neutron emission). As regards the total energy of deuterons accelerated to fusion energies $W_{\mathrm{d}} = N_{\mathrm{d}} \langle E_{\mathrm{d}} \rangle$, it was above 1.5 kJ which is more than 15% of the energy input into a plasma during the implosion $W_{\mathrm{input}} = \frac{1}{2}\int_0^{t_{\mathrm{imp}}} \dot{L} I^2\,\mathrm{d}t$.

Since that is a surprisingly high efficiency, we wanted to be quite certain about this value. Firstly, the neutron yield was measured by several independent methods. Secondly, it was necessary to discuss the strong dependence of the fusion cross-section on the deuteron energy E_{d}. The total energy W_{d} is proportional to $\int f_{\mathrm{d}}(E_{\mathrm{d}}) E_{\mathrm{d}}/\sigma_{\mathrm{fusion}}(E_{\mathrm{d}})\,\mathrm{d}E_{\mathrm{d}}$. Since the ratio $E_{\mathrm{d}}/\sigma_{\mathrm{fusion}}(E_{\mathrm{d}})$ is the smallest exactly for $E_{\mathrm{d}} = 150\,\mathrm{keV}$, it means that we did a lower estimate of the total energy $W_{\mathrm{d}} \geqslant N_{\mathrm{n}} \langle E_{\mathrm{d}} \rangle / \sigma_{\mathrm{fusion}}(\langle E_{\mathrm{d}} \rangle) n_{\mathrm{d}} l$. Thirdly, the path length of 3 cm should be a credible estimation because such a distance is on the order of the anode–cathode separation. The length of 3 cm is also travelled by 150 keV deuterons during 10 ns which is the characteristic time of observed changes in neutron emission.

Finally, the most uncertain parameter was the density of target deuterons. We calculated the upper value of the density from the known linear mass density and from the observed diameter of globally expanding plasma which was detected by the streak camera. The density could have been higher than $7.5 \times 10^{18}\,\mathrm{cm^{-3}}$ in two cases. In the first case, the density could have been increased by secondary, local implosions; however, such implosions occurred usually before the main neutron pulse and were not observed during the peak of neutron emission. Moreover, there is a question of how to confine fast deuterons in a small, dense locality to

Table 3. Basic parameters and results achieved on Angara [14] and S-300 (this work).

	Angara	S-300
Current	2–3 MA	1.35–1.65 MA
Energy input W_{input}	20–30 kJ	<10 kJ
Linear mass density	5–50 μg cm^{-1} axial gradient of linear density	20 μg cm^{-1}
Anode–cathode separation	2–4 cm	1–2 cm
Initial diameter of solid gas puff	1.5–3.0 cm at cath. <6 cm at anode	4 cm
Implosion velocity	(4–5) $\times$ 10^5 m s^{-1}	(3–4) $\times$ 10^5 m s^{-1}
Zipper	35 ns	<10 ns
Time of neutron emission	after implosion after voltage drop	after implosion after voltage drop
Duration of neutron emission	40–50 ns FWHM	35 $\pm$ 5 ns FWHM
Peak neutron yield	$\approx 10^{12}$	6 $\times$ 10^{10}
FWHM of side-on energy spectrum	300 keV	600 $\pm$ 200 keV

achieve a sufficiently high pass length. In the second case, there might have remained a high density plasma near the Z-pinch axis even though the outer plasma shell expanded. We should exclude this possibility by laser probing in future experiments. Now we can argue that a dense region should be visible if it is heated by Coulomb collisions with a large number of fast deuterons. Further, it is possible to exclude neutron production outside the inter-electrode region: since the cathode was not hollow, the significant number of neutrons produced above the anode should cause a neutron emission anisotropy and a large shift of upstream neutron energies above 2.5 MeV. Such a result has, however, not been observed.

We conclude this discussion with an important argument about high efficiency of deuteron acceleration observed in PF and on the Angara Z-pinch. In PF devices, almost 10% conversion efficiency of stored energy into >25 keV deuterons is reported [43]. On the Angara [14], the neutron yield of 10^{12}, the deuteron energies of about 500 keV, the plasma (target) density of 10^{20} cm^{-3} with the path length of 4 cm imply the total number of deuterons of 4×10^{16} with an energy of 3 kJ. Since the energy input on the Angara was 20–30 kJ, the conversion efficiency to the energy of fast deuterons was also about 15%. Such a value is similar to the one achieved in our experiment with comparable electrical parameters.

4.4. Comparison with deuterium gas puffs on the Angara Z-pinch

The previous paragraph shows that the total numbers of accelerated deuterons are similar on the S-300 as well as on the Angara. At this point it seems proper to also provide a comparison of other parameters in both experiments (see table 3).

As regards the neutron emission, there were a lot of similarities. In both experiments, neutrons were produced for quite a long period after the implosion and after the voltage peak. The principal distinction between both experiments was the strong axial gradient of the linear gas puff density and the subsequent zipper. This difference could explain relatively high neutron yields achieved on the Angara Z-pinch and one order lower yield on the S-300 generator. On the one hand, the neutron yield on the S-300 was lower. But on the other hand, homogeneous plasma with the zipper below 10 ns and also the solid centre of the cathode are more convenient for the discussion of where and when deuterons are accelerated and where and when fusion neutrons are produced. The experiment at the Kurchatov Institute clearly showed that deuterons were accelerated in a lower density plasma during the global plasma

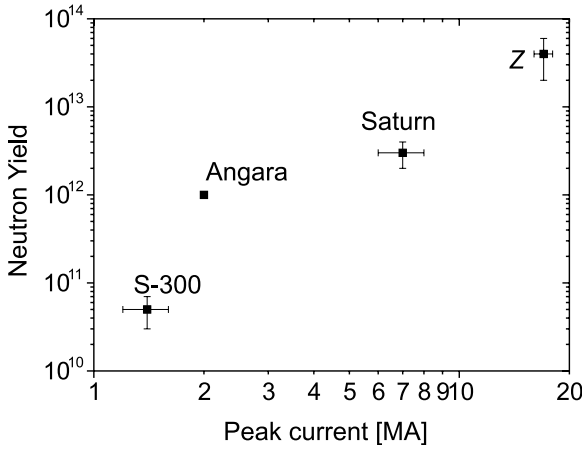

Figure 10. Neutron yields from deuterium gas puff Z-pinches [14, 16, 17].

expansion. Because of the axially homogeneous gas puff, also the density of a target plasma was low and subsequently the neutron yield was lower than on the Angara. On the Angara, deuterons were supposed to be accelerated also in a low density plasma. However, because of the axial gradient of plasma density, these deuterons could produce more neutrons in a dense plasma near the hollow cathode. We note that an analogical axial density gradient influences neutron yields in PF where a large number of neutrons are produced in a dense structure at the heel of the current sheath [6, 44, 45]).

4.5. Neutron yield scaling with current

To know the scaling law for a neutron yield is of crucial importance for future applications of Z-pinch facilities as sources of neutrons. This is why we present peak neutron yields achieved with deuterium gas puffs in figure 10.

The neutron yield from the S-300 is important for two reasons. Firstly, it makes it possible to enlarge the neutron scaling law for deuterium gas puffs below 2 MA currents. Secondly, it provides a reasonable comparison with experiments on Sandia's Saturn and Z-machine because all these gas puffs were more axially homogeneous than the one used on the Angara. If we leave out the neutron yield on the Angara, the total number of neutrons scales as $I^{2.9\pm0.2}$ in the 1.5–17 MA region. At 15 MA current, there is a hope of a large thermonuclear component. As regards the thermonuclear source, the neutron yield should theoretically increase as the fourth power of an electric current, i.e. $Y_n \propto n^2 \propto I^4$. If this I^4 law is valid above 20 MA currents, high current Z-pinches might be powerful sources of neutrons.

When thermonuclear fusion is concerned, the neutron yield, however, is not the most relevant parameter. A much more important value is the ratio between the energy released from fusion and the energy input into a plasma. In order to have this ratio high enough, it is not sufficient just to reach a high temperature, it means to accelerate a significant fraction of deuterons by elastic collisions in a Maxwellian plasma. It is also necessary to keep these fast deuterons in this high temperature region. (If deuterons escape a high temperature region, they are slowed down by cold deuterons usually without undergoing fusion reactions. Since $\sigma_{\text{fusion}}(E_\text{d})Q \ll \sigma_{\text{Coulomb}}(E_\text{d})E_\text{d}$, the fusion energy released is always smaller than the energy expended on the acceleration of fast deuterons. The only way to achieve the energy gain is to transfer the lost energy of fast deuterons to the acceleration of other deuterons in the same

plasma). In other words, it is necessary to have a sufficiently long time and enough high plasma density to produce a large number of fusion reactions. This condition has been expressed by the known Lawson criterion. At this stage we found it interesting to calculate the necessary density of Z-pinch plasmas from the Lawson criterion $n\tau \approx 10^{14}\,\mathrm{cm}^{-3}\,\mathrm{s}$.

Let us assume the confinement time of a gas puff Z-pinch $\tau = R/v_{T_i}$ on the order of 5 ns. Then the required density is about $2 \times 10^{22}\,\mathrm{cm}^{-3}$. This value is about 60 times higher than the plasma density achieved with 17 MA on the Z-machine [19]. If we consider the same character of implosions, i.e. the same value of dimensionless scaling parameter Π [46], then $n \propto m \propto I^2$ and the Lawson criterion could be achieved with 100 MA current drivers. It is a fairly high current. However, only a few experiments have been carried out with deuterium gas puffs. Therefore, more shots with multi-MA drivers and with various Z-pinch configurations (see, e.g., [46, 47] and references herein) are needed in order to study neutron production mechanism and to find out if it is possible to increase the plasma density and mainly the confinement time.

5. Conclusions

The neutron production and dynamics of deuterium gas puffs were studied on the S-300 generator. The axially homogeneous gas puff with the zipper below 10 ns and with the solid centre of the cathode was well suited for the discussion of where and when deuterons were accelerated and fusion neutrons were produced. The study of neutron emission was focused mainly on the estimation of neutron energies and neutron emission time, the anisotropy of neutron emission and the energy distribution of deuterons which produced fusion neutrons.

In the case of the linear mass density of $20\,\mu\mathrm{g\,cm}^{-1}$, the gas puff imploded onto the axis before the current peak at about 100 ns. The fusion neutrons were generated after the gas puff implosion during the global expansion of a plasma column. The neutron emission lasted on average 35 ± 5 ns. In the downstream direction (on the Z-pinch axis behind the cathode), the mean neutron energy was 2.6 ± 0.1 MeV. The side-on neutron energy spectra peaked at 2.40 ± 0.05 MeV with about 600 ± 150 keV FWHMs. The broad width of the side-on neutron spectra implied a high radial component of deuteron velocity. The average kinetic energy of fast deuterons, which produced fusion neutrons, was about 150 keV. Most of the fusion neutrons were produced by deuterons with the kinetic energy below 300 keV. At the current level of 1.5 MA, the peak neutron yield reached a value of 6×10^{10}. It is by one order higher in comparison with previous experiments with deuterated fibres, X-pinches, deuterated foams and imploding wire-arrays on the same current generator.

On the basis of the above-mentioned experimental data and observed plasma parameters, we concluded that, on the one hand, most of the neutrons were not of thermonuclear origin. On the other hand, however, the total energy of deuterons accelerated to fusion energies was above 1.5 kJ. It is more than 15% of the energy input into a plasma and therefore gas puff Z-pinches seem to be not only powerful sources of x-ray radiation but also efficient sources of $\approx$100 keV deuterons. Such a result is consistent with a high neutron yield observed on the Angara Z-pinch and PF with similar currents.

Acknowledgments

This research has been supported by project No LC528, No LA08024, No ME09087 of the Ministry of Education of the Czech Republic, by grant No SGS10/266/OHK3/3T/13 of the Grant Agency of the Czech Technical University in Prague, by the GACR grant No 202-08-P084 and by the IAEA Grant RC14817.

References

[1] Andrianov A M *et al* 1958 *Proc. 2nd United Nations Int. Conf. on Peaceful Uses of Atomic Energy, Geneva, 1958* vol 31 ed J H Martens *et al (United Nations, Geneva, Switzerland, 1958)* p 348
[2] Mather J W and Williams A H 1958 *Proc. 2nd United Nations Int. Conf. on Peaceful Uses of Atomic Energy, Geneva, 1958* vol 32 ed J H Martens *et al (United Nations, Geneva, Switzerland, 1958)* p 26
[3] Anderson O A *et al* 1958 *Phys. Rev.* **110** 1375
[4] Bernard A *et al* 1979 *Plasma Physics and Controlled Fusion Research (IAEA-CN-37), 7th IAEA Conf. on Plasma Physics and Controlled Nuclear Fusion (Innsbruck, Austria, 1978)* vol 2 (Vienna: IAEA) p 159
[5] Soto L 2005 *Plasma Phys. Control. Fusion* **47** A361
[6] Gribkov V A *et al* 2007 *J. Phys. D: Appl. Phys.* **40** 3592
[7] Lee S and Saw SH 2008 *J. Fusion Energy* **27** 292
[8] Kubes P *et al* 2009 *IEEE Trans. Plasma Sci.* **37** 2191
[9] Sethian J D *et al* 1987 *Phys. Rev. Lett.* **59** 892
[10] Sethian J *et al* 1991 *Workshop on Physics of Alternative Magnetic Confinement Schemes (Varenna, Italy, 1990)* ed S Ortolani and E Sindoni (Bologna, Italy: Editrice Compositori) p 511
[11] Scudder D W 1991 *Workshop on Physics of Alternative Magnetic Confinement Schemes (Varenna, Italy, 1990)* ed S Ortolani and E Sindoni (Bologna, Italy: Editrice Compositori) p 519
[12] Kies W *et al* 1991 *J. Appl. Phys.* **70** 7261
[13] Lebedev S *et al* 1998 *Phys.Plasmas* **5** 3366
[14] Batyunin A V *et al* 1990 *Sov. J. Plasma Phys.* **16** 597
[15] Smirnov V P 1991 *Plasma Phys. Control. Fusion* **33** 1697
[16] Spielman R B *et al* 1998 *D–D Fusion Experiments Using Fast Z Pinches* (Sandia National Laboratories) Rep. SAND98-0705
[17] Coverdale C A *et al* 2007 *Phys. Plasmas* **14** 022706
[18] Coverdale C A *et al* 2007 *Phys. Plasmas* **14** 056309
[19] Velikovich A L *et al* 2007 *Phys. Plasmas* **14** 022701
[20] Welch D R *et al* 2009 *Phys. Rev. Lett.* **103** 255002
[21] Scholz M *et al* 2001 *Nukleonika* **46** 35
[22] Krauz V I 2006 *Plasma Phys. Control. Fusion* **48** B221
[23] Klir D *et al* 2009 *IEEE Trans. Plasma Sci.* **37** 425
[24] Chernenko A S *et al* 1996 *11th Int. Conf. on High Power Particle Beams (Prague, Czech Republic)* vol 1 ed J Ullschmied (Prague: Academy of Science of Czech Republic) p 154
[25] Bakshaev Yu L *et al* 1996 *11th Int. Conf. on High Power Particle Beams (Prague, Czech Republic)* vol 2 ed J Ullschmied (Prague: Academy of Science of Czech Republic) p 962
[26] Klir D *et al* 2008 *Phys. Plasmas* **15** 032701
[27] Anan'ev S S *et al* 2008 *Plasma Phys. Rep.* **34** 574
[28] Waisman E M *et al* 2008 *Phys. Plasmas* **15** 042702
[29] Velyhan A *et al* 2006 *Phys. Scr.* **T123** 112
[30] Tiseanu I, Decker G and Kies W 1996 *Nucl. Instrum. Methods Phys. Res.* A **373** 73
[31] Tiseanu I and Craciunescu I 1996 *Nucl. Sci. Eng.* **122** 384
[32] Klir D *et al* 2006 *Phys. Scr.* **T123** 116
[33] Bakshaev Yu B *et al* 2006 *Plasma Phys. Rep.* **32** 531
[34] Akunets A A *et al* 2009 *Eur. Phys. J.* D **54** 499
[35] Řezáč K *et al* 2006 *Czech J. Phys.* **56** B357
[36] Decker G *et al* 1983 *Phys. Fluids* **26** 571
[37] Bernard A 1978 *Atomkernenergie* **32** 73
[38] Bernard A *et al* 1975 *Phys. Fluids* **18** 180
[39] Schmidt H *et al* 2006 *IEEE Trans. Plasma Sci.* **34** 2363
[40] Wolle B 1999 *Phys. Rep.* **312** 1
[41] Huba J D 2009 *NRL Plasma Formulary* (Washinghton DC: Naval Research Laboratory) p 45
[42] Chadwick M B *et al* 2006 *Nucl. Data Sheets* **107** 2931
[43] Stygar W, Gerdin G, Venneri F and Mandrekas J 1982 *Nucl. Fusion* **22** 1161
[44] Sadowski M J and Malinowska A 2006 *Czech. J. Phys.* **56** B364
[45] Kubes P *et al* 2010 *IEEE Trans. Plasma Sci.* **38** 672
[46] Ryutov D D, Derzon M S and Matzen M K 2000 *Rev. Mod. Phys.* **72** 167
[47] Slutz S A *et al* 2010 *Phys. Plasmas* **17** 056303

ARTICLE NO. 5

Experimental evidence of thermonuclear neutrons in a modified plasma focus

D. Klir,[1,a)] P. Kubes,[1] M. Paduch,[2] T. Pisarczyk,[2] T. Chodukowski,[2] M. Scholz,[2] Z. Kalinowska,[2] E. Zielinska,[2] B. Bienkowska,[2] J. Hitschfel,[1] S. Jednorog,[2] L. Karpinski,[2] J. Kortanek,[1] J. Kravarik,[1] K. Rezac,[1] I. Ivanova-Stanik,[2] and K. Tomaszewski[3]
[1]*FEE, Czech Technical University in Prague, Technicka 2, 16627 Prague 6, Czech Republic*
[2]*Institute of Plasma Physics and Laser Microfusion, 23 Hery St., 00-908 Warsaw, Poland*
[3]*ACS Ltd., Advanced Diagnostics Laboratory, 23 Hery St., 01-497 Warsaw, Poland*

(Received 20 December 2010; accepted 24 January 2011; published online 14 February 2011)

The PF-1000 plasma focus was modified by adding the cathode disk 3 cm in front of the anode. This modification facilitated the evaluation of neutron energy spectra. Two neutron pulses were distinguishable. As regards the first neutron pulse, it lasted 40 ns during the plasma stagnation and it demonstrated high isotropy of neutron emission. A peak neutron energy detected upstream was 2.46 ± 0.02 MeV. The full width of neutron energy spectra of 90 ± 20 keV enabled to calculate an ion temperature of 1.2 keV. These parameters and a neutron yield of 10^9 corresponded to theoretical predictions for thermonuclear neutrons. © *2011 American Institute of Physics*.
[doi:10.1063/1.3555447]

The search for thermonuclear neutrons in Z-pinches and plasma foci began in the 1950s. At the outset of controlled thermonuclear fusion research, compressional Z-pinches were found to produce a large number of neutrons which originated from $D(d,n)^3He$ reactions; however, neutrons were not of thermonuclear origin.[1] The dominant fraction of beam-target neutrons and no direct evidence of thermonuclear neutrons were also reported in plasma focus studies in the 1970s and 1980s.[2] More recently, on a 10 MA current level, significant thermonuclear neutron yield has been simulated for deuterium gas puff Z-pinches on *Z*,[3,4] but insufficient experimental evidence has been provided. As for late plasma focus experiments,[5,6] the possibility of thermonuclear neutrons was identified during the pinch phase; however, the interpretation of results was not unambiguous. In this paper, we would like to provide more explicit experimental evidence of thermonuclear neutrons.

The experiments were carried out at the PF-1000 plasma focus (2.0 MA peak current, 24 kV charging voltage, 400 kJ stored energy).[7] The facility was equipped with Mather-type coaxial electrodes (48 cm length, 23 cm anode diameter). The cathode was composed of 12 stainless-steel rods distributed around a cylinder of 40 cm diameter. The initial pressure of a deuterium gas was between 160 and 240 Pa (i.e., relatively low for the sake of increasing an implosion velocity). In order to search for thermonuclear neutrons, the plasma focus was modified by placing a cathode disk 3 cm in front of the anode and by adding a copper plug into the hollow anode (see Fig. 1). The fixed length of a plasma column enabled to correlate plasma dynamics with neutron emission and to calculate an inductance and a power input during the radial phase more precisely. In addition to that, the shorter length caused a higher current during the pinch phase, a less significant zipper, and shorter neutron emission which facilitated the evaluation of neutron energy spectra.

Plasma dynamics was studied by means of a 16-frame laser interferometric system.[9] An illustrative example of analyzed interferograms[10] is shown in Fig. 2. Figure 3 then presents the neutron emission detected by a radial time-of-flight (TOF) detector[11] at 3 m. In shot 9006, a quite stable snowplough implosion was seen. The maximum implosion velocity v_{imp} exceeded 3.5×10^5 m/s. During a quiet phase at 10 ns, the first neutron peak was observed. The stagnation at about 15 mm diameter lasted 40 ns and then the second implosion with $m=0$ instabilities occurred. The main neutron emission started after the disruptive development of instabilities at 100 ns. Two neutron pulses were also observed in other mega-ampere plasma foci[12] and gas puff Z-pinches.[13,14] In what follows, we would like to deal with the question whether a fraction of neutrons in the first pulse may be explained by thermonuclear mechanism.

On the basis of analyzed interferograms and electric measurements, we were able to calculate important plasma parameters. To start with data from interferograms, we received a total number of deuterons of 4×10^{19} and a peak electron density of 10^{19} cm^{-3}. The implosion velocity of 3.5×10^5 m/s implied an ion temperature of 850 eV. This value was increased by adiabatic compression. In order to include this effect, we calculated the ion temperature from the energy input assuming that 80% of measured current is flowing inside the current sheath (this fraction corresponded to the observed implosion velocity). For the measured energy

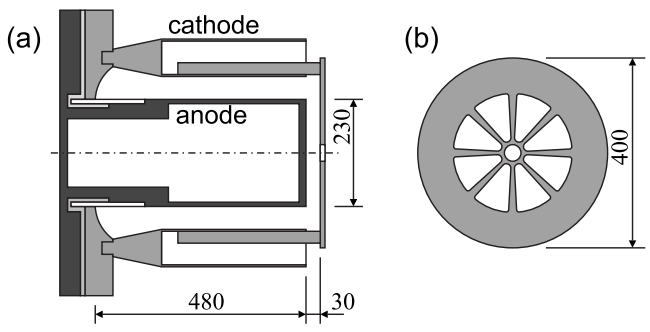

FIG. 1. (a) The side-on and (b) the end-on schematic of electrodes at a modified PF-1000 plasma focus (cf. with Ref. 8). Dimensions are in mm.

a)Electronic mail: daniel.klir@fel.cvut.cz.

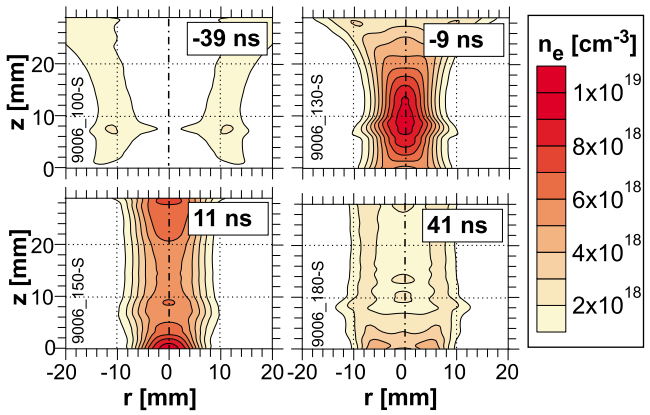

FIG. 2. (Color online) The sequence of electron density distributions in shot 9006.

input during the radial phase $W=\frac{1}{2}\int_{\text{rad}} dL/dt I^2 dt = 13$ kJ, we received $k(T_i+T_e)=\frac{2}{3}W/N=1.3$ keV. Since the density is below 10^{19} cm^{-3}, the electron-ion temperature equilibration time is above 80 ns for $T_e \geq 300$ eV. Therefore, the lower estimate of the ion temperature during the stagnation is 1.0 keV. At this ion temperature, the ion-ion collision time of 8 ns is several times shorter than the duration of the pinch phase. Then, for the total ion density N of 4×10^{19}, the average density $\bar{n}_i$ of 8×10^{18} cm^{-3}, the confinement time τ of 40 ns and the D(d,n)^{3}He fusion reaction rate $\langle\sigma v\rangle_{1\text{ keV}}$ of 0.75×10^{-22} cm^3, we obtain the thermonuclear yield $Y=\frac{1}{2}N\bar{n}_i\langle\sigma v\rangle_{1\text{ keV}}\tau$ of 5×10^8. It is on the order of several percents of measured neutron yields.

Such a small fraction of neutrons is, however, difficult to observe. For this reason, neutron detectors should be placed on the axis in a so-called upstream direction.[15] In this direction, 2.45 MeV neutrons are one of the fastest and they could be distinguished from beam-target and scattered neutrons which are emitted during the second pulse. Downstream, on the contrary, it was not possible to observe the first neutron pulse at the distance of 16 m since it was concealed by the second pulse. Therefore, we placed one TOF detector side-on at 3 m, one detector downstream at 7 m, and four detectors upstream at 7, 24, 50, and 83.7 m. In Fig. 4(a), there are TOF signals which were recorded by the upstream detectors at 7 and 24 m in the shot described above. We chose this shot with a modest neutron yield because the first pulse of

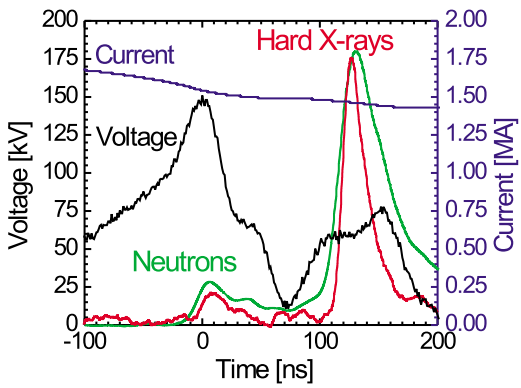

FIG. 3. (Color online) Waveforms of current, $V-LdI/dt$ voltage, hard x-rays, and radial neutrons at 3 m. Neutrons were shifted by TOF of 2.45 MeV neutrons. The time $t=0$ corresponds to the voltage peak. Shot 9006, 190 Pa D_2 pressure, 2×10^{10} neutron yield.

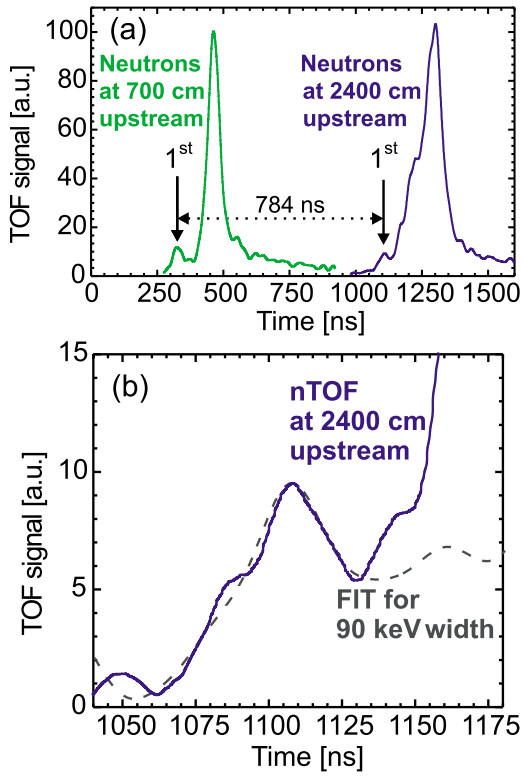

FIG. 4. (Color online) (a) Neutron signals detected upstream at 7 and 24 m in shot 9006. 784 ns corresponds to 2.46 MeV neutrons. (b) The first neutron pulse at 24 m and the fit for the energy spectrum with the 2.46 MeV peak and 90 keV width.

6×10^8 neutrons was still clearly visible at these detectors and therefore neutron energies could be inferred.

From the time-of-flight of the first peak at 7 and 24 m, it was possible to find with precision that these neutrons were emitted during the stagnation and their peak energy was 2.46 ± 0.02 MeV. This is a very important finding because most of beam-target mechanisms are based on axially accelerated deuterons which produce lower energetic neutrons in the upstream direction.[1] Nevertheless, the thermonuclear mechanism is not the only one which could provide a 2.45 MeV peak in the axial direction. Such a peak could be produced, for instance, by deuterons accelerated in the radial direction by the gyroreflecting mechanism.[16] Therefore, more unambiguous support for the thermonuclear mechanism here should be the measurement of a width of neutron energy spectra. For that purpose, we used the Monte Carlo method and we simulated TOF signals at 7 and 24 m for the instant neutron source with the Gaussian energy spectrum with 2.46 MeV peak and various widths. Then, the simulated TOF signal at 24 m was deconvoluted by the response at 7 m. Finally, the obtained response was convoluted with the measured neutron signal at 7 m and the result was compared with the signal at 24 m. In shot 9006, the best fit of the neutron TOF signal at 24 m was found for a 90 keV width [see Fig. 4(b)].

As regards average values from seven shots, we received the neutron yield of 7×10^8 and the width ΔE_n of 90 ± 20 keV. On the one hand, such a narrow spectrum is inconsistent with proposed beam-target models. On the other hand, this spectrum and the observed neutron yield could be easily explained by thermonuclear plasma. According to the relation $\Delta E_n(\text{keV})=82.5\sqrt{kT_i[\text{keV}]}$, the ion temperature T_i

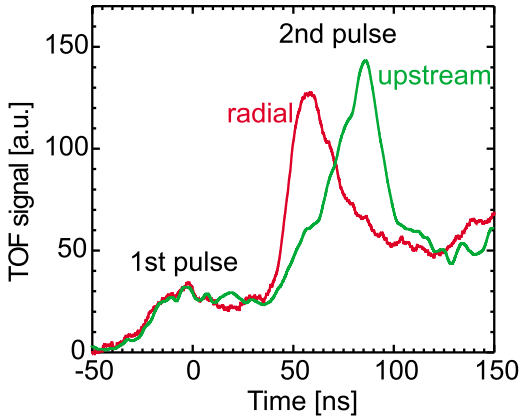

FIG. 5. (Color online) Neutron signals at the radial and upstream TOF detectors. Neutrons are shifted by TOF of 2.45 MeV neutrons. Shot 9008, 190 Pa D_2 pressure, 3×10^{10} neutron yield.

was 1.2 keV. It is for the first time when the ion temperature of thermonuclear Z-pinch plasma is calculated from the width of neutron energy spectrum.

Up to this point, the results from the upstream detectors were presented. The final issue that should be discussed here is neutron emission isotropy.

As far as the neutron energy spectrum is concerned, it was highly isotropic since the peak energy of the first pulse was ≈2.45 MeV in the axial as well as in the radial direction. In several shots, a fraction of the first neutron pulse (up to 30%) seemed to be anisotropic with the downstream energy above 2.45 MeV. Although the shift could be explained mostly by a plasma moving downstream with $\approx10^5$ m/s fluid velocity, a small contribution of beam-target neutrons cannot be ruled out.

As for the neutron flux anisotropy, results from indium samples demonstrated a relatively high isotropy in the case of the modified plasma focus. However, this time-integrated technique is not a deciding factor since only the small fraction of the total neutron yield was produced during the first pulse. Therefore, it is useful to compare the ratio of the first and the second neutron pulses at the radial and axial detectors. In shot 9008 with a high ratio between the first and the second pulses (see Fig. 5), the ratio at the radial detector was about 1.2 times higher than at the upstream detector (the sensitivity of a scintillator on neutrons with different energies was taken into account). Such a result could be influenced by the anisotropy of the second pulse which is most likely produced by axially accelerated deuterons. In any case, the neutron flux anisotropy during the first pulse was low and it was possible to exclude the acceleration of >10 keV deuteron beams only in the radial direction. Nevertheless, it was still possible to think that some neutrons were produced by head-on collisions of deuterons interacting with $2v_{\mathrm{imp}}$ relative velocity near the axis. However, since the product of the fusion cross-section and the velocity $\sigma(2v_{\mathrm{imp}})\cdot v_{\mathrm{imp}}$ is for $2v_{\mathrm{imp}}=7\times10^5$ m/s by two orders of magnitude smaller than the reaction rate $\langle\sigma v\rangle_T$ of 1 keV thermalized plasma, this contribution to the neutron yield can be neglected.

In conclusion, from the facts presented above, it is possible to summarize that (i) the time, (ii) the energy spectrum, (iii) the emission isotropy, and (iv) the yield during the first neutron pulse corresponded to the theoretical predictions for thermonuclear neutrons. The thermonuclear yield of 7×10^8 was achieved in shots with the modest total neutron yield of 2×10^{10} which were suitable for data processing. Since some thermonuclear neutrons could be expected also after the first neutron pulse,[17] we estimate the fraction of thermonuclear neutrons on the order of 5%. On higher current machines such as *Z*, this fraction should be more significant.[4]

This research has been supported by the Grant Agency of the Czech Republic (Grant Nos. 202-08-P084 and 202-08-H057), the research programs of the Ministry of Education (Grant Nos. LA08024, ME09087, and LC528), the IAEA (Grant No. RC14817), and the CTU (Grant No. SGS10/266/OHK3/3T/13).

[1]O. A. Anderson, W. R. Baker, S. A. Colgate, J. Ise, and R. V. Pyle, Phys. Rev. **110**, 1375 (1958).
[2]A. Bernard, Atomkernenergie **32**, 73 (1978).
[3]A. L. Velikovich, R. W. Clark, J. Davis, Y. K. Chong, C. Deeney, C. A. Coverdale, C. L. Ruiz, G. W. Cooper, A. J. Nelson, J. Franklin, and L. I. Rudakov, Phys. Plasmas **14**, 022701 (2007).
[4]D. R. Welch, D. V. Rose, C. Thoma, R. E. Clark, C. B. Mostrom, W. A. Stygar, and R. J. Leeper, Phys. Plasmas **17**, 072702 (2010).
[5]A. Serban and S. Lee, J. Plasma Phys. **60**, 3 (1998).
[6]V. A. Gribkov, A. Banaszak, B. Bienkowska, A. V. Dubrovsky, I. Ivanova-Stanik, L. Jakubowski, L. Karpinski, R. A. Miklaszewski, M. Paduch, M. J. Sadowski, M. Scholz, A. Szydlowski, and K. Tomaszewski, J. Phys. D **40**, 3592 (2007).
[7]M. Scholz, L. Karpinski, M. Paduch, K. Tomaszewski, R. Miklaszewski, and A. Szydlowski, Nukleonika **46**(1), 35 (2001).
[8]N. V. Filippov, T. I. Filippova, and V. P. Vinogradov, Nucl. Fusion Suppl. **2**, 577 (1962).
[9]P. Kubes, M. Paduch, T. Pisarczyk, M. Scholz, D. Klir, J. Kravarik, K. Rezac, T. Chodukowski, I. Ivanova-Stanik, L. Karpinski, E. Zielinska, K. Tomaszewski, and M. J. Sadowski, IEEE Trans. Plasma Sci. **38**, 672 (2010).
[10]A. Kasperczuk and T. Pisarczyk, Opt. Appl. **31**, 571 (2001).
[11]D. Klir, J. Kravarik, P. Kubes, K. Rezac, E. Litseva, K. Tomaszewski, L. Karpinski, M. Paduch, and M. Scholz, "Fusion neutron detector for time-of-flight measurements in Z-pinch and plasma focus experiments," Rev. Sci. Instrum. (to be published).
[12]H. Schmidt, P. Kubes, M. J. Sadowski, and M. Scholz, IEEE Trans. Plasma Sci. **34**, 2363 (2006).
[13]C. A. Coverdale, C. Deeney, A. L. Velikovich, J. Davis, R. W. Clark, Y. K. Chong, J. Chittenden, S. Chantrenne, C. L. Ruiz, G. W. Cooper, A. J. Nelson, J. Franklin, P. D. LePell, J. P. Apruzese, J. Levine, and J. Banister, Phys. Plasmas **14**, 056309 (2007).
[14]D. Klir, J. Kravarik, P. Kubes, K. Rezac, J. Cikhardt, E. Litseva, T. Hyhlik, S. S. Ananev, Yu. L. Bakshaev, V. A. Bryzgunov, A. S. Chernenko, Yu. G. Kalinin, E. D. Kazakov, V. D. Korolev, G. I. Ustroev, A. A. Zelenin, L. Juha, J. Krasa, A. Velyhan, L. Vysin, J. Sonsky, and I. V. Volobuev, Plasma Phys. Controlled Fusion **52**, 065013 (2010).
[15]P. Kubes, J. Kravarik, D. Klir, K. Rezac, M. Scholz, M. Paduch, K. Tomaszewski, I. Ivanova-Stanik, B. Bienkowska, L. Karpinski, M. Jan Sadowski, and H. Schmidt, IEEE Trans. Plasma Sci. **34**, 2349 (2006).
[16]R. Deutsch and W. Kies, Plasma Phys. Controlled Fusion **30**, 263 (1988).
[17]V. V. Vikhrev and V. D. Korolev, Plasma Phys. Rep. **33**, 356 (2007).

ARTICLE NO. 6

Response to "Comment on 'Experimental evidence of thermonuclear neutrons in a modified plasma focus'" [Appl. Phys. Lett. 100, 016101 (2012)]

D. Klir,[1,a)] P. Kubes,[1] M. Paduch,[2] T. Pisarczyk,[2] T. Chodukowski,[2] M. Scholz,[2] Z. Kalinowska,[2] E. Zielinska,[2] B. Bienkowska,[2] J. Hitschfel,[1] S. Jednorog,[2] L. Karpinski,[2] J. Kortanek,[1] J. Kravarik,[1] K. Rezac,[1] I. Ivanova-Stanik,[2] and K. Tomaszewski[3]
[1]*Czech Technical University in Prague, FEE, Technicka 2, 16627 Prague 6, Czech Republic*
[2]*Institute of Plasma Physics and Laser Microfusion, 23 Hery St., 00-908 Warsaw, Poland*
[3]*ACS Ltd., Advanced Diagnostics Laboratory, Warsaw, Poland*

(Received 9 November 2011; accepted 13 December 2011; published online 3 January 2012)

[doi:10.1063/1.3674315]

In our letter,[1] we reported measurements of an ion temperature of thermonuclear Z-pinch plasmas from the width of neutron energy spectra. The main point of the comment[2] raised by Dr. M. M. Milanese is to remark that deuteron temperatures were measured earlier on the mega-joule plasma focus in Frascati.[3] To respond this comment, we will clarify our statement in more detail in the following paragraphs.

From the very beginning of the controlled thermonuclear fusion research, it has been known that neutron energy spectra carry important information about ions. Assuming the isotropic Maxwell velocity distribution of ions, the dependence of the width of neutron energy spectra ΔE_n on the square root of ion temperatures T_i was published by Faust and Harris[4] in 1960. In 1967, Lehner and Pohl[5] calculated the full width at half maximum of DD neutron energy spectra as

$$\Delta E_n(\mathrm{keV}) = 82.5\sqrt{kT_i[\mathrm{keV}]}. \quad (1)$$

As far as plasma foci are concerned, this relation was used for the analysis of neutron emission, e.g., by Bernstein and Hai[6] in the 1971, by Bernard *et al.*[7] in 1975, and also by Milanese and Pouzo[3] in 1978. However, since neutrons are produced mostly by the tail of the distribution,[8] the temperature from Eq. (1) describes primarily the high energy tail of a deuteron velocity distribution in one dimension. Equation (1) cannot be used for the estimation of average ion energies or ion temperatures of anisotropic non-Maxwellian distributions which were often observed in plasma foci.[6,7,9] Before the ion temperature is calculated from Eq. (1), it is necessary to prove the neutron emission isotropy and the thermal equilibrium of the high energy tail of a distribution with ions of average kinetic energies. This equilibrium can be verified, for instance, by a sufficiently short ion-ion collision time or by the agreement of "temperatures" of the high energy tail with ion temperatures estimated theoretically or experimentally by different techniques. We believe that we verified the fulfillment of these conditions in Refs. 1 and 10, and that we provided an unambiguous experimental evidence of thermonuclear neutrons during the first pulse at the PF-1000 plasma focus.

In the mega-joule plasma focus at Frascati, the neutron emission isotropy and the thermonuclear mechanism during a main neutron pulse were not confirmed. In Ref. 3, a radial detector at 140 m enabled precise time-of-flight measurements. According to Eq. (1), the widths of neutron energy spectra in Ref. 3 corresponded to ion temperatures of 6-37 keV. These temperatures and plasma densities of 10^{18}–10^{19} cm^{-3} imply ion–ion collision times of 0.1-10 μs. Since neutrons were produced for 0.15 μs, the high energy tail could not be produced by multiple elastic collisions of ions. Therefore, we suppose that neutron energy spectra in Ref. 3 (i) did not correspond to the thermonuclear mechanism and (ii) did not provide information about average energies of ions, i.e., about ion temperatures. On the contrary, the width of spectra gave "equivalent" temperatures of the high energy tail which were higher than temperatures estimated by other diagnostic techniques, e.g., laser scattering.[11]

More recently, neutron measurements have been used as diagnostics of ions in deuterium gas puff Z-pinches.[12,13] At multi-megaampere currents, the number of thermonuclear neutrons should be more significant and measured widths of spectra could be used as the argument for and against the thermonuclear mechanism.[14] However, it should be noted that the fluid motion can also lead to a broadening of neutron spectra and to an inaccurate measurement of ion temperatures from spectrum widths.[15]

Our research has been supported by research program No. ME09087 of the Czech Ministry of Education and by Grant No. 0661/B/H03/2011/40 of National Science Center, Poland.

[1]D. Klir, P. Kubes, M. Paduch, T. Pisarczyk, T. Chodukowski, M. Scholz, Z. Kalinowska, E. Zielinska, B. Bienkowska, J. Hitschfel *et al.*, Appl. Phys. Lett. **98**, 071501 (2011).
[2]M. M. Milanese, Appl. Phys. Lett. **100**, 016101 (2012).
[3]M. M. Milanese and J. Pouzo, Nucl. Fusion **18**, 533 (1978).
[4]W. R. Faust and E. G. Harris, Nucl. Fusion **1**, 62 (1960).
[5]G. Lehner and F. Pohl, Z. Phys. **207**, 83 (1967).
[6]M. J. Bernstein and F. Hai, Phys. Fluids **14**, 1010 (1971).
[7]A. Bernard, A. Coudeville, A. Jolas, J. Launspach, and J. de Mascureau, Phys. Fluids **18**, 180 (1975).
[8]H. Brysk, Plasma Phys. **15**, 611 (1973).
[9]U. Jager and H. Herold, Nucl. Fusion **27**, 407 (1987).

[a)]Electronic mail: daniel.klir@fel.cvut.cz.

[10]D. Klir, P. Kubes, M. Paduch, T. Pisarczyk, T. Chodukowski, M. Scholz, Z. Kalinowska, B. Bienkowska, L. Karpinski, J. Kortanek *et al.*, Plasma Phys. Controlled Fusion **54**, 015001 (2012).
[11]M. J. Forrest and N. J. Peacock, Plasma Phys. **16**, 489 (1974).
[12]C. Coverdale, C. Deeney, A. L. Velikovich, J. Davis, R. W. Clark, Y. K. Chong, J. Chittenden, S. Chantrenne, C. L. Ruiz, G. W. Cooper *et al.*, Phys. Plasmas **14**, 056309 (2007).
[13]D. Klir, J. Kravarik, P. Kubes, K. Rezac, J. Cikhardt, E. Litseva, T. Hyhlik, S. S. Ananev, Yu. L. Bakshaev, V. A. Bryzgunov *et al.*, Plasma Phys. Controlled Fusion **52**, 065013 (2010).
[14]D. R. Welch, D. V. Rose, C. Thoma, R. E. Clark, C. B. Mostrom, W. A. Stygar, and R. J. Leeper, Phys. Plasmas **17**, 072702 (2010).
[15]B. Appelbe and J. Chittenden, Plasma Phys. Controlled Fusion **53**, 045002 (2011).

ARTICLE NO. 7

Plasma Phys. Control. Fusion **54** (2012) 015001 (11pp) doi:10.1088/0741-3335/54/1/015001

Search for thermonuclear neutrons in a mega-ampere plasma focus

D Klir[1], P Kubes[1], M Paduch[2], T Pisarczyk[2], T Chodukowski[2], M Scholz[2], Z Kalinowska[2], B Bienkowska[2], L Karpinski[2], J Kortanek[1], J Kravarik[1], K Rezac[1], I Ivanova-Stanik[2], K Tomaszewski[3] and E Zielinska[2]

[1] Department of Physics, Faculty of Electrical Engineering, Czech Technical University in Prague, Technicka 2, 166 27 Prague 6, Czech Republic
[2] Institute of Plasma Physics and Laser Microfusion, 23 Hery St., 00-908 Warsaw, Poland
[3] ACS Ltd, Advanced Diagnostics Laboratory, Warsaw, Poland

E-mail: klirdani@fel.cvut.cz

Received 19 August 2011, in final form 26 October 2011
Published 1 December 2011
Online at stacks.iop.org/PPCF/54/015001

Abstract
Plasma focus experiments were carried out at a modified PF-1000 where the cathode disc was added in front of the anode. Experimental results indicated a fraction of thermonuclear neutrons on the mega-ampere current level. In order to prove the thermonuclear mechanism, the time of neutron production and the neutron energy spectrum were measured by time-of-flight (TOF) diagnostics. Neutron TOF signals showed that the neutron production was a multiphase process and more than one mechanism occurred simultaneously. The occurrence of the thermonuclear mechanism was most evident during the plasma stagnation at low deuterium pressures. At low filling pressures, the narrow width of the neutron energy spectra demonstrated an ion temperature of about 1 keV. The possibility of thermonuclear neutrons was studied also after the stagnation, during the main neutron emission. In this case, the thermonuclear mechanism could be verified by calculating the number of deuterons that participate in the fusion process. For the bulk of thermonuclear plasmas, a significant fraction of plasma should participate in fusion. Finally, the basic consideration of the thermonuclear mechanism in Z-pinches showed the reasonableness of the MagLIF concept.

(Some figures may appear in colour only in the online journal)

1. Introduction

At present, Z-pinches are being studied as powerful and efficient laboratory x-ray generators [1, 2] and as sources for high energy density physics (HEDP) experiments [3, 4]. In addition, Z-pinches have been used as efficient sources of fast neutrons from the very beginning of fusion research. A large number of neutrons produced in Z-pinches led to the study of acceleration of deuterons to fusion energies. Soon, neutrons from ≈100 kA compressional Z-pinches were discovered to be produced by the beam-target mechanism whereas the fraction of thermonuclear neutrons was negligible. From that time on, thermonuclear mechanism in Z-pinches has been a source of controversy (see [5–8] and references therein). Recently, the issue of thermonuclear mechanism has emerged again in connection with Z-pinch fusion experiments on a 10 MA current level. In the case of the Z-machine at the Sandia National Laboratories, thermonuclear neutrons have been confirmed experimentally [9, 10]. However, these neutrons were not produced by Z-pinch plasmas themselves but by a deuterium filled capsule driven by a dynamic hohlraum. As far as a Z-pinch plasma is concerned, a significant thermonuclear neutron yield was simulated for deuterium gas puffs on Z [11, 12], but only a few experimental results were accumulated during several shots [13, 14]. A significantly larger amount of data was acquired within plasma focus research, however, with mega-ampere currents.

In dense plasma foci, multiple neutron pulses were distinguished. The first neutron pulse was observed during a so-called quiet phase; however, the main neutron emission occurred at about 100 ns later, after the disruptive development of $m = 0$ instabilities (cf [15–18]). In this paper, we present

experimental results from the PF-1000 plasma focus [19] and we intend to search for thermonuclear neutrons at 2 MA currents. This knowledge is important for scaling to higher currents where the contribution of thermonuclear neutrons should be more significant. This paper is structured as follows. In section 2 the importance of the thermonuclear mechanism and the way to recognize thermonuclear neutrons are described. The occurrence of thermonuclear neutrons during plasma compression at the PF-1000 is presented in section 3. The search for thermonuclear neutrons during the principal, second neutron pulse is provided in section 4. Some conclusions on the thermonuclear mechanism in Z-pinches are summarized in section 5.

2. Thermonuclear mechanism

The thermonuclear mechanism of fusion reactions in Z-pinches has been studied intensively from the 1950s because it has a crucial impact on the energy gain and the development of energy sources based on nuclear fusion. The controversy about the thermonuclear mechanism often arises from an ambiguous definition of neutrons which can be considered as thermonuclear and which cannot. For this reason, we would like to first discuss why the thermonuclear mechanism is important and then how thermonuclear neutrons can be discerned from neutrons of beam-target mechanisms.

2.1. Uniqueness of thermonuclear mechanism

Already in 1934, significant fusion yields were achieved by shooting of deuterium nuclei onto targets from deuterium or tritium [20]. However, as far as fusion power production is concerned, yield is not the most relevant parameter and beam fusion does not provide a possibility to achieve energy gain [21]. Since the ratio of the fusion and Coulomb cross-sections is much lower than the ratio between the deuteron energy and fusion energy, the fusion energy released is always smaller than the energy expended on the acceleration of fast deuterons. One possibility of achieving energy gain is to transfer the lost energy of fast deuterons to the acceleration of other deuterons within the same plasma. The only known mechanism with this energy feedback is the thermonuclear mechanism. That is why the conclusion about the beam-target mechanism led to the abandonment of Z-pinches as fusion power sources even though the produced neutron yields were surprisingly high. In addition to that, the saturation of beam-target neutron yields might occur at high currents which is not the case of the thermonuclear mechanism.

Within the thermonuclear mechanism, deuterons are accelerated to fusion energies by multiple elastic collisions in a high-temperature plasma. For instance at 1 keV temperature of a deuterium plasma, a Maxwellian tail of >5 keV deuterons has to be created in order to produce a significant number of DD fusion neutrons. At 10 keV temperatures, a large number of neutrons are produced by 30 keV deuterons from the main part of the velocity distribution (see e.g. [22]). In both cases, i.e. at 1 and 10 keV temperatures, the Maxwell distribution of deuteron velocities needs some time to develop. There is also another reason for keeping the plasma confined for a sufficient period of time—it is necessary for equilibrium between ions and electrons. In the case of the DT reaction, an exploitable energy is carried by an alpha-particle. The 3.5 MeV kinetic energy of an alpha-particle is so high that in 10 keV plasmas, it is deposited by Coulomb collisions mostly to electrons rather than to ions. Therefore, the thermonuclear mechanism cannot fully work with hot ions and cold electrons. Finally, when the Maxwellian distribution is established and hot ions are in equilibrium with electrons, additional time is necessary to produce a large number of fusion reactions and to achieve the energy gain. All these requirements on the confinement time at sufficiently high plasma densities and temperatures have been expressed by the known Lawson criterion [23].

2.2. Thermonuclear neutrons

Mostly it is agreed that neutrons are of thermonuclear origin if they are produced by deuterons accelerated by elastic collisions inside a high-temperature plasma. As mentioned above, a truly thermonuclear plasma requires sufficient time to produce the energy gain. Then, the production of thermonuclear neutrons at the centre of mass frame of the reference is characterized by the isotropic neutron emission, i.e. an isotropic neutron flux as well as an isotropic neutron energy spectrum. Furthermore, neutron energy spectra should be centred at about 2.45 MeV, or slightly above in the case of a high-temperature plasma.

During the compressional Z-pinch experiments in the 1950s, the axial neutron flux was higher than the radial one. As for the peak neutron energy detected downstream, it was shifted from 2.45 MeV towards higher energies, e.g. above 2.7 MeV [24]. Although the small flux anisotropy and the small shift above 2.45 MeV could be partially explained by the fluid velocity of a thermal plasma, it is generally accepted that neutrons were produced by the beam-target neutrons. From that time on, the thermonuclear mechanism in Z-pinches has often been verified by flux anisotropy measurements and by the time-of-flight (TOF) analysis of axial neutron energy spectra.

However, 2.5 MeV neutrons detected on the Z-axis is not a sufficient verification of the thermonuclear mechanism since these neutrons might be explained by fast deuterons moving in a radial direction. Such deuterons can be accelerated, for instance, by the Fermi acceleration mechanism or they can originate from axially accelerated deuterons which are trapped by the strong magnetic fields of high-current Z-pinches (cf generalized beam-target model [15, 25]). The strong magnetic fields also suppress the neutron flux anisotropy (which might vary in time) and therefore other diagnostic methods should be used to distinguish thermonuclear neutrons from beam-target ones.

In order to verify the thermonuclear mechanism, it seems appropriate to observe the time and duration of neutron production. The temporal evolution of neutron production is often compared with soft and hard x-ray (HXR) emission [26–28]. Thermonuclear neutrons are expected to be accompanied by intensive soft x-ray (bremsstrahlung) radiation during the maximum compression. In contrast, beam-target neutrons are often correlated with a sudden

onset of >100 keV HXRs after the disruptive development of plasma instabilities. Thus, the correlation of neutrons with x-rays might be useful as an auxiliary argument for or against the thermonuclear mechanism. Nevertheless, it cannot be recommended as the only method of verifying the thermonuclear origin since beam-target mechanisms could also be accompanied by soft x-ray emission.

What is more decisive here, is the total number of deuterons that participated in the neutron production mechanism. In the 1950s, fusion neutrons were produced by a small fraction of deuterons which were accelerated to >100 keV energies and this small fraction of fast deuterons produced a significant neutron yield. From the experimental point of view, >100 keV deuterons could be identified by a significant shift of neutron energies from 2.45 MeV and also by a broad width of neutron energy spectra either in the axial or in the radial direction. From the width of the neutron energy spectrum $\triangle E_n$, we can calculate the equivalent ion temperature kT_D as $\triangle E_n(\text{keV}) = 82.5\sqrt{kT_D[\text{keV}]}$ (we talk about the equivalent temperature since the Maxwellian distribution is assumed). When the equivalent ion temperature and neutron yield are known, it is possible to estimate the amount of plasma that participates in neutron production (see section 4.3). Within beam-target mechanisms, a high equivalent temperature and observed neutron yields imply a very small fraction of a fusion plasma. Further, it is appropriate to compare the equivalent ion temperature with the average energy deposited to one ion. If the equivalent temperature is significantly higher, only a fraction of a plasma can produce the observed neutron spectra otherwise the total energy of deuterons would be higher than the energy deposited into the plasma.

On the basis of what has been written so far we can address several implications here.

Firstly, the thermonuclear stationary plasma with an ion temperature of about 1 keV can be easily recognized. The ion temperature of 1 keV implies a <100 keV width of neutron energy spectra. Such a narrow width can be easily observed in neutron TOF (nTOF) signals. This idea was applied to fusion protons in order to verify thermonuclear neutrons on the Scylla theta pinch where the first thermonuclear fusion is said to be proved [29].

Secondly, if there is a significant kinetic energy in a residual (non-thermalized) fluid motion the neutron energy spectrum will be broadened [30, 31]. But on the other hand, since there is a smaller amount of energy spent on the creation of a Maxwellian tail, the neutron yield should be smaller.

Thirdly, there is a possibility of a high-temperature spot which could be the result of the adiabatic compression of an $m = 0$ instability. Such a spot could produce a broad width of neutron energy spectra and reasonable neutron yields [6, 32]. In addition to that, if deuterons escape a high-temperature region, neutron emission anisotropy could be the result of external fields [33] and/or of the anisotropy of target neutrons. Such a situation could be hardly distinguished from the beam-target mechanism. If fast deuterons escape a high-temperature region, fusion neutrons could be referred to as 'beam-target' even though deuterons are accelerated by elastic collisions. However, if the beams of deuterons and fusion products are intense enough, they could heat the surrounding plasma to fusion temperature and cause the thermonuclear wave to propagate from the $m = 0$ neck [34].

Fourthly, plasmas with a high ion temperature, e.g. 10 keV, might have the same neutron spectrum width produced by both the thermonuclear and beam-target mechanisms (cf [11]). If so, it is almost impossible to prove experimentally whether the deuteron velocity distribution is formed from the thermalization of a stagnating plasma or by the slowing down of deuterons accelerated by electric fields and trapped by strong magnetic fields. Nevertheless, if widths of neutron energy spectra and observed neutron yields imply that the bulk of the plasma participates in fusion and if the equilibrium deuterium velocity distribution is reached, we can call the neutron production mechanism as 'thermonuclear'.

Finally, we may conclude this section by saying that it is not perhaps important to know for sure whether to call neutrons 'thermal' or 'beam-target'. Much more useful seems to be to know how neutrons are produced, what is the neutron yield scaling with current, and whether it is useful for fusion energy.

3. Thermonuclear neutrons during the plasma stagnation

3.1. The first neutron pulse in compressional Z-pinches and mega-ampere plasma foci

The first compressional Z-pinches at ≈100 kA currents did not produce a sufficiently high implosion velocity and an ion temperature to create substantial thermonuclear yields at stagnation. As a consequence, neutrons were not observed during the first compression [24, 35]. In contrast with MA currents, neutron emission was observed during the first compression in plasma foci at the CEA in Limeil [36], on the Poseidon at the Stuttgart University [15], on the PF-1000 at the IPPLM in Warsaw [18, 37] as well as in a deuterium gas puff Z-pinch on the S-300 generator at the KIAE in Moscow [38]. In addition to that, energy spectra of neutrons emitted in the axial direction peaked at 2.45 MeV. It is therefore natural to ask whether a fraction of neutrons in the first pulse may be explained by the thermonuclear mechanism. The affirmative answer to this question was not provided during the intensive plasma focus research in the 1970s and 1980s. At the end of the well-diagnosed experiment at the CEA, Dr A Bernard said that he had never seen any piece of evidence indicating that neutrons have thermonuclear origin [39]. Similarly on the Poseidon, the large width of neutron energy spectra during the quiet phase did not correspond to thermonuclear mechanism and an expected ion temperature of 1 keV [15]. Therefore Deutsch and Kies suggested that the first neutron pulse can be explained by the gyro-reflection acceleration by Fermi's mechanism [40]. However, there remains the unanswered question of how electrons were accelerated and HXRs produced during the first compression.

Most of the above-mentioned experiments were optimized for a high neutron yield which was produced during the second neutron pulse. The filling pressure of the deuterium gas and the total number of deuterons were too high to achieve a fusion

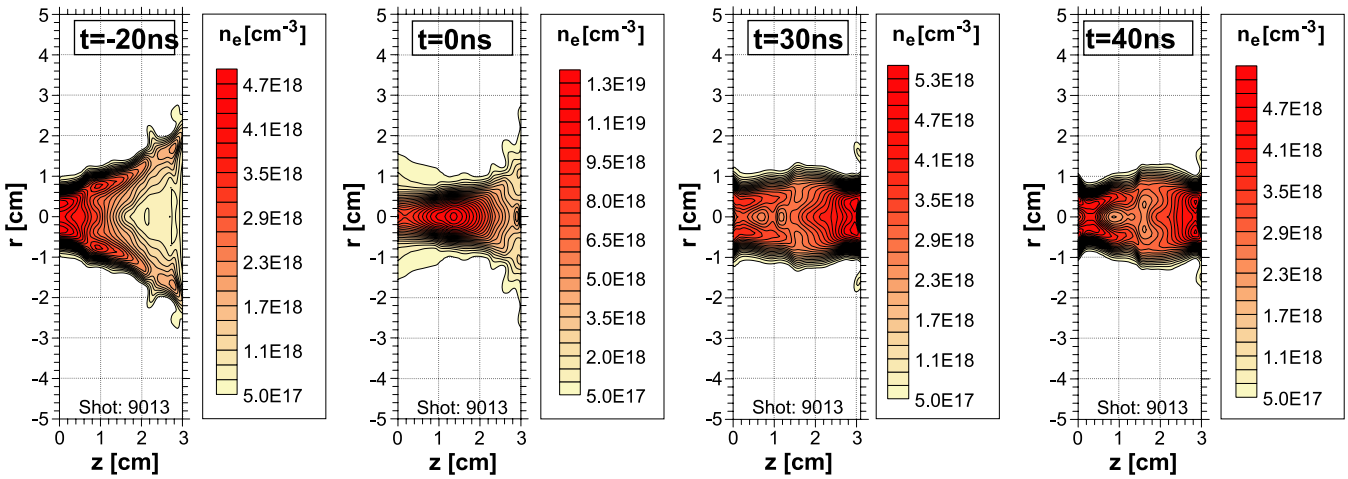

Figure 1. The sequence of electron density distributions in shot 9013. Neutron signals and other waveforms are displayed in figure 6.

temperature and a significant thermonuclear yield. When the filling pressure was lower, the fusion yield was lower but it was possible to observe a narrow peak at 3.0 MeV in the end-on proton energy spectra. At a low pressure of 3 mbar, the narrow 3.0 MeV peak was separated well from the beam-target peak at 3.9 MeV (see figure 2(*a*) in [41]). It is the one and only indication of the thermonuclear mechanism that we have found to be published. More data about this peak have not been provided and the influence of plasma and fields on the measurement of proton energies has not been discussed.

3.2. The first neutron pulse at the PF-1000

In order to search for thermonuclear neutrons, we carried out experiments on the PF-1000 plasma focus at the IPPLM in Warsaw (2.0 MA peak current, 24 kV charging voltage, 400 kJ stored energy) [18]. The facility was equipped with Mather-type coaxial electrodes (480 mm length, 230 mm anode diameter). The cathode was composed of twelve 80 mm diameter stainless-steel rods distributed around a cylinder of 400 mm diameter. The initial pressure of the deuterium gas was between 160 and 240 Pa, i.e. lower than usual for the sake of increasing the implosion velocity and ion temperature. Due to the fact that we wanted to localize the region where deuterons are accelerated, we modified the plasma focus discharge. We placed a cathode disc 3 cm in front of the anode and we added a copper plug into the hollow anode (see figure 1 in [18]). In this way we constructed the compressional Z-pinch with metal walls, i.e. the configuration initially studied by Filippov and his colleagues [35, 42]. The fixed length of the plasma column enabled us to calculate the basic plasma parameters more precisely, e.g. the inductance and the energy deposited to one ion, since the region of the power input was localized. The length of 3 cm implied lower inductance of the plasma column and a higher current during the pinch phase. In addition to that, the shorter length caused a less significant zipper and shorter neutron emission which facilitated the evaluation of neutron energy spectra. The main disadvantages of this modification are the larger amount of material evaporated from the electrodes and a lower neutron yield. The neutron yield decreased by a factor of 2 or 3 with 6 cm or 3 cm anode–cathode distance, respectively.

In order to study plasma dynamics, we applied a 16-frame laser interferometric system (527 nm wavelength, <1 ns pulse duration, 10 or 20 ns interframe delay [43]) and nTOF diagnostics [44]. The expected fraction of thermonuclear neutrons was of the order of a few percent of the total neutron yield of 10^{11}. Such a small fraction of neutrons is difficult to observe. For this reason, neutron TOF detectors were placed on the axis in an upstream direction. In this direction, 2.45 MeV neutrons were one of the fastest and they could be distinguished from beam-target and scattered neutrons which were emitted after the first compression. It was therefore decided that we place one nTOF detector side-on at 3 m, one detector downstream at 7 m and four detectors upstream at 7, 24, 50 and 83.7 m.

The exemplary sequence of electron density distribution recorded during the first compression is shown in figure 1. In the case of a modified plasma focus, the final stage of implosion was similar to that of a cylindrical Z-pinch. In [18], the most important results about the first neutron pulse were presented. On the basis of neutron and interferometric measurements we proved that (i) the time, (ii) the energy spectrum, (iii) the emission isotropy and (iv) the neutron yield of 10^9 during the first neutron pulse corresponded to theoretical predictions for thermonuclear neutrons. The ion temperature of 1.2 keV was calculated from the width of the neutron energy spectrum. It was actually for the first time in the plasma focus research that the ion temperature of a thermonuclear plasma was calculated from the neutron energy spectrum. Before that, the deuterium temperature was measured, e.g. by Forrest and Peacock [46], Bernard *et al* [36] and Herold *et al* [47] with laser scattering. In the following paragraphs, we elaborate, in more detail, on the results which were published in [18].

First, we would like to point out the difference between the first pulse observed during the stagnation and the second pulse detected after the disruptive development of instabilities. In figure 2, HXRs detected in shot No. 9008 are presented. Comparing the first and second pulses, it can be seen that photon energies substantially differed. Because the first HXR

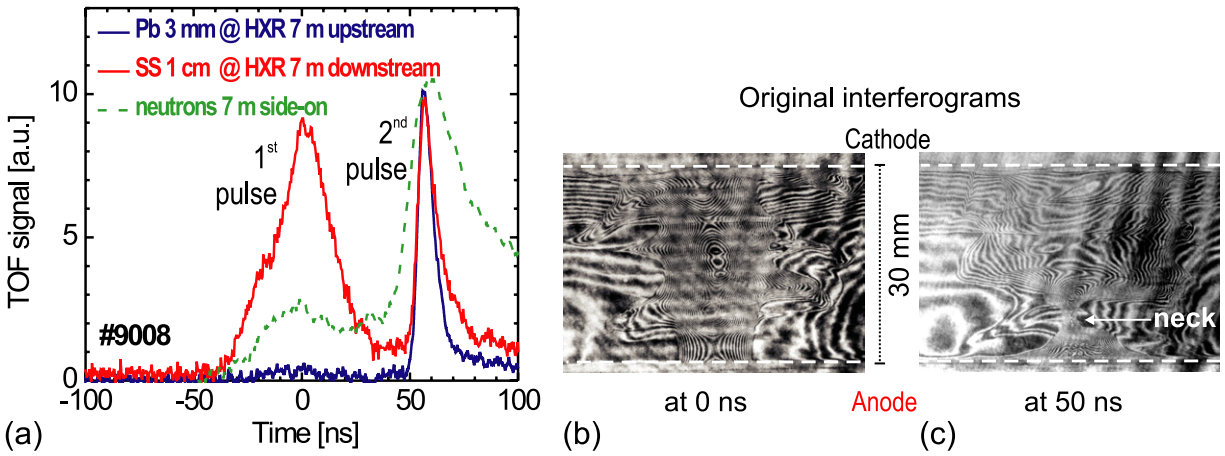

Figure 2. (*a*) The HXR and neutron pulses detected by TOF detectors. (*b*), (*c*) Original interferograms recorded at 0 and 50 ns. Neutrons were shifted by the TOF of 2.45 MeV neutrons. nTOF signal is broadened due to various kinetic energies of neutrons; shot no 9008, 190 Pa D_2 pressure, 3×10^{10} neutron yield.

pulse was effectively filtered by a lead of 3 mm thickness, the energy of photons was below 200 keV (note that the peak $V - L\,\mathrm{d}I/\mathrm{d}t$ voltage was 150 kV). Nevertheless, the different time history was an even more important result. Whereas the rise time of the first HXR pulse was about 30 ns, the measured rise time of the second HXR pulse was significantly shorter, namely of the order of the temporal resolution of the nTOF detector. All these facts considered together indicate that the acceleration mechanism was not the same.

Second, we would like to emphasize that all neutrons observed during the plasma stagnation were not necessarily of thermonuclear origin (see [15, 40]). As an example, we can analyse the above-mentioned shot. Figure 3 shows the nTOF signals recorded at 3 and 24 m in shot 9008. Comparing signals shifted by the TOF of 2.45 MeV neutrons, it is evident that the main part of neutrons emitted in the axial upstream direction had an energy of 2.45 MeV. On the one hand, the observed broadening of the TOF signal at 24 m was small which indicates a low (longitudinal) plasma temperature of ≈1 keV. On the other hand, the deuteron distribution was not fully Maxwellian during the first neutron pulse. A fraction of neutrons with energy higher than 2.5 MeV is marked in figure 3. Also at 0 ns, i.e. at the time of the HXR peak, a narrow peak is missing in the TOF signal at 24 m.

Finally, as far as the ratio of thermonuclear neutrons in the first pulse is concerned, it was strongly dependent on the filling pressure. At lower pressures (<200 Pa), the fraction of thermonuclear neutrons was up to 80% with some shot-to-shot variation. With increasing pressure, the neutron yield of the first pulse rose; however, the neutron energy spectrum was significantly broadened and the 2.5 MeV peak decreased in the axial neutron energy spectrum.

All these results show that the neutron production mechanism is a rather complex process even during the first pulse. We have to take into account at least these five processes: (i) thermonuclear plasma, (ii) moving thermal plasma, (iii) the contribution of head-on collisions of deuterons interacting with $2v_{\mathrm{imp}}$ relative velocity near the axis, (iv) the fraction of ions accelerated by several reflections at the magnetic piston

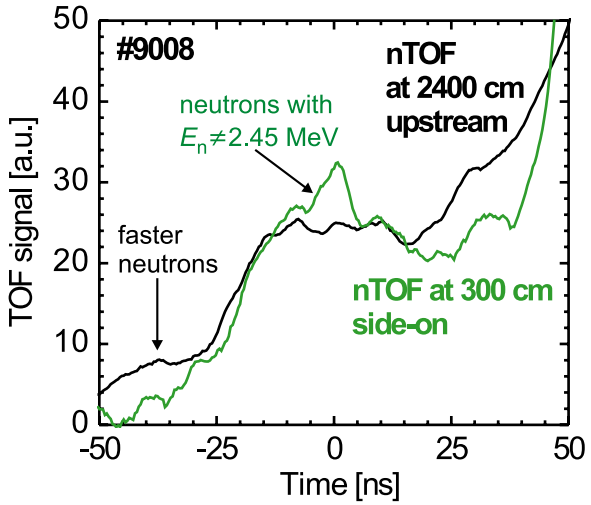

Figure 3. Neutron signals detected side-on at 3 m and upstream at 24 m. Neutrons were shifted by the TOF of 2.45 MeV neutrons; shot No. 9008, 190 Pa D_2 pressure, 3×10^{10} neutron yield.

(cf [15, 40]) and (v) also axial acceleration of deuterons by a transient voltage, e.g. during current redistribution [47]. A high transient voltage could produce run away electrons and could cause HXR (<200 keV) emission observed at the stagnation in figure 2. On the one hand, it can be difficult to find the contribution of these mechanisms (e.g. acceleration by elastic collisions may be confused with the acceleration by two or three reflections at the magnetic piston). But on the other hand, if the neutron production mechanisms are distinguished, neutron detection could provide important information about ions during stagnation.

4. 2.45 MeV neutrons during the main neutron emission

4.1. Main neutron emission in Z-pinches and plasma foci

The main neutron emission is usually connected with the disruptive development of $m = 0$ instabilities and with the

beam-target production of neutrons [5, 8, 24]. Nevertheless, a fraction of deuterons could also be accelerated by elastic collisions during the adiabatic compression and heating of necks [6, 48]. Therefore, we decided to search for thermonuclear neutrons shortly before and within the main neutron pulse. In the following subsections, we present the experimental results which were achieved on the PF-1000 at the IPPLM in Warsaw.

4.2. Principal neutron pulse at the PF-1000

The plasma dynamics observed during the main neutron emission on the PF-1000 plasma focus was described in [17]. Before the main neutron pulse occurred, the compression of the neck was clearly visible (see figure 5 in [17]). According to figure 2, the modified PF-1000 demonstrated the same evolution of the neck before the second neutron pulse. An axial ejection of ions from the neck decreased the peak ion density. The ion density inside the neck was about 10^{19} cm^{-3} shortly before the disruption. It is possible to estimate the adiabatic heating of ions to temperatures of several kilo elecronvolts. At these temperatures and densities, the collisionality of ions is low. At a reasonable temperature of 5 keV and ion density of 10^{20} cm^{-3}, the ion–ion collision time is about 10 ns and there is no sufficient time to form the Maxwellian tail by elastic collisions (the tail of the velocity distribution could be formed by gyro-reflections at the imploding magnetic piston during the collisionless compression [40]). Therefore, the expected thermonuclear neutron yield is limited by the short ($\lesssim$10 ns) confinement time, low collisionality of ions and low total number of deuterons in the neck. Then, a significantly larger number of neutrons could be produced later by fast deuterons flowing from the neck into the surrounding dense plasma.

The fact that thermonuclear neutrons are concealed by the beam-target mechanism makes the search for thermonuclear mechanism during the main neutron emission rather difficult. Nevertheless, the horizontal orientation of the PF-1000 plasma focus enabled us to place distant TOF detectors at 50.0, 67.0 and 83.7 m upstream, i.e. in the axial direction behind the anode. These distances of the detectors allowed us to reconstruct the upstream neutron energy spectra accurately. A typical example of TOF signals is displayed in figure 4(*a*). It can be seen how $\approx$2.5 MeV neutrons emerged in these TOF signals with increasing distance of the upstream detectors. The neutron energy spectrum was calculated from the detector at 83.7 m by the basic TOF method (see figure 4(*b*)). Even though there is an indication of a 2.5 MeV peak in the energy spectrum, it still does not provide unambiguous evidence of thermonuclear neutrons. It can be simply a result of fast deuterons trapped by magnetic fields [15] or a large number of off-axis deuterons proceeding towards the anode with a smaller kinetic energy [49].

The latter mechanism described also by Haines on pages 57 and 114 in [8] is, however, interesting for other reasons too. In this model, the low linear density of plasmas after the disruptive development of necks causes the occurrence of microturbulences, high resistivity, rapid dissipation of magnetic fields, and high Alfvén and ion-acoustic velocities.

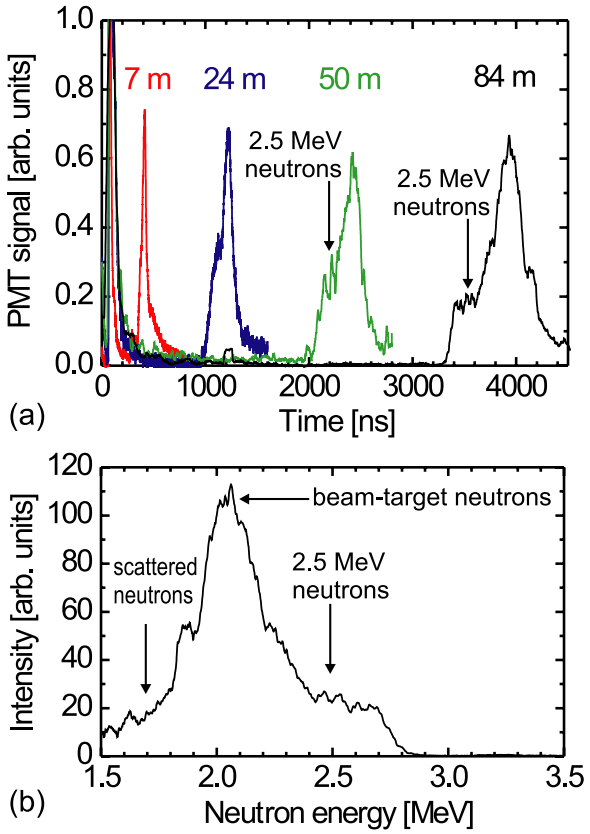

Figure 4. (*a*) Neutron signals detected upstream at 7.0, 24.0, 50.0 and 83.7 m. TOF signals were shifted by the TOF of photons. (*b*) Upstream neutron spectrum reconstructed with a 75 keV resolution from the TOF detector at 83.7 m. The single neutron sensitivity for various neutron energies was taken into consideration [44]; shot no 9012, 240 Pa D_2 pressure, 9×10^{10} neutron yield.

Then, a fast redistribution of current and magnetic fields together with a rapid plasma expansion leads to the acceleration of ions to high velocities towards the cathode near the axis and to lower velocities towards the anode at larger radii. This model satisfactorily explains the observed neutron energy spectra, neutron emission anisotropy, peak neutron production after the disruption, the correlation of neutron emission with HRXs above 1 MeV and the conservation of axial momentum. In contrast, the Fermi acceleration mechanism [40] and the adiabatic heating of necks [32] produce the peak neutron emission exactly at the maximum compression of the neck and they cannot account for the occurrence of 1 MeV HXRs. As for the formation of a high-energy ion tail due to the onset of ion-acoustic turbulences [5], it cannot explain the observed end-on neutron emission anisotropy. Therefore, in our opinion, the mechanism described by Haines is able to explain most of the features of the principal neutron emission in a modified plasma focus.

4.3. Lower yield shots without disruptions at the PF-1000

The search for thermonuclear mechanism is made more difficult by a large number of beam-target neutrons. Therefore it is natural to ask what happens if the influence of the beam-target mechanism is reduced. Since we did not have the

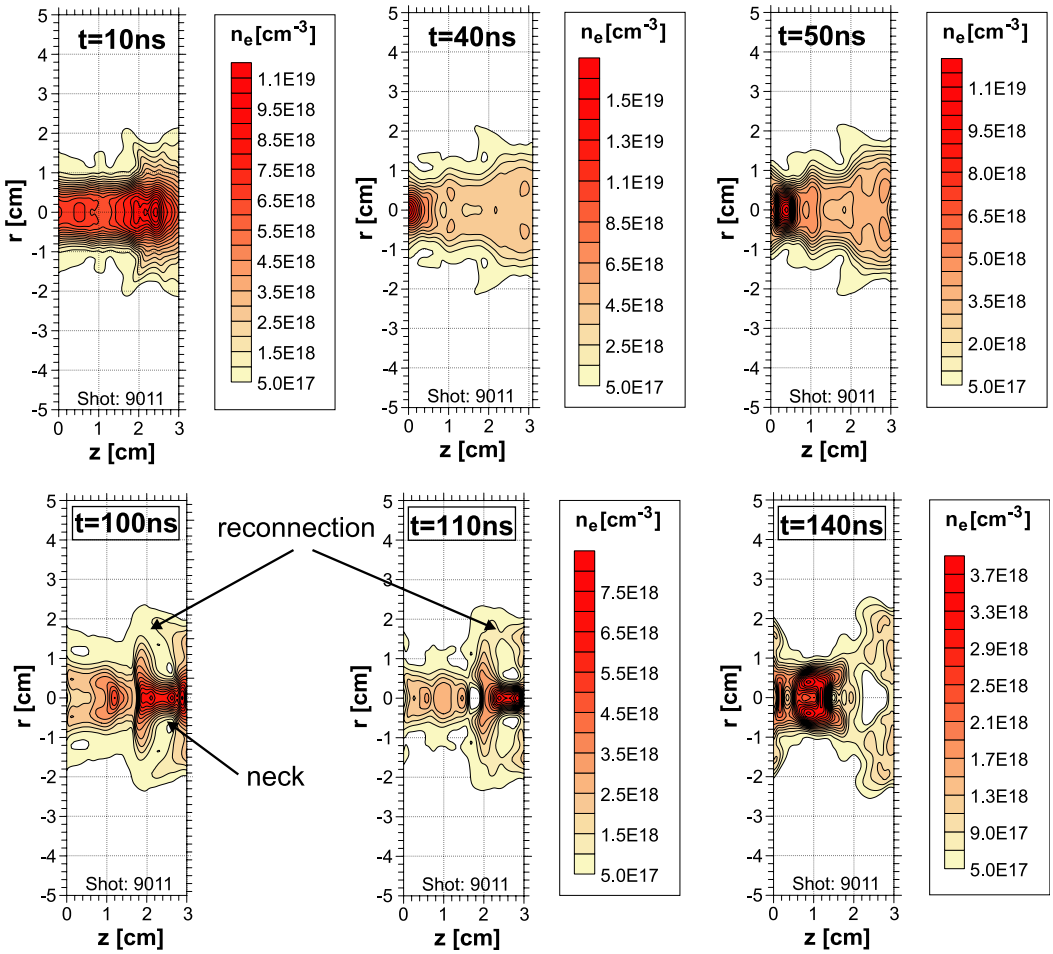

Figure 5. The sequence of electron density distributions; shot No 9011, 240 Pa D_2 pressure, 2×10^{10} neutron yield.

opportunity for the application of an axial magnetic field (cf [24, 45]), we selected shots with a low neutron yield where the development of instabilities was suppressed. The suppression occurred relatively more frequently in the case of the modified plasma focus with the cathode disc. The suppression was caused, for instance, by a current pass reconnection from the central part of an imploding neck to peripheries. One example was recorded between 100 and 110 ns in shot 9011 (see figure 5). As a result, the disruption was not observed and the second intense HXR and neutron pulse were missing in this shot. In figure 6, it is possible to compare shot no. 9011 with no. 9013. In these shots, the first neutron pulse seemed to be very similar even though the plasma column during the stagnation was more stable in shot no. 9013 (cf figure 1 with figure 5). However in shot no. 9013, the development of instabilities led to the intense second HXR and neutron pulse with a yield of 10^{11}.

The TOF signals in figure 6(*b*) show that neutrons with low energies, i.e. longer TOF, were missing at 83.7 m upstream in shot no. 9011. Because of the long neutron production time, we were not able to unambiguously determine the shape of the neutron energy spectrum; nevertheless, the mean energy could be estimated. The averaged neutron energy detected upstream was about 2.39 ± 0.03 MeV and 2.22 ± 0.03 MeV in shot nos 9011 and 9013, respectively. A small shift below 2.45 MeV energy can be explained by (i) the downstream fluid motion of the plasma, (ii) a small fraction of beam-target neutrons, (iii) the anisotropy of target deuterons, and/or (iv) scattered neutrons (see the results in [50]). As far as the spectrum width is concerned, it was calculated by the extended TOF method from the TOF signals at 7, 24, 50 and 83.7 m [51–53]. The long neutron emission in shot 9011 caused a relatively significant uncertainty. Therefore, we made an average from five shots with a lower neutron yield and we obtained the time-integrated width (FWHM) of the neutron energy spectrum as 220 ± 50 keV. Such a width corresponds to the effective ion temperature of a stationary plasma $T_D = (\triangle E_n/82.5)^2 = (220/82.5)^2 = 7$ keV.

Now we can apply the procedure which was described in section 2.2. Since we know the average ion density, the diameter of the plasma column and the total number of ions from the analysed interferograms, we are able to calculate the expected thermonuclear yield for the effective temperature $T_D = 7$ keV. For an ion density $n_D = 2 \times 10^{18}$ cm^{-3}, column diameter $2R = 2$ cm, length $l = 3$ cm, DD fusion reaction rate $\langle \sigma v \rangle_{7\,\mathrm{keV}} \doteq 3.5 \times 10^{-19}$ cm^3 s^{-1} [54] and emission time $\tau = 150$ ns in shot 9011, we obtain the thermonuclear neutron yield $Y_{\mathrm{thermonuclear}} = \frac{1}{4} n_D^2 \langle \sigma v \rangle_T \pi R^2 l \tau$ of 5×10^{11}. Since the observed neutron yield was 2×10^{10}, this means that not all but roughly 5% of the plasma participated in the nuclear fusion.

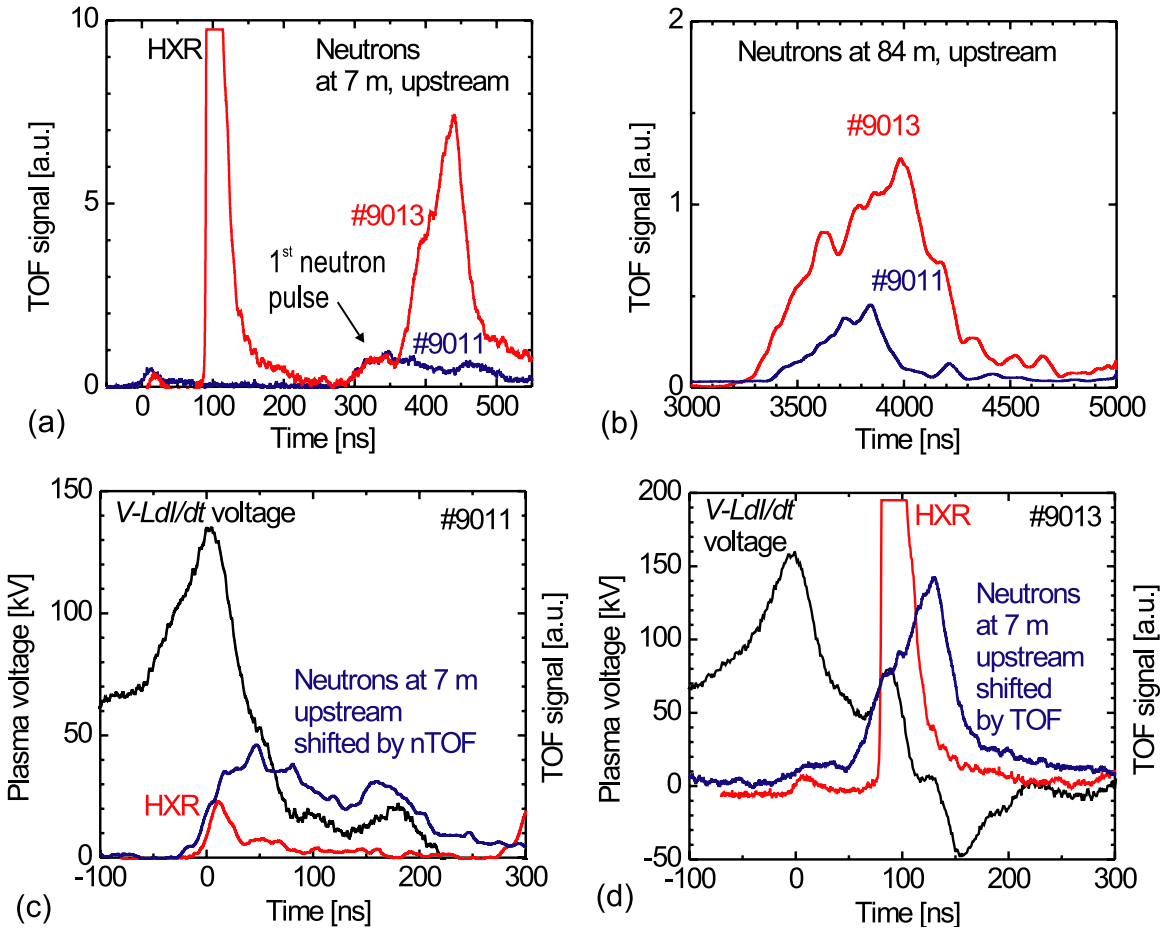

Figure 6. (*a*) Neutron signals detected upstream at 7.0 m in shots 9011 and 9013. (*b*) Neutron signals detected upstream at 84.0 m in shots 9011 and 9013. (*c*) Voltage, HXRs and the neutron signal detected upstream at 7.0 m in shot 9011. nTOF signals were shifted by the TOF of 2.45 MeV neutrons. (*d*) Voltage, HXRs and the neutron signal detected upstream at 7.0 m in shot 9013. nTOF signals were shifted by the TOF of 2.45 MeV neutrons; shot no. 9011, 240 Pa D_2 pressure, 2×10^{10} neutron yield; shot no. 9013, 240 Pa D_2 pressure, 1×10^{11} neutron yield. The voltage $V - L\mathrm{d}I/\mathrm{d}t$ was calculated neglecting the plasma resistance. However, since the voltage was given mainly by the $-L\mathrm{d}I/\mathrm{d}t$ term and since the inductance increase during the stagnation was small in comparison with the total inductance including coaxial electrodes $L \approx 70$ nH, the error estimate of the voltage was below 10%.

In comparison with beam-target mechanisms with $\leqslant 0.1\%$ of fast ions, 5% can be considered a large fraction of the plasma and we can call the neutron production mechanism as quasi-thermonuclear (it demonstrates some properties similar to the thermonuclear mechanism). The equivalent temperature of 7 keV does not correspond to the bulk plasma temperature of about 1 keV that was expected from the deposited energy per ion [18]. However, the temperature of 7 keV does not necessarily imply the violation of the energy conservation law since the deuteron velocity distribution does not have to be Maxwellian. Then, the temperature of 1 keV describes the average ion energy whereas the equivalent temperature describes the high-energy tail of the deuteron velocity distribution, which produces fusion reactions. In addition to that, not all but 'only' 5% of the plasma demonstrated the high-energy tail corresponding to the 7 keV temperature.

At 7 keV temperature, neutrons were produced mainly by 20–30 keV deuterons. The question that remains unanswered here is how these deuterons were accelerated? Figure 6(*c*) demonstrates the correlation between the neutron emission and the plasma voltage measured in shot 9011. But it is still not clear whether the acceleration to 30 keV energies was connected with the power input into the plasma or with the voltage induced across the plasma column. Therefore it is not possible to decide unambiguously whether the neutrons were thermonuclear or whether they were produced by a large number of lower energetic deuteron beams trapped by magnetic fields.

5. Discussion

The previous paragraphs gave the indication of thermonuclear neutrons in mega-ampere Z-pinches. The occurrence of the thermonuclear mechanism was the most evident during the plasma stagnation. Nevertheless, it was still a very small fraction of the total neutron yield on a mega-ampere current level. Therefore, we can now derive parameters of a current generator and a load which are suitable for higher thermonuclear yields during the pinch phase. The following derivation may be somewhat simplified, nevertheless it may be useful for the discussion of the thermonuclear mechanism in fast, dynamic Z-pinches.

We start the derivation from the Lawson criterion. If we assume the optimal ion temperature during the stagnation T_D,

the thermonuclear mechanism requires a high product $n_D\tau$. Here, n_D represents the ion density, and τ stands for the confinement time.

As far as the final plasma density is concerned, it can be expressed as

$$\bar{n}_D = \frac{\hat{m}}{m_D}\frac{1}{\pi R_{final}^2} = \frac{\hat{m}}{m_D}\frac{C^2}{\pi R_0^2}, \quad (1)$$

where $\hat{m}$ is the linear mass density, m_D is the mass of one deuteron, R_{final} is the final radius, R_0 is the initial radius and $C = R_0/R_{final}$ is the compressional ratio. The linear mass density $\hat{m}$ is connected with the dimensionless parameter Π, the peak current I and the rise time to current maximum t_{MAX} as

$$\hat{m} = \frac{\mu I^2 t_{MAX}^2}{4\pi\Pi R_0^2}. \quad (2)$$

This equation with the parameter Π was derived for the implosion of a thin shell (see [5]). Similar equations can be derived for other configurations. For instance, the optimal parameters for dense plasma foci with comparable implosion velocities are given by the constant value of I^2/pR_0^2, where p is the initial filling pressure [55].

By inserting equation (2) into (1), we have

$$\bar{n}_D = \frac{\mu I^2 t_{MAX}^2}{4\pi\Pi R_0^2 m_D}\frac{C^2}{\pi R_0^2} = \frac{\mu\beta^2 C^2}{4\pi^2\Pi m_D}\frac{I^2}{R_0^2 v_{imp}^2}, \quad (3)$$

where we considered the matching of the current rise time with the implosion time which depends on the initial radius, the implosion time and the dimensionless constant β as $t_{MAX} = t_{imp} = \beta R_0/v_{imp}$.

As for the confinement time τ, it depends on the final radius R_{final}, the ion thermal velocity $v_{T_D} = \sqrt{kT_D/m_D}$ and the coefficient α as follows

$$\tau = \alpha\frac{R_{final}}{v_{T_D}} = \alpha\frac{R_0}{C\sqrt{kT_D/m_D}}. \quad (4)$$

From (3) and (4), we obtain the product

$$\bar{n}_D\tau = \left(\frac{\alpha\beta^2 C^2\mu}{4\, m_D^{1/2}\Pi\pi^2}\right)\frac{I^2}{v_{imp}^2 R_0\sqrt{kT_D}}. \quad (5)$$

If we consider the same character of implosion, i.e. the coefficients α, β, C and Π are constant, we can write

$$\bar{n}_D\tau \propto \frac{I^2}{v_{imp}^2 R_0\sqrt{kT_D}} \propto \frac{I^2}{v_{imp}^3 t_{MAX}\sqrt{kT_D}}. \quad (6)$$

On the basis of this formula, we are able to make the following conclusions.

Firstly, it should be emphasized that the thermonuclear yield is important mainly for higher current machines. The fusion yield scales as $Y \propto \hat{m}^2 \propto I^4$ assuming a constant ion temperature. Because the energy input into a plasma also increases with rising current, the product $\bar{n}_D\tau$ depends on the second power of the current as I^2.

Secondly, at higher currents and higher plasma densities, the thermonuclear mechanism can be improved by significant plasma heating with alpha particles and/or by higher plasma stability. On the other hand, however, the energy transfer from ions to electrons reduces the ion temperature and consequently it reduces the neutron yield. In addition to that, at high currents, there is a question of how to achieve enough high mass densities. Using gas puffs may not be sufficient. Deuterium fibre Z-pinches can provide higher densities but experiments have not been very successful so far.

Thirdly, a high implosion velocity means a shorter confinement time as well as a large initial diameter and a lower plasma density. As a result, the product $\bar{n}_D\tau$ strongly decreases with increasing implosion velocity. Also at high velocities, the implosion can become unstable. If the final ion temperature is proportional to the kinetic energy $T_D \propto v_{imp}^2$, then it is always a trade-off between a high ion temperature T_D and a high product $\bar{n}_D\tau \propto (kT_D)^{-2}$. In addition to that, at high plasma temperatures and low ion densities, the frequency of ion–ion collisions could be too low to produce the Maxwellian tail during the stagnation.

Fourthly, provided that the compressional ratio C and the final ion temperature T_D are kept constant, it is better to use a high current generator with a shorter rise time t_{MAX}, and to start with a higher initial density and smaller diameter R_0. It follows that the thermonuclear yield of 100 ns deuterium solid gas puffs should be higher than with 1 μs plasma foci, if currents are the same. To start with the initial small diameter was also the idea of gas embedded and fibre Z-pinches [56–58]. However, since the compressional ratio cannot be considered as fully independent of the initial radius and the early development of instabilities, this idea proved to be wrong [7, 59–64].

Fifthly, the product $\bar{n}_D\tau$ increases with a longer confinement time and thus with a higher coefficient α. In this respect, the duration of neutron emission of about 150–200 ns in figure 6(*c*) and $\alpha \doteq$ 4–6 seem to be interesting. Even though such a duration is not sufficient for thermonuclear fusion energy, it is worthwhile to find the cause of this enhanced confinement.

Finally, we may use relation (6) to discuss the MagLIF concept [65]. This concept is a modification of magnetized target fusion [5, 66] to a faster current generator. It is based on laser preheating, the implosion of a heavy metal liner and the use of an axial magnetic field. Because of the laser preheating, a high implosion velocity $v_{imp} \sim 10^6\,m\,s^{-1}$ is not required in order to achieve a high plasma temperature $T_D \sim 10$ keV. A sufficiently high temperature can be reached by an adiabatic compression with a moderate ($\sim 10^5\,m\,s^{-1}$) implosion velocity of the metal liner. The heavy metal liner with a moderate velocity is suitable for a longer confinement time $\tau \propto R_{final}/v_{imp} > R_{final}/\sqrt{kT_D/M_D}$. In addition to that, the metal liner and the fast current generator enable us to start from a small initial radius $R_0 \sim 3$ mm and from an initial DT gas density of $\sim 10^{21}\,cm^{-3}$ which is substantially higher than contemporary possibilities of deuterium gas puffs and plasma foci. Another advantage of the heavy metal liner is the sufficient electrical conductivity which has been a serious issue in the case of deuterium frozen fibres [61]. All these facts

strongly support the reasonableness of the MagLIF concept. However, only experiments can confirm the feasibility of this concept, the sufficient compressional ratio in particular, and its usefulness for fusion energy.

6. Conclusions

In this paper we have presented the experimental search for thermonuclear neutrons in a mega-ampere plasma focus. In this respect, neutron TOF diagnostics proved to be useful. Nevertheless, the isotropic emission and neutrons with 2.45 MeV energies do not necessarily imply the thermonuclear origin. In order to prove the thermonuclear mechanism, we measured the width of neutron energy spectra which should be small in the case of a low ion temperature of 1 keV. This approach was used to verify a fraction of thermonuclear neutrons during the stagnation. In the case of high temperatures, we suggested to calculate the number of deuterons which participate in the fusion process. For the bulk of thermonuclear plasmas, a significant fraction of the plasma should participate in fusion. It was the case of lower yield shots where it was possible to see the long-lasting neutron emission which was produced by an equivalent deuteron temperature of 7 keV. It is beyond the scope of this paper to go into more details on this neutron production mechanism, however, it would be interesting to study its connection with high ion temperatures measured in imploding wire arrays [67].

Acknowledgments

This work was supported by the MSMT Grant Nos LC528, LA08024 and ME09087 of the Ministry of Education of the Czech Republic, by the GACR grant No. 202-08-H057, by the IAEA Grant RC14817 and by the CTU grant No. SGS10/266/OHK3/3T/13.

References

[1] Sandford T *et al* 1996 *Phys. Rev. Lett.* **77** 5063
[2] Spielman R *et al* 1998 *Phys. Plasmas* **5** 2105
[3] Matzen M K *et al* 2005 *Phys. Plasmas* **12** 055503
[4] Remington B A, Drake R P and Ryutov D D 2006 *Rev. Mod. Phys.* **78** 755
[5] Ryutov D D, Derzon M S and Matzen M K 2000 *Rev. Mod. Phys.* **72** 167
[6] Vikhrev V V and Korolev V D 2007 *Plasma Phys. Rep.* **33** 356
[7] Klir D *et al* 2008 *Phys. Plasmas* **15** 032701
[8] Haines M G 2011 *Plasma Phys. Control. Fusion* **53** 093001
[9] Ruiz C L *et al* 2004 *Phys. Rev. Lett.* **93** 015001
[10] Rochau G A *et al* 2007 *Plasma Phys. Control. Fusion* **49** B591
[11] Welch D R, Rose D V, Thoma C, Clark R E, Mostrom C B, Stygar W A and Leeper R J 2010 *Phys. Plasmas* **17** 072702
[12] Velikovich A L *et al* 2007 *Phys. Plasmas* **14** 022701
[13] Coverdale C A *et al* 2007 *Phys. Plasmas* **14** 022706
[14] Coverdale C *et al* 2007 *Phys. Plasmas* **14** 056309
[15] Jager U and Herold H 1987 *Nucl. Fusion* **27** 407
[16] Schmidt H *et al* 2006 *IEEE Trans. Plasma. Sci.* **34** 2363
[17] Kubes P *et al* 2010 *IEEE Trans. Plasma Sci.* **38** 672
[18] Klir D *et al* 2011 *Appl. Phys. Lett.* **98** 071501
[19] Scholz M, Miklaszewski R, Gribkov V A and Mezzetti F 2001 *Nukleonika* **46** 35
[20] Oliphant M L, Harteck P and Rutherford E 1934 *Nature* **133** 413
[21] Post R F 1956 *Rev. Mod. Phys.* **28** 338
[22] Brysk H 1973 *Plasma Phys. Control. Fusion* **15** 611
[23] Lawson J D 1957 *Proc. Phys. Soc.* B **70** 6
[24] Anderson O A *et al* 1958 *Phys. Rev.* **110** 1375
[25] Bernstein M J and Comisar G G 1972 *Phys. Fluids* **15** 700
[26] Serban A and Lee S 1998 *J. Plasma Phys.* **60** 3
[27] Goudarzi S, Sadat Kiai S, Morshedian N, Nasiri A and Amrollahi R 2005 *Czech. J. Phys.* **55** 45
[28] Castillo F, Milanese M, Moroso R and Pouzo J 2000 *J. Phys. D: Appl. Phys.* **33** 141
[29] Nagle D E, Quinn W E, Riesenfeld W B and Leland W 1959 *Phys. Rev. Lett.* **3** 318
[30] Appelbe B and Chittenden J 2011 *Plasma Phys. Control. Fusion* **53** 045002
[31] Murphy T J, Chrien R E and Klare K A 1997 *Rev. Sci. Instrum.* **68** 614
[32] Vikhrev V V 1986 *Sov. J. Plasma Phys.* **12** 262
[33] Vikhrev V V 1989 *Sov. J. Plasma Phys.* **15** 339
[34] Yankov V V 1991 *Sov. J. Plasma Phys.* **17** 305
[35] Andrianov A M *et al* 1958 *Proc. 2nd United Nations Int. Conf. on Peaceful Uses of Atomic Energy (Geneva, Switzerland, 1958)* vol 31 ed J H Martens *et al* (Geneva: United Nations) p 348
[36] Bernard A *et al* 1975 *Phys. Fluids* **18** 180
[37] Gribkov V A *et al* 2007 *J. Phys. D: Appl. Phys.* **40** 3592
[38] Klir D *et al* 2010 *Plasma Phys. Control. Fusion* **52** 065013
[39] Bernard A 1978 *Atomkernenergie* **32** 73
[40] Deutsch R and Kies W 1988 *Plasma Phys. Control. Fusion* **30** 263
[41] Van Calker C, Decker G, Jager U, Kies W and Rybach J 1985 *Phys. Lett.* A **113** 203
[42] Filippov N V, Filippova T I and Vinogradov V P 1962 *Nucl. Fusion* **2** 577
[43] Zielinska E, Paduch M and Scholz M 2011 *Control. Plasma. Phys* **51** 279
[44] Klir D *et al* 2011 *Rev. Sci. Instrum.* **82** 033505
[45] Mather J W and Williams A H 1958 *Proc. 2nd United Nations Int. Conf. on Peaceful Uses of Atomic Energy (Geneva, Switzerland, 1958)* ed J H Martens *et al* (Geneva: United Nations) vol 32, p 26
[46] Forrest M J and Peacock N J 1974 *Plasma Phys.* **16** 489
[47] Herold H *et al* 1985 *Proc. 10th Int. Conf. on Plasma Physics and Controlled Nuclear Fusion Research 1984 (London, UK, 1984)* vol 2 (IAEA: Vienna) p 579
[48] Chittenden J P *et al* 2006 *6th Int. Conf. on Dense Z-Pinches (Oxford, UK, 25–28 July 2005) AIP Conf. Proc.* **808** 335–8
[49] Haines M G 1983 *Nucl. Instrum. Methods* **207** 179
[50] Krasa J *et al* 2008 *Plasma Phys. Control. Fusion* **50** 125006
[51] Tiseanu I, Decker G and Kies W 1996 *Nucl. Instrum. Methods Phys. Res.* A **373** 73
[52] Rezac K *et al* 2006 *Czech J. Phys.* **56** B357
[53] Rezac K 2011 *Ph.D. Thesis* Czech Technical University in Prague
[54] Huba J D 2009 *NRL Plasma Formulary* (Washinghton, DC: Naval Research Laboratory) p 45
[55] Lee S and Serban A 1996 *IEEE Trans. Plasma Sci.* **24** 1101
[56] Hammel J E, Scudder D W and Shlachter J S 1983 *Nucl. Intrum. Methods* **207** 161
[57] Pereira N R, Rostoker N, Riordan J and Gersten M 1985 *Proc. 1st Int. Conf. on Dense Z-Pinches for Fusion (Alexandria, VA, 1984)* ed J D Sethian and K A Gerber (Washington, DC: Naval Research Laboratory) p 71
Hammel J E, Scudder D W and Schlachter J S 1985 *Proc. 1st Int. Conf. on Dense Z-Pinches for Fusion (Alexandria, VA, 1984)* ed J D Sethian and K A Gerber (Washington, DC: Naval Research Laboratory) p 13

[58] Scudder D W 1985 *Bull. Am. Phys. Soc.* **30** 1408
[59] Sethian J, Robson A, Gerber K and DeSilva A 1991 *Conf. Proc. Workshop on Physics of Alternative Magnetic Confinement Schemes (Varenna, Italy, 1990)* ed S Ortolani and E Sindoni (Bologna: Editrice Compositori) p 511
[60] Scudder D W 1991 *Conf. Proc. Workshop on Physics of Alternative Magnetic Confinement Schemes (Varenna, Italy, 1990)* ed S Ortolani and E Sindoni (Bologna: Editrice Compositori) p 519
[61] Kies W *et al* 1991 *J. Appl. Phys.* **70** 7261
[62] Lebedev S *et al* 1998 *Phys. Plasmas* **5** 3366
[63] Klir D *et al* 2005 *Plasma Devices Operations* **13** 39
[64] Klir D *et al* 2006 *IEEE Trans. Plasma Sci.* **34** 2303
[65] Slutz S A *et al* 2010 *Phys. Plasmas* **17** 056303
[66] Lindemuth I R and Kirkpatrick R C 1983 *Nucl. Fusion* **23** 263
[67] Haines M G, LePell P D, Coverdale C A, Jones B, Deeney C and Apruzese J P 2006 *Phys. Rev. Lett.* **96** 075003

ARTICLE NO. 8

Drive Parameter of Neutron-Optimized Dense Plasma Foci

Daniel Klir and Leopoldo Soto

***Abstract*—A dense plasma focus is being studied as a source of fusion neutrons. Lee and Serban noticed (*IEEE Trans. Plasma Sci.*, vol. 24, no. 3, pp. 1101–1105, 1996) that neutron-optimized Mather-type plasma foci have an almost constant drive parameter $I_0/(a\sqrt{\rho_0})$. The origin of this parameter goes back to the 1960s. Recently, it has been pointed out that the constant value of the drive parameter means almost the same values of axial and radial velocities, ion temperatures, Alfvén velocities, and magnetic energy per unit mass. Several physical mechanisms were suggested to explain the constant characteristic velocities in plasma foci. This paper presents the relation between the drive parameter and the rise rate of a current. The dependence of the drive parameter on plasma focus geometry is also derived. The obtained results are illustrated by neutron-optimized plasma foci with significantly higher drive parameters. Possible consequences on plasma focus research are mentioned.**

***Index Terms*—Deuterium, drive parameter, neutron, plasma focus.**

I. Introduction

A DENSE plasma focus (DPF) is an efficient pulsed plasma neutron source when deuterium is used as a filling gas. In order to design a neutron-optimized plasma focus, the drive parameter $I_0/(a\sqrt{\rho_0})$ has been discussed in the last 15 years [1]–[7]. Here, I_0, a, and ρ_0 represent the peak discharge current, the inner electrode radius, and the initial gas density, respectively.

The origin of the drive parameter and its importance for plasma focus dynamics go back to the 1960s. In 1967, for instance, the drive parameter occurred in [8], where Dyachenko and Imshennik derived it during the nondimensionalization of MHD equations. Later, Imshennik with his colleagues used dimensionless parameters and similarity transformations in order to make predictions for thermonuclear yields and lifetimes of a high-energy plasma focus [9]. In their derivation, they used the dimensionless parameter $(\rho_0^{1/2}R_0^2)/(t_0I_0)$ to express the ratio of the plasma and circuit times t_p/t_0, where I_0, R_0, and v are the characteristic values of current, length, and velocity, respectively. The ratio $t_p/t_0 \propto (\rho_0^{1/2}R_0)/I_0 \cdot v$ was said to be constant because it ensured that "the energy from the circuit is fed into the plasma at the right time" [9].

At the beginning of the 1970s, the similarity law $E_0/(p_0z_0) = \text{const}$ for the stored energy E_0, the initial pressure p_0, and the electrode length z_0 was established experimentally by Rapp [10]. In order to design plasma focus devices, only the acceleration length was determined such that the peak current occurred at the end of the acceleration phase. Thereafter, the deuterium pressure was adjusted for the highest neutron yield. Trunk attempted to optimize electrical parameters of an energy supply and the geometry of a plasma focus for the maximum current and the maximum utilization of the stored energy [11]. He extended the aforementioned law $E_0/(p_0z_0) = \text{const}$ by including the optimum radius of the inner electrode a. For a constant critical acceleration of the plasma layer, he obtained $E_0/(p_0a^2) \propto I^2/(p_0a^2) = \text{const}$. This relation was used as a scaling law for low-voltage plasma foci by Kaeppeler [12], [13]. In the 1980s, during the research of high-voltage (> 60 kV) plasma foci, the $I_0^2/(\rho_0a^2)$ parameter was assumed to be constant for all charging voltages [14].

The constant value of $(\mu_0I^2/8\pi^2a^2\rho_0u^2)^{1/2}$, which is closely related to the drive parameter, can also be found in the paper written by Herziger *et al.* [15]. This expression, where u is the axial speed, was derived in an analytic model describing the plasma focus with a shock front driven by a magnetic piston. Due to the criterion of thermodynamic stability, $(\mu_0I^2/8\pi^2a^2\rho_0u^2)^{1/2}$ was assumed to be constant and equal to one. This value was later used to estimate the ratio between sheath currents and measured total currents in plasma focus experiments [16].

The importance of the drive parameter $(I_0/a)/\rho_0^{1/2}$ was emphasized by Lee and Serban in a well-known IEEE paper in 1996 [1]. The authors showed that the drive parameter is approximately constant for Mather-type plasma foci with a wide range of stored energies. Soto extended this range to subkilojoule plasma foci [4]. It has been pointed out that the constant value of the drive parameter means almost the same values of axial and radial velocities, ion temperatures, plasma energy density [1], magnetic energy per unit mass [3], and Alfvén velocities [6]. The fixed value of the axial speed was attributed to a good focusing effect at a particular velocity [2]. The lower speed limit was explained by an insufficient coupling of the magnetic piston with the shock plasma layer. The upper

Manuscript received April 30, 2012; revised July 31, 2012 and September 6, 2012; accepted September 17, 2012. Date of publication October 18, 2012; date of current version December 7, 2012. This work was supported in part by the Grant Agency of the Czech Republic under Grant P205/12/0454, by the Czech Ministry of Education under Grants LA08024, ME09087, and LC528, by the IAEA under Grant RC17088, and by FONDECYT-Chile under Grant 1110940.

D. Klir is with the Department of Physics, Faculty of Electrical Engineering, Czech Technical University in Prague, 166 27 Prague, Czech Republic, and also with the Extreme Light Infrastructure Beamlines, Institute of Physics, AS CR, v.v.i., 182 21 Prague, Czech Republic (e-mail: klirdani@fel.cvut.cz).

L. Soto is with the Thermonuclear Plasma Department and the Center for Research and Applications in Plasma Physics and Pulsed Power, Comisión Chilena de Energía Nuclear, Santiago 8340701, Chile. He is also with the Center for Research and Applications in Plasma Physics and Pulsed Power, University of Talca, Curicó 3340000, Chile, and also with the Universidad Andrés Bello, Santiago 8370251, Chile (e-mail: lsoto@cchen.cl).

Color versions of one or more of the figures in this paper are available online at http://ieeexplore.ieee.org.

Digital Object Identifier 10.1109/TPS.2012.2220380

boundary was ascribed to the following: 1) a separation of the magnetic piston from the plasma layer; 2) Rayleigh–Taylor instabilities; 3) plasma–anode interactions; and 4) a higher mean free path causing the diffusive shock (see [2] and references herein). In order to increase the axial sheath velocity and not to influence the focusing effect, the shape of the inner electrode was modified [2], [7].

In this paper, we would like to relate the drive parameter with properties of a current generator, namely, with the rise rate of a current. This relationship, which is derived in Section II, could partially explain small variations of the drive parameter of low-voltage lower inductance Mather-type plasma foci. Illustrative examples of neutron-optimized DPFs with significantly higher drive parameters are presented in Section III. The dependence of characteristic velocities and drive parameters on plasma focus geometry and other quantities is discussed in Section IV. Some conclusions on the drive parameter and consequences for the plasma focus research are summarized in Section V.

II. Drive Parameter

The axial motion of the plasma focus current sheath in the z-direction can be described by the snow-plow model (cf. [1], [17], and [18])

$$\frac{d}{dt}\left[\pi(b^2-a^2)zf_m\rho_0\frac{dz}{dt}\right]=\frac{\mu}{4\pi}\ln\left(\frac{b}{a}\right)f_c^2I^2 \tag{1}$$

where ρ_0 is the initial gas density, f_m is the fraction of mass participated in the snow plow, I is the total current, f_c is the fraction of the current in the sheath, and a and b are the radii of the inner and outer electrodes, respectively.

Let us assume that the current I is measured in units of the peak current I_0, the axial position z in units of the inner electrode length z_0, and the time t in units of the time to the maximum current t_0. It means that we introduce the dimensionless quantities $\zeta=z/z_0$, $\tau=t/t_0$, and $\iota=I/I_0$.

Then, the equation

$$\frac{d}{dt}\left(z\frac{dz}{dt}\right)=\frac{\mu f_c^2}{4\pi^2 f_m}\frac{\ln\left(\frac{b}{a}\right)}{\left(\frac{b}{a}\right)^2-1}\frac{I^2}{\rho_0 a^2} \tag{2}$$

can be rewritten as

$$\frac{d}{d\tau}\left(\zeta\frac{d\zeta}{d\tau}\right)=\Lambda\iota^2 \tag{3}$$

where

$$\Lambda=\frac{\mu}{4\pi^2}\frac{f_c^2}{f_m}\frac{\ln\left(\frac{b}{a}\right)}{\left(\frac{b}{a}\right)^2-1}\frac{I_0^2}{\rho_0 a^2}\frac{t_0^2}{z_0^2}. \tag{4}$$

If we have two plasma foci with the same dimensionless parameter Λ and with the same dependence of the current on time $\iota(\tau)=I(t/t_0)/I_0$, the axial phase will occur in a similar way, and conversely, if Mather-type plasma foci are optimized and the end of the axial phase coincides with the time of the peak current, then these DPFs have very similar dimensionless parameters Λ. For the sinusoidal dependence of currents on time $\iota(\tau)=\sin((\pi/2)\tau)$, the axial phase ends at the peak current for $\Lambda\doteq 3$. If Λ is lower than three, the Mather-type plasma focus is "overmassed," and the axial phase ends too late. On the contrary, if Λ is higher than four, the axial phase ends too early.

Since the velocity is given by

$$\frac{dz}{dt}=\frac{z_0}{t_0}\frac{d\zeta}{d\tau} \tag{5}$$

we arrive at the characteristic axial velocity

$$v_a=\frac{z_0}{t_0}=\sqrt{\frac{\mu\ln\left(\frac{b}{a}\right)}{4\pi^2\Lambda\left(\left(\frac{b}{a}\right)^2-1\right)}}\frac{f_c}{\sqrt{f_m}}\frac{I_0}{\sqrt{\rho_0}a}. \tag{6}$$

It should be noted that this characteristic velocity differs from the one derived in [1] by a factor of $\Lambda^{-1/2}$. Our characteristic velocity is very close to the average velocity $\bar{v}_a$. The average axial velocity depends on the real axial transit time t_a as

$$\bar{v}_a=\frac{z_0}{t_a}=\frac{z_0\alpha}{t_0}=\alpha v_a \tag{7}$$

where $\alpha=t_0/t_a$ is about one for Mather-type DPFs. Usually, α is slightly higher than one since the duration of the current sheath formation and the radial phase t_r have to be included in t_0. Nevertheless, $\alpha<1$ could also occur, particularly in low-impedance high-current generators where the current reaches the peak before the end of the axial phase because of the damping effect (e.g., PF-1000 [19]).

If we express the initial density ρ_0 in terms of the pressure p_0, the temperature k_BT, and the D_2 mass M_{D_2} as $\rho_0=M_{D_2}p_0/(k_BT)$, we have

$$v_a=\frac{z_0}{t_0}=\sqrt{\frac{\mu k_BT\ln\left(\frac{b}{a}\right)}{4\pi^2M_{D_2}\Lambda\left(\left(\frac{b}{a}\right)^2-1\right)}}\frac{f_c}{\sqrt{f_m}}\frac{I_0}{\sqrt{p_0}a} \tag{8}$$

$$v_a=\frac{z_0}{t_0}=L\cdot\frac{I_0}{\sqrt{p_0}a}. \tag{9}$$

As a result, the drive parameter is constant if velocities in Mather-type plasma foci are similar and if values of L are the same (i.e., the ratios b/a and $f_c/\sqrt{f_m}$ are comparable and the end of the axial phase is matched with the peak current). In most of the Mather-type plasma foci (e.g., PF-1000, PF-360, FN-II, Paco, PF-400, UNU/ICTP, and KSU), L varies between 0.6 and 0.9 $\mathrm{m^2\cdot s^{-1}\cdot Pa^{1/2}\cdot A^{-1}}$. For instance, typical values of $b/a=2$, $f_c=0.7$, $f_m=0.1$, $T=300$ K, and $\Lambda=3$ lead to

$$v_a\doteq 0.09\cdot\frac{I_0}{\sqrt{p_0}a}. \tag{10}$$

Then, the average drive parameter of 7.7×10^5 $\mathrm{A/(Pa^{1/2}\cdot m)}$ (77 $\mathrm{kA\cdot cm^{-1}\cdot mbar^{-1/2}}$ [1]) gives the axial velocity

$$v_a\doteq 7\times10^4\ \mathrm{m/s} \tag{11}$$

which corresponds to the typical average axial velocity observed in plasma focus experiments.

The question that we should ask here is why DPFs operate in a narrow range of velocities. The fixed velocities were

TABLE I
IMPORTANT PARAMETERS OF LOW-VOLTAGE DPFS. NOTE THAT, IF AVAILABLE, THE VALUE OF f_c^2/f_m WAS TAKEN FROM [20]; OTHERWISE, IT WAS ASSUMED TO BE TWO

Name	Voltage V_0 (kV)	Peak current I_0 (kA)	Rise time t_0 (μs)	Anode radius a (cm)	Cathode radius b (cm)	Anode length z_0 (cm)	Optimal pressure p_0 (mbar)	Ratio f_c^2/f_m	Parameter $\sqrt{F/L\sqrt{p_0}}$ $\sqrt{\frac{\mathrm{As}}{\mathrm{m^2Pa}}}$	Current rise rate $\sqrt{I_0/t_0}$ $10^4\sqrt{\frac{\mathrm{A}}{\mathrm{s}}}$	Drive parameter $I_0/\sqrt{p_0}a$ $10^4\ \frac{\mathrm{A}}{\sqrt{\mathrm{Pa}}\mathrm{m}}$	Ref.
PF-1000	35	2300	7	12.2	18.4	60	6.6	2.0	1.5	57	74	[21]
Bernstein		820	3	3.9	7.5	22	6.7	2.0	1.7	57	82	[22]
Mather	17	500	2.5	2.5	5	20	9	2.0	1.8	45	67	[23]
7 kJ Japan	25	390	1.7	1.75	4	13	6	2.3	1.9	48	91	[24]
Paco	30	250	0.7	2	5	4	1.5	1.9	1.6	60	100	[25]
AASC	10	230	1.25	1.5	3	6.5	6	2.0	1.6	43	63	[26]
PF-400	30	130	0.31	0.6	1.3	2.8/1.7	9	2.5	1.3/1.0	66	72	[6]
FMPF-3	14	100	0.35	0.6	1.5	2.2	4.5	2.3	1.5	47	81	[27]

ascribed to the stability of the snow-plow implosion, to the efficient coupling of the magnetic piston with the shocked plasma layer, to the lower limit of magnetic Reynolds number and specific energy, to the good focusing effect, etc. [2]. All these phenomena might play a significant role. Nevertheless, at this point, we would like to point out the relationship between the drive parameter and a current generator, namely, the rise rate of a current. Thus far, little mention has been made of such a relationship.

In order to express the characteristic and average velocities in terms of generator parameters, it is useful to eliminate the length $z_0 = F \cdot a$ from (9)

$$z_0 = L \cdot \frac{I_0 t_0}{\frac{z_0}{F}\sqrt{p_0}} \tag{12}$$

$$z_0 = \sqrt{\frac{LFI_0 t_0}{\sqrt{p_0}}}. \tag{13}$$

Substituting z_0 into $v_a = z_0/t_0$ and using L from (8), the axial velocity is given by

$$v_a = L \cdot \frac{I_0}{\sqrt{p_0}a} = \sqrt{\frac{LFI_0}{\sqrt{p_0}t_0}} \tag{14}$$

$$v_a = \sqrt[4]{\frac{\mu k_B T f_c^2 \ln\left(\frac{b}{a}\right) F^2}{4\pi^2 M_{D_2} \Lambda f_m \left(\left(\frac{b}{a}\right)^2 - 1\right)}} \cdot \sqrt{\frac{I_0}{\sqrt{p_0}t_0}} \tag{15}$$

whereas the drive parameter is equal to

$$\frac{I_0}{\sqrt{p_0}a} = \sqrt{\frac{F}{L\sqrt{p_0}}} \cdot \sqrt{\frac{I_0}{t_0}}. \tag{16}$$

These equations show that the axial velocity and the drive parameter depend on the geometry of a tube, the deuterium pressure, the f_c^2/f_m ratio, and the rise rate of a current. As a result, axial velocities and drive parameters should be almost constant in Mather-type plasma foci with similar current rise rates $\sqrt{I_0/t_0}$ and with comparable $\sqrt{F/(L\sqrt{p_0})}$ parameters (variations in F^2, b/a, f_c^2/f_m, Λ, and p_0 are reduced by the fourth root). This is demonstrated in Table I, where several lower inductance (< 100 nH) Mather-type plasma foci are presented. Indeed, Table I shows that these Mather-type plasma foci with similar $\sqrt{I_0/t_0}$ have drive parameters in a quite narrow range of 60–100 kA/cm/mbar$^{1/2}$.

Another consequence of (16) could be illustrated by higher voltage generators with fast rising currents. According to (16), faster generators could provide higher values of the drive parameter. Several Mather-type plasma foci with various initial voltages are presented in Table II. Even though $\sqrt{F/(L\sqrt{p_0})}$ varies over these DPFs, it can be seen how the drive parameter increases with higher voltages and with higher values of $\sqrt{I_0/t_0}$.

III. HIGH-VOLTAGE GENERATORS WITH SHORTER CURRENT RISE TIMES

It has been shown in the previous section that the drive parameter and the characteristic velocity can be increased with high-voltage generators. Of course, the increased drive parameter and the higher velocity are in themselves valueless if the efficient neutron production is not achieved. The most advanced research of high-voltage plasma foci was performed by the group of Decker and Kies in Düsseldorf. The main idea of their research was to increase the current and neutron production efficiency for a given energy stored in a generator [14]. During the first experiments, several issues of high-voltage operation had to be addressed. The first problem was if it is possible to create a high-quality plasma sheath and a proper rundown phase. The second problem was to find the optimal plasma focus geometry and initial gas density. Finally, it had to be studied if the higher voltage does not change plasma properties which are convenient for the efficient neutron production. These issues were successfully solved with an 85-kV generator [14]. The average neutron yield of 3×10^9 and the stored energy of 12 kJ implied the efficiency of 2.5×10^5 neutrons/J. A similar efficiency was achieved with a 160-kV 20-kJ SPEED-1 generator [31]. The optimization procedure was pursued also with a 300-kV 187-kJ SPEED-2 generator [32], [33], but only a few results from neutron measurements have been published (e.g., [34]). Therefore, more experiments are needed to confirm that DPFs can operate efficiently at voltages above 100 kV. Nowadays, DPFs usually employ low-voltage (≤ 35 kV) discharges. The only exception is the SPEED-2 generator with the voltage of 180 kV and the impedance of 60 mΩ. In this respect, the SPEED-2 generator at Comisión Chilena de Energía Nuclear (CCHEN) could provide unique results. One disadvantage is that the insulator and the anode radius of the SPEED-2 were optimized for the 300-kV voltage [32], [33],

TABLE II
IMPORTANT PARAMETERS OF DPFS WITH VARIOUS CHARGING VOLTAGES

Name	Voltage V_0 (kV)	Peak current I_0 (kA)	Rise time t_0 (μs)	Anode radius a (cm)	Cathode radius b (cm)	Anode length z_0 (cm)	Optimal pressure p_0 (mbar)	Ratio f_c^2/f_m	Parameter $\sqrt{F/L\sqrt{p_0}}$ $\sqrt{\frac{\mathrm{As}}{\mathrm{m^2Pa}}}$	Current rise rate $\sqrt{I_0/t_0}$ $10^4\sqrt{\frac{\mathrm{A}}{\mathrm{s}}}$	Drive parameter $I_0/\sqrt{p_0}a$ $10^4\ \frac{\mathrm{A}}{\sqrt{\mathrm{Pa}}\mathrm{m}}$	Ref.
AASC	10	230	1.25	1.5	3	6.5	6	2.0	1.6	43	62	[26]
Mather	17	500	2.5	2.5	5	20	9	2.0	1.8	45	67	[23]
PF-1000	27	1750	5.5	11.5	18	48	2.75	2.0	1.7	57	92	[28]
PF-360	38	2100	3	6	8.5	30	6.6	1.9	1.3	80	100	[29]
DPF-78	60	880	1.4	2.5	5	15	10	3.1	1.3	80	110	[30]
HV-focus	85	560	0.6	1.2	3	5.5	10	2.0	1.6	100	150	[14]
Poseidon	60	3800	3	10.4	14.6	42.3	4	2.0	1.6	110	180	[29]
SPEED-1	160	900	0.4	2.5	7.5	6.5/5	3.5	2.0	1.6/1.4	150	190	[31]
SPEED-2	300	2500	0.4	5.4	11	9/5.8	5	2.0	1.0/0.85	250	210	[32]

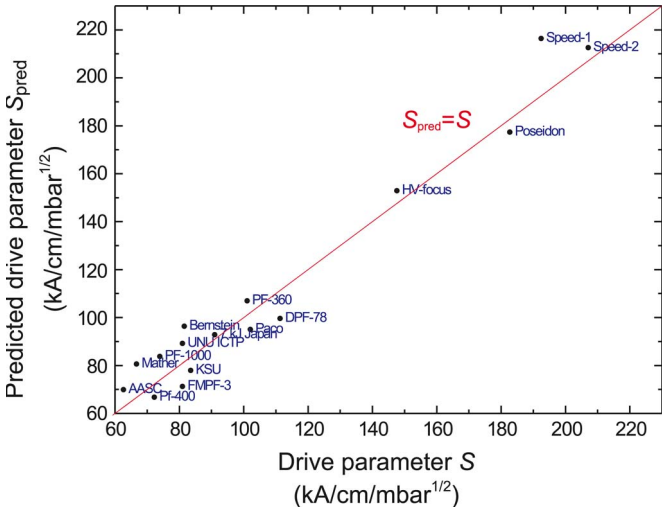

Fig. 1. Comparison of the drive parameter evaluated from $S = I_0/(\sqrt{p_0}a)$ and derived from $S_{\mathrm{pred}} = \sqrt{F/(L\sqrt{p_0})}\sqrt{I_0/t_0}$). Parameters were taken from Tables I–III. The anode lengths of PF-400, SPEED-1, and SPEED-2 were 1.7, 5.0, and 5.8 cm, respectively.

whereas the present operation at 180 kV would require smaller dimensions.

At the end of this section, we may verify our derivation by comparison of the drive parameter evaluated from $S = I_0/(\sqrt{p_0}a)$ and from $S_{\mathrm{pred}} = \sqrt{F/(L\sqrt{p_0})}\sqrt{I_0/t_0}$). The obtained results are shown in Fig. 1.

Fig. 1 shows that S_{pred} is proportional to S. Deviations from the linear dependence can be explained by incorrect values of Λ and f_c^2/f_m.

Another uncertainty arises from the anode length z_0. A rather complicated shape of the current sheath could cause that the axial position in (1) is not well defined. As a result, it is not always clear if the insulator length has to be included into z_0 or not. The uncertainty is substantial if the length of the insulator is comparable with the effective anode length such as at the PF-50, PF-400, SPEED-1, and SPEED-2 plasma foci. In these cases, we use the "average" anode length, i.e., the distance from the center of the insulator to the anode tip. This corresponds to the numerical experiments on the PF-400 J using the Lee model code where the 1.7-cm anode length was used instead of the full length of 2.8 cm [35]. In the case of the PF-50J, we obtained the best agreement between S and S_{pred} for the effective anode length of 0.48 cm.

It is also not certain if all plasma foci in Fig. 1 are optimized with respect to neutron yields. We should note that the optimization procedure significantly differs between various plasma foci. It is not rare that only the length of the anode and the pressure are adjusted whereas insulator dimensions and anode and cathode radii are kept constant. However, even in the case of neutron-optimized plasma foci, it is not easy to find published papers with all parameters of the highest neutron yield shot.

Despite all these effects, (16) seems to be valid. This equation enables us to split the drive parameter into two parts. The first part is determined mainly by the tube geometry and the initial pressure, whereas the second one is dependent on the rise rate of a current. For instance, as shown in Table III, the rise rate of the higher impedance plasma foci at Kansas State University and at the UNU/ICTP is about $26 \times 10^4\ \sqrt{\mathrm{A/s}}$ which is significantly lower than the values in Table I. However, because of long anodes and higher values of $F = z_0/a$, the drive parameters and the characteristic velocities are comparable with those in Table I.

IV. DISCUSSION

The equations in Section II were derived for the Mather-type plasma focus and for the sinusoidal dependence of a current on time. In this section, we can discuss our assumptions and the influence of various phenomena on our results.

A. Pinch Current

Recently, the role of the current limitation effect has been pointed out [36]. A high dynamic resistance during the axial and radial phases causes the damping of the current (see also [11], [14], and [31]). As a result, the current rise rate I_0/t_0 is smaller than V_0/L_0, where V_0 is the initial voltage and L_0 is the static inductance. Particularly in the case of high-current low-impedance generators with long electrodes, the peak current is significantly reduced, and the sinusoidal dependence is distorted. The former effect is already included in our nondimensionalization of MHD equations. The latter, i.e., the distortion of the sinusoidal shape, changes the optimal value of Λ. For instance, the optimal value for the $\sqrt{\sin((\pi/2)\iota)}$ dependence is $\Lambda \doteq 2$. It is a small shift from $\Lambda \doteq 3$ considering the $\Lambda^{1/4}$ power law for the drive parameter in (16). A more

TABLE III
IMPORTANT PARAMETERS OF HIGHER INDUCTANCE ($>$ 100 nH) DPFS

Name	Voltage V_0 (kV)	Peak current I_0 (kA)	Rise time t_0 (μs)	Anode radius a (cm)	Cathode radius b (cm)	Anode length z_0 (cm)	Optimal pressure p_0 (mbar)	Ratio f_c^2/f_m	Parameter $\sqrt{F/L\sqrt{p_0}}$ $\sqrt{\frac{\mathrm{As}}{\mathrm{m^2Pa}}}$	Current rise rate $\sqrt{I_0/t_0}$ $10^4\sqrt{\frac{\mathrm{A}}{\mathrm{s}}}$	Drive parameter $I_0/\sqrt{p_0}a$ $10^4\ \frac{\mathrm{A}}{\sqrt{\mathrm{Pa}}\mathrm{m}}$	Ref.
KSU	17	140	2.1	0.75	2.5	9	5	2.1	3.0	26	83	[18]
UNU/ICTP	14	172	2.5	0.95	3.2	16	5	2.3	3.4	26	81	[3]

important effect of the damping is its influence on the matching of the peak current with the end of the axial phase. In low-impedance high-current generators, the current reaches the peak before the end of the axial phase. Such a case corresponds to an "overmassed" plasma focus where Λ is significantly lower than three.

Another phenomenon that should be considered here is the difference between the maximum current I_0 and the pinch current I_{pinch}. On the one hand, it is assumed that the pinch current I_{pinch} has a decisive influence on the total neutron yields [36]. On the other hand, the peak current I_0 is more important for the matching with the axial phase, and therefore, it is the appropriate current in (14) and (16).

B. Filippov-Type Plasma Focus

In 2006, Zhang *et al.* showed that the drive parameter depends on the type of plasma focus, in other words, whether the plasma focus is of the Filippov, Mather, or hybrid type [5]. From (7) and (8), it is evident that the average velocity in DPFs is influenced not only by the drive parameter but also by the geometry of a plasma focus, namely, by α, Λ, a, and b. Therefore, different drive parameters do not necessarily imply different velocities or different physical processes. For instance, one of the most important distinctions between Filippov- and Mather-type plasma foci lies in different α's in (7). In the case of Filippov-type plasma foci, the values of $\alpha = t_0/t_a$ and Λ are significantly higher than one and three, respectively. Then, according to (7) and (9), the same average axial velocity $\bar{v}_a$ leads to the lower characteristic velocity v_a and, if $\alpha/\sqrt{\Lambda} > 1/\sqrt{3}$, also to the lower drive parameter $I_0/(p_0^{1/2}a)$ in Filippov-type plasma foci. Such a result agrees with the conclusion drawn earlier [5].

In the case of a Filippov-type plasma focus, the duration of a radial phase is comparable with the rise time of the current to the peak. Also, fast current generators, such as SPEED-1 and SPEED-2, have a short axial phase, and their tube geometry tends to be similar to that of a Filippov-type plasma focus. Therefore, it is more reasonable to calculate the radial velocity rather than the axial one. Even though the snow-plow model from the 1950s could be used as the first approximation, the "slug" model is more appropriate to describe the motion of a weakly radiating plasma current sheath. According to the slug model devised by Potter in 1978 [37], the average radial velocity of the piston is proportional to the drive parameter

$$\bar{v}_r = K \cdot \frac{I_0}{p_0^{\frac{1}{2}} a} \tag{17}$$

where K is the constant which is dependent on the shape of a current pulse. In order to match the pinch phase with the maximum current, we have

$$\frac{a}{t_r} = \beta \frac{a}{t_0} = \bar{v}_r = K \cdot \frac{I_0}{p_0^{\frac{1}{2}} a} \tag{18}$$

$$a = \sqrt{\frac{K I_0 t_0}{\beta \sqrt{p_0}}} \tag{19}$$

where β stands for the ratio of the circuit time t_0 to the radial transit time t_r.

Substituting a from (19) back into (18), we obtain the dependence

$$\bar{v}_r = \beta \frac{a}{t_0} = \sqrt{\frac{\beta K I_0}{\sqrt{p_0} t_0}} \tag{20}$$

which is analogous to (14). As a result, our conclusions for Mather-type DPFs are valid also for Filippov-type devices.

The derived equation (20) can be explained as follows. The characteristic velocities in DPFs depend on $I_0/\sqrt{\rho_0 a^2}$. This drive parameter is closely related to $I_0/\sqrt{\hat{m}}$ that is proportional to an implosion velocity of Z-pinches with the linear mass $\hat{m}$. In hollow gas puff or wire-array Z-pinches, a wide range of velocities for a given current could be achieved simply by changing the linear mass. Thereafter, the initial radius is set to match the stagnation with the current peak.

Such a procedure cannot be applied to dense Filippov-type plasma foci. In a Filippov-type plasma focus, it is also conceivable to decrease the initial gas density with a hope that it will lead to higher velocities $\bar{v}_r \propto 1/\rho_0^{1/2}$. Nevertheless, the lower mass in the current sheath causes the shift of the pinch phase to the instant of time when the current is still low. In order to reach the pinch phase at the maximum current, it is necessary to increase electrode dimensions $a \propto \bar{v}_r t_0 \propto 1/\rho_0^{1/2}$. Because "standard" plasma foci are homogeneously filled with the gas, the enlargement of electrodes results in the increase of the total mass per unit length $\rho_0 a^2$. Then, the mass in the current sheath is similar to that of the case with a higher initial gas density and a smaller anode radius. In the end, the dependence of characteristic velocities on pressure is quite weak. One possibility of how to decrease the linear mass density $\rho_0 a^2$ for a given current I_0 is to use faster current generators with the shorter rise time to the peak current t_0. This is the physical meaning of (20).

C. Other Possibilities of Increasing Velocity

Approximately constant values of characteristic velocities mean almost the same values of ion temperature and mass density of magnetic energy in neutron-optimized DPFs. For several purposes, e.g., the increase of thermonuclear yields of deuterium plasmas [2], [40] or K-shell yields of medium-Z plasmas, it would be advantageous to increase the temperature, the energy density, and, therefore, the final velocity. As mentioned previously, one possibility of increasing the average velocity is the use of a faster high-voltage generator. Another possibility of how to influence the velocity in DPFs is as follows: 1) to modify the geometry of electrodes or 2) to change the gas density at the breakdown and the pinch phase. The former led to higher axial velocities in the case of a stepped-down composite anode used by Serban and Lee [2], Verma *et al.* [38], and Aghamir and Behbahani [7]. The latter is related to the use of gas puffs near the insulator and/or at the anode tip (e.g., [39] and references therein). By using gas puffs, more "degrees of freedom" are introduced to a DPF since they enable to change independently conditions convenient for the breakdown, for the rundown, and for the pinch phase.

Finally, the following question arises: What is the upper limit of the velocity at which the current sheath is stable and the good focusing effect occurs? It is likely that optimized DPFs can operate reliably at fixed velocities only. If optimized DPFs are really restricted to constant velocities, it seems reasonable to research deuterium gas puff Z-pinches that possess higher variability than plasma foci [41].

V. Conclusion

In this paper, we are interested in the axial and radial velocities and in the drive parameter of neutron-optimized DPFs. We intended to point out the importance of the plasma focus geometry and the basic parameters of current generators. It was derived that the plasma foci with similar tube geometries and with comparable current rise rates I_0/t_0 should have the same drive parameter and the same velocities. In order to increase velocities, higher voltages and fast rising currents are desirable. On the one hand, high voltages and higher velocities might have deleterious effects on the breakdown phase, on the stability of the snow-plow mechanism, and on the focusing effect. It is still questionable if DPFs can operate efficiently at voltages above 100 kV and if high-voltage DPFs can sustain plasma properties and physical processes convenient for neutron production. On the other hand, however, high-voltage generators can be used for several interesting purposes and for the greater efficiency of energy conversion to neutron yields. Therefore, it is of high importance to continue with the research of high-voltage high-impedance generators such as the SPEED-2 at CCHEN.

References

[1] S. Lee and A. Serban, "Dimensions and lifetime of the plasma focus pinch," *IEEE Trans. Plasma Sci.*, vol. 24, no. 3, pp. 1101–1105, Jun. 1996.

[2] A. Serban and S. Lee, "Experiments on speed-enhanced neutron yield from a small plasma focus," *J. Plasma Phys.*, vol. 60, no. 1, pp. 3–15, Aug. 1998.

[3] S. Lee, P. Lee, G. Zhang, X. Feng, V. A. Gribkov, M. Liu, A. Serban, and T. K. S. Wong, "High rep rate high performance plasma focus as a powerful radiation source," *IEEE Trans. Plasma Sci.*, vol. 26, no. 4, pp. 1119–1126, Aug. 1998.

[4] L. Soto, "New trends and future perspectives on plasma focus research," *Plasma Phys. Control. Fusion*, vol. 47, no. 5A, p. A361, May 2005.

[5] T. Zhang, R. S. Rawat, S. M. Hassan, J. J. Lin, S. Mahmood, T. L. Tan, S. V. Springham, V. A. Gribkov, P. Lee, and S. Lee, "Drive parameter as a design consideration for Mather and Filippov types of plasma focus," *IEEE Trans. Plasma Sci.*, vol. 34, no. 5, pp. 2356–2362, Oct. 2006.

[6] L. Soto, C. Pavez, A. Tarife, J. Moreno, and F. Veloso, "Studies on scalability and scaling laws for the plasma focus: Similarities and differences in devices from 1 MJ to 0.1 J," *Plasma Sources Sci. Technol.*, vol. 19, no. 5, p. 055017, Oct. 2010.

[7] F. M. Aghamir and R. A. Behbahani, "Current sheath behavior and its velocity enhancement in a low energy Mather-type plasma focus device," *J. Appl. Phys.*, vol. 109, no. 4, p. 043301, Feb. 2011.

[8] V. F. Dyachenko and V. S. Imshennik, *Voprosy Teorii Plazmy (Problems of Plasma Theory)*, M. A. Leontovich, Ed. Moscow, Russia: Atomizdat, 1967, p. 432, No. 5.

[9] V. Imshennik, N. Filippov, and T. Filippova, "Similarity theory and increased neutron yield in a plasma focus," *Nucl. Fusion*, vol. 13, no. 6, pp. 929–934, Dec. 1973.

[10] H. Rapp, "Measurements referring to plasma focus scaling laws," *Phys. Lett. A*, vol. 43, no. 5, pp. 420–422, Apr. 1973.

[11] M. Trunk, "Numerical parameter studies for the dense plasma focus," *Plasma Phys.*, vol. 17, no. 4, p. 237, Apr. 1975.

[12] H. J. Kaeppeler, "Ahnlichkeitsbetrachtungen und skalierungsgesetze fur den plasmafokus," Univ. Stuttgart, Stuttgart, Germany, Rep. IPF-74-7, 1974.

[13] H. J. Kaeppeler, "Neutron production in the dense plasma focus," in *6th Int. Conf. on Plasma Physics and Controlled Nuclear Fusion Research*, Berchtesgaden, Germany, 1976, pp. 437–439.

[14] G. Decker, L. Flemming, H. J. Kaeppeler, T. Oppenlander, G. Pross, P. Schilling, H. Schmidt, M. Shakhatre, and M. Trunk, "Current and neutron yield scaling of fast high voltage plasma focus," *Plasma Phys.*, vol. 22, no. 3, pp. 245–260, Mar. 1980.

[15] G. Herziger, H. Krompholz, W. Schneider, and K. Schonbach, "A steady-state fluid model of the coaxial plasma gun," *Phys. Lett. A*, vol. 71, no. 1, pp. 54–56, Apr. 1979.

[16] H. Krompholz, F. Ruhl, W. Schneider, K. Schonbach, and G. Herziger, "A scaling law for plasma focus devices," *Phys. Lett. A*, vol. 82, no. 2, pp. 82–84, Mar. 1981.

[17] S. Lee, "A sequential plasma focus," *IEEE Trans. Plasma Sci.*, vol. 19, no. 5, pp. 912–919, Oct. 1991.

[18] S. Lee, Radiative Dense Plasma Focus Computation Package RADPF. [Online]. Available: http://www.plasmafocus.net/IPFS/modelpackage/File1RADPF.htm

[19] S. Lee and S. H. Saw, "Pinch current limitation effect in plasma focus," *Appl. Phys. Lett.*, vol. 92, no. 2, p. 021503, Jan. 2008.

[20] Institute for Plasma Focus Studies. [Online]. Available: http://www.plasmafocus.net

[21] H. Schmidt, A. Kasperczuk, M. Paduch, T. Pisarczyk, M. Scholz, K. Tomaszewski, and A. Szydlowsky, "Review of recent experiments with the megajoule PF-1000 plasma focus device," *Phys. Scr.*, vol. 66, no. 2, p. 168, 2002.

[22] M. Bernstein, D. Meskan, and H. van Paassen, "Space, time, and energy distributions of neutrons and x rays from a focused plasma discharge," *Phys. Fluids*, vol. 12, no. 10, p. 2193, Oct. 1969.

[23] J. W. Mather and P. J. Bottoms, "Characteristics of the dense plasma focus discharge," *Phys. Fluids*, vol. 11, no. 3, p. 611, Mar. 1968.

[24] M. Kashani and T. Miyamoto, in *Proc. 5th Int. Conf. Dense Z-Pinches*, J. Davis, C. Deeney, and N. R. Pereira, Eds., Albuquerque, NM, 2002, vol. 651, p. 249.

[25] F. Castillo, J. J. E. Herrera, J. Rangel, M. Milanese, R. Moroso, J. Pouzo, J. I. Golzarri, and G. Espinosa, "Isotropic and anisotropic components of neutron emissions at the FN-II and PACO dense plasma focus devices," *Plasma Phys. Control. Fusion*, vol. 45, no. 3, p. 289, Mar. 2003.

[26] B. L. Bures, M. Krishnan, and R. E. Madden, "Relationship between neutron yield and macroscale pinch dynamics of a 1.4-kJ plasma focus over hundreds of pulses," *IEEE Trans. Plasma Sci.*, vol. 39, no. 12, pp. 3351–3357, Dec. 2011.

[27] R. Verma, R. S. Rawat, P. Lee, S. V. Springham, and T. L. Tan, "High performance high repetition rate miniature plasma focus device: Record time averaged neutron yield at 200 J with enhanced reproducibility," *J. Fusion Energy*, vol. 31, pp. 1–9, Jan. 2012.

[28] P. Kubes, M. Paduch, T. Pisarczyk, M. Scholz, D. Klir, J. Kravarik, K. Rezac, T. Chodukowski, I. Ivanova-Stanik, L. Karpinski, E. Zielinska, K. Tomaszewski, and M. J. Sadowski, "Transformation of the pinched column at a period of the neutron production," *IEEE Trans. Plasma Sci.*, vol. 38, no. 4, pp. 672–679, Apr. 2010.
[29] H. Herold, A. Jerzykiewicz, M. Sadowski, and H. Schmidt, "Comparative analysis of large plasma focus experiments performed at IPF, Stuttgart, and IPJ, Świerk," *Nucl. Fusion*, vol. 29, no. 8, pp. 1255–1269, Aug. 1989.
[30] S. Lee, S. H. Saw, P. C. K. Lee, R. S. Rawat, and H. Schmidt, "Computing plasma focus pinch current from total current measurement," *Appl. Phys. Lett.*, vol. 92, no. 11, p. 111 501, Mar. 2008.
[31] G. Decker, W. Kies, and G. Pross, "The first and the final fifty nanoseconds of a fast focus discharge," *Phys. Fluids*, vol. 26, no. 2, p. 571, Feb. 1983.
[32] G. Decker, W. Kies, M. Malzig, C. van Calker, and G. Ziethen, "High performance 300 kV driver speed 2 for MA pinch discharges," *Nucl. Instrum. Methods Phys. Res. A, Accel. Spectrom. Detect. Assoc. Equip.*, vol. 249, no. 2/3, pp. 473–483, Sep. 10, 1986.
[33] W. Kies, "Power limits for dynamical pinch discharges," *Plasma Phys. Control. Fusion*, vol. 28, no. 11, pp. 1645–1657, Nov. 1986.
[34] I. Tiseanu, G. Decker, and W. Kies, "A Monte-Carlo technique for the reconstruction of time dependent spectra of short-pulse neutron sources," *Nucl. Instrum. Methods Phys. Res. A, Accel. Spectrom. Detect. Assoc. Equip.*, vol. 373, no. 1, pp. 73–80, Apr. 1996.
[35] S. Lee, S. H. Saw, L. Soto, S. V. Springham, and S. P. Moo, "Numerical experiments on plasma focus neutron yield versus pressure compared with laboratory experiments," *Plasma Phys. Control. Fusion*, vol. 51, no. 7, p. 075006, Jul. 2009.
[36] S. Lee and S. H. Saw, "Pinch current limitation effect in plasma focus," *Appl. Phys. Lett.*, vol. 92, no. 2, p. 021503, Jan. 2008.
[37] D. Potter, "The formation of high-density z-pinches," *Nucl. Fusion*, vol. 18, no. 6, pp. 813–823, Jun. 1978.
[38] R. Verma, R. S. Rawat, P. Lee, M. Krishnan, S. V. Springham, and T. L. Tan, "Experimental study of neutron emission characteristics in a compact sub-kilojoule range miniature plasma focus device," *Plasma Phys. Control. Fusion*, vol. 51, no. 7, p. 075008, Jul. 2009.
[39] H. Schmidt, M. Sadowski, L. Jakubowski, E. Skladnik-Sadowska, and J. Stanislawski, "Gas-puff target experiments with the Poseidon plasma focus facility," *Plasma Phys. Control. Fusion*, vol. 36, no. 1, pp. 13–24, Jan. 1994.
[40] D. Klir, P. Kubes, M. Paduch, T. Pisarczyk, T. Chodukowski, M. Scholz, Z. Kalinowska, B. Bienkowska, L. Karpinski, J. Kortanek, J. Kravarik, K. Rezac, I. Ivanova-Stanik, K. Tomaszewski, and E. Zielinska, "Search for thermonuclear neutrons in a mega-ampere plasma focus," *Plasma Phys. Control. Fusion*, vol. 54, no. 1, p. 015001, Jan. 2012.
[41] D. Klir, A. V. Shishlov, P. Kubes, K. Rezac, F. I. Fursov, V. A. Kokshenev, B. M. Kovalchuk, J. Kravarik, N. E. Kurmaev, A. Y. Labetsky, and N. A. Ratakhin, "Deuterium gas puff Z-pinch at currents of 2 to 3 mega-ampere," *Phys. Plasmas*, vol. 19, no. 3, p. 032706, Mar. 2012.

Daniel Klir was born in Podebrady, Czech Republic, in 1979. He received the M.Sc. degree in applied physics and the Ph.D. degree in plasma physics from the Czech Technical University (CTU) in Prague, Prague, Czech Republic, in 2002 and 2005, respectively.

Since 2005, he has been a Research Associate with the Department of Physics, Faculty of Electrical Engineering, CTU in Prague. Since 2012, he has also been a Senior Researcher with the Extreme Light Infrastructure Beamlines, Institute of Physics, AS CR, v.v.i., Prague. His research interests include Z-pinch physics, plasma diagnostics, and controlled thermonuclear fusion.

Leopoldo Soto was born in Santiago, Chile, in 1964. He received the B.S., M.S., and Ph.D. degrees in physics from the Pontificia Universidad Católica de Chile, Santiago, in 1989, 1990, and 1993, respectively.

He is currently the Head of the Thermonuclear Plasma Department, Comisión Chilena de Energía Nuclear (CCHEN), Santiago, and the Director of the Center for Research and Applications in Plasma Physics and Pulsed Power, CCHEN–University of Talca, Santiago. He is also an Associate Professor of the Ph.D. program in physics with the University of Concepción, Concepción, Chile, an Associate Professor of the Ph.D. program in applied science with the University of Talca, Talca, Chile, and a Full Professor with the Universidad Andrés Bello, Santiago. His main research interests are related to dense transient plasmas, pulsed power, and applied optics, including Z-pinch, plasma focus, capillary discharges, pulsed-power miniature devices, transient plasma diagnostics, holography, interferometry, and optical refractive diagnostics.

Dr. Soto was recognized as a Presidential Chair in Science by the President of Chile in 1999. In 2007, he was elected as a fellow of the Institute of Physics, U.K. He was the President of the Chilean Physical Society for two periods, from April 2003 to April 2008.

ARTICLE NO. 9

Deuterium gas puff Z-pinch at currents of 2 to 3 mega-ampere

D. Klir,[1] A. V. Shishlov,[2,3] P. Kubes,[1] K. Rezac,[1] F. I. Fursov,[2] V. A. Kokshenev,[2]
B. M. Kovalchuk,[2,3] J. Kravarik,[1] N. E. Kurmaev,[2] A. Yu. Labetsky,[2] and N. A. Ratakhin[2,3]
[1]*Faculty of Electrical Engineering, Czech Technical University in Prague, Technicka 2, 16627 Prague 6, Czech Republic*
[2]*Institute of High Current Electronics SB RAS, 2/3 Akademichesky Ave., Tomsk 634055, Russia*
[3]*National Research Tomsk Polytechnic University, 30 Lenina Ave., Tomsk 634050, Russia*

(Received 21 December 2011; accepted 5 March 2012; published online 30 March 2012)

Deuterium gas-puff experiments have been carried out on the GIT-12 generator at the Institute of High Current Electronics in Tomsk. The emphasis was put on the study of plasma dynamics and neutron production in double shell gas puffs. A linear mass density of deuterium (D_2) varied between 50 and 85 μg/cm. Somewhat problematic was a spread of the D_2 gas at a large diameter in the central anode–cathode region. The generator operated in two regimes, with and without a plasma opening switch (POS). When the POS was used, a current reached a peak of 2.7 MA with a 200 ns rise time. Without the POS, a current rise time approached 1500 ns. The influence of different current rise times on neutron production was researched. Obtained results were important for comparison of fast deuterium Z-pinches with plasma foci. Average DD neutron yields with and without the POS were about 10^{11}. The neutron yield seems to be dependent on a peak voltage at the Z-pinch load. In all shots, the neutron emission started during stagnation. At the beginning of the neutron production, the neutron emission correlated with soft x-rays and a significant fraction of neutrons could be explained by the thermonuclear mechanism. Nevertheless, a peak of the neutron emission occurred 40 ns after a soft x-ray peak. At this very moment, hard x-rays above 1 MeV were detected and a rapid expansion with a velocity of 3×10^5 m/s was observed. In the case of the POS, 1 MeV widths of radial neutron spectra implied that there are deuterons with the energy above 200 keV moving in the radial direction. On the basis of D_2 gas puff experiments in the 0.3–17 MA region, the neutron yield dependence on a current as $Y \propto I^{3.0\pm0.2}$ was proposed. © *2012 American Institute of Physics*. [http://dx.doi.org/10.1063/1.3696859]

I. INTRODUCTION

Deuterium Z-pinches have produced a large number of fast neutrons from the very beginning of fusion research.[1] Even though the thermonuclear origin of neutrons was not confirmed in the first compressional Z-pinch experiments,[1,2] a high efficiency of neutron production led to the study of Z-pinches as neutron sources. In order to produce a significant number of fusion reactions, various Z-pinch configurations have been tested from that time on. In particular, a plasma focus with a deuterium filling was optimized for a high neutron yield. At present, higher repetitive ≈100 kA plasma foci are being investigated as portable neutron sources for radiation material science,[3] radiobiology, nuclear medicine (PET radioisotope production,[4] brachytherapy), cargo inspection,[5] improvised-explosive-device detection,[6] etc. In the case of mega-ampere plasma foci, many experimental results were achieved[7–15] and a record yield from the D(d,n)^{3}He fusion reaction approached 10^{12} neutrons/shot.[16] The further increase of the neutron yield has not been achieved since the pinch current dropped below 2 MA due to a low impedance of low voltage MJ capacitive discharges.[14] In this respect, multi-megaampere Z-pinch experiments with deuterium gas puffs in vacuum could provide important information about neutron production mechanisms and scaling laws of neutron yields above 2 MA. In comparison with plasma foci, deuterium gas puffs are much more variable. To be more precise, deuterium gas puffs allow us to study the influence of various gas density profiles, various implosion velocities, and shorter current rise times. They also allow to research the influence of different gases and admixtures inside an inner and/or outer shell. They possess the advantage of causing no difficulties with an insulator, namely, with its conditioning and re-strikes during the pinch phase.

The first experiment with a deuterium gas jet, i.e., with a narrow solid gas puff, was carried out with a 200 kA generator at the University of California in Irvine.[17] In the following experiments, the influence of argon admixture on plasma dynamics of a hollow deuterium gas puff was studied.[18] A peak neutron yield of 2×10^8 was achieved with pure deuterium in a lower density regime. At the end of the 1980s, solid deuterium gas puffs with a strong axial gradient of a linear density were used on the Angara-5-1 generator at 2-3 MA currents.[19,20] On the Angara-5-1, deuterons were supposed to be accelerated in a low density plasma. However, because of the strong axial gradient of a plasma density, accelerated deuterons could produce abundance of neutrons in a dense target plasma near a hollow cathode. As a result, more than 10^{12} beam-target neutrons were emitted within 50 ns. With a hollow gas puff, similar neutron yields of 2×10^{12} were achieved at significantly higher currents of about 8 MA on the Saturn generator.[21] The "saturation" of a neutron yield at a value of ≈10^{12} was overcome first on the Z machine with a double-shell deuterium gas-puff at a 17 MA current.[22,23]

With regard to the overall neutron yield of 4×10^{13}, MHD (Ref. 24) and particle-in-cell (Ref. 25) simulations showed that there is a hope of a large thermonuclear component but only a few experimental results were accumulated during several shots.

In order to provide more experimental results, we carried out deuterium gas puff experiments at 2 MA on the S-300 generator at the Kurchatov Institute in Moscow. On the S-300, a comprehensive set of neutron and x-ray diagnostics was prepared[26] and efficient production of 100 keV deuterons was demonstrated.[27] A total energy of deuterons accelerated to fusion energies was calculated as 15% of the energy input into a plasma, i.e., similar value to plasma foci.

In this paper, we present results from the GIT-12 generator at the Institute of High Current Electronics in Tomsk. The experiments were carried out at currents of about 3 MA with 200 and 1500 ns rise times. Experiments at such rise times are unique since previous MA deuterium Z-pinch experiments were carried out with a shorter rise time of 100 ns. On the other hand, current rise times of MA plasma foci were usually of the order of several microseconds. The neutron emission at two different current rise times was researched. The emphasis was put on neutron time-of-flight diagnostics. The current generator, gas puff hardware, an experimental arrangement, and diagnostics used in our experiment are described in Sec. II. Section III provides the most important experimental results. The discussion of these results is the subject of Sec. IV. Finally, conclusions are summarized in Sec. V.

II. APPARATUS AND DIAGNOSTICS

A. Current generator

The experimental series of 11 shots with a deuterium gas puff was carried out on the GIT-12 generator at the Institute of High Current Electronics in Tomsk.[28] The GIT-12 is the current generator with an intermediate inductive storage of the energy and a microsecond plasma opening switch. At a 50 kV charging voltage, the generator stored an energy of 2.6 MJ. When the plasma-opening-switch (POS) was applied, a current reached a peak of about 2.7 MA with a $\approx$ 200 ns risetime (10%–90%) and a rate of up to 20 kA/ns. The generator was also used without the POS in 3 shots. In these shots, the generator approached a current of 3.5 MA with a rate of 3 kA/ns and a current rise time of 1.5 μs.

B. Gas puff

During the experimental campaign on the GIT-12, we used an electromagnetic valve, nozzles, preionization, and also experience from previous experiments with argon gas puffs (see Refs. 29 and 30 and references herein). The design of the dual-plenum valve, which was described in Ref. 31, enabled a different pressure of up to 6 bars in each plenum. This valve was coupled to concentric convergent-divergent nozzles with a throat width of about 500 μm. During our initial experiments in May 2011, we used mainly double shell gas puffs with an inner and outer shell diameter of 30 mm and 80 mm, respectively (see Fig. 1). In order to research the dependence of neutron emission on a gas density profile, single hollow shell and shell-on-solid fill gas puffs were also tested. Before each shot, the linear mass injected between the anode and cathode was estimated by a piezoelectric pressure sensor and by the procedure which was described in Ref. 32. The linear mass density of deuterium varied between 50 and 85 μg/cm. An inner-to-outer shell mass ratio was set close to 1. The nozzles were placed inside the anode. The cathode was formed by a stainless-steel mesh with a transparency of 71%. The diameter of the cathode reached 320 mm, and the inner diameter of a return-current conductor was 370 mm. The separation between the cathode and the anode was 20 mm. The time delay between the valve opening and the triggering of the generator was set at 300–450 μs. Usually, the gas-puff inside a vacuum chamber was preionized by 4 UV flashboards at about 1 μs before the onset of the load current.

FIG. 1. Nozzle of a double shell gas puff with an inner and outer diameter of 30 and 80 mm, respectively.

C. Diagnostics

The dynamics of a deuterium gas puff Z-pinch was studied by optical, x-ray, and neutron diagnostics. Each shot was observed with the following set of diagnostic tools.

First, in order to provide time- and space-resolved information about visible emission, a streak camera was performed in the radial mode, i.e., with a slit perpendicular to the Z-pinch axis. A streak camera sweep rate was 250 ns/cm. The plasma located in a plane at 10.0 ± 0.2 mm above the cathode was imaged on the slit of the streak camera.

Second, x-ray radiation was detected by a pinhole camera, by two x-ray vacuum diodes with copper cathodes, and by a photoconducting detector (PCD).[33] The x-ray pinhole camera was differentially filtered with 10 and 25 μm thick Be filters. Time-integrated images of a plasma column were recorded on RAR 2497 film with a $\approx$ 200 μm spatial resolution. The first vacuum diode filtered by a 1.5 μm Mylar foil had the peak sensitivity in a 150–280 eV window. The second x-ray vacuum diode was filtered with a 6 μm thick Kimfoil and a 600 nm thick Al layer in order to detect the

radiation above 700 eV. The photoconducting detector with 30 μm thick Teflon and 20 μm thick polypropylen filters detected the bremsstrahlung radiation above 1.7 keV.

Third, electrical characteristics and the power input into a Z-pinch load were monitored by high-voltage, current, and dI/dt probes.[28,34]

Fourth, neutron energies and the emission time of neutrons as well as hard x-rays (> 1 MeV) were measured by 4 radial neutron time-of-flight (ToF) detectors. These detectors were composed of a BC-408 fast plastic scintillator and a Hamamatsu H1949-51 PMT assembly.[35] A temporal resolution of the neutron detectors was about 5 ns. Time of neutron production was estimated from the nearest neutron detector which was placed as close to the neutron source as possible. Since energies of neutrons are determined mainly by the most distant detector, one neutron ToF detector was placed far from the Z-pinch load, i.e., at 25 m. For preventing hard x-rays from saturating the photomultipliers, the detectors were shielded up to 10 cm of lead, and neutral density filters were placed between the scintillator and the photomultiplier. As regards hard x-rays and neutron signals, they were obtained from the same waveform. Therefore, the temporal uncertainty between x-rays and neutrons was determined only by the accuracy of the distance from the source to the detectors. In the case of 2.5 MeV neutrons, the distance of about 2 cm corresponds to the 1 ns temporal uncertainty.

Finally, a neutron flux was measured by a silver activation counter, by calibrated time-of-flight (ToF) detectors,[35] and by two bubble detectors-personal neutron dosimeters (BD-PNDs)[36] in the radial direction. A total neutron yield was estimated from the radial neutron flux assuming the flux isotropy.

The most recent layout of diagnostics with 4 neutron ToF detectors is displayed in Fig. 2. This set of diagnostic tools enabled us to obtain results which are described in Sec. III. All times that are described in this paper refer to the start of the generator when the load current reached 100 kA ($t = 0$ ns).

III. EXPERIMENTAL RESULTS

A. Double shell gas puff with a 200 ns current rise-time

During the experimental campaign in 2011, 6 shots with a double shell gas puff were carried out in the plasma opening switch regime. Figure 3 presents exemplary results which were achieved with the outer and the inner shell diameter of 80 mm and 30 mm, respectively. The linear mass density in each shell was 40 ± 5 μg/cm.

Evidently, the streak camera shows that the inner shell imploded onto the axis even before the implosion of the outer shell. Assuming the thin-shell model[37] for the inner shell of the 40 μg/cm linear mass density and the 30 mm initial diameter, the implosion time of 400 ns indicates that more than 10% of the total current flowed inside the inner shell before the collision with the outer shell. The outer shell

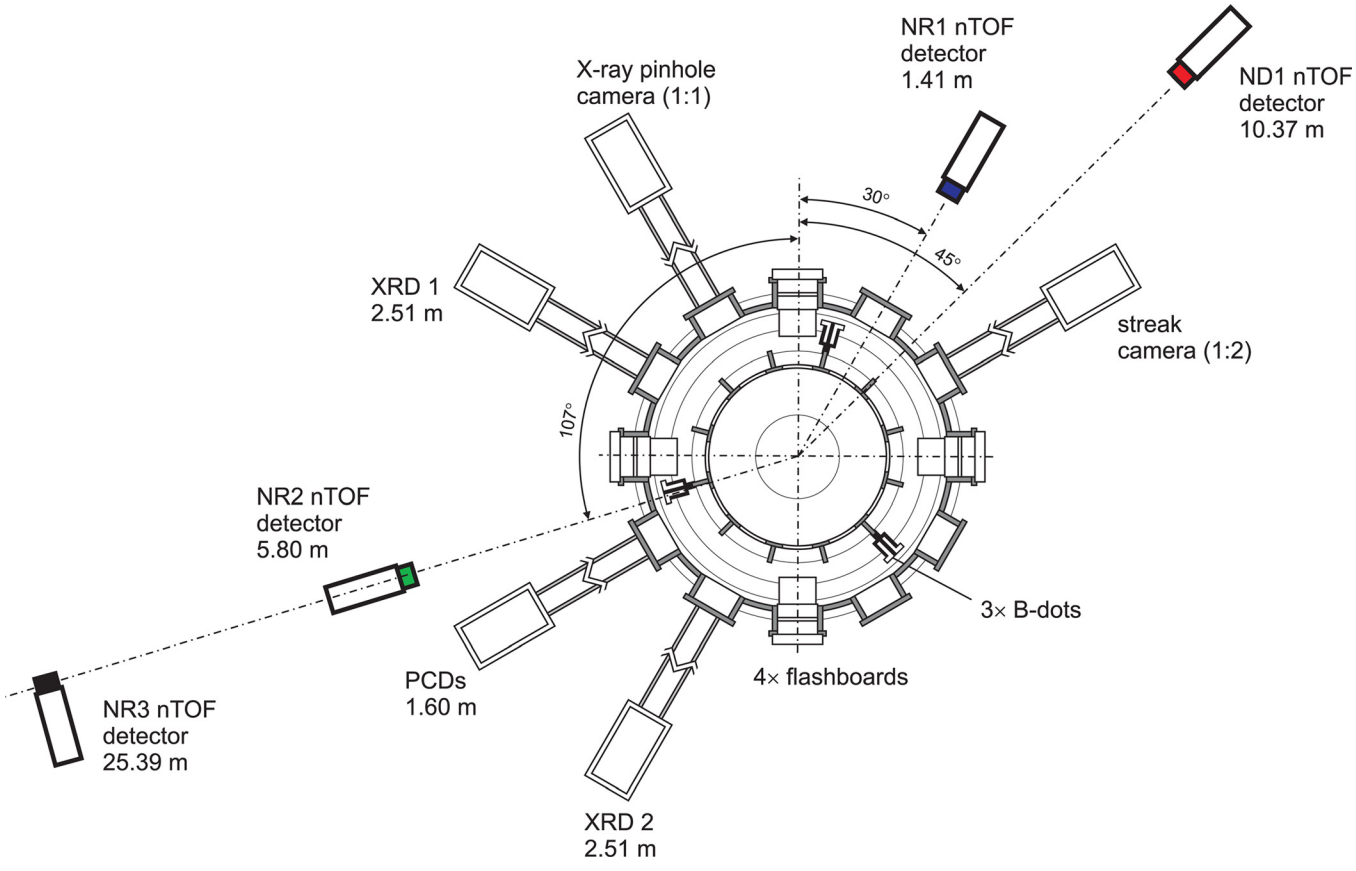

FIG. 2. Schematic diagram of diagnostic setup with 4 neutron ToF detectors.

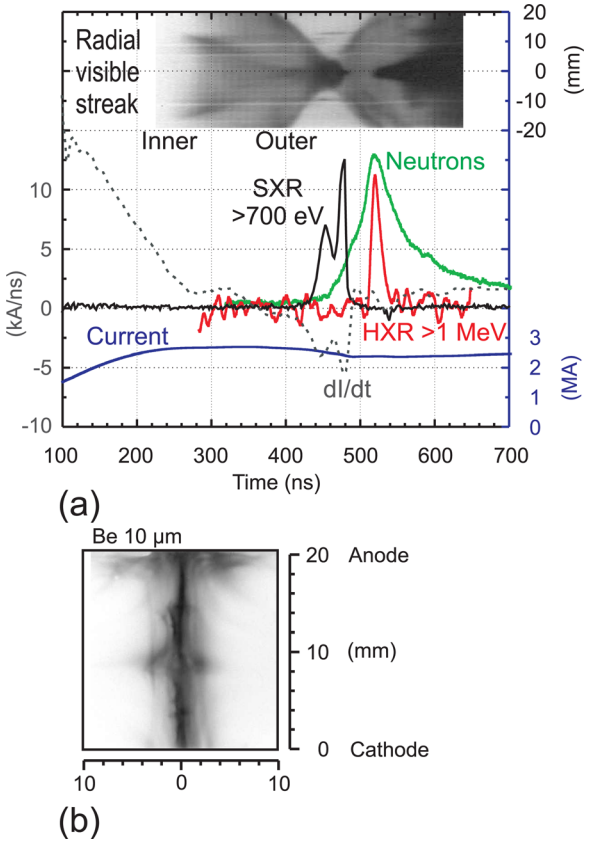

FIG. 3. (a) Visible streak image and waveforms of current, current derivative, soft x-rays, hard x-rays, neutron emission, and (b) a time-integrated x-ray pinhole image recorded in shot No. 1409 (with the POS). D_2 double shell gas puff, 80 μg/cm total linear mass density, $(1.0 \pm 0.2) \times 10^{11}$ neutrons.

stagnated on the axis at about 475 ns with an implosion velocity of 3.2×10^5 m/s. The plasma diameter in the pinhole image was 5 mm with a narrow submillimeter central column. The time-integrated pinhole image was quite similar to the one observed in a MA plasma focus.[38] During the stagnation, two dips in the dI/dt and two x-ray peaks were observed 25 ns apart from each other. The x-rays above 1.7 keV were emitted within one pulse at the end of the stagnation, i.e., during the second x-ray pulse in Fig. 3. After the stagnation, the plasma column rapidly expanded at a speed comparable with the velocity of implosion. The energy input into the Z-pinch load during the implosion $W_{\text{input}} = \frac{1}{2}\int_{\text{imp}} \dot{L} I^2 \mathrm{d}t$ exceeded 35 kJ.

1. Neutron and hard x-ray emission

The total number of neutrons measured by the BD-PND detectors in shot No. 1409 was $(1.0 \pm 0.2) \times 10^{11}$. Fig. 3 shows also waveforms of hard x-rays and neutrons. All signals were adjusted to account for different transit times from each detector to the oscilloscopes. The time of the neutron production in shot No. 1409 was estimated from the side-on ToF detectors at 5.8 m. We shifted the observed neutron signal by 267 ns, i.e., by the ToF of 2.45 MeV neutrons. Therefore, the temporal resolution of the neutron detection was given not only by the 5 ns pulse response of the neutron detector but also by the width of a neutron energy spectrum.

In all shots with the POS, the neutron emission started at the stagnation. However, the peak of the neutron emission occurred 40 ns after the peak of soft x-rays and after the dip in the dI/dt when the voltage at the Z-pinch load was low. At this very moment, hard x-rays above 1 MeV and a central bright region in the streak camera image were detected. The FWHM of neutron emission was 50 ns. This scenario was very similar to that observed on the S-300 Z-pinch, the PF-1000 plasma focus, and the Poseidon plasma focus. On the S-300 gas puff[27] and on the MA plasma foci,[10,46] the bright spot after the main stagnation corresponded to the secondary local implosion of unstable plasmas and to the disruptive development of instabilities. In general, the outset of a bright region could be a result of (1) the secondary local implosion, (2) the interaction of e-beams with plasmas, or (3) the evaporation of electrode material. With our set of diagnostic tools, we are not able to tell which phenomenon was the most important on the GIT-12. But it is clear that the hard x-ray radiation above 1 MeV is the evidence of the interaction of e-beams with higher-Z material, e.g., the anode. Therefore, the correlation of hard x-ray and neutron peaks could be explained by the simultaneous acceleration of electron and ion beams.

The information about neutron energies was obtained from the time-of-flight (ToF) analysis of fusion neutrons emitted in the radial direction. The ToF analysis was enabled by four plastic scintillators and photomultiplier tubes. In Fig. 4(a), we can see an example of ToF signals measured at various distances in shot No. 1414. Initial parameters of this shot were the same as those of shot No. 1409 which was described above. Figures 4(a) and 4(b) show how the neutron signal was shifted and broadened with the increasing distance from the neutron source. The broadening was caused by different velocities of neutrons. Quantitatively, we calculated a neutron energy spectrum from the most distant ToF detector by the time-of-flight method. An energy resolution ΔE was determined mainly by the duration of neutron emission $\Delta\tau$ as $\Delta E/E = 2\Delta\tau/\tau$, where τ is the neutron time-of-flight from the source to the detector. In shot No. 1414, the FWHM of the neutron emission $\Delta\tau$ was about 50 ns. Then, for the 25.4 m distance and for 2.45 MeV neutrons with the ToF of 1170 ns, we obtained the energy resolution ΔE of the order of 0.2 MeV. The neutron spectrum which we received is displayed in Fig. 4(c). A sensitivity of the scintillator on neutrons with different energies was taken into account.[35] A mean neutron energy of 2.42 ± 0.03 MeV was close to the expectation of $\approx$2.5 MeV. The slight shift of the mean neutron energy to 2.42 MeV provides the quantitative information about the influence of scattered neutrons. A width of the neutron spectra ΔE_n was 1000 ± 150 keV (the error estimate includes the effect of neutron scattering). Such a broad width cannot be influenced by the expansion with the fluid velocity of 3×10^5 m/s (cf. Ref. 39). 1 MeV widths of radial neutron spectra implied that there was a large number of deuterons with a 200–300 keV radial component of a kinetic energy.[27] According to the relation between an ion temperature and a spectrum width $T_D(\text{keV}) = (\Delta E_n[\text{keV}]/82.5)^2$, an effective[40] ion temperature of a stationary plasma was 150 ± 50 keV. As regards the neutron spectra from all 6 shots with

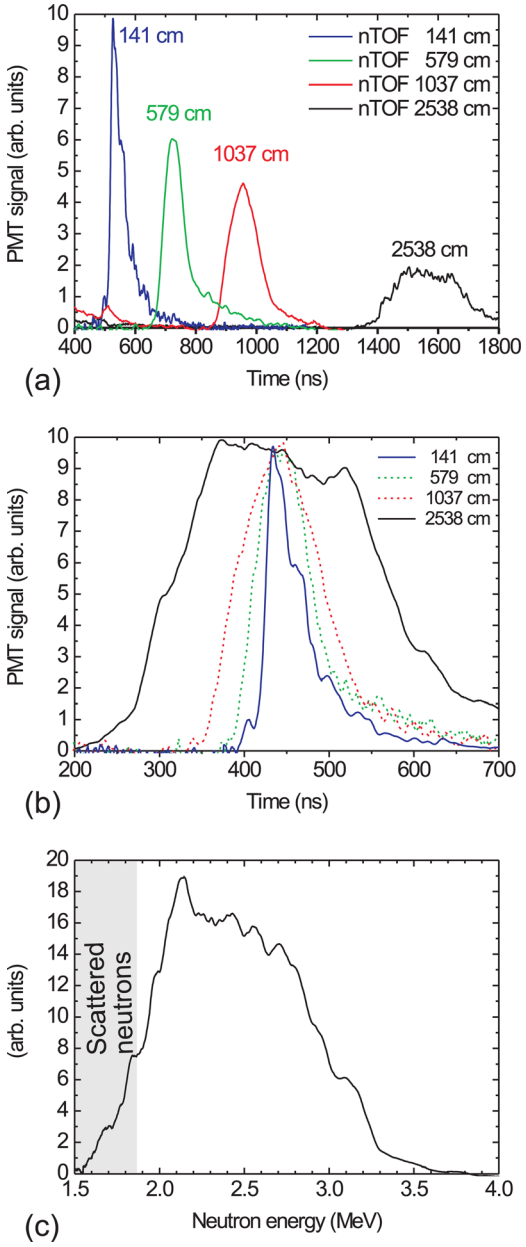

FIG. 4. (a) Neutron ToF signals on the radial detectors at various radial positions. (b) Side-on nToF signals shifted by the ToF of 2.45 MeV neutrons. (c) Time-integrated neutron energy distribution function $f(E, \phi, \vartheta)$ in the side-on direction ($\vartheta = 90^{o}$). Shot No. 1414 (with the POS), D_2 double shell gas puff, 80 μg/cm total linear mass density, $(1.3 \pm 0.3) \times 10^{11}$ neutrons.

the POS, average values were almost the same as in shot No. 1414.

The broad spectrum was the cause why the neutron ToF signal at 5.8 m was significantly broadened and why it was not possible to observe multiple neutron peaks in Fig. 3. From this reason, we placed one nToF detector as close to the source as possible. The shortest possible distance was given by the experimental arrangement and by the fact that a neutron signal had to be temporally separated from hard x-ray emission and harsh electromagnetic noise. When one detector was placed at 140 cm, the first small neutron pulse was clearly visible during the stagnation (see Fig. 4(b)). This short peak at 400 ns with 3×10^9 neutrons and 10 ns duration occurred at about 6 ns after the soft x-ray peak.

B. Double shell gas puff with a 1500 ns current rise-time

During the first experiments with deuterium gas puffs on the GIT-12, the neutron ToF detectors were saturated by a huge number of >500 keV photons from the plasma opening switch. This saturation was eliminated by shielding of the detectors with 10 cm of lead from all sides. Before the detectors were shielded, we had tried also 3 deuterium gas puff shots without the POS. Fig. 5 shows exemplary results which were achieved with the double shell gas puff with the outer and inner shell mass of 40 and 30 μg/cm, respectively. In this shot, the gas puff imploded onto the axis at about 720 ns, i.e., during the rise of the current. An implosion velocity exceeded 3×10^5 m/s and the diameter in the pinhole image was about 6 mm during the stagnation. Similarly as with the POS, two dips in the dI/dt and two x-ray peaks were observed during the stagnation 25 ns apart from each other. The energy input into the Z-pinch load during the implosion $W_{\text{input}} = \frac{1}{2}\int_{\text{imp}} \dot{L} I^2 \mathrm{d}t$ reached 25 kJ.

1. Neutron and hard x-ray emission

The neutron yield in shot No. 1408 reached $(2.0 \pm 0.6) \times 10^{11}$. It was the maximum neutron yield in our experimental campaign even though, without the POS, the load current during the stagnation approached "only" 2 MA. The neutron

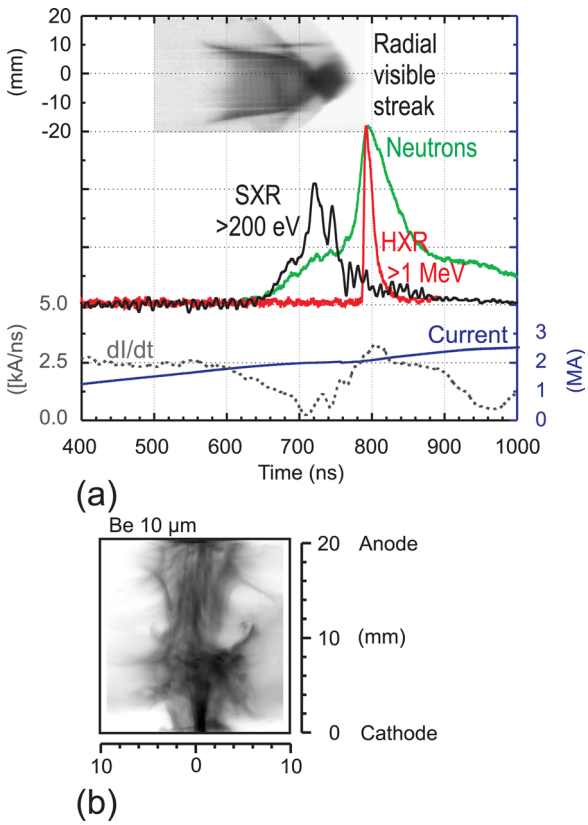

FIG. 5. (a) A visible streak image and waveforms of current, current derivative, soft x-rays, hard x-rays, neutron emission, and (b) a time-integrated x-ray pinhole image recorded in shot No. 1408 (without the POS). D_2 double shell gas puff, 70 μg/cm total linear mass density, $(2.0 \pm 0.6) \times 10^{11}$ neutrons. Note: The whole image of the streak camera was recorded in shot No. 1406, see Fig. 9.

emission started during the collision of the outer shell onto the inner shell and lasted more than 200 ns. At the beginning of the neutron emission, there was a nice correlation between the neutron emission and soft x-rays. Similarly to shots with the POS, the main neutron pulse together with hard x-rays (HXRs) peaked 40 ns after the stagnation.

Figure 6 shows ToF signals measured at 5.8 m and 25.4 m. We calculated the neutron energy spectrum from these ToF signals by a Monte Carlo reconstruction.[26,41,42] A 200 keV FWHM of the side-on spectrum was substantially smaller in comparison with shots when the POS was applied (cf. Fig. 4(c)). Such a width implies that the neutron energy resolution of our measurements was better than 200 keV and that the broad spectrum in Fig. 4(c) was not significantly influenced by neutron scattering.

Another difference between shots with and without the POS was the intensity of the neutron emission during the stagnation. Figure 7 displays soft x-rays above 700 eV together with the neutron emission detected at 5.8 m in shots Nos. 1408 and 1409. Clearly, the neutron emission during the stagnation, i.e., during the soft x-ray emission, was more intense in shot No. 1408 without the POS. In contrast, the soft x-ray emission above 700 eV was comparable in both regimes of the generator. Furthermore with the POS, an electron temperature seems to be higher since the PCD detected

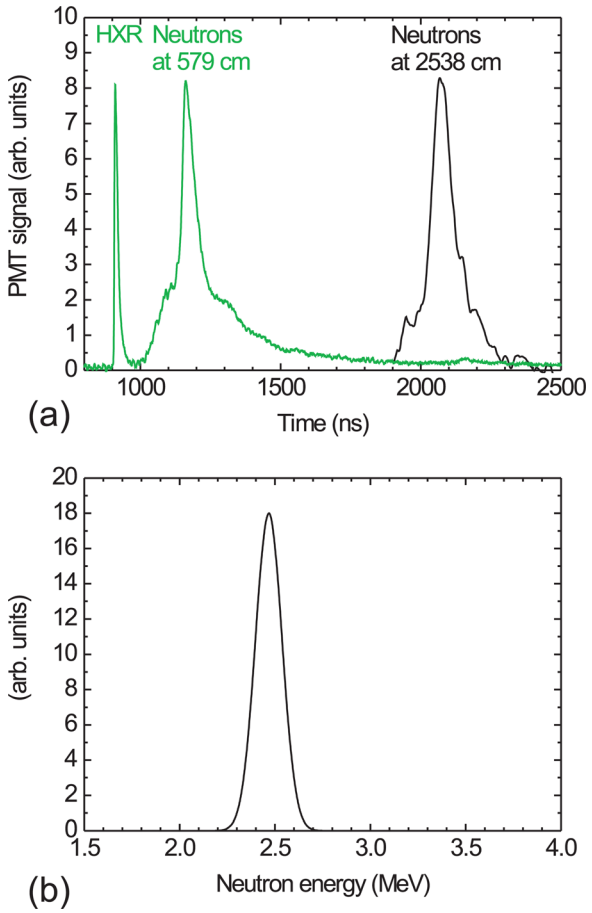

FIG. 6. (a) Neutron ToF signals on the radial detectors at 580 and 2539 cm. (b) Time integrated neutron energy distribution function $f(E, \phi, \vartheta)$ in the side-on direction ($\vartheta = 90^{o}$). Shot No. 1408 (w/o POS), D_2 double shell gas puff, 70 μg/cm total linear mass density, $(2.0 \pm 0.6) \times 10^{11}$ neutrons.

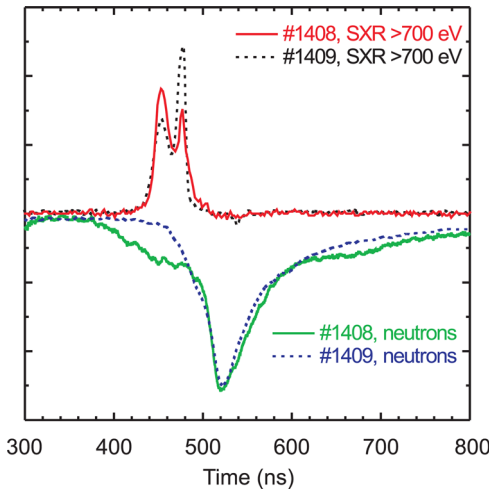

FIG. 7. Comparison of the x-rays and the neutron emission in shots with the POS (No. 1409) and without the POS (No. 1408). The waveforms of shot No. 1408 are shifted by 270 ns in order to fit shot No. 1409.

a much more intense signal of x-rays above 1.7 keV. Also, the plasma diameter in the pinhole image was lower in shot No. 1409 with the POS as illustrated in Figs. 3 and 5. In this respect, a lower neutron yield during the stagnation in shot No. 1409 might be a surprising result.

C. Neutron yield

The average neutron yields produced with and without the POS were about 10^{11}. These neutron yields were estimated from the radial detectors assuming flux isotropy. Because of the neutron flux anisotropy in favor of the z-axis, the real neutron yield could be even several times higher than the estimated one. It is particularly the case of the slower current rise rate where the width of side-on neutron energy spectra and, therefore, also the radial components of deuteron kinetic energies were significantly smaller.

One important fact to know is whether the neutron yield was dependent on any measurable parameter of the gas puff implosion. One parameter that we recognized that played some role was the peak of the "effective" voltage at the Z-pinch load $V_{\text{eff}} = V - (L_0 + L_l)dI/dt$, where V is the voltage at the microsecond plasma-opening-switch, $L_0 + L_l$ is the total downstream inductance, and L_l is the inductance of a Z-pinch load.[28,34] We call this voltage "effective" since we subtract the $(L_0 + L_l)dI/dt$ inductive term. The load inductance $L_l(t)$ was calculated numerically from the differential equation $\dot{L}_l I = V - (L_0 + L_l)\dot{I}$, where a Z-pinch resistivity R_l was assumed to be negligible.

Figure 8 shows the dependence of the neutron yield on the magnitude of the load voltage in 6 shots with the total linear mass density of 80 μg/cm. In this figure, the neutron yield increases with a peak load voltage during the stagnation (cf. Ref. 43). A higher load voltage seems to be connected with a higher compression ratio of the current sheath. For instance in shots without the POS, a higher neutron yield correlated with a higher increase of the load inductance ΔL_l, with a smaller diameter in x-ray pinhole images and with a more intense soft x-ray emission.

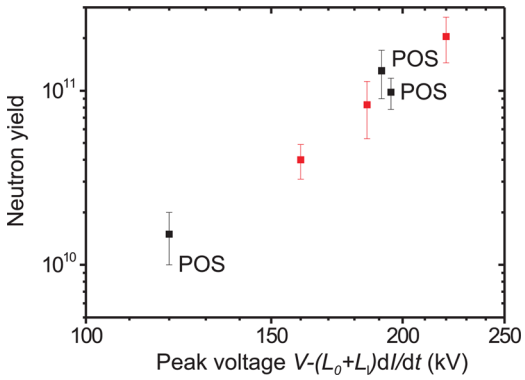

FIG. 8. The dependence of neutron yields on the peak of effective voltage at a load $V_{\text{eff}} = V - (L_0 + L_l)dI/dt$. Double shell gas puffs, 80 μg/cm total linear mass density, and the inner and outer shell diameter of 30 mm and 80 mm, respectively.

D. Load voltage

We showed in Sec. III C that the peak of the effective voltage during the stagnation $V_{\text{eff}} = V - (L_0 + L_l)dI/dt$ correlated with the neutron yield. At this point, it seems reasonable to look at the load voltage in more detail. Results will be illustrated on shot No. 1406. In this exemplary shot without the POS, the effective voltage V_{eff} could be calculated more precisely than in shots with the POS. Fig. 9 presents a voltage waveform together with a total inductance $L_0 + L_l$, soft x-rays, hard x-rays, and a streak camera image. It can be seen that the voltage started to rise at 400 ns, i.e., 300 ns before the stagnation. The load inductance L_l increased by about 15 nH during the implosion. Calculating with the 6 mm diameter at the stagnation, the 15 nH increase requires the initial diameter of about 300 mm, i.e., the diameter of the cathode. At such large diameters, even a low voltage of the order of 10 kV implies a high implosion velocity (e.g., $v_{\text{imp}} \approx 5 \times 10^5$ m/s for 40 kV and 20 cm diameter at 200 ns before the stagnation). At the stagnation, the moderate peak voltage of 200 kV indicates either a large final diameter or a slow velocity of the current sheath. For the current sheath velocity of (2–3) $\times 10^5$ m/s,

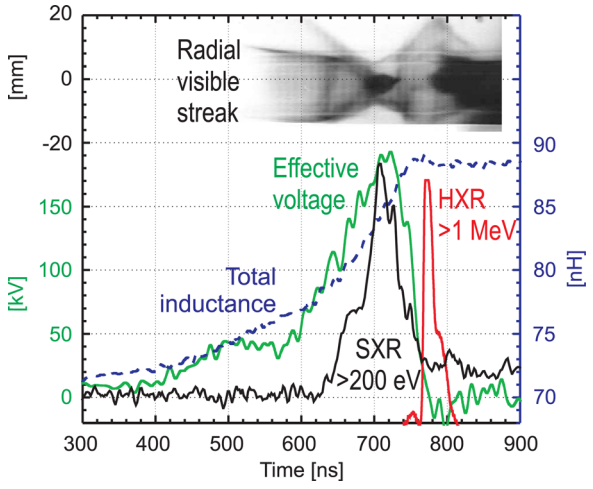

FIG. 9. A visible streak image and waveforms of a voltage V_{eff}, a total inductance $L_0 + L_l$, soft x-rays, hard x-rays in shot No. 1406 (without the POS). D_2 double shell gas puff, 80 μg/cm total linear mass density, $(0.8 \pm 0.2) \times 10^{11}$ neutrons.

the peak voltage implies the final plasma radius of 1.0–1.5 cm (cf. the diameter in the streak image in Fig. 9).

Analyzing voltage and inductance waveforms also in other shots, we concluded that the implosion started at a large diameter in a low density plasma. First, the initial inductance of the gas puff was lower than that of a short circuit where the conducting cylinder of a 10 cm diameter was used as a load. Second, there was a relatively large difference in the inductance at the beginning of the discharge and at the end of the implosion. Third, the 80 μg/cm deuterium gas puff imploded later than a 170 μg/cm neon gas puff when the same nozzles were used. The longer implosion times were observed also in previous experiments with argon–hydrogen gas puffs in the case of a high hydrogen fraction in an outer shell (cf. shot Nos. 368 and 395 in Ref. 29). All these facts together imply that the deuterium gas was spread at a large distance in the central anode–cathode region.

The significant spread of hydrogen is likely caused by a lower mass of hydrogen molecules and a higher thermal velocity. The spread of the gas inside the energy concentrator is the serious issue of hydrogen and deuterium gas puffs since it influences a gas puff implosion. First, the spread of the gas could cause the occurrence of the stagnation after the peak current implying poor efficiency of the energy conversion. Second, it could give rise to the early implosion of the inner shell before the arrival of the outer shell. Third, it could influence the implosion velocity, the plasma diameter at the stagnation, and consequently the peak load voltage. Because these parameters are important for the optimization of neutron yields, we would like to focus on this issue in our future gas-puff experiments on the GIT-12 generator.

IV. DISCUSSION

A. Multiple neutron pulses in deuterium gas puffs

The characteristic feature of the deuterium gas puff experiment on the GIT-12 was the occurrence of multiple neutron pulses. Two neutron pulses were observed also in previous experiments on the S-300 (Ref. 27) as well as in the plasma foci on the mega-ampere current level.[9,10,44] The GIT-12 generator with the POS provided the current rise-time of about 200 ns. In comparison with the rise times achieved on the S-300 and the MA plasma foci, such a value is in between. Besides on the GIT-12, it was possible to compare results at 200 ns and 1500 ns rise times, i.e., with and without the POS.

Deuterium gas puffs with and without the POS demonstrated a lot of similarities in the neutron emission. For instance, the first neutron pulse was observed at the stagnation and at the peak of the soft x-ray emission. However, the hard x-rays above 1 MeV were observed about 40 ns later. This hard x-ray emission was accompanied with the principal neutron emission. The main neutron emission will be discussed in Sec. IV C, while the following paragraphs are devoted to the first neutron pulse.

B. The first neutron pulse

As far as the first neutron pulse is concerned, it is natural to ask whether a fraction of neutrons may be explained by the

thermonuclear mechanism? In order to answer this question, we calculate an ion temperature and an expected thermonuclear yield from plasma parameters reached in our experiment.

The thermonuclear neutron yield is given by the equation

$$Y_{\text{thermonuclear}} = \frac{1}{4} n_i^2 \langle \sigma v \rangle_T \pi R^2 l \tau, \quad (1)$$

where n_i is the ion density, $\langle \sigma v \rangle$ stands for the DD fusion reaction rate, R is the plasma radius, l is the plasma length, and τ means the confinement time. For the 80 μg/cm linear mass density and the plasma radius of 3 mm, we obtain the plasma density of 8×10^{19} cm^{-3}. The plasma length l was 2 cm and the total ion number N was 4.8×10^{19}. Then, the neutron yield of 3×10^9 and the duration of the first neutron pulse of 10 ns in shot No. 1414 (see Fig. 4) imply the reaction rate of 6×10^{-22} cm^{-3}/s and the ion temperature of about 1.3 keV. We can compare this value with the temperature derived from the implosion velocity, the expansion velocity, and from the energy input into a plasma.

From the implosion velocity of 3.5×10^5 m/s, we obtain the ion temperature $kT_i \approx \frac{2}{3} \cdot \frac{1}{2} m_i v_{\text{imp}}^2 = 0.8$ keV. This value was influenced by the adiabatic compression and the ion energy loss to electrons. The significant adiabatic heating and the temperature above 1 keV can be deduced from a fast expansion with the 3×10^5 m/s velocity. Assuming the free expansion with an ion sound speed and neglecting T_e, the ion temperature $kT_i \approx m_i v_{\text{exp}}^2$ is about 1.8 keV. From the energy input $W = 30$ kJ, we have $k(T_i + T_e) = \frac{2}{3} W/N \approx 2.5$ keV. On the basis of these estimations, the "effective temperature" of 1.3 keV seems to be a reasonable value. We use the term "effective temperature" since it describes primarily the high energy tail of a deuteron velocity distribution. The average ion temperature could be higher. However, at temperatures higher than 1.3 keV, the collisionality of ions is low. At the 1.3 keV ion temperature, the ion-ion collision time of 2 ns is several times shorter than the duration of the stagnation and the Maxwellian tail of the velocity distribution has some time to develop. Therefore, the neutrons produced during the stagnation in shot No. 1414 can be explained by the thermonuclear mechanism and the temperature of 1.3 keV.

There is indeed an interesting question of why the neutron production during the stagnation was more intense in shot No. 1408 without the POS as illustrated in Fig. 7. In shots without the POS, the PCD detected much less intensive signals of x-rays above 1.7 keV and the current together with the energy input during the implosion were lower. However, the neutron yield during the stagnation reached 2×10^{10} in shot No. 1408 (cf. 2×10^9 neutrons in shot No. 1409 with the POS). The higher neutron yield was caused by a long duration of the neutron emission of about 70 ns. The effective temperature calculated from the neutron yield was the same, i.e., 1.3 keV, as in shots with the POS. The longer duration of the neutron emission without the POS shows that the neutron production is not a simple process even during the first pulse.

The first neutron pulse was intense also in MA plasma foci with a micro-second quarter period.[9,10,45,46] Deutsch and Kies suggested Fermi's mechanism to explain the neutron emission before and during the stagnation.[11] In addition to that, we have to take into account also the contribution of head-on collisions of deuterons interacting with $2v_{\text{imp}}$ relative velocity near the axis as well as axial acceleration of deuterons by a transient voltage, e.g., during current redistribution.[9] The experimental evidence of the thermonuclear mechanism has been provided only recently in Refs. 40, 44 and 46.

C. Main neutron emission

The main neutron emission occurred 40 ns after the soft x-ray peak as shown in Fig. 7. It was the case of the shots with a 3 kA/ns as well as with a 20 kA/ns current rise rate even though there was a difference in the width of radial neutron spectra. On the basis of previous plasma focus experiments,[10,15,47] we believe that these neutrons were produced by the beam-target mechanism after the disruptive development of instabilities. Therefore, we may ask if conditions convenient for a high x-ray yield are also optimal for a high neutron yield. On the one hand, the fast current rise time did not imply higher neutron yields (see, e.g., high neutron yield in shot No. 1408 without the POS or high neutron yields in microsecond plasma foci). On the other hand, the neutron yield of the post-stagnation phase depended on the effective load voltage reached during the stagnation (see Fig. 8). It means that the neutron yield was somehow connected with the quality of the implosion, e.g., with the final plasma diameter. To confirm this observation and to find optimal conditions for the highest neutron yield will be the subject of our future experiment.

D. Neutron yield scaling with current

To know the scaling law for a neutron yield is important for future applications of Z-pinch facilities as sources of neutrons. This is why we present peak neutron yields achieved with other deuterium gas puffs in Fig. 10. In these experiments, the cathode–anode gap was 20 mm except the 1 cm long gas puff at the University of California in Irvine. Figure 10 shows that the total number of neutrons scales as $I^{3.0\pm0.2}$ in the 0.3–17 MA region.

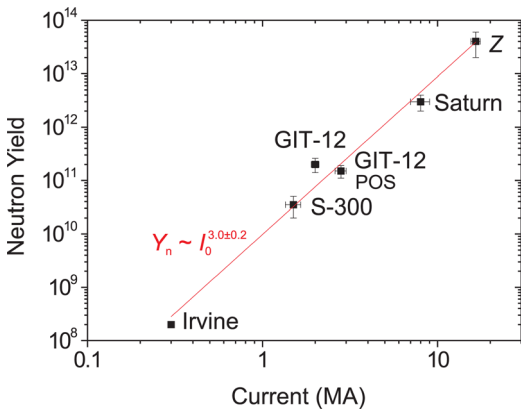

FIG. 10. Neutron yields from deuterium gas puff Z-pinches.[18,21,22,27] We left out the peak neutron yield at 2-3 MA on the Angara-5-1 (Ref. 19) because it was achieved with a strong axial gradient of linear density. In case of more axially homogeneous gas puffs on the Angara-5-1, neutron yields were smaller and very close to those achieved on the GIT-12.

This scaling is close to $Y_n \propto I^{3.3\pm0.3}$ which was obtained with Mather-type plasma foci by Bernard.[48] Milanese[49] and Soto[50] found a more favorable dependence for plasma foci $Y_n \propto I^{4.7}$. At this point, we should note perhaps that neutron yields produced in mega-ampere plasma foci are higher than these of deuterium Z-pinches with similar currents. Therefore, one may ask why the configuration of a Mather-type plasma focus is more efficient with respect to neutron production. A possible explanation could be related to a longer plasma column (i.e., higher inductances and lower currents during the pinch phase together with an abundance of neutrons for a given neutron yield per 1 cm), to an extra neutron yield produced in a surrounding gas, or to a better optimization due to a larger amount of experiments. In our opinion, the principal distinction between both configurations is a higher axial gradient of the linear density and more significant zipper in a plasma focus. Mega-ampere D_2 gas puffs on the S-300 (Ref. 27) clearly showed that 100 keV deuterons are accelerated with a high efficiency in a lower density plasma after the stagnation. Because of the axially homogeneous gas puff, also the density of a target plasma is low. Subsequently, neutron yields are lower than those in PFs where a large number of neutrons are produced in a dense structure at the heel of the current sheath.[47] In order to achieve higher neutron yields in mega-ampere deuterium Z-pinches, it seems convenient to "simulate" a plasma focus-like geometry. Such a geometry has been tried on the Angara-5-1 Z-pinch in Troitsk where a strong axial gradient of a linear density was achieved with a short delay between the initiation of the current generator and the breakdown pin pulse. This way, more than 10^{12} neutrons were emitted within 50 ns at a current of 2 MA.

E. Comparison with plasma foci

Our previous experiments on the S-300 demonstrated several similarities between deuterium gas puffs and plasma foci on a MA level.[27] We could give two neutron pulses,[9,10,45,46] the efficient production of 100 keV deuterons[10,52] and broad radial spectra[7,8,10,53,54] as examples. The experiment on the GIT-12, which provides two different current rise-times somewhere between fast Z-pinches and plasma foci, confirmed these observation. Such conclusion has significant implications for Z-pinch and plasma focus research. First, as far as Z-pinch research is concerned, it is possible to use experimental results which have been achieved in well-diagnosed plasma foci during the long-lasting plasma focus research. As for the plasma focus study, deuterium gas puff Z-pinches could provide important results about fusion processes at currents above 2 MA. At these currents, successful plasma focus experiments have not been carried out because of a low impedance of generators.[14] In Z-pinches, neutron yields are usually lower. But, on the other hand, the fixed length of a Z-pinch column and a less significant zipper enable to correlate plasma dynamics and neutron emission and to calculate plasma energetics more precisely.

As far as differences between gas puff Z-pinches and plasma foci are concerned, one might also like to discuss the contribution of the thermonuclear mechanism which depends on ion temperatures T, ion densities n, and confinement times τ. All plasma foci maintain almost the same value of ion densities and implosion velocities of $10^{18} - 10^{19}$ cm^{-3} and (2–3) $\times 10^5$ m/s, respectively.[50] With increasing currents of plasma foci I, it is necessary to increase the dimensions of these devices[51] as $R \propto a \propto I$, where R and a stand for a final pinch radius and an anode radius, respectively. The product of density n and confinement time τ is given by $n\tau \propto nR/\sqrt{T}$. Since ion densities and plasma temperatures in plasma foci are almost constant, $n\tau$ is proportional to the current $n\tau \propto R \propto I$.

Deuterium gas puffs are not so restricted by initial parameters as plasma foci. This way, higher implosion velocities or higher ion densities could be achieved. For instance on the GIT-12 as well as on the S-300 generators, the ion densities and implosion velocities were about 10^{20} ions/cm^3 and (3–4) $\times 10^5$ m/s, respectively. On the Z accelerator, the ion density reached 2×10^{20} cm^{-3}, whereas the implosion velocity was estimated as approximately 10^6 m/s. In comparison with plasma foci, higher temperatures and smaller dimensions of gas puffs result in shorter stagnation and neutron emission times. All these facts influence the product of density n and confinement time τ. Assuming the constant initial diameter of gas puffs and the same current rise-time, higher currents I require higher initial and final densities of deuterium ions $n \propto I^2$. Then, keeping the temperature constant, the product $n\tau$ scales as $\propto nR/\sqrt{T} \propto n \propto I^2$. It means that in Z-pinches, the Lawson product increases with higher currents faster than in plasma foci. Besides, Z-pinches are able to reach higher implosion velocities and temperatures more convenient for fusion. With regard to this, neutron measurements at higher implosion velocities are very rare and more experiments are needed to draw substantial conclusions about neutron production mechanisms in gas puff Z-pinches.

V. SUMMARY AND FUTURE WORK

In conclusion, the plasma dynamics and the neutron production in the deuterium gas puff Z-pinch were studied on the GIT-12 generator. The experiment was carried out with the double shell gas puff on the 2–3 MA current level. The influence of two different current rise rates (3 kA/ns and 20 kA/ns) on the neutron emission was researched. At the beginning of the neutron production, the neutron emission correlated with soft x-rays and a significant fraction of neutrons could be explained by the thermonuclear mechanism. Nevertheless, the peak of the neutron emission occurred 40 ns after the soft x-ray peak. The peak neutron yield of $(2.0 \pm 0.6) \times 10^{11}$ was achieved without the POS when the load current approached 2 MA during the stagnation. We believe that the neutron yield can be further increased if the two following issues are solved: First, the spread of deuterium inside the experimental chamber should be reduced; second, it is necessary to suppress early current penetration inside the inner shell and to prevent an inner shell from imploding before an outer shell arrives. We would like to focus on these phenomena during our future gas-puff experiments on the GIT-12 generator. The neutron TOF detectors, mainly the detector at 1.4 m, are now able to distinguish the first neutron pulse

from the main neutron emission. Therefore, it will be possible (1) to study the influence of various parameters on the first neutron pulse and (2) to optimize the neutron emission. Obtained results can be valuable to benchmark numerical codes and to address issues specific for deuterium. While a large number of studies are devoted to x-ray radiation of high-Z materials, the information about mega-ampere deuterium Z-pinches is rather rare. In this respect, we believe that our experiment contributes at least a little to this unexplored area.

ACKNOWLEDGMENTS

We wish to thank Dr. A. Velikovich and Dr. M. Krishnan for their valuable comments. This research has been supported by the Grant Agency of the Czech Republic (Grant No. P205/12/0454), the Czech Ministry of Education (Grant Nos. LA08024, ME09087, and LC528), the IAEA (Grant No. RC14817), the CTU (Grant No. SGS10/266/OHK3/3T/13).

[1]A. M. Andrianov, O. A. Bazilevskaia, S. I. Braginskii, B. G. Brezhnev, S. Khvaschevski, V. A. Khrabrov, N. G. Kovalski, N. V. Filippov, T. I. Filippova, V. E. Palchikov, I. M. Podgorny, Y. G. Prokhorov, and M. M. Sulkovskaya, *in Proc. 2nd United Nations International Conference on Peaceful Uses of Atomic Energy, Geneva, 1958*, edited by John H. Martens, Miss L. Ourom, Dr. Walter M. Barss, Dr. Lewis G. Bassett, Mr. K. R. E. Smith, Martha Gerrard, Mr. F. Hudswell, Betty Guttman, Dr. John H. Pomeroy, Mr. W. B. Woollen, Dr. K. S. Singwi, Mr. T. E. F. Carr, Dr. A. C. Kolb, Dr. A. H. S. Matterson, Mr. S. Peter Welgos, Dr. I. D. Rojanski, and Dr. David Finkelstein, (United Nations, Geneva, Switzerland, 1958), Vol. 31, p. 348; L. A. Artsimovich, *ibid*., p. 6; I. V. Kurchatov, Atomic Energy **1**, 359 (1956).
[2]O. A. Anderson, W. R. Baker, S. A. Colgate, J. Ise, and R. V. Pyle, Phys. Rev. **110**, 1375 (1958).
[3]Ye. P. Bogolubov, M. V. Koltunov, B. D. Lemeshko, V. I. Mikerov, V. N. Samosyuk, P. P. Sidorov, and D. I. Yurkov, Nucl. Instrum. Methods Phys. Res. A **605**, 62 (2009).
[4]M. V. Roshan, S. V. Springham, R. S. Rawat, and P. Lee, IEEE Trans. Plasma Sci. **38**, 3393 (2010).
[5]B. L. Bures, M. Krishnan, R. E. Madden, and F. Blobner, IEEE Trans. Plasma Sci. **38**, 667 (2010).
[6]V. A. Gribkov, S. V. Latyshev, R. A. Miklaszewski, M. Chernyshova, K. Drozdowicz, U. Wiacek, K. Tomaszewski, and B. D. Lemeshko, Phys. Scr. **81**, 035502 (2010).
[7]M. J. Bernstein and G. G. Comisar, Phys. Fluids **15**, 700 (1972).
[8]A. Bernard, A. Coudeville, A. Jolas, J. Launspach, and J. de Mascureau, Phys. Fluids **18**, 180 (1975).
[9]H. Herold, L. Bertalot, K. Hirano, U. Jaeger, H. J. Kaeppeler, M. J. Sadowski, H. Schmidt, R. Schmidt, M. Shakhatre, and A. Shyam, in *Plasma Physics and Controlled Nuclear Fusion Research, Proc. 10th Int. Conf., London, 1984* (IAEA, Vienna, 1985), Vol. 2, p. 579.
[10]U. Jager and H. Herold, Nucl. Fusion **27**, 407 (1987).
[11]R. Deutsch and W. Kies, Plasma Phys. Controlled Fusion **30**, 263 (1988).
[12]L. Soto, Plasma Phys. Controlled Fusion **47**, A361 (2005).
[13]V. A. Gribkov, A. Banaszak, B. Bienkowska, A. V. Dubrovsky, I. Ivanova-Stanik, L. Jakubowski, L. Karpinski, R. A. Miklaszewski, M. Paduch, M. J. Sadowski, M. Scholz, A. Szydlowski, and K. Tomaszewski, J. Phys. D **40**, 3592 (2007).
[14]S. Lee and S. H. Saw, J. Fusion Energy **27**, 292 (2008).
[15]P. Kubes, M. Paduch, T. Pisarczyk, M. Scholz, T. Chodukowski, D. Klir, J. Kravarik, K. Rezac, I. Ivanova-Stanik, L. Karpinski, K. Tomaszewski, and E. Zielinska, IEEE Trans. Plasma Sci. **37**, 2191 (2009).
[16]A. Bernard, J. P. Garconnet, A. Jolas, J. P. Le Breton, and J. de Mascureau, in *Plasma Physics and Controlled Fusion Research (IAEA-CN-37), 7th IAEA Conf. on Plasma Physics and Controlled Nuclear Fusion, Innsbruck, 1978* (IAEA, Vienna, 1979), Vol. 2, p. 159.
[17]J. Shiloh, A. Fisher, and N. Rostoker, Phys. Rev. Lett. **40**, 515518 (1978); J. Shiloh, Ph.D. dissertation, University of California, Irvine, 1978.
[18]J. Bailey, Y. Ettinger, A. Fisher, and N. Rostoker, Appl. Phys. Lett. **40**, 460 (1982).
[19]A. V. Batyunin, A. N. Bulatov, and V. D. Vikharev, Sov. J. Plasma Phys. **16**, 597 (1990).
[20]V. P. Smirnov, Plasma Phys. Controlled Fusion **33**, 1697 (1991).
[21]R. B. Spielman, G. T. Baldwin, G. Cooper, D. Hebron, R. J. Leeper, S. F. Lopez, J. S. McGurn, D. J. Muron, C. L. Ruiz, A. Schmidlapp, and M. Vargas, "D–D fusion experiments using fast Z pinches," Report No. SAND98-0705, Sandia National Laboratories, 1998.
[22]C. A. Coverdale, C. Deeney, A. L. Velikovich, R. W. Clark, Y. K. Chong, J. Davis, J. Chittenden, C. L. Ruiz, G. W. Cooper, A. J. Nelson, J. Franklin, P. D. LePell, J. P. Apruzese, J. Levine, J. Banister, and N. Qi, Phys. Plasmas **14**, 022706 (2007).
[23]C. A. Coverdale, C. Deeney, A. L. Velikovich, J. Davis, R. W. Clark, Y. K. Chong, J. Chittenden, S. Chantrenne, C. L. Ruiz, G. W. Cooper, A. J. Nelson, J. Franklin, P. D. LePell, J. P. Apruzese, J. Levine, and J. Banister, Phys. Plasmas **14**, 056309 (2007).
[24]A. L. Velikovich, R. W. Clark, J. Davis, Y. K. Chong, C. Deeney, C. A. Coverdale, C. L. Ruiz, G. W. Cooper, A. J. Nelson, J. Franklin, and L. I. Rudakov, Phys. Plasmas **14**, 022701 (2007).
[25]D. R. Welch, D. V. Rose, R. E. Clark, C. B. Mostrom, W. A. Stygar, and R. J. Leeper, Phys. Rev. Lett. **103**, 255002 (2009); D. R. Welch, D. V. Rose, C. Thoma, R. E. Clark, C. B. Mostrom, W. A. Stygar, and R. J. Leeper, Phys. Plasmas **17**, 072702 (2010); D. R. Welch, D. V. Rose, C. Thoma, R. E. Clark, C. B. Mostrom, W. A. Stygar, and R. J. Leeper, Phys. Plasmas **18**, 056303 (2011).
[26]D. Klir, J. Kravarik, P. Kubes, K. Rezac, S. S. Ananev, Yu. L. Bakshaev, P. I. Blinov, A. S. Chernenko, E. D. Kazakov, V. D. Korolev, G. I. Ustroev, L. Juha, J. Krasa, and A. Velyhan, IEEE Trans. Plasma Sci. **37**, 425 (2009).
[27]D. Klir, J. Kravarik, P. Kubes, K. Rezac, J. Cikhardt, E. Litseva, T. Hyhlik, S. S. Ananev, Yu. L. Bakshaev, V. A. Bryzgunov, A. S. Chernenko, Yu. G. Kalinin, E. D. Kazakov, V. D. Korolev, G. I. Ustroev, A. A. Zelenin, L. Juha, J. Krasa, A. Velyhan, L. Vysin, J. Sonsky, and I. V. Volobuev, Plasma Phys. Controlled Fusion **52**, 065013 (2010).
[28]S. P. Bugaev, A. M. Volkov, A. A. Kim, V. N. Kiselev, B. M. Kovalchuk, N. F. Kovsharov, V. A. Kokshenev, N. E. Kurmaev, S. V. Loginov, G. A. Mesyats, F. I. Fursov, and A. P. Khuzeev, Russ. Phys. J. **40**, 1154 (1997).
[29]A. V. Shishlov, R. B. Baksht, A. Yu Labetsky, V. I. Oreshkin, A. G. Rousskikh, A. V. Fedunin, S. A. Chaikovsky, V. A. Kokshenev, N. E. Kurmaev, and F. I. Fursov, IEEE Trans. Plasma Sci. **30**, 498 (2002).
[30]A. Yu. Labetsky, V. A. Kokshenev, N. E. Kurmaev, V. I. Oreshkin, A. G. Rousskikh, A. V. Fedyunin, F. I. Fursov, S. A. Chaikovsky, A. V. Shishlov, and N. A. Zhidkova, Plasma Phys. Rep. **34**, 228 (2008).
[31]R. Baksht, A. Fedyunin, A. Chuvatin, C. Rouaie, and B. Etlicher, Instrum. Exp. Tech. **41**, 536 (1998).
[32]A. Yu. Labetsky, A. G. Rousskikh, A. V. Fedunin, and A. V. Shishlov, Russ. Phys. J. **42**, 1048 (1999).
[33]R. B. Spielman, Rev. Sci. Instrum. **63**, 5056 (1992).
[34]V. A. Kokshenev, I. E. Kurmaev, and F. I. Fursov, Russ. Phys. J. **42**, 1056 (1999).
[35]D. Klir, J. Kravarik, P. Kubes, K. Rezac, E. Litseva, K. Tomaszewski, L. Karpinski, M. Paduch, and M. Scholz, Rev. Sci. Instrum. **82**, 033505 (2011).
[36]H. Ing, R. A. Noulty, and T. D. McLean, Radiat. Meas. **27**, 1 (1997).
[37]D. D. Ryutov, M. S. Derzon, and M. K. Matzen, Rev. Mod. Phys. **72**, 167 (2000).
[38]M. Sadowski, H. Herold, H. Schmidt, and M. Shakhatre, Phys. Lett. **105A**, 117 (1984).
[39]B. Appelbe and J. Chittenden, Plasma Phys. Controlled Fusion **53**, 045002 (2011).
[40]D. Klir, P. Kubes, M. Paduch, T. Pisarczyk, T. Chodukowski, M. Scholz, Z. Kalinowska, E. Zielinska, B. Bienkowska, J. Hitschfel, S. Jednorog, L. Karpinski, J. Kortanek, J. Kravarik, K. Rezac, I. Ivanova-Stanik, and K. Tomaszewski, Appl. Phys. Lett. **100**, 016102 (2012).
[41]K. Rezac, D. Klir, P. Kubes, J. Kravarik, and M. Stransky, Czech J. Phys. **56**, B357 (2006).
[42]K. Rezac, Ph.D. dissertation, Czech Technical University in Prague, 2011.
[43]B. L. Bures, M. Krishnan, and R. E. Madden, IEEE Trans. Plasma Sci. **40**, 3351 (2011).
[44]D. Klir, P. Kubes, M. Paduch, T. Pisarczyk, T. Chodukowski, M. Scholz, Z. Kalinowska, B. Bienkowska, L. Karpinski, J. Kortanek, J. Kravarik, K. Rezac, I. Ivanova-Stanik, K. Tomaszewski, and E. Zielinska, Plasma Phys. Controlled Fusion **54**, 015001 (2012).

[45]H. Schmidt, P. Kubes, M. J. Sadowski, and M. Scholz, IEEE Trans. Plasma. Sci. **34**, 2363 (2006).
[46]D. Klir, P. Kubes, M. Paduch, T. Pisarczyk, T. Chodukowski, M. Scholz, Z. Kalinowska, E. Zielinska, B. Bienkowska, J. Hitschfel, S. Jednorog, L. Karpinski, J. Kortanek, J. Kravarik, K. Rezac, I. Ivanova-Stanik, and K. Tomaszewski, Appl. Phys. Lett. **98**, 071501 (2011).
[47]P. Kubes, M. Paduch, T. Pisarczyk, M. Scholz, D. Klir, J. Kravarik, K. Rezac, T. Chodukowski, I. Ivanova-Stanik, L. Karpinski, E. Zielinska, K. Tomaszewski, and M. J. Sadowski, IEEE Trans. Plasma Sci. **38**, 672 (2010).
[48]A. Bernard, A. Coudeville, J. P. Garconnet, A. Jolas, J. de Mascureau, C. Nazet, in *Plasma Physics and Controlled Nuclear Fusion Research, Proc. 6th Int. Conf., Berchtesgaden, 1976* (International Atomic Energy Agency, Vienna, 1977), Vol. 3, p. 471.
[49]M. M. Milanese, R. Moroso, and J. Pouzo, Eur. Phys. J. D **27**, 77 (2003).
[50]L. Soto, C. Pavez, A. Tarife, J. Moreno, and F. Veloso, Plasma Sources Sci. Technol. **19**, 055017 (2010).
[51]S. Lee and A. Serban, IEEE Trans. Plasma Sci. **24**, 1101 (1996).
[52]W. Stygar, G. Gerdin, F. Venneri, and J. Mandrekas, Nucl. Fusion **22**, 1161 (1982).
[53]M. J. Bernstein and F. Hai, Phys. Fluids **14**, 1010 (1971).
[54]M. M. Milanese and J. Pouzo, Nucl. Fusion **18**, 533 (1978).